Hydrogen bonding for the stabilization of different peptide conformations

Dayi Liu

▶ **To cite this version:**

Dayi Liu. Hydrogen bonding for the stabilization of different peptide conformations. Organic chemistry. Université Paris-Saclay, 2023. English. NNT : 2023UPASF041 . tel-04166042

HAL Id: tel-04166042
https://theses.hal.science/tel-04166042

Submitted on 19 Jul 2023

HAL is a multi-disciplinary open access archive for the deposit and dissemination of scientific research documents, whether they are published or not. The documents may come from teaching and research institutions in France or abroad, or from public or private research centers.

L'archive ouverte pluridisciplinaire **HAL**, est destinée au dépôt et à la diffusion de documents scientifiques de niveau recherche, publiés ou non, émanant des établissements d'enseignement et de recherche français ou étrangers, des laboratoires publics ou privés.

THÈSE DE DOCTORAT

NNT : 2023UPASF041

université PARIS-SACLAY

Hydrogen bonding for the stabilization of different peptide conformations

Liaison hydrogène pour la stabilisation de différentes conformations de peptides

Thèse de doctorat de l'université Paris-Saclay

École doctorale n° 571 : sciences chimiques : molécules, matériaux, instrumentation et biosystèmes (2MIB)
Spécialité de doctorat : Chimie
Graduate School : Chimie. Référent : Faculté des sciences d'Orsay

Thèse préparée à l'**Institut de Chimie Moléculaire et des Matériaux d'Orsay** (Université Paris-Saclay, CNRS), sous la direction de **David AITKEN**, professeur

Thèse soutenue à Paris-Saclay, le 3 juillet 2023, par

Dayi LIU

Composition du Jury

Membres du jury avec voix délibérative

Marie-Christine SCHERRMANN Professeure, Université Paris-Saclay	Présidente
Sophie FAURE Directrice de Recherche, Institut de Chimie de Clermont-Ferrand	Rapporteur & Examinatrice
Sylvain BROUSSY Professeur, Université Paris Cité	Rapporteur & Examinateur
Karen WRIGHT Chargée de recherche, Université Versailles St-Quentin-en-Yvelines	Examinatrice

université PARIS-SACLAY

ÉCOLE DOCTORALE
Sciences Chimiques : Molécules, Matériaux, Instrumentation et Biosystèmes (2MIB)

Titre : Liaison hydrogène pour la stabilisation de différentes conformations de peptides

Mots clés : liaisons hydrogène, peptides, acides aminés, hélice, interaction C5, synthèse organique

Résumé : Les liaisons H jouent un rôle essentiel dans la stabilisation des peptides et des protéines. Parmi ces interactions, la plus courante est la liaison N–H···O=C, une liaison H du squelette qui pousse les peptides à se replier en structures secondaires. En outre, d'autres types de liaisons H contribuent également de manière significative à la stabilisation des peptides.

Tout d'abord, nous avons étudié le comportement de conformation des peptides hybrides γ/α alternant *cis*-^{3,4}CB-GABA et alanine, qui étaient stabilisés par des liaisons H N–H···O=C. Ces peptides ont été caractérisés par calcul, par solution et par des techniques expérimentales à l'état solide, ce qui suggère que les peptides adoptent une hélice 12/10.

Nous avons ensuite étudié les interactions entre le squelette et la chaîne latérale dans la stabilisation d'une faible interaction C5.

La conformation des dérivés de l'Aatc(Me) a été caractérisée par le calcul, par l'expérience en phase gazeuse et en solution, ce qui suggère qu'une liaison H N–H···N C6γ stabilise l'interaction C5, et le système de liaison H C5-C6γ prédominant dans les oligomères de l'Aatc(Me). Les conformations des dérivés oxydés de l'Aatc(Me) et de l'Attc ont révélé qu'une liaison H C7δ N–H···O–X (X=N, S) stabilisait l'interaction C5, ce qui a donné lieu à une forme étendue.

Enfin, la conformation des dérivés *trans*-ACBC de la *N*-benzoxazolinone a été étudiée et a démontré que la partie *N*-benzoxazolinone avait un impact significatif sur la conformation locale en C8 des dérivés *trans*-ACBC.

Title : Hydrogen bonding for the stabilization of different peptide conformations

Keywords : H-bonds, peptides, amino acids, helix, C5 interaction, organic synthesis

Abstract : H-bond plays an essential role in stabilizing peptides and proteins. Among these interactions, the most common one is N–H···O=C, a backbone–backbone H-bond that drives peptides to fold into secondary structures. Additionally, other types of H-bonds also contribute significantly to peptide stabilization.

Firstly, we investigated the conformation behavior of γ/α-hybrid peptides alternating *cis*-^{3,4}CB-GABA and alanine, which were stabilized by common N–H···O=C H-bonds. These peptides were characterized by computation, by solution and solid states experimental techniques, suggested that *R*,*R*,*S* peptides adopt a 12/10 helix.

Then, we explored the backbone–sidechain interactions in stabilizing a weak C5 interaction.

The conformation of Aatc(Me) derivatives were characterized by computation, by experimentally in gas and solution phases suggesting that an N–H···N C6γ H-bond stabilized the C5 interaction, and the C5-C6γ H-bonding system prevalent in Aatc(Me) oligomers. The conformations of oxidized Aatc(Me) and Attc derivatives revealed that a C7δ N–H···O–X (X=N, S) H-bond stabilized the C5 interaction, resulting in an extended form.

Lastly, the conformation of *N*-benzoxazolinone *trans*-ACBC derivatives was studied and demonstrated that the *N*-benzoxazolinone moiety had a significant impact on the C8 local conformation of *trans*-ACBC derivatives.

AUTHOR'S STATEMENT

The research work presented in this thesis was conducted between autumn 2019 and summer 2023 under the joint supervision of Pr David J Aitken and Dr Sylvie Robin. For administrative reasons, I have not been allowed to include Dr Sylvie Robin's name on the front cover of thesis to testify her supervisory capacity. Through the present statement, I wish it to be known and recognized that Dr Robin acted as my co-supervisor throughout the indicated research period.

July 2023, Dayi Liu

DECLARATION DE L'AUTEUR

Les travaux de recherche présentés dans cette thèse ont été réalisés entre l'automne 2019 et l'été 2023 sous la direction du Pr David J Aitken et le co-encadrement du Dr Sylvie Robin. Pour des raisons administratives, je n'ai pas été autorisé à inclure le nom du Dr Sylvie Robin sur la couverture de thèse pour témoigner de son rôle. Par la présente déclaration, je souhaite que ce soit reconnu que le Dr Robin a été co-encadrante de la thèse tout au long de la période de recherche indiquée.

Juillet 2023, Dayi Liu

Acknowledgement

Firstly, I would like to thank Dr. Sophie FAURE and Dr. Sylvain BROUSSY for being reporters of my PhD thesis, and Prof. Marie-Christine SCHERRMANN and Dr. Karen WRIGHT for being examiners of my jury members.

I am also deeply grateful to Prof. David. J. AITKEN for his guidance and supervision throughout my four-year doctoral program. He provided invaluable suggestions for my projects, helped the correction of my thesis manuscript, and scheduled an appropriate time for my defense. Many thanks to Dr. Sylvie ROBIN, the co-supervisor of my thesis, for her supervision and manuscript corrections, as well as for her support with administrative tasks. I still remember those moments that she helped me handle applications such as bank card, Navigo card, vitale card, etc. She has magic power to manage all those stuffs.

I would like to extend my appreciation to Dr. Etienne Brachet, for my comite de suivi, he provided lots of suggestions on my projects.

Special thanks to other permanents in CP^3A team. Thanks to the director, Marie-Christine Schermann, who provided a warm and supportive environment for our team. Thanks to Thomas for his gentle and motivated demeanor, and he shared lots of fun with us. Thanks to Omar, a new addition to the lab who is both energetic and helpful. Many thanks to him for his suggestions and willingness to listen to me during my difficult period. Thanks to Valerie for her kindness, to Sandrine for her humorous and outgoing personality, to Catherine for HPLC purification and for teaching me how to use it, to Fatima, who left the team but helped us a lot during her stay.

I cannot forget my colleagues in the student office, first thanks to Zeynab, who worked with me in the lab for one year, shared many experiences with me. Many thanks to Peng for his help and cheerful personality. Great appreciation to Xuefeng, who accompanied me in the team for three years, for my manuscript correction and gave me lots of suggestions. Thanks to Ivana for her kindness and her suggestions. Great thanks to Xiaodan for her humor and daily support, nice experience working together in the lab for one year. Many thanks to Gabriel for his generous and funny character, who made lots of laughing moments with us. Thanks to Chiara for her funny and helpful nature. I am also thankful for the support and cooperation of all the interns, Vincent, Williams, Slimane, Cloe, Nakid, Emeric, Timothe, etc.

Additionally, thanks to Jean-Pierre and Amandine for the NMR techniques support. Jean-Pierre is the gentlest man I have ever met. He taught me NMR techniques always with patience, thanks for his kindness. Thanks to Helene for the mass support and Regis for the XRD analysis.

I want to thank Michel Mons for his collaboration on the project. He is very nice and gentle, thanks for his contributions and suggestions on our projects.

I also want to express my great appreciation to my friends who accompanied me during these years. They made me feel less alone and gave me the strength to keep going. In particular, I am grateful to Shanyu for her accompany, she always helped me to fix stuff, is a thoughtful person at working

and in the daily. Thanks to Chanjuan, Wei, Donghuang, Dan, etc for all the happy times we shared in daily.

Importantly, thanks to CSC (Chinese scholarship council) for financial support in accomplishing my PhD study in France.

最后，我非常感谢我的家人，如果没有他们的支持我很难走出这一步，并且不能走到顺利完成博士学业。

Table of contents

PART I GENERAL INTRODUCTION

PART II RESULTS AND DISCUSSION

PART I

GENERAL INTRODUCTION

1 The hydrogen bond: a universal role

The hydrogen bond (H-bond) is a non-covalent interaction which takes many forms. Gilbert Lewis first proposed the concept of H-bond in his "Valence and the Structure of Atoms and Molecules" in 1923[1]: This interaction is an electrostatic attraction (Figure 1, dashed line) between a hydrogen (H) atom covalently bonded (Figure 1, solid line) to a strongly electronegative atom (X) and an atom (Y) possessing a lone pair of electrons with high electronegativity too. X and Y atoms are commonly the second-row elements N, O and F.

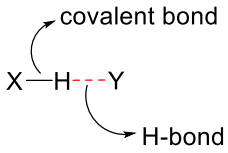

Figure 1. The presence of a H-bond

H-bonds could be inter- or intramolecular in nature. The intermolecular H-bond occurs between the atoms of different molecules, and the intramolecular H-bond occurs between the atoms of the same molecule.

The energy of the H-bond typically ranges from 4 to 167 kJ/mol considering its geometry, environment and the nature of the specific X and Y atoms. For example, the bond strength of O–H···O of water is 21 kJ/mol, and N–H···N of liquid ammonia is 13 kJ/mol. This type of bonding used is weaker than ionic or covalent bonding but stronger than van der Waals forces. Its easy formation or disruption under a wide range of physiological temperatures and conditions induces different effects on diverse substances (inorganic and organic molecules). These properties of H-bonds have led to broad applications in the universal fields.

1.1 H-bonds in daily life

1.1.1 H-bonds in water

Water is essential for life and is the human body's most abundant substance (60%–70%). H-bonding determines the structure and dynamics of water. Water molecules are highly polarized and can form an extensive network of H-bonds owing to their oxygen atoms having a partial negative (δ-) charge and their hydrogen atoms having a partial positive (δ+) charge. The lone pairs of electrons on the oxygen atom are attracted to the δ+ of the hydrogen of

nearby water molecules. Each water molecule can form a total of four H-bonds in the network (Figure 2).

H-bonds in water are essential to sustain life.[2] For example, H-bonds are responsible for the high boiling point of water at 100 °C. Without them, water would be in a gas state at room temperature as well as ammonia (two H-bond) (Figure 2). Other properties of water, such as adhesion, surface tension, and ability to dissolve polar substances are the results of H-bonds.

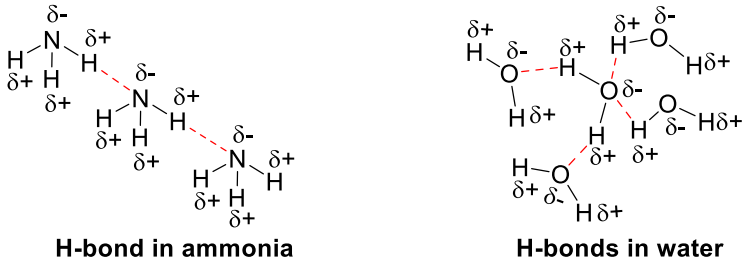

Figure 2. H-bonds in ammonia and water

1.1.2 H-bonds in paints and dyes

H-bonds play an important role in the properties of paints and dyes, particularly in the formation of their solid films. In paint and dye systems, H-bonds can occur between various components, such as binders, pigments, and solvents.[3] For example, indigo dye is sticky, driven by adhesive force resulting in H-bonds, which can tightly hold molecules together (Figure 3).[4]

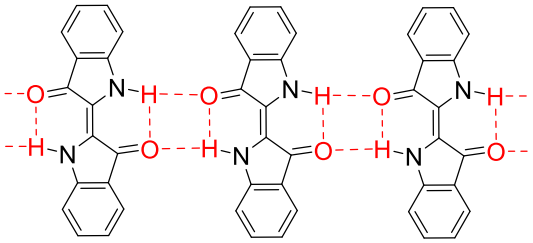

Figure 3. H-bonds in indigo structure

1.1.3 H-bonds in clothing materials

The materials for our clothing are derived from natural fibers including wool, silk and cotton, or from synthetic fibers like polyester and nylon.

Natural fibers such as wool, silk, and cotton contain complex protein structures that are held together by H-bonds, which contribute to their strength, elasticity, and texture.

In synthetic fibers such as polyester and nylon (Figure 4), H-bonding can also modify their properties. Controlling the H-bonding interactions between the fibers makes it possible to produce materials with improved strength, durability, and resistance to heat and chemicals.[5,6]

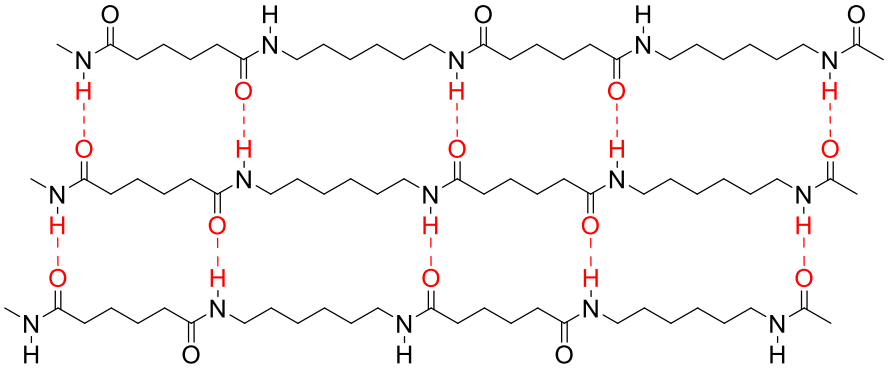

Figure 4. H-bonds in nylon 6,6 hold the chains together to form fibers

1.1.4 H-bonds in cleaning action of soaps

The dirt (grease) on clothes is insoluble in water, meaning that it cannot be removed by only using water. Soap is designed to do this job, and H-bonds are the main player thereof. Soap is an amphipathic structure with hydrophobic and hydrophilic portions. Once soap is dissolved in water containing dirty clothes, the hydrophilic portion is H-bonded to the water, and its hydrophobic portion binds with the grease. The dirt can then be removed easily from clothes (Figure 5).

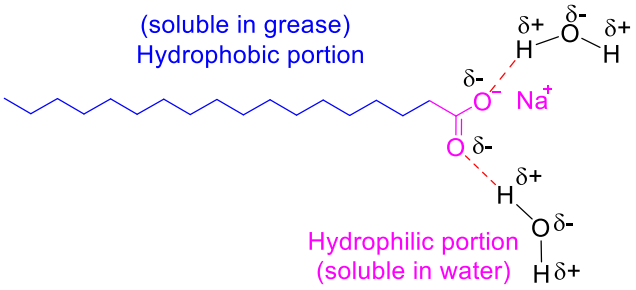

Figure 5. Soap forms H-bonds with water

1.2 H-bonds in living organisms

The interactions between nucleic acids, proteins, carbohydrates and/or lipids are involved in almost every process in life on earth. H-bonds play an essential role in these interactions and are critical to the systems of living organisms.

1.2.1 H-bonds in nucleic acids

H-bonds play a key role in the structure and function of nucleic acids, especially in DNA (Deoxyribonucleic Acid) and RNA (Ribonucleic Acid).

In 1953, Watson and Crick described the structure of DNA as based on H-bonds between purine and pyrimidine bases.[7]

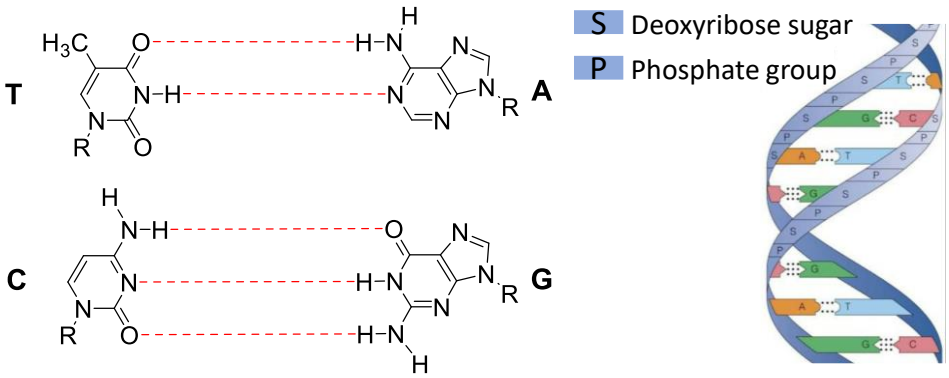

Figure 6. Part of Watson and Crick's DNA structure

Thymine (T) forms two H-bonds with adenine (A), and cytosine (C) forms three H-bonds with guanine (G) (Figure 6, left).

These H-bonds between base pairs in DNA hold the two strands of nucleotides together into a double helix (Figure 6, right). Without H-bonding, DNA would exist as a different structure.

RNA forms H-bonds much like DNA. H-bonding also plays a crucial role in the formation of its secondary structures, such as stems and loops, which are involved in many important biological processes, for example, in RNA–protein interactions[8].

1.2.2 H-bonds in proteins

In 1936, Mirsky and Pauling suggested that, the formation of the H-bonds between the peptide backbone amide protons and carbonyl oxygens, and also between the free amine and carboxylate groups of diamino and dicarboxylic amino acid residues, respectively, define the conformation of the polypeptide chain of a native protein molecule.[9] The concept was supported by Pauling's further work in 1951: he verified the importance of intramolecular H-bonds in model structures for α-helix[10] and β-sheet[11], which are the main secondary structures of natural proteins.

Approximately 50% of polar groups are buried within the interior of folded native proteins, and isolated from bulk solvents. They may form intramolecular H-bonds in the constrained microenvironment and contribute to protein folding and stability. Even in the unfolded state, those polar groups may form intermolecular H-bonds with solvent.[12,13]

Protein folding is a complex process including four stages, primary, secondary, tertiary and quaternary structures. The **primary** structure of a protein is the linear sequence of amino acids residues in the polypeptide chain, and it is the starting point for all subsequent stages of protein structure; The polypeptide chain folds back on itself via the formation of H-bonds to generate a **secondary** structure; Different interactions between amino acid side chains, such as disulfide bonds, hydrophobic interactions and H-bonds, then associate to produce a **tertiary** structure; The **quaternary** structure of a protein refers to the way in which multiple protein subunits associate to form a multi-subunit protein. This stage of protein structure is particularly important for enzymes, which often require multiple subunits to function properly.

H-bonding is crucial in determining the secondary structure of proteins. The two most common secondary structural elements are α-helices and β-sheets, accompanied by less common β-turns and Ω-loops. In addition to stabilizing the overall shape of the protein, H-bonding is also important for the specific functions of individual proteins. In particular, H-bonding is crucial in determining the specificity of an enzyme by helping to position substrate molecules in the active site, as well as in the stability of protein-protein interactions and in the formation of protein-DNA complexes.

1.2.2.1 Helices in natural proteins

Helices in natural proteins include the α-helix, the 3_{10}-helix and the π-helix (Figure 7).[14,15]

The **α-helix** is the most prevalent type of helix that occurs in protein secondary structures. Every backbone amide proton forms an H-bond with the backbone carbonyl oxygen located four residues earlier along the protein sequence, this repeated i+4→i H-bonding is the most predominant feature and is exhibited as a right-handed helix.[16]

The **3_{10}-helix** is the fourth most common type of secondary structure found in proteins, after α-helix, β-sheets and β-turns. They are typically observed as extensions of α-helices, found at either their *N*- or *C*- terminus. Every backbone amide proton forms an H-bond with the backbone carbonyl oxygen located three residues earlier along the protein sequence, which shows repeated i+3→i H-bonding.[17,18]

The **π-helix** was discovered by crystallographer Barbara Low in 1952. Short π-helices are found in 15% of known protein structures and are believed to be an evolutionary adaptation derived by the insertion of a single amino acid into an α-helix. Every backbone amide proton forms an H-bond with the backbone carbonyl oxygen located five residues earlier along the protein sequence, which shows repeated i+5→i H-bonding.[19–21]

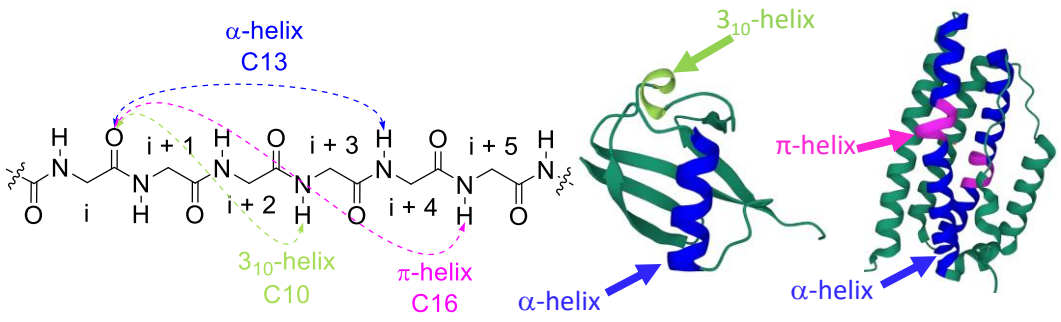

Figure 7. H-bonding folding patterns of helices (left); Structure of ubiquitin refined at 1.8 angstroms resolution (middle) (PDB: 1UBQ); Crystal structure of oxidized symerythrin from cyanophora paradoxa (right) (PDB: 3QHB)

1.2.2.2 Sheets in natural proteins

The β-sheet is a common motif of the regular protein secondary structure, and its basic unit in protein is the β-strand. A β-strand is a stretch of polypeptide chain typically 3 to 10 amino acids long with the backbone in an extended conformation, these polypeptide chains run alongside each other and are linked in a regular manner by H-bonds between the main chain C=O and N–H groups.[22] Adjacent β-strands can form parallel, antiparallel, or mixed sheets. If the amino acids in the interacting β-strands are aligned in the same direction (amino terminal to carboxyl terminal), the β-sheet is described as a parallel β-sheet (Figure 8, left). If the amino

acids in successive strands have alternating directions, the β-sheet is called an antiparallel β-sheet (Figure 8, right).

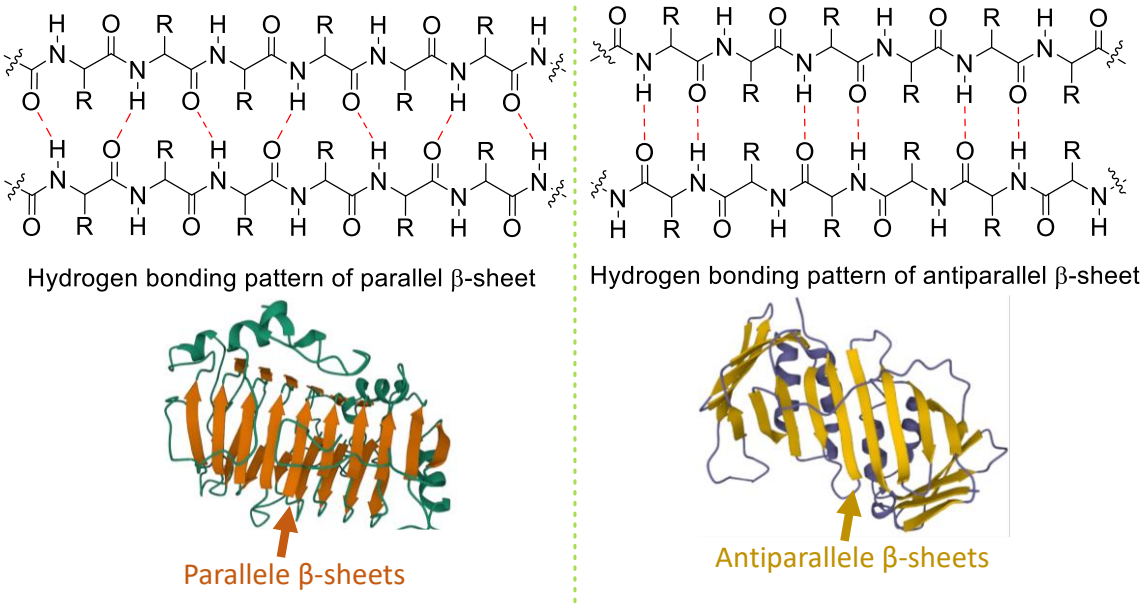

Figure 8. H-bonding patterns of β-sheets (upper); The refined three-dimensional structure of pectate lyase c from erwinia chrysanthemi (bottom left) (PDB: 2PEC); Human pcna (bottom right) (PDB: 1AXC)

C5 interaction accompanies β-sheets in native proteins (Figure 9), it is a H-bond formed between the amide proton and the carbonyl oxygen of the same α-amino acid residue. This unusual and elusive H-bond has been noticed by chemists since the 1960s.[23–25] In recent years, the Raines group showed via experimental and computational methods that this H-bond is presented in 94% of proteins and contributes significantly to protein stabilization in some cases.[26] Raines suggested that the C5 H-bond may play a key role in stabilizing amyloid-forming proteins in β-sheets, such as those involved in Alzheimer's disease.[27]

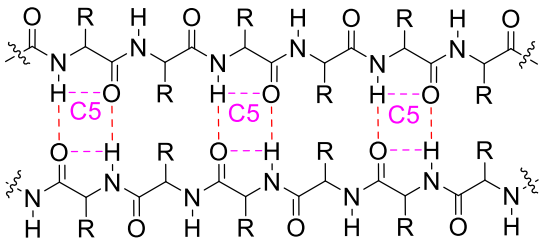

Figure 9. C5 H-bonds in β-sheets

1.2.2.3 Turns in natural proteins

Turns are short segments of a protein's structure that are often referred to as "loops" or "bends". They generally occur when polypeptide chains reverse their overall direction and eventually generate the tertiary structure. They serve as connecting regions between two other elements of secondary structure.

The most common turns are β-turns, in which the direction change is executed in the space of four residues. The defining feature of a β-turn is an H-bond between the C=O of residue i and the N–H of residue i+3 (Figure 10). Proline and glycine play key roles in turns, which proline provides less flexibility (starting the turn) and glycine provides greater flexibility (facilitating the turn).

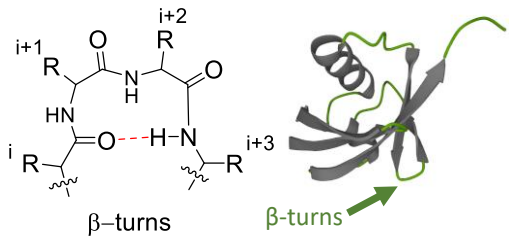

Figure 10. H-bonding folding patterns of β-turns (left); Structure of ubiquitin refined at 1.8 angstroms resolution (right) (PDB: 1UBQ)

1.2.3 H-bonds in carbohydrates

Carbohydrates are probably the most abundant and widespread families of organic substances in Nature and are essential constituents of all living things. With the general chemical formula $C_x(H_2O)_y$, composed of carbon (C), hydrogen (H), and oxygen (O). In carbohydrates, both intermolecular and intramolecular H-bonds help to hold the carbohydrate chains together and contribute to the stability of the overall structure.[28]

For example, cellulose (Figure 11) is the structural component of plants principally. In its structure, the H-bonds between the oxygen atoms and the hydrogen atoms of hydroxyl groups (–OH) of adjacent glucose units help to form a strong, rigid structure. Such stability is essential for the function of cellulose as a component of plant cell walls, providing mechanical support to the plant.[29]

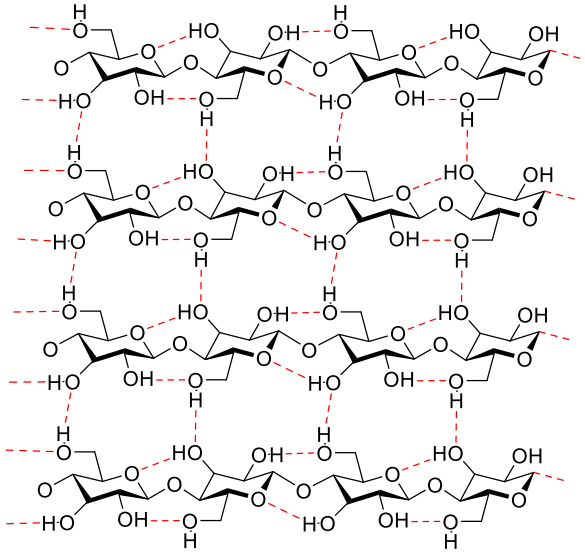

Figure 11. The structure of cellulose, stabilized by H-bonds

1.2.4 H-bonds in lipids

Lipids are any organic compounds that are insoluble in water, including fats, waxes, oils, hormones, and specific components of membranes. They function as energy-storage molecules and chemical messengers. Together with proteins and carbohydrates, lipids are one of the principal structural components of living cells.

H-bonds are involved in the interactions between lipids and other biomolecules, such as proteins and carbohydrates. To name a few, H-bonds between the polar head groups of phospholipids help the stabilization of the lipid bilayer structure and regulate the membrane's fluidity.[30,31]

1.3 H-bonds in organic synthesis

In chemical processes, H-bonds participate in molecular structure stability, reactivity, function, conformational dynamics, etc.

1.3.1 H-bonds in catalysts

Catalytic operations are essential in many complex synthetic processes. Numerous catalysts are used daily in laboratory research in synthetic fields, since they speed up chemical

reactions and improve the efficiency of such processes. Exploiting novel and efficient catalysts for chemical reactions is one of the most active areas in organic chemistry.

In addition to its primacy as a structural determinant, H-bond has played a considerable role in catalysts, being implicated in transition metal catalysts, organocatalysts, enzyme catalysts, etc.

1.3.1.1 H-bonds in transition metal catalysts

Transition metals are highly efficient catalysts for organic synthesis and have been used for almost a hundred years.[32,33]

H-bonding can occur in many metal complexes, and this interaction assisted transition metal catalysts has been widely studied.[34,35]

In 2001, the Rheingold group showed that the combination of a Ru complex and a phosphinoimidazole ligand, which could provide exceptionally effective catalysis for the anti-Markovnikov hydration of terminal alkynes to the corresponding aldehydes. It is remarkable that these relatively simple organometallic complexes were stabilized by H-bonds formed in the structure (Scheme 1).[36]

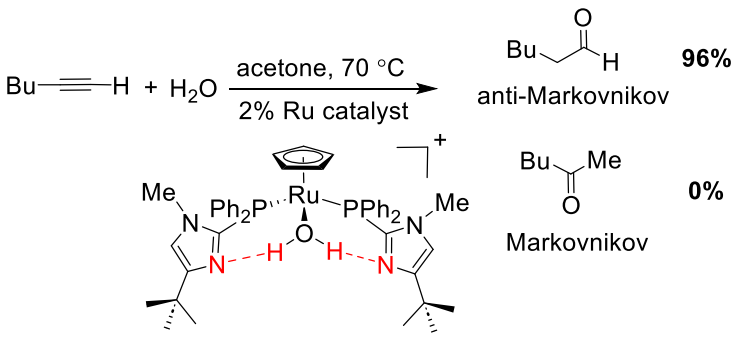

Scheme 1. Ru complex catalyst for anti-Markovnikov hydration

In 2018, the Bosch group reported a copper-mediated oxidation process for alcohols, using Cu complexes with bidentate redox-active ligands featuring H-bonding donor groups. In the single-crystal structure, the authors observed that the Cu complexes were stabilized through the formation of intramolecular H-bonds between the two ligand scaffolds (Scheme 2).[37]

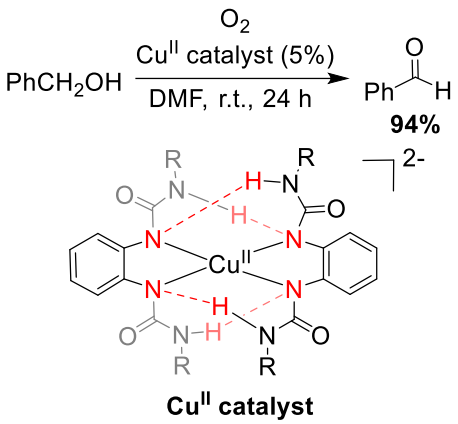

Scheme 2. Cu complex catalyst for the oxidation of alcohols

In 2022, the Shi group showed that an Ir complex catalyst for the asymmetric C–H activation/annulation of sulfoximines was facilitated by the H-bonding interactions. By theoretical calculations, the authors indicated that the N–H···O H-bonding between the sulfoximine and the chiral carboxylic acid ligand was essential to achieve high enantioselectivity (Scheme 3).[38]

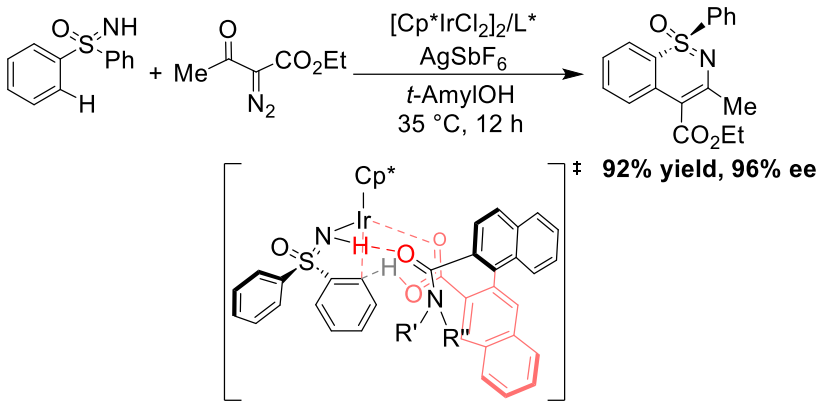

Scheme 3. Ir complex catalyst for asymmetric C–H activation/annulation of sulfoximines enabled by H-bonds

1.3.1.2 H-bonds in organocatalysts

Organocatalysts are appreciated for their stability, lack of metal, sustainability, and eco-friendliness in chemical reactions. They have garnered widespread attention in organic synthesis.

H-bonding organic catalysts can drive chemical reactions forward by stabilizing anionic intermediates and transition states. For instance, the extensive use of urea and thiourea derivatives as organocatalysts has led to remarkable accomplishments.[39]

In 1994, Curran proved that diaryl urea derivatives could act as catalysts for the allylation of cyclic-sulfinyl radicals. Without additive, the product was obtained in 60% yield with a ratio of (*trans*/*cis* = 2.5/1). Using diaryl urea as catalyst, the product was obtained in 81% yield and with a ratio of (*trans*/*cis* = 7/1). It was proposed that the enhancements could be attributed to H-bonding. In the transition state, the urea derivative H-bonded to sulfoxide which may promote the addition of the radical to allylstannane (Scheme 4).[40]

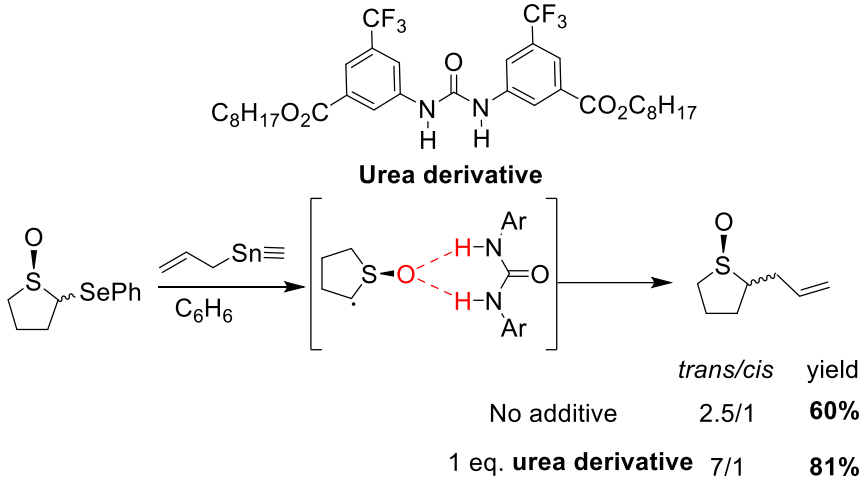

Scheme 4. The allylations of cyclic-sulfinyl radicals with diaryl urea

One year later, Curran used diaryl urea derivatives as catalyst in the Claisen rearrangements of allyl vinyl ester. He observed a significant acceleration of the reaction rate: without additive, the rate factor (K_{rel}) was 1.0 whereas with 1 eq. of urea derivative the rate factor (K_{rel}) was 4.2. It was suggested that these accelerations were also due to H-bonds (Scheme 5).[41]

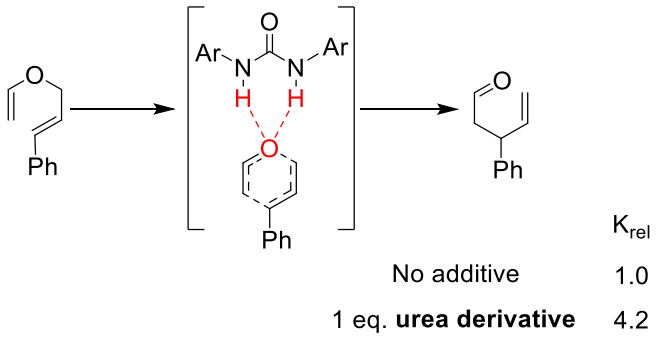

Scheme 5. The Claisen rearrangements of allyl vinyl ester by diaryl urea

The structural and mechanical characteristics of H-bonding catalysts also can play a crucial role in determining the high enantioselectivity in asymmetric reactions.[42,43] Earlier studies of asymmetric catalysis utilizing small chiral molecules revealed that H-bonding between the catalyst and electrophiles is a crucial interaction for activating the electrophile and organizing the transition state.[44,45]

In 1989, the Inoue group discovered that the diketopiperazine cyclo(L-phenylalanine-L-histidine) acted as a catalyst for the hydrocyanation of benzaldehyde to (*S*)-mandelonitriles in 97% yield with 97% ee (Scheme 6). The carbonyl oxygen of benzaldehyde is proposed to H-bond to the amide proton of the histidine residue of cyclo(L-phenylalanine-L-histidine). Then hydrogen cyanide reacts with the imidazolyl moiety of the histidine residue, forming cyanide ion which then attacks the *Si* face of the activated carbonyl group to give (*S*)-mandelonitriles, while the *Re* face is blocked by the aromatic ring of phenylalanine residue.[46]

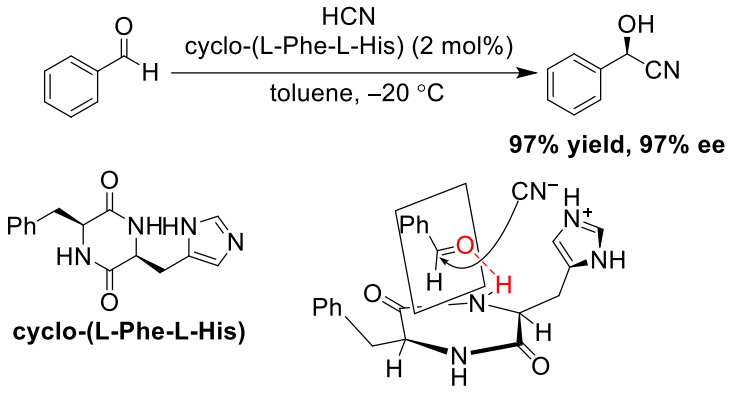

Scheme 6. Asymmetric addition of hydrogen cyanide to aldehydes

The application of chiral ureas and thioureas as H-bonding donor catalysts in asymmetric reactions has seen significant progress.[47]

In 1998, the Jacobsen group described the enantioselective hydrocyanations of imines using chiral thiourea derivatives as catalysts, to provide the corresponding aminonitriles in high yield and enantioselectivity (Scheme 7).[48]

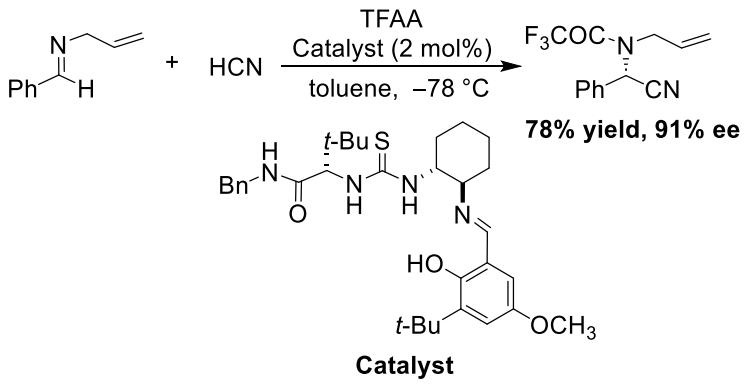

Scheme 7. Thiourea-catalyzed enantioselective hydrocyanation of imines

In 2004, the Nagasawa group developed a bis-thiourea-catalyzed asymmetric Baylis–Hillman reaction between cyclohexenone and aldehydes. It was proposed that, in the transition state, both aldehyde and enone coordinate to the thiourea group of the bis-thiourea catalyst

through H-bonds, such that the Ph group in the aldehyde is located on the opposite side from the thiourea group, which interacts with the enone. The activated enone attacks the *Re* face of the aldehyde to give the (*R*)-allylic alcohol in 88% yield with 33% ee (Scheme 8).[49]

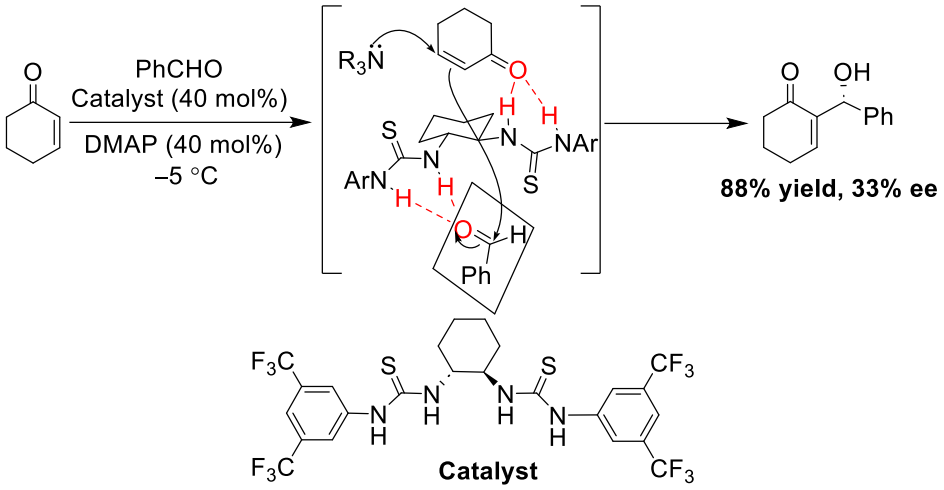

Scheme 8. Asymmetric Baylis-Hillman reaction catalyzed by bis thiourea of cyclohexanone with aldehydes

1.3.1.3 H-bonds in enzyme catalysts

Almost all chemical transformations in the human body are catalyzed. Many proteins in our body are catalysts called enzymes, that are responsible form many phenomena, ranging from creating signals that move our limbs to helping to digest our food. They are indeed a fundamental part of life.

H-bonds are essential in many enzymatic reactions, both in orienting the substrate molecules in the active site and in lowering energy barriers of reactions. Firstly, substrate binding is facilitated by the specific shape and H-bonding sites within the active site, which allows the enzyme to selectively bind its specific substrate. Once the substrate is bound, the enzyme stabilizes the reaction transition state via many interactions, including H-bonding, lowering the activation energy required for the reaction to occur and thus increasing its rate. Finally, the stabilized transition state proceeds to the final product, which is then released from the active site.[50–53]

In 2000, the Churchill group showed the amino methylation by DNA methyltransferases. As the amino nitrogen begins its nucleophilic attack on the methyl group of *S*-adenosylmethionine (AdoMet), the amine is deprotonated by a nearby aspartate side chain and forms a H-bond with the main chain carbonyl of an active site proline, which increases the electron density of the nitrogen, making it more nucleophilic (Scheme 9).[54]

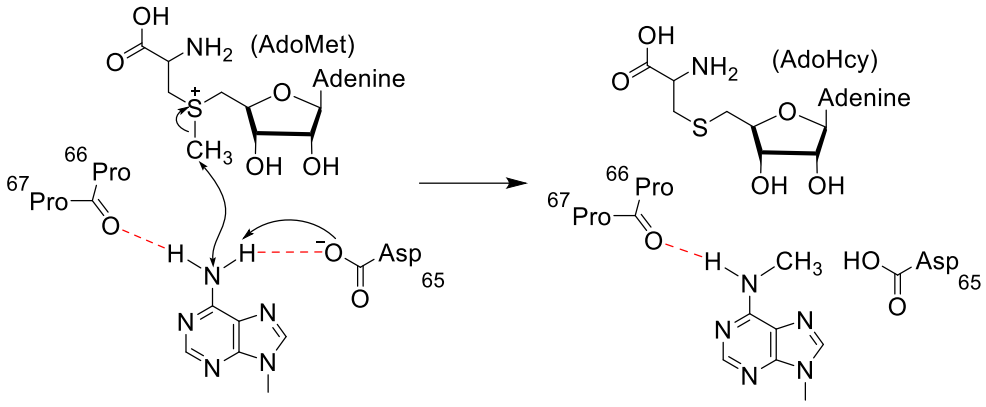

Scheme 9. Amino methylation by DNA methyltransferases

1.3.2 H-bonds in the selectivity of non-covalent synthesis

In non-covalent synthesis, the precise orientation and arrangement of H-bonding groups can determine which molecule will bind to which partner, leading to selective interactions and specific product formations. H-bonding groups are commonly found in organic molecules and biopolymers, such as amino acids, peptides, and nucleic acids, and can be used to drive non-covalent recognition events and selective reactions.

For example, in supramolecular chemistry, H-bonds are commonly used to design host-guest complexes, where a host molecule with specific H-bonding sites can selectively recognize and interact with a guest molecule with complementary H-bonding groups. The H-bonds between the host and guest provide stability to the complex and can be used to control the outcome of chemical reactions.[55–57]

Chemists are intrigued by the challenge of applying self-assembly techniques at nanoscale, and a major focus is the selectivity in non-covalent syntheses, including regio-, stereo-, chemo-, and enantioselectivity.[58]

In the 1990s, the Hamilton group showed that controlling the direction of H-bonding sites could induce simple monomeric subunits to interact with aliphatic dicarboxylic acids and self-assemble into an extended helical structure. The association of 2-aminopyrimidines and carboxylic acids is highly chemoselective for heteromeric assembly (Scheme 10).[59,60]

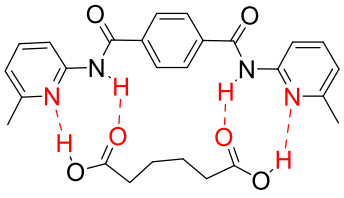

Scheme 10. The association of 2-aminopyrimidines and carboxylic acids

1.3.3 H-bonds in total synthesis

In total synthesis, H-bonds can control the conformation or stabilize the geometric structure of molecules. In addition, H-bonds can be used to design and execute synthetic transformations that are guided by the formation and manipulation of weak interactions between reactive groups. For example, H-bonds can be used to stabilize reaction intermediates and promote the formation of desired products over other competing pathways.[61,62]

In 2004, the Bouzas group developed a total synthesis of both *trans*- **E** and *cis*-Resorcylide **F** and, which was carried out from corresponding alcohol **B** and benzoic acid **A**. The starting materials underwent several transformations to obtain the dienes **C** and **D**. The final step was performed by ring-closing metathesis on dienes **C** and **D**. Diene **D** possessed an intramolecular H-bond that could control the coplanar conformation between aromatic moiety and the carboxylate plane to afford *cis*-Resorcylide **F**. Whereas diene **C**, without benefits from H-bonding, afforded *trans*-Resorcylide **E** (Scheme 11).[63]

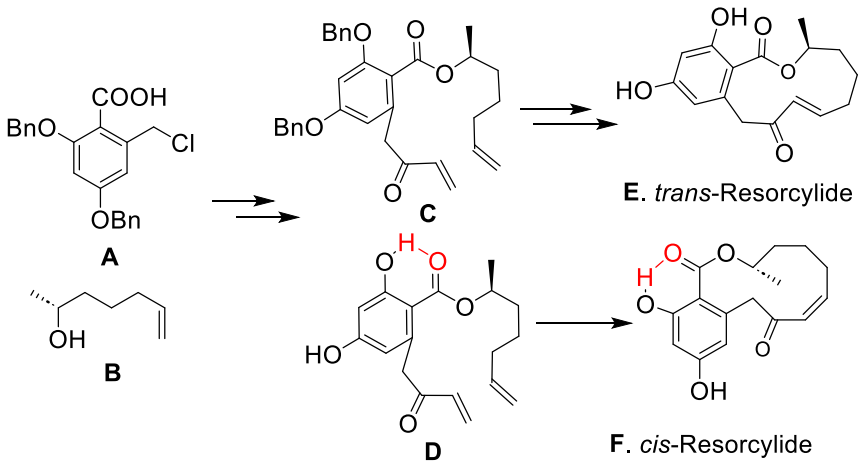

Scheme 11. Synthesis of *trans*- and *cis*-Resorcylide **E** and **F**, controlled by intramolecular H-bond in their precursors **C** and **D**

In 2011, the Rizzacasa group described the stereoselective total synthesis of (–)-Spirofungin A (**O**). The synthesis was carried out from enone **H** and alkene **I**, via a cross-metathesis to obtain ketone **J**. Selective TES group removal from **J** was followed by spiroketal formation and debenzylation to afford terminal alkynes **K** and **L** in a ratio of 3:1. The mixture of **K** and **L** was then subjected to TBS group removal and isomerization to give a mixture of spiroketals **M** and **N** (ratio 9/1). The spiroketal **M** was more stable and benefited from the intramolecular H-bond in the structure. Efficient subsequent transformations of spiroketal **M** afforded (–)-Spirofungin A (**O**) (Scheme 12).[64]

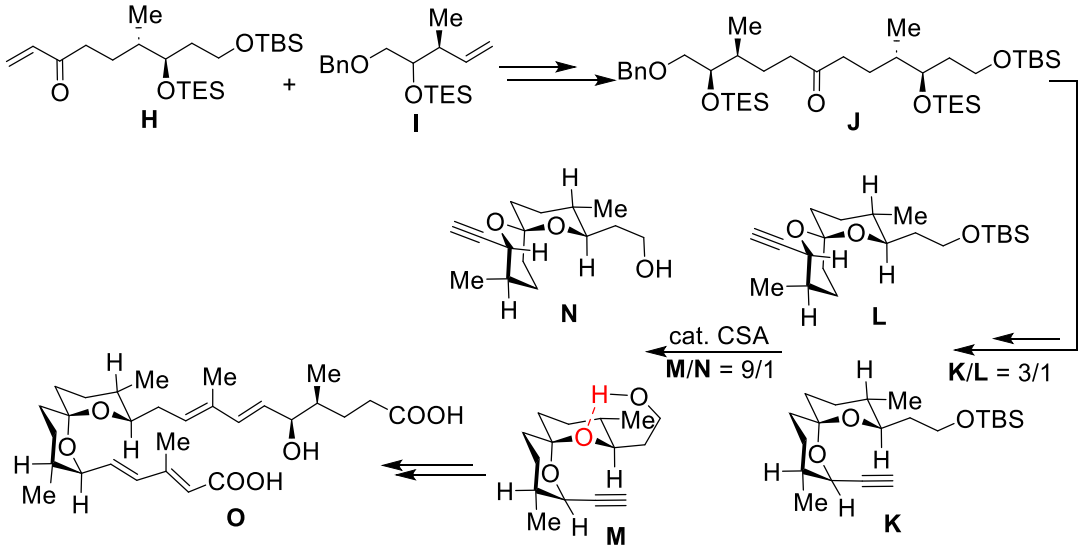

Scheme 12. The stereoselective total synthesis of the (–)-Spirofungin A (**O**)

2 Intramolecular H-bonding, a major driving force in peptide science

The fundamental roles that peptides and proteins play in biological processes make them indispensable in all forms of life.

Peptides and proteins are made up of oligomers of Nature's fundamental building blocks (amino acids) and are held together by peptide bonds. In basic terms, the difference is that peptides are made up of smaller chains of amino acids than proteins, peptides are defined as molecules that consist of between two and fifty amino acids, whereas proteins are made up of 50 or more amino acids. Hence, proteins essentially are very large peptides.

2.1 Types of intramolecular H-bonding

In peptides and proteins, three types of intramolecular H-bonds are present and simultaneously organize stability and folding. These H-bond types are 1). backbone to backbone interactions, 2). backbone to side chain interactions and 3). side chain to side chain interactions.

2.1.1 Backbone–backbone H-bonding

The most abundant type of intramolecular H-bonding in peptides and proteins is backbone–backbone H-bonding. H-bonds formed between backbone atoms (mainly N–H···O=C) of peptide are fundamental for protein secondary structures, such as helices, sheets and turns. This type of H-bonding exhibits the H-bonding donor (N–H) and the H-bonding acceptor (O=C), and they are both from the main chain (Figure 12).

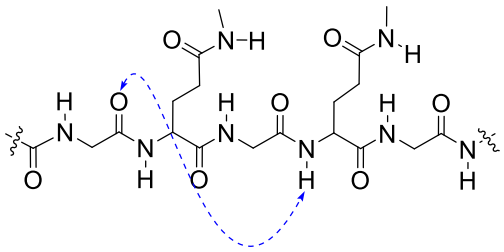

Figure 12. Schematic diagram of a backbone–backbone H-bond

2.1.2 Backbone–side chain H-bonding

Backbone–side chain H-bonds are the second most abundant in peptides and proteins. This type of H-bond includes both, side chain donor to backbone acceptor H-bonds, and backbone donor to side chain acceptor H-bonds (Figure 13).

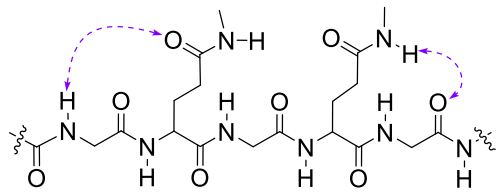

Figure 13. Schematic diagram of a backbone–side chain H-bond

2.1.3 Side chain–side chain H-bonding

In contrast with the other two H-bonding types, side chain–side chain H-bonding is one of the reasons for proteins' tertiary structure. In proteins, four factors are responsible for the tertiary structure: (1) disulfide linkages (2) H-bonding (3) electrostatic interactions (4) hydrophobic interactions. As the name suggests, the H-bonding donor and acceptor are both from the peptide side chain (Figure 14).

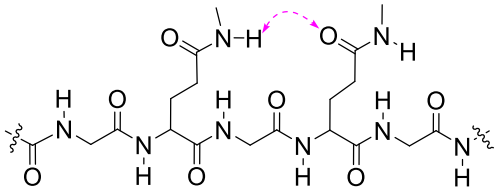

Figure 14. Schematic diagram of a side chain–side chain H-bond

2.2 Peptide foldamers

The term “foldamer” was defined by Gellman in 1996. Foldamers are artificial molecular structures, these sequence-specific oligomers of proper length are inclined to fold into well-defined secondary and tertiary conformations. In peptide foldamers, the typical secondary structures are helices, sheets, turns, and the intramolecular non-covalent interactions in these structures are principally H-bonds.[65,66]

2.2.1 Helices

Helices in peptide foldamers are attractive targets for researchers because they may mimic the helical structures found in natural peptides and proteins, allowing the study of the relationship between structure and function in biological systems and the development of new therapeutic approaches.

2.2.1.1 Homogeneous oligomers

Synthetic peptide structures may be constituted of homogeneous amino acids leading to homogeneous peptide sequences. β-peptides are the closest relatives of the natural α-peptides and are proposed to have similar interesting properties; they are among the most

thoroughly characterized at present. Compared with the structure of α-peptides, β-peptides have an additional carbon atom introduced between successive backbone peptide bonds that may induce a broader range of shapes and functions.

The Hofmann group predicted the different helices that could be adopted by a β-peptide via theoretical calculations (Figure 15).[67]

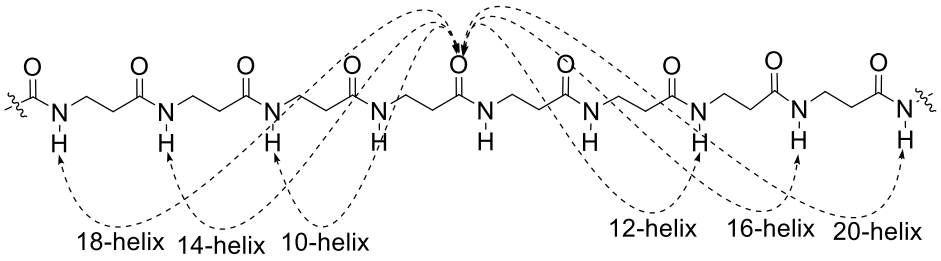

Figure 15. Possible helices that could be adopted by a β-peptide

These predictions of the β-peptides have been confirmed by experimental methods, which have exhibited many types of helices, such as 8-[68,69], 10-[70–72], 12-[73–76], 12/10 (or 10/12)-[77–80], 14-[65,81–83], 14/16-[84], 18-[85] and 18/20-[86] helices.

In 1996, the Seebach group showed a β-hexapeptide (from homologated valine, alanine and leucine) adopts 14-helix conformation in solution. Additionally, the peptide was found to be stable against the peptidase pepsin (Figure 16).[87,88]

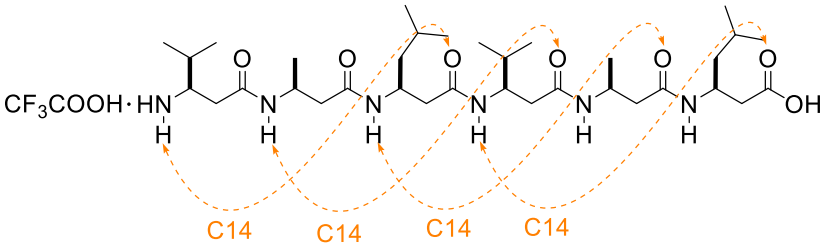

Figure 16. A β-hexapeptide adopts a 14-helix conformation

In 1996, the Gellman group presented a homogeneous β-peptide derived from *trans*-aminocyclohexanecarboxylic acid (ACHC) adopting a 14-helical conformation. Structuration of the peptide was confirmed by single-crystal structure and its conformation in solution was also studied (Figure 17).[65]

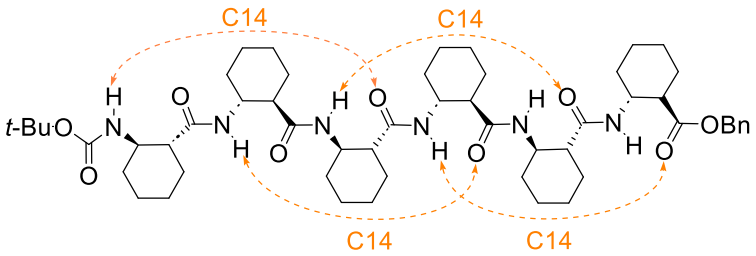

Figure 17. The hexamer of *trans*-ACHC adopts a 14-helix conformation

In 1999, the Gellman group designed a homogeneous β-peptide that was constrained by five-membered rings using *trans*-aminocyclopentanecarboxylic acid (ACPC). This β-peptide adopts a 12-helix conformation, characterized by circular dichroism and crystal structures (Figure 18).[73]

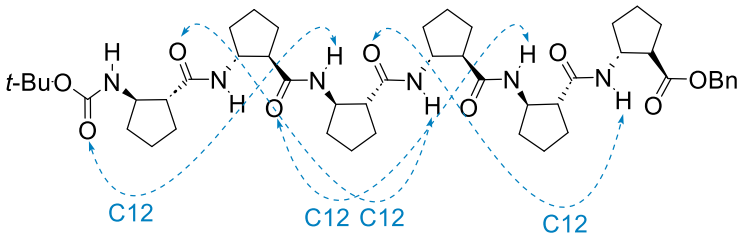

Figure 18. The hexamer of *trans*-ACPC adopts a 12-helix conformation

The homopeptides of *trans*-aminocyclobutanecarboxylic acid (ACBC) constrained by four-membered rings, if the homopeptide shorter than tetramer tend to adopt 8-helix conformation, described by the Ortuno group in 2012.[89] Whereas, if the homopeptide longer than hexamer prefer 12-helix (Figure 19), presented by the Aitken group in 2020.[90]

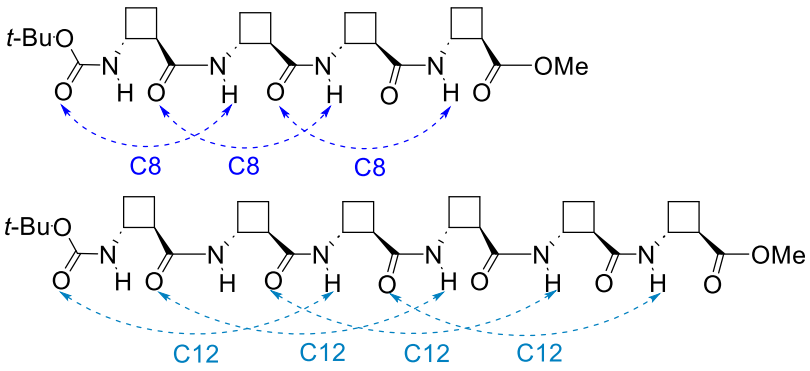

Figure 19. The tetramer of *trans*-ACBC adopts an 8-helix (top), the octamer of *trans*-ACBC adopts a 12-helix (bottom)

In 2020, the Aitken group investigated the control of the 8-helix conformation of *trans*-ACBC in longer peptides, they introduced *N*-aminoazetidine-2-carboxylic acid (AAzC) residues at *N*-terminal and *C*-terminal of *trans*-ACBC peptides, and examined these peptides adopt an 8-helical conformation in solution. The AAzC residue provided an additional 5-membered ring

(C5) N–H···N H-bond, which helped to sustain the 8-helix of *trans*-ACBC in longer peptides (Figure 20).[91]

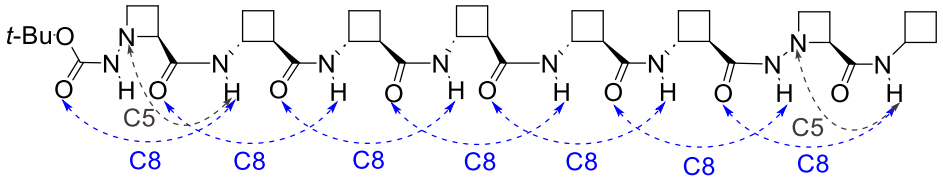

Figure 20. *trans*-ACBC derived octapeptide bearing AAzC residues adopts an 8-helix conformation

In 2012, the Hofmann group reported left-handed 12/10- and 10/12-mixed helices. The β^2-peptide was derived from a C-linked carbo-β^2-amino acid (β^2-Caa) with a carbohydrate side chain at the Cα stereocenter, and the configuration is alternating. These conformations were confirmed both by experimental in solution state and by theoretical studies (Figure 21).[78]

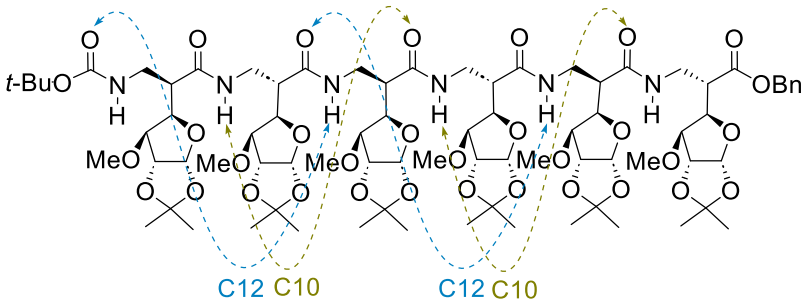

Figure 21. A C-linked carbon-β^2-peptide exhibited a 12/10-helix conformation

In 2018, the Aitken group described the conformational behavior of the *cis*-3-amino-2-oxetanecarboxylic acid (oxetin) derived homo-β-peptides. The hexamer exhibited a predominant 10-helix conformation suggested by 1D/2D NMR and infrared studies in solution. Furthermore, the 10-helix conformation was stabilized by C5 N–H···O H-bonds implicating ring oxygens and neighboring amide hydrogen atoms (Figure 22).[92]

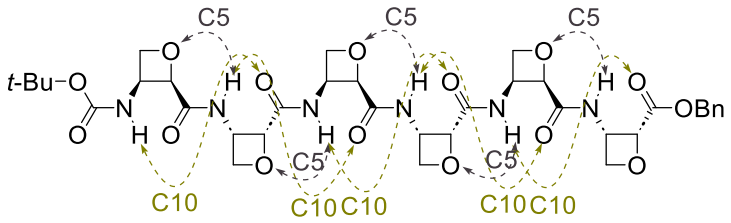

Figure 22. Oxetin derived hexapeptide adopts a 10-helix conformation

In 2015, Tanaka described the conformational behavior of (*R*,*R*)-Ac$_6$c^{35dBu} derived homopeptide, in which two chiral acetal moieties located at 3,5 positions of the cyclohexane. Peptide backbone N–H was intramolecularly H-bonded with the acetal oxygen of the same

amino acid residue in the side chain. It was proposed that the C6δ N–H···O H-bonds stabilized the helix conformation both in solution and solid states (Figure 23).[93]

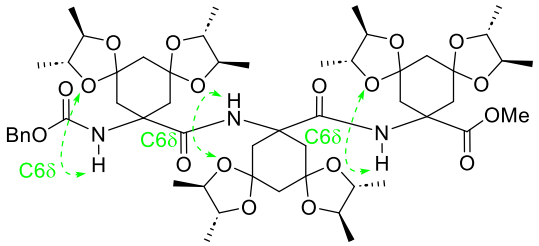

Figure 23. (*R*,*R*)-Ac$_6$c^{35dBu} derived homopeptide adopts a helical conformation stabilized by consecutive C6δ H-bonds

Homogeneous γ-peptide foldamers have also emerged and reveal attractive properties. They have shown their capability to adopt various stable conformations. Compared with the structure of α-peptides, γ-peptides have two additional carbon atoms introduced between consecutive peptide bonds.

In 2003, Hofmann described a total of eight different helices that a γ-peptide could adopt by theoretical calculations, (Figure 24).[94]

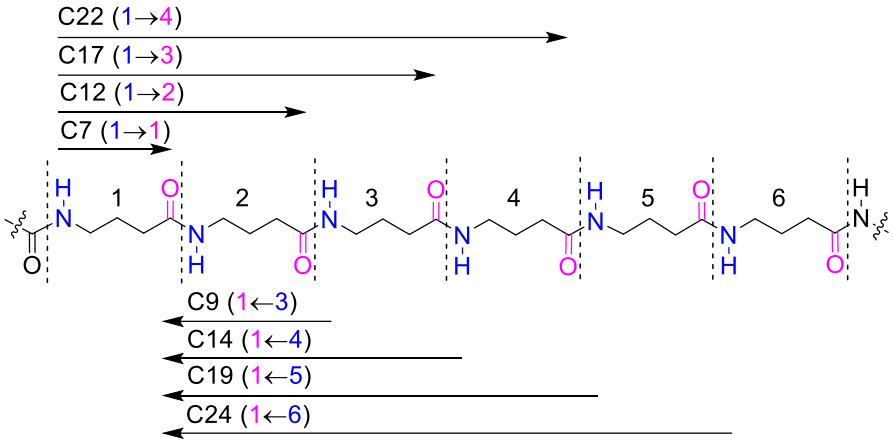

Figure 24. Different helices possibly adopted by a γ-peptide

Nevertheless, to date, only 7-[95], 9-[96–98] and 14-[99–102] helical structures have been experimentally observed for γ-peptides.

In 2013, the Maillard group developed a thiazole based γ-peptide that adopts a right-handed C9 helical conformation. The thiazole ring played a key role in providing a high constraint in the backbone. The conformation was confirmed both in solid and solution states (Figure 25).[98]

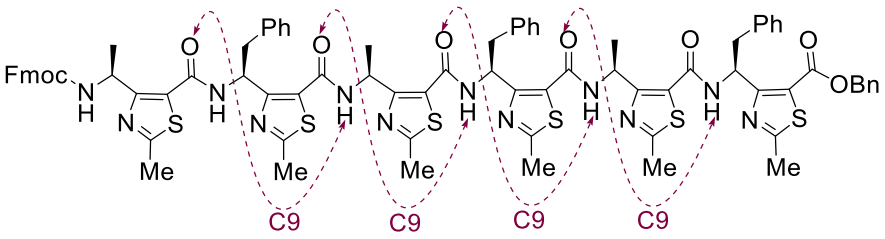

Figure 25. A thiazole-based γ-peptide that adopts a 9-helix conformation

In 2017, the Aitken group described the conformational behavior of *cis*-^{2,3}CB-GABA derived homopeptides. In dilute solutions, these peptides showed rare intra-residue C7 intramolecular H-bonds, supported by theoretical calculations (Figure 26).[95]

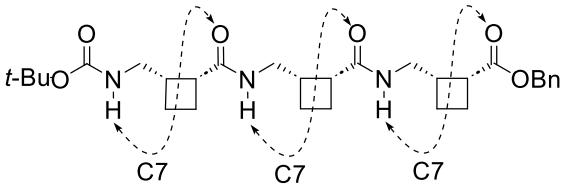

Figure 26. *cis*-^{2,3}CB-GABA derived tripeptide showed rare C7 intra-residue H-bonds

2.2.1.2 Heterogeneous oligomers

Peptides with a heterogeneous backbone composed of different classes of amino acids (α, β, γ) have been investigated in a systematic way. The introduction of different residues in a homogeneous backbone may induce further options for helix types. Common hybrid peptide sequences are composed of repeated units. In a hybrid α/β-peptide, for example, the sequence could be αβαβαβαβ, ααβααβ, ααββααββ, or ββαββα to name just a few.

The Hofmann group described the possible helices that could be adopted by alternating α/β-[103], α/γ-[104], and β/γ-[104] hybrid peptides.

Experimental observations of hybrid peptides have revealed various helical patterns. α/β-Peptides have shown 9/11-[105–107], 10/11-[108], 11-[109,110], 11/12-[108], 13-[105], 14/13-[111], 14/15-[109,110] and 18-[109] helical folding patterns. α/γ-Peptides have shown 12-[112–114], 12/10-[115–117] and 15/17-[114] helices. β/γ-Peptides have shown 13-[118] and 11/13-[115] helical conformations. Moreover, some of those scaffolds have contributed to biological applications, such as peptidomimetics inhibitors of protein–protein interactions.[119]

In 2005, the Kunwar group reported the adoption of 9/11 helical structures by α/β-hybrid peptides, which were characterized by experimental studies in solution and theoretical

methods. The peptides were derived from C-linked carbo-β^3-amino acid (β^3-Caa) and L-alanine in alternation (Figure 27).[106]

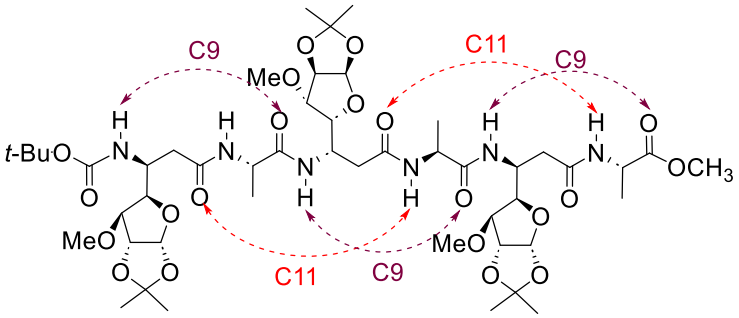

Figure 27. A α/γ-hybrid peptide that adopts a 9/11-helix conformation

In 2014, the Gellman group described α/γ-hybrid peptides derived from the cyclic constrained γ-amino acid, (1*R*,2*R*,3*S*)-2-(1-aminopropyl)cyclohexane carboxylic acid (APCH) and D-alanine in alternation. The 12/10-helical secondary conformation was observed in both solution and crystalline states of these peptide derivatives (Figure 28).[116]

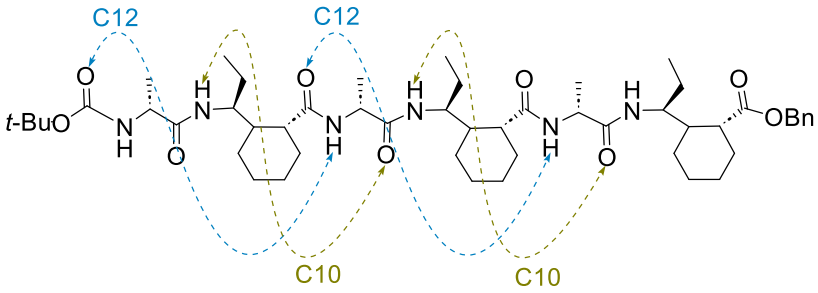

Figure 28. A α/γ-hybrid peptide that adopts a 12/10-helix conformation

In 2016, the Aitken group described the 13-helix folding pattern adopted by a β/γ-hybrid peptide. The hybrid peptide was constituted of *trans*-2-aminocyclobutanecarboxylic acid (ACBC) and singly substituted γ^4-amino acid in alternation (Figure 29).[120]

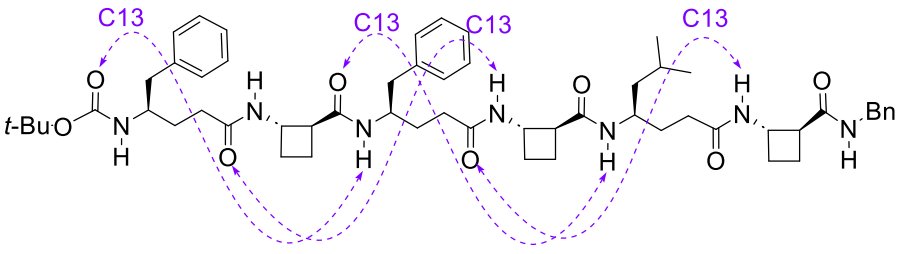

Figure 29. A β/γ-hybrid peptide that adopts a 13-helix folding pattern

2.2.1.3 Peptidomimetics

The most fundamental interactions in living beings are the so-called protein–protein interactions (PPIs). Therefore, peptidic foldamers bear the promise to be an important tool for the inhibition of PPIs, as they are structurally most akin to the original proteins, particularly α-helix.[121–123]

In 2015, the Fairlie group developed a stapled α/β-peptide in a helical conformation[124] that structurally and functionally mimicked the parent stapled α-peptide in its ability to enter specific types of cells while showing increased protease stability (Figure 30).[125]

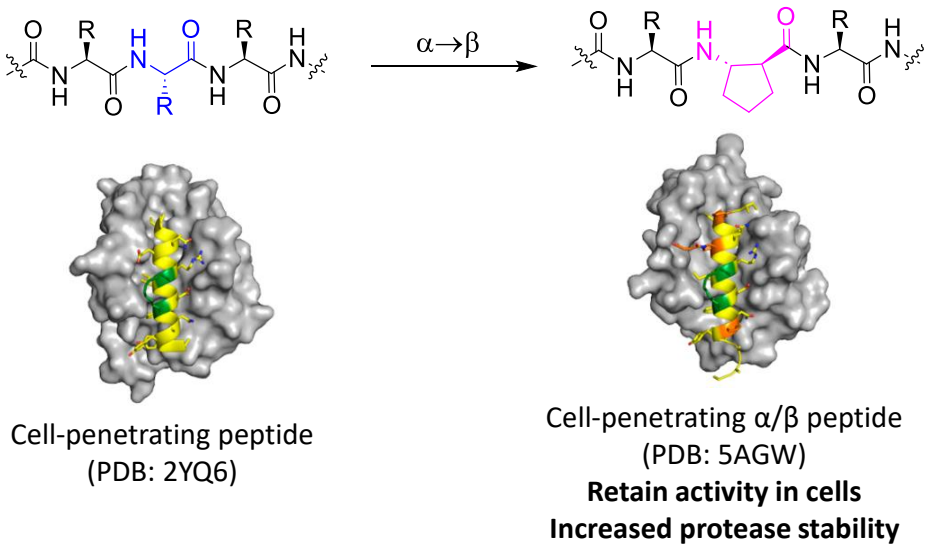

Figure 30. A stapled α/β-peptide foldamer that structurally and functionally mimics the parent stapled α-peptide: the protein images were reproduced from the literature[125]

In 2016, the Aitken and Wilson groups designed an α/β/γ-hybrid peptide using the *trans*-ACBC that structurally mimicked a native α-helix. Suitably functionalized α/β/γ-peptides assumed an α-helix mimicking 12,13-helix conformation in solution, exhibited enhanced proteolytic stability compared to the wild-type α-peptide parent sequence from which they are derived, and acted as selective inhibitors of the p53/hDM2 interaction (Figure 31).[126]

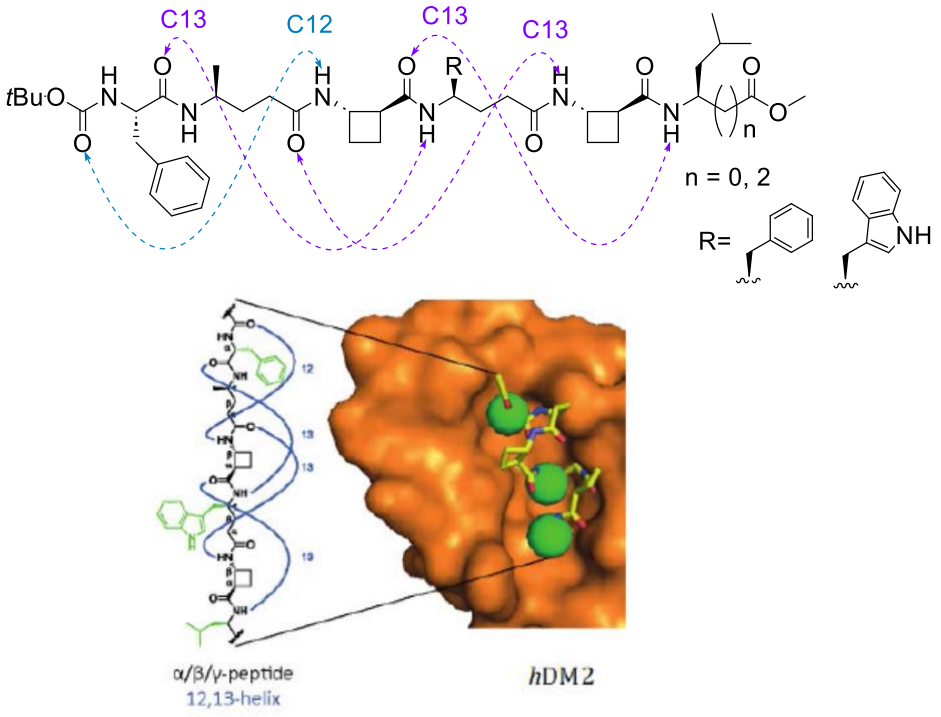

Figure 31. H-bonding pattern (left) of an α/β/γ-hybrid peptide that acts as a selective inhibitor of the p53/hDM2 interaction, the image (bottom) was reproduced from the literature[126]

2.2.2 Sheets

Mimicking the chemical and biological functions found in Nature has been a major objective behind the growth and development of foldamer research. Sheets, as a common protein secondary structure, have inspired scientists to design sheet-like structures.

β-Sheets, also known as β-pleated sheets, are a prevalent secondary structure in proteins and play a significant role in the structure and function of many of them. They are made up of β-strands linked by two or three backbone H-bonds (N–H···O=C), forming a twisted sheet-like structure. Since the 1980s, researchers have focused on designing artificial β-sheet-like foldamers to gain a deeper understanding of the factors that influence β-sheet structure and stability. A particular goal of the research is to develop new treatments for Alzheimer's disease and other diseases.[127]

In 1994, the Feigel group reported an artificial antiparallel β-sheet structure. The biphenyl moieties provided the rigid spacers in the backbone of those cyclic peptides. The β-sheet solution conformation was proved experimentally and also by theoretical calculations (Figure 32).[128]

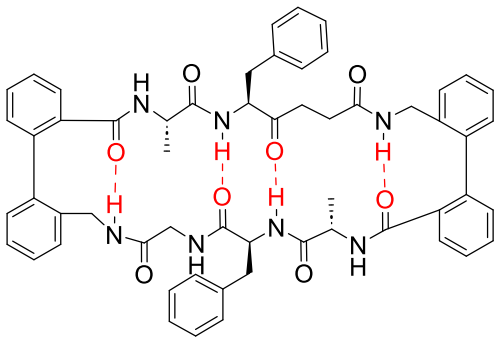

Figure 32. An artificial antiparallel β-sheet structure of a cyclic peptide

In 1988, the Kemp group developed artificial parallel β-sheets, by connecting two tetrapeptides to a 2,8-diaminoepindolidione template. In solution, these tetrapeptides adopted β-sheet structures (Figure 33).[129]

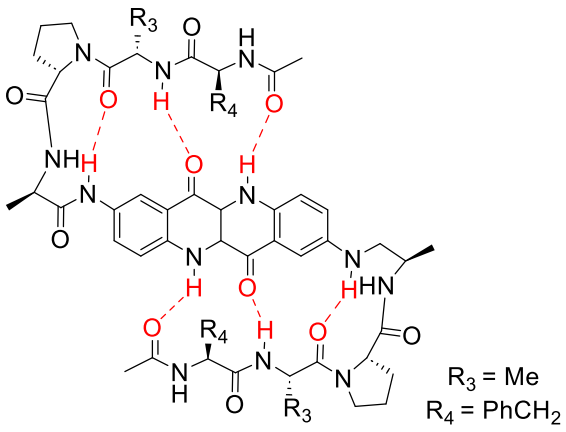

Figure 33. An artificial parallel β-sheet was promoted by a 2,8-diaminoepindolidione template

In 2007, the Linton group showed a β-sheet conformation in cystine linked peptides. The conformation was demonstrated experimentally in solution state (Figure 34).[130]

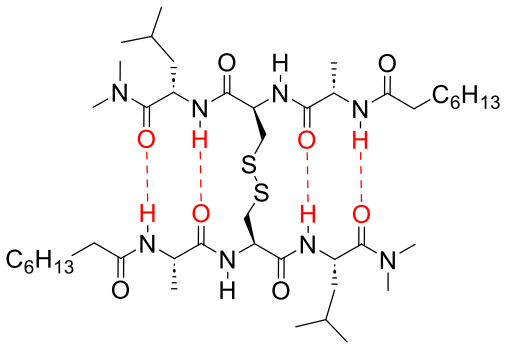

Figure 34. β-sheet H-bonding patterns in cystine linked peptide

2.2.3 Turns

In addition to their biological importance, turn structures are also attractive targets for synthetic chemistry because they can be designed and synthesized in a controlled and predictable manner. This allows researchers to precisely tailor the properties of the peptide to suit researchers' needs, it is essential for many applications in biochemistry, pharmaceuticals, and other fields.[131–134]

In 2007, the Sanjayan group described a hybrid foldamer derived from regularly repeating α-aminoisobutyric acid (Aib), proline (Pro) and 3-amino-4,6-dimethoxy benzoic acid (Adb) residues as subunits (Aib-Pro-Adb), that display a β-turn conformation in solution and solid states (Figure 35).[135]

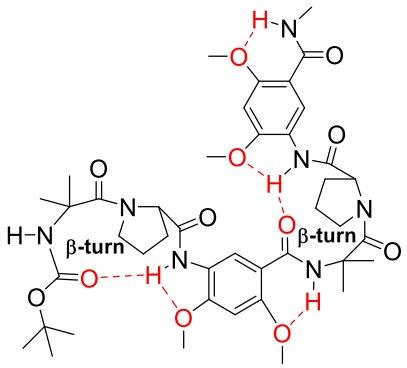

Figure 35. Aib-Pro-Adb derived hybrid peptide adopts a β-turn conformation

In 2001, the Seebach group designed a linear substituted β-tetrapeptide composed of Thr, Lys, Trp and Phe residues. It was proved that this peptide folds into a β-turn conformation in solution (Figure 36).[136]

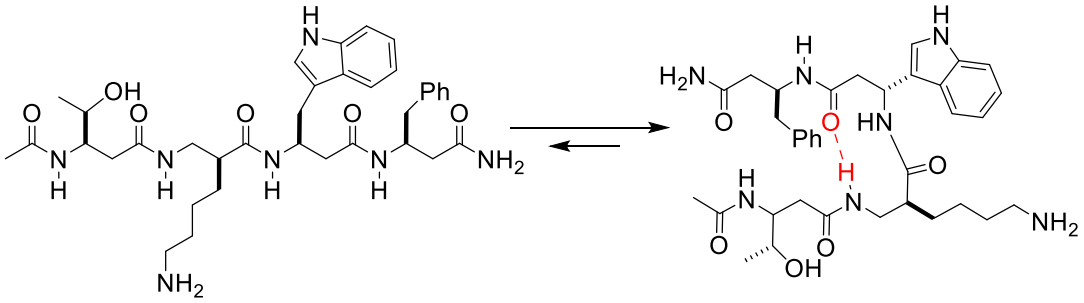

Figure 36. A linear β-tetrapeptide folds into a β-turn conformation

2.2.4 The C5 interaction: 2.0_5-helix—extended conformation

As introduced in section 1.2.2.2, the C5 interaction accompanies β-sheets in native proteins. In synthetic C^{α}-tetrasubstituted amino acid derivatives, the adoption of a fully extended 2.0_5-helix conformation with successive C5 H-bonds relies essentially on steric constraints. Toniolo suggested that C^{α}-tetrasubstituted amino acids with at least two carbon atoms in each side chain, their homopeptides are more inclined to adopt a 2.0_5-helix conformation, for example, Deg, Dp_ng, and Db_zg (Figure 37).[137,138]

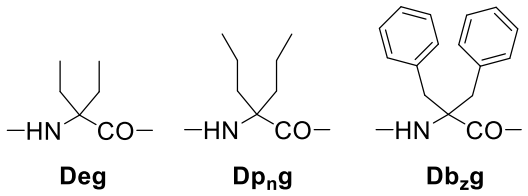

Figure 37. Some C^{α}-tetrasubstituted amino acids prefer the 2.0_5-helix conformation

In 1988, the Toniolo group described the conformation preference of α,α-diethylglycine (Deg) derived homopeptides. Deg residue is sterically restricted and forces its homopeptides to adopt fully extended C5 H-bonding conformation supported by theoretical calculations, and confirmed experimentally both in solution and solid states (Figure 38).[139,140]

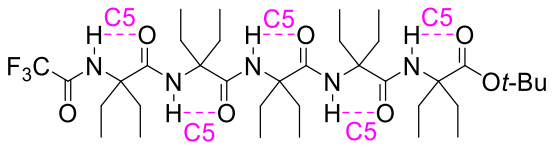

Tfa-(Deg)$_5$-O*t*-Bu

Figure 38. The H-bonding pattern of Tfa-$(Deg)_5$-O*t*-Bu

In 1994, Toniolo described α-methylated D-Leucine derived homopeptide adopts a fully extended 2.0_5-helix conformation. This conformation was found in the crystal structure (Figure 39).[141]

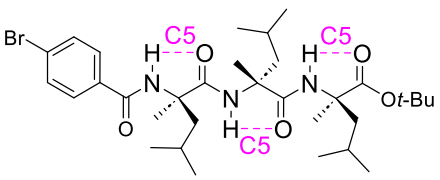

***p*-BrBz-[D-(Me) Leu]$_3$-O*t*-Bu**

Figure 39. The H-bonding pattern of *p*-BrBz-[D-(Me) Leu]$_3$-O*t*-Bu

Since the C5 H-bond is weak, studies have been particularly useful in gas phase using laser spectroscopy methods to characterize the interaction in model compounds.[142–149]

In 2019, the Das group observed a C5 H-bond in an *N*-capped hybrid dipeptide Cbz-Gly-Pro. The weak intra-residue H-bond was confirmed via infrared spectroscopy studies in gas phase and by computational methods (Figure 40).[146]

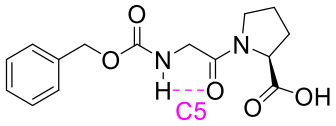

Figure 40. The weak intra-residue C5 H-bond was observed in a Cbz-Gly-Pro dipeptide

Moreover, in many cases of hybrid peptides, C5 interactions have been stabilized by additional H-bonds in the structure.[142,150,151]

In 2010, the Zwier group investigated the conformational preference of constrained α/β-peptides. The peptide Ac-L-Phe-ACPC-NHMe exhibited a C5-C8 H-bonding conformation, suggested by IR spectroscopy studies in gas phase and by theoretical calculations (Figure 41).[152]

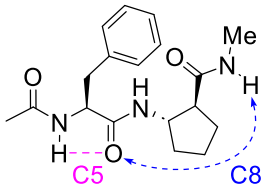

Figure 41. The Ac-L-Phe-ACPC-NHMe peptide adopts a C5-C8 H-bonding conformation

In 2020, the Aitken and Mons groups described the conformational behavior of 3-aminothietane-3-carboxylic acid (Attc) derivatives. The sulfur atom from the Attc residue formed a C6γ H-bond that stabilized a weak intra-residue C5 H-bond in the peptide backbone. The consecutive C5-C6γ H-bonding systems exhibited extended conformation suggested by infrared spectroscopy in gas and solution phases and NMR spectroscopy studies in solution (Figure 42).[153]

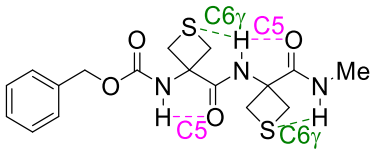

Cbz-(Attc)$_2$-NHMe

Figure 42. The Cbz-(Attc)$_2$-NHMe adopts a C5-C6γ extended conformation

In 2021, the Aitken and Mons groups compared the conformational behaviors of Attc with three other cyclic α,α-disubstituted α-amino acids: 3-amino-1-methylazetidine-3-carboxylic acid [Aatc(Me)], 3-aminooxetane-3-carboxylic acid (Aotc) and 1-aminocyclobutanecarboxylic acid (Ac4c). The aim was to evaluate the ability of the C6γ N–H···X (S, N and O) backbone–side chain interaction to stabilize the C5 H-bond in the peptide backbone, and compare this with the case which does not have this interaction (Ac4c). Infrared in gas and solution phases results showed that Aatc(Me) and Attc derivatives adopt a predominant C5-C6γ extended conformation, supported by theoretical calculations. Aotc derivative adopted a C5-C6γ extended conformation in gas phase, while this extended conformation was challenged by other conformations (C7 and free) in solution (Figure 43).[154]

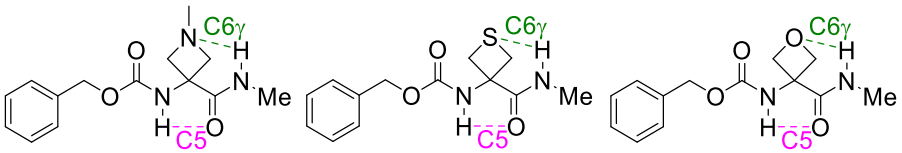

Figure 43. The C5 H-bond stabilized by a C6γ H-bond in three cyclic α-amino acids

In the case of Ac4c derivative, due to the absence of C6γ H-bond from the side chain, only adopts a minor C5 H-bonding conformation, suggested by infrared in gas phase. In the solution state, no evidence for a C5 H-bond conformation but replaced by free and C7 H-bond conformations (Figure 44).

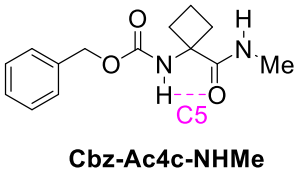

Figure 44. The Cbz-Ac4c-NHMe adopts a minor C5 H-bond conformation in gas phase

3 Project of the thesis

Overall, the section of general introduction described the contributions of H-bond in the universe, and this non-covalent interaction plays a crucial role in stabilizing the conformation of peptides. Studying the role of H-bonds in peptide foldamers enables a deeper understanding of how changes in the amino acid residues or modifications to the peptide backbone affect the stability and conformation of the molecule. This knowledge may guide the design of new peptide-based drugs, catalysts, or materials with improved stability,

specificity, and functionality. Therefore, in this thesis, we are going to explore different types of H-bonding for the stabilization of peptide conformations.

Among the peptide foldamers, the most common type of H-bond is N–H···O=C formed in the peptide backbone, which is between the carbonyl oxygen and amide proton. This H-bond is the predominant force that drives peptides to fold into well-defined secondary structures. Additionally, the 12/10-helix conformation adopted by γ/α-hybrid peptides is still limited. Therefore, in the first chapter, we aim to study the conformational behaviors of a series of γ/α-hybrid peptides controlled by the common N–H···O=C backbone–backbone H-bonds. The candidate γ-amino acid is (*R*,*R*)-*cis*-^{3,4}CB-GABA, which bears a four-membered ring, while alanine is selected as α-amino acid component. The peptide sequence is an alternation of (*R*,*R*)-*cis*-^{3,4}CB-GABA and alanine, arranged in γαγαγα order (Figure 45).

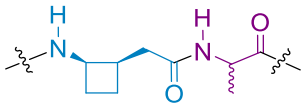

Figure 45. The sequence of γ/α-hybrid peptide

In the second chapter, we are going to expand our understanding to study a short-range, intra-residue C5 H-bond and an inter-residue N–H···N H-bond formed from side chain, implicating an azetidine moiety. Compared with the conventional N–H···O=C H-bond found in the peptide backbone, these H-bonds are considered weak and unusual interactions. We introduce *N*-methyl azetidine residue to the α-position of α-amino acid derivative and aim to evaluate the ability of the backbone–side chain C6γ H-bond for stabilizing the C5 H-bond in peptide backbone (Figure 46).

Figure 46. The chemical structure of Aatc(Me) derivatives

In the third chapter, we will continue to study the stabilization of the intra-residue C5 H-bond using the oxidized derivatives of Aatc(Me) (3-amino-1-methylazetidine-3-carboxylic acid) and Attc (3-amino-thietane-3-carboxylic acid). The generated oxygen atom has a higher electronegativity than nitrogen and sulfur, which may exert a significant influence and form an inter-residue C7δ H-bond that can stabilize the C5 H-bond in the peptide backbone (Figure 47).

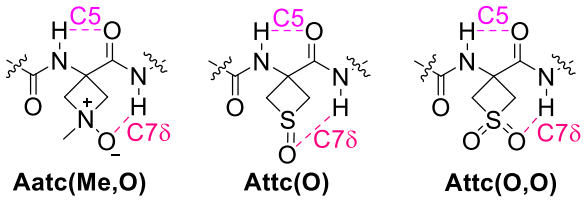

Figure 47. The chemical structures of Aatc(Me,O), Attc(O) and Attc(O,O) derivatives

In the fourth chapter, the conformations of two *trans*-ACBC (2-aminocyclobutane-1-carboxylic acid) derivatives that are capped with *N*-benzoxazolinone moiety will be investigated. The cyclic carbamate moiety, unlike common protecting groups such as Cbz and Boc, may affect the C8 H-bonding local feature of the *trans*-ACBC derivative. Hence, we aim to evaluate the influence of this cyclic carbamate moiety on *trans*-ACBC and whether the C8 H-bonding feature is retained (Figure 48).

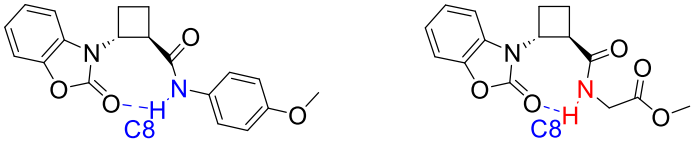

Figure 48. The chemical structures of two *trans*-ACBC derivatives

PART II

RESULTS AND DISCUSSION

Chapter 1. Synthesis and conformational studies of γ/α-hybrid peptides

Chapter 1. Synthesis and conformational studies of γ/α-hybrid peptides

1.1 Introduction

1.1.1 Presentation of γ-amino acid

GABA (γ-aminobutyric acid) is a completely unrestricted γ-amino acid and plays an essential role in the mammalian central nervous system and serves as a major neurotransmitter[155]. The presence of substituents in different locations gives rise to sub-families of compounds; some are shown below, γ^3-amino acid (γ^3-GABA), $\gamma^{2,3}$-amino acid ($\gamma^{2,3}$-GABA), $\gamma^{3,4}$- amino acid ($\gamma^{3,4}$-GABA) (Figure 49).

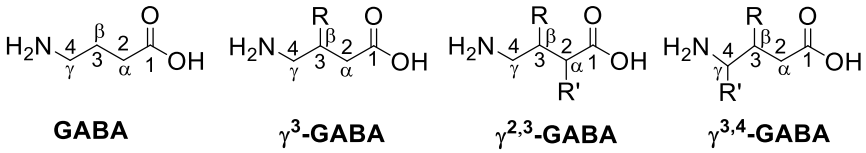

Figure 49. Some examples of GABA derivatives

Owing to the high flexibility of GABA, it can exist in numerous low-energy conformations. Analogs of GABA have been employed to explore the binding mode of these molecules and their structure-activity relationship. In particular, conformationally restricted analogs that contain a rigid backbone can mimic specific conformations of GABA and help to elucidate the molecular mechanisms of GABA receptor function. Therefore, to discover and develop selective ligands for GABA receptors, cyclic analogs of GABA have been of particular interest (Figure 50).[156,157]

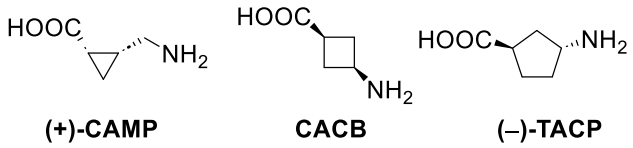

Figure 50. Some examples of restricted cyclic GABA derivatives

In the host group, the synthesis of GABA analogs featuring a cyclobutane ring constraint has been described in recent years, ^{3,4}CB-GABA and ^{2,3}CB-GABA (Figure 51).[158,159]

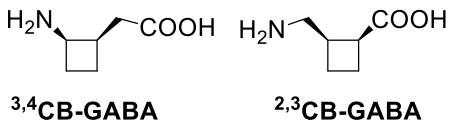

Figure 51. The chemical structures of ^{3,4}CB-GABA and ^{2,3}CB-GABA

In 2017, the host group described the conformational behavior of *cis*-^{2,3}CB-GABA derived homopeptides (di-, tri- and tetramers). In dilute solutions, FT-IR and NMR spectroscopic results of these peptides showed rare intra-residue C7 H-bonds, supported by theoretical calculations. In more concentrated solutions, these peptides displayed a supramolecular assembly leading to sheet-like arrays that allow gel formation (Figure 52).[95]

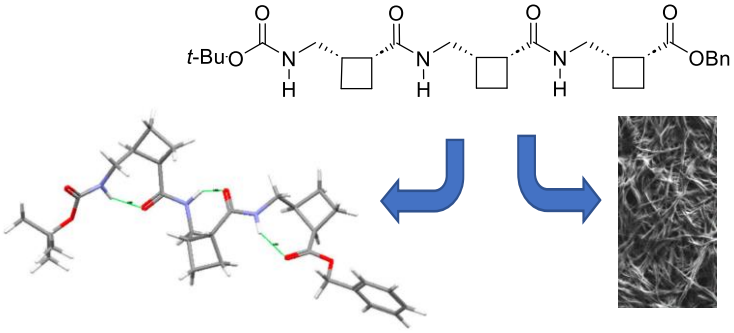

Figure 52. *cis*-^{2,3}CB-GABA derived homopeptides showed rare C7 intra-residue H-bonds, two images (bottom) were reproduced from the literature[95]

1.1.2 Hofmann's theoretical calculations

In 2006, the Hofmann group investigated the helix formation in α/γ- and β/γ-hybrid peptides by theoretical calculations.[160] In this work, they calculated the backbone torsion angles of the most stable helices of alternating α/γ-hybrid peptides. Based on ab initio MO theory methods, Hofmann's left-handed 12/10-helix conformer I displayed backbone torsion angles for each peptide residue is shown in Table 1 (top), and the structure of conformer I is shown in Figure 53 (top). In this model, the torsion angles for α-amino acid residue are around +68° for ϕ and around –148° for ψ. The torsion angels for a γ-amino acid residue: around –64° for ϕ, around –32° for θ, around –48° for ζ and around +132° for ψ. The combinations of these torsion angels in each residue might privilege a 12/10-helix conformation. In this work, they also calculated the backbone torsion angles for a left-handed 12-helix conformer, and its conformer I displayed dihedrals for each residue is shown in Table 1 (bottom), and the structure of conformer I is shown in Figure 53 (middle).

	Peptide residue	ϕ (°)	θ (°)	ζ (°)	ψ (°)
Hofmann's left-handed 12/10-helix	γ	–64 ± 1	–32 ± 1	–48 ± 1	+132 ± 5
	α	+68 ± 2			–148 ± 1
Hofmann's left-handed 12-helix	γ	+122 ± 1	–52 ± 1	–63 ± 1	+132 ± 5
	α	+70 ± 2			+29 ± 1

Table 1. Backbone torsion angles for Hofmann's 12/10-helix conformer I (top) and 12-helix conformer I (bottom)

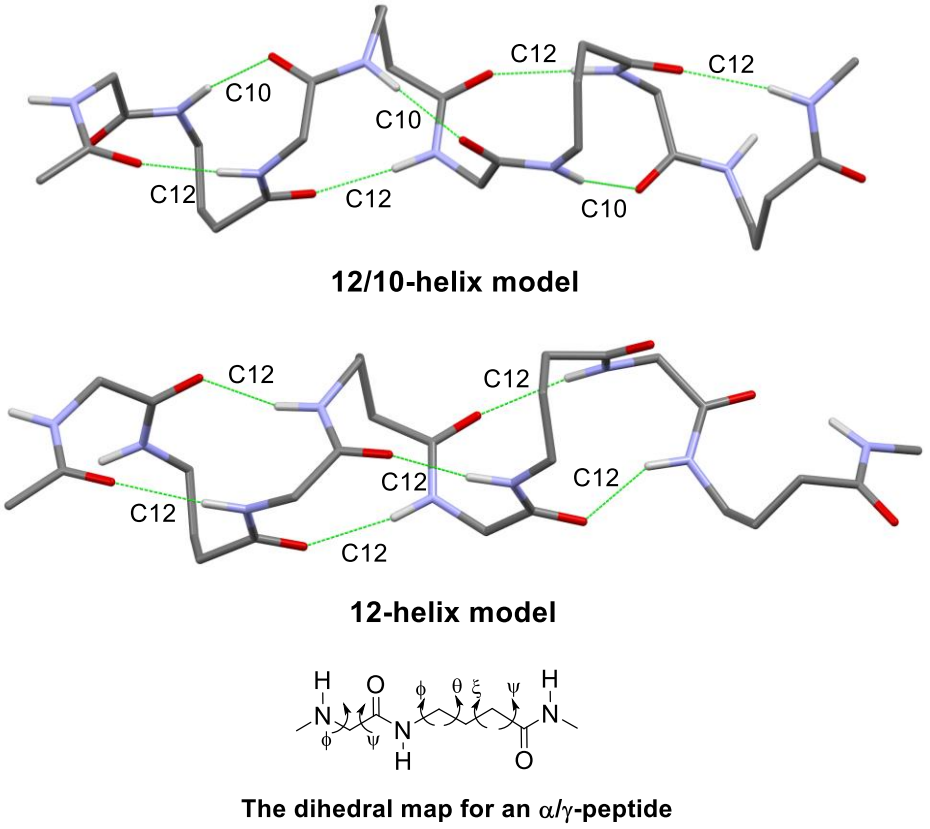

Figure 53. A α/γ-peptide for 12/10-helix conformer I (top), image was reproduced from the literature[160], for 12-helix conformer I (middle), image was reproduced from the literature[160], and the schematic structure of α/γ-peptide with dihedrals (bottom)

1.1.3 The 12/10-helix in α/γ-hybrid peptides

Conventional helical structures in peptide foldamers arise from a single type of N–H···O=C H-bond that have a consistent directionality, where the *N*-terminal side C=O bonds to the *C*-terminal side N–H. However, a number of helical structures of peptide foldamers feature two types of H-bonding directionality alternates along the backbone, resulting in helices with

alternating H-bond directions. In this case, the mixed helices give rise to relatively small macrodipoles, may be more stable secondary structures in hybrid peptides.

In 2006, the Sharma group described α/γ-hybrid peptides containing residues with bulky side chain, a C-linked carbo-γ-amino acid. These peptides adopt a 12/10-helix conformation, a secondary structure in which neighboring amide groups form H-bonds with opposite orientations. The conformation was suggested by NMR studies in solution (Figure 54).[115]

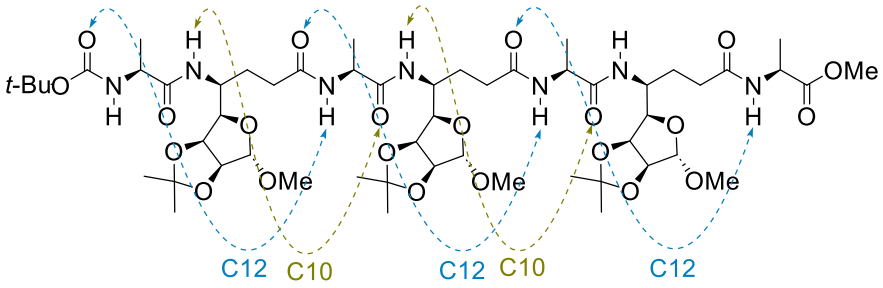

Figure 54. A γ-Caa derived α/γ-hybrid peptide that adopts a 12/10-helix conformation

In 2008, the Balaram group reported a tetrapeptide (Boc-Leu-Gpn-Leu-Aib-OMe) that showed a 12/10-helix conformation in crystal structure, the C12 H-bond was observed between the carbonyl oxygen of Boc motif and the NH(3) of the Leu residue, the C10 H-bond was observed between the NH(2) of Gpn residue and the carbonyl oxygen of Leu residue (Figure 55).[117]

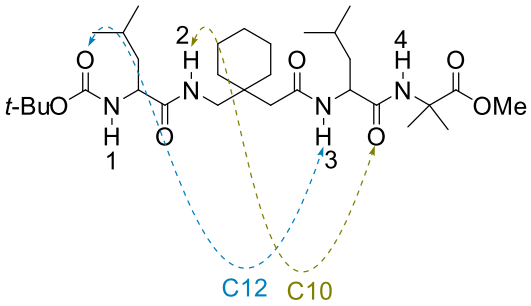

Figure 55. A tetrapeptide Boc-Leu-Gpn-Leu-Aib-OMe that adopts a 12/10-helix conformation

In 2014, the Gellman group reported an α/γ-hybrid peptide, in which the γ-peptide residue was derived from constraint (1*R*,2*R*,3*S*)-2-(1-aminopropyl)cyclohexane carboxylic acid (APCH) moiety, and the α-peptide residue was an unconstraint alanine moiety. The crystal structure of α/γ-tetramer exhibited two intramolecular H-bonds: one C=O(i)···H−N(i+3), 12-membered ring H-bond between the Boc carbonyl oxygen and the NH(3) of the alanine residue, another one C=O(i)···H−N(i−1), 10-membered ring H-bond between the carbonyl oxygen of alanine residue and the NH(2) of APCH residue. This α/γ-hybrid peptide adopts a 12/10-helix conformation, which features alternating H-bond directionality, in both solution and solid states (Figure 56).[116]

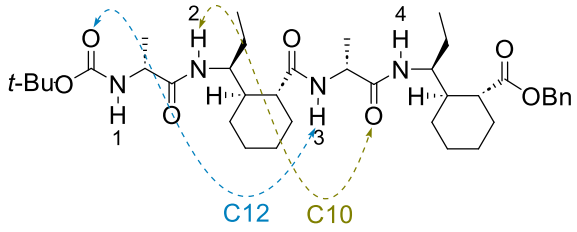

Figure 56. An APCH derived α/γ-hybrid peptide that adopts a 12/10-helix conformation

1.1.4 Aim of this chapter

On the basis of these observations, the helical structures of peptide foldamers with alternating H-bonding directions along the helical axis are interesting, but the cases of α/γ-peptides adopt 12/10-helix conformation are still limited, and it is worthy to continue to do the exploration.

In a previous study from the host group,[161] X-ray crystallographic analyses of an absolute configuration of Boc-*cis*-^{3,4}CB-GABA-OBn (Figure 57, top) revealed a torsion angle θ of +22°, but the same configuration of Boc-*cis*-^{3,4}CB-GABA-OX[158] (Figure 57, bottom) showed a torsion angel θ in opposite sign of –28°, which both quite close to Hofmann's theoretical value in a 12/10-helix. Moreover, this compound is a rotationally restricted cyclic amino acid that can provide sufficient backbone rigidity to enhance overall conformational stability. As such, it could be an excellent candidate for use as the γ-amino acid component in the design of γ/α-hybrid peptides that fold into 12/10-helix. The unconstraint alanine was selected as the α-amino acid component, and to account for the dihedral cooperations for the helical formation, both enantiomers of alanine were prepared, resulting in *R,R,R* and *R,R,S* peptides.

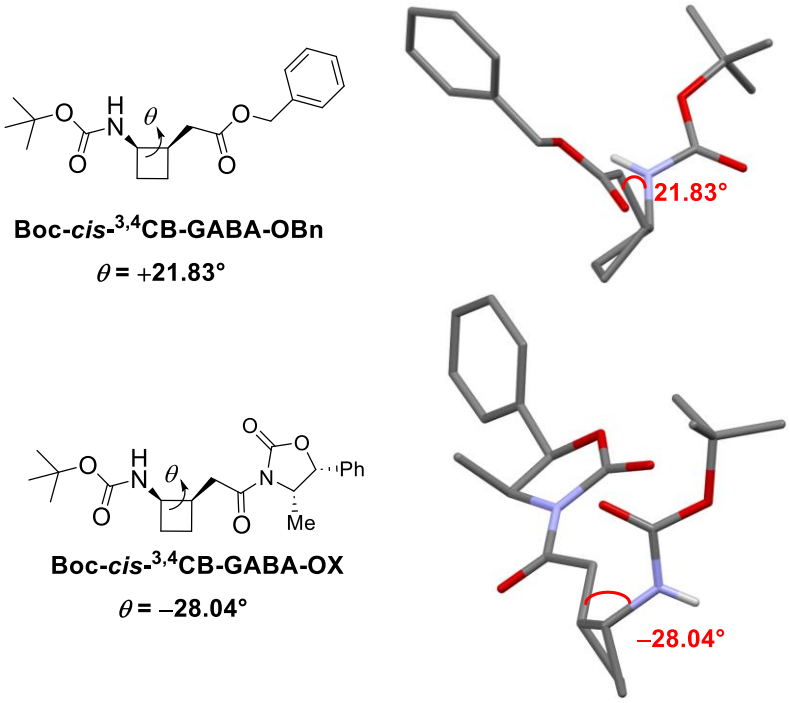

Figure 57. Crystal structures of the absolute configuration of Boc-*cis*-^{3,4}CB-GABA-OBn (top) [161] and Boc-*cis*-^{3,4}CB-GABA-OX (bottom)[158], images were reproduced from the literature

In this chapter, we proposed to explore the conformational behavior of γ/α-peptides composed alternately of (*R*,*R*)-*cis*-^{3,4}CB-GABA and either (*R*) or (*S*)-alanine (Figure 58).

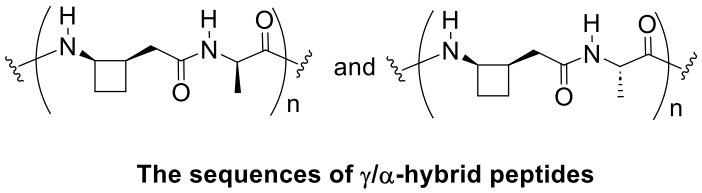

Figure 58. γ/α-peptides composed alternately of (*R*,*R*)-*cis*-^{3,4}CB-GABA and either (*R*) or (*S*)-alanine

1.2 Synthesis of γ/α-peptides

1.2.1 Preparation of (*R*,*R*)-*cis*-^{3,4}CB-GABA

To prepare (*R*,*R*)-*cis*-^{3,4}CB-GABA, we first to obtain racemic *cis*-^{3,4}CB-GABA, followed by a chiral resolution step for separation of two enantiomers, finally cleavage of the chiral auxiliary to obtain the absolute configuration of (*R*,*R*)-*cis*-^{3,4}CB-GABA for peptide coupling.

1.2.1.1 Preparation of *N*-Boc-*cis*-^{3,4}CB-GABA (±)-**7**

Two synthetic routes have been developed in the host laboratory for *cis*-^{3,4}CB-GABA.[158] The first method involves the homologation of the corresponding β-amino acid, *cis*-2-amino-cyclobutanecarboxylic acid (*cis*-ACBC). The second approach involves the photochemical 2+2 electrocyclization of an azepin-2-one. For our work, we used this second approach (Scheme 13).

Azepin-2-one **3** was prepared from commercially available caprolactam **1** in two steps. Caprolactam **1** was reacted with PCl_5, ZnI_2 and Br_2 in $CHCl_3$ on gram scale, according to the procedure from the Brown group,[162] to give dibrominated lactam **2** in 78% crude yield. Lactam **2** was converted to azepin-2-one **3** via a double elimination in the presence of LiCl. Purification by column chromatography produced azepin-2-one **3** as a yellow solid in 77% yield. This material was pure enough for further reactions. The yellow solid could be recrystallized from pentane to give colorless crystals.

Azepin-2-one **3** was submitted to a photochemical electrocyclization. Irradiation of a solution of azepin-2-one **3** in Et_2O in a quartz tube in a Rayonet reactor at –25 °C for 8 hours gave lactam **4** in 96% crude yield. Without further purification, lactam **4** was treated with Pd/C under an H_2 atmosphere to afford lactam **5** in 88% crude yield without purification. Lactam **5** was treated with Boc_2O in the presence of DMAP to give *N*-Boc lactam **6** in 83% yield after purification by column chromatography. *N*-Boc lactam **6** was hydrolyzed with LiOH in H_2O/THF at room temperature overnight. After purification by column chromatography, racemic *N*-Boc-*cis*-^{3,4}CB-GABA (±)-**7** was obtained as a white solid in 97% yield.

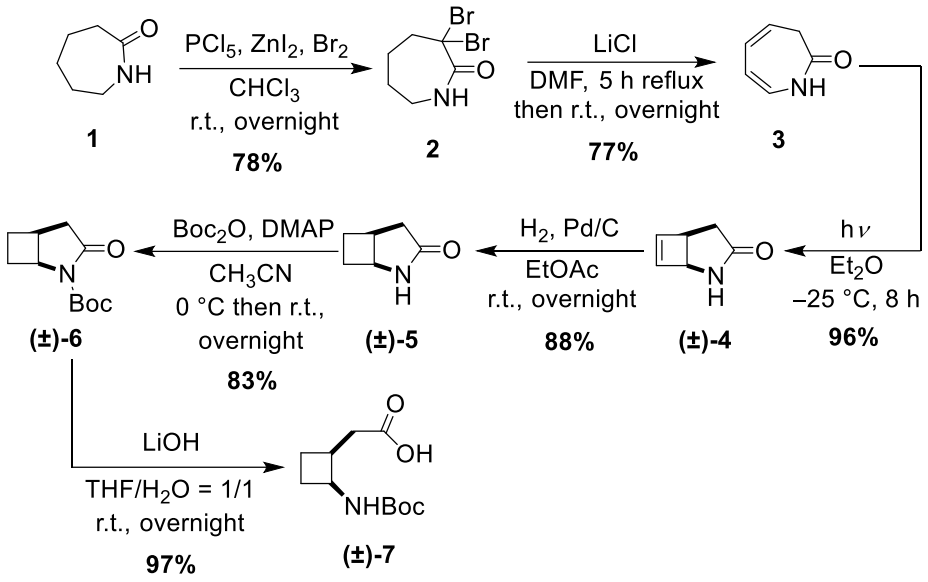

Scheme 13. Synthesis of *N*-Boc-*cis*-[3,4]CB-GABA (±)-**7**

1.2.1.2 Preparation of oxazolidinone (–)-**9**

The established procedure[158] for the resolution of (±)-**7** required the use of oxazolidinone (–)-**9**. This compound was prepared by treating commercial (1*S*,2*R*)-(+)-norephedrine **8** with triphosgene, in the presence of dry triethylamine at room temperature for 1 hour. The reaction afforded oxazolidinone (–)-**9** in 99% yield, which was used without further purification (Scheme 14).

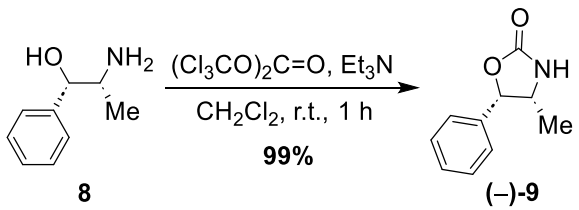

Scheme 14. Preparation of oxazolidinone (–)-**9**

1.2.1.3 Preparation of Boc-(*S*,*S*)-*cis*-[3,4]CB-GABA **11** and Boc-(*R*,*R*)-*cis*-[3,4]CB-GABA **12**

The Boc protected racemic amino acid (±)-**7** was coupled with chiral oxazolidinone (–)-**9** in order to perform a chiral resolution. Activation of (±)-**7** as a mixed anhydride was achieved by treatment with PivCl (trimethylacetyl chloride) and Et_3N. The oxazolidinone (–)-**9** was deprotonated with *n*-BuLi, then added to the activated Boc-amino acid solution affording the formation of a mixture of two diastereomers (+)-**10a** and (–)-**10b**. The separation of these two

diastereomers was performed by flash chromatography on silica four times and gave (+)-**10a** and (–)-**10b** in 41% and 47% yields, respectively (Scheme 15).

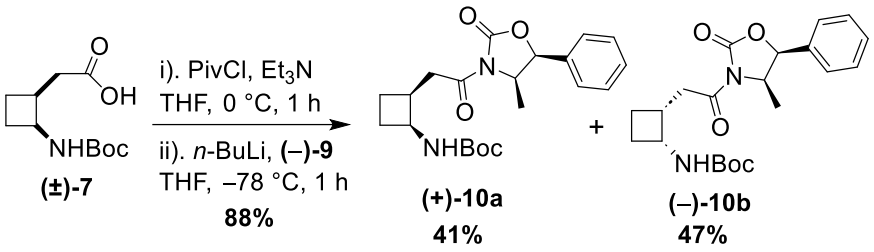

Scheme 15. Chiral resolution of racemic *N*-Boc-*cis*-^{3,4}CB-GABA (±)-**7**

Cleavage of the chiral auxiliary was then performed on each diastereomer (+)-**10a** and (–)-**10b** (Scheme 16). The hydrolysis was carried out using H_2O_2 in the presence of LiOH. After the reaction was completed, a first extraction was done to recover chiral oxazolidinone (–)-**9** for recycling. Then the lithium salts of **11** and **12** were acidified with concentrated HCl solution, extracted with CH_2Cl_2 to afford enantiomerically pure Boc-(*S*,*S*)-*cis*-^{3,4}CB-GABA **11** and Boc-(*R*,*R*)-*cis*-^{3,4}CB-GABA **12**, with 96% and 98% yields, respectively.

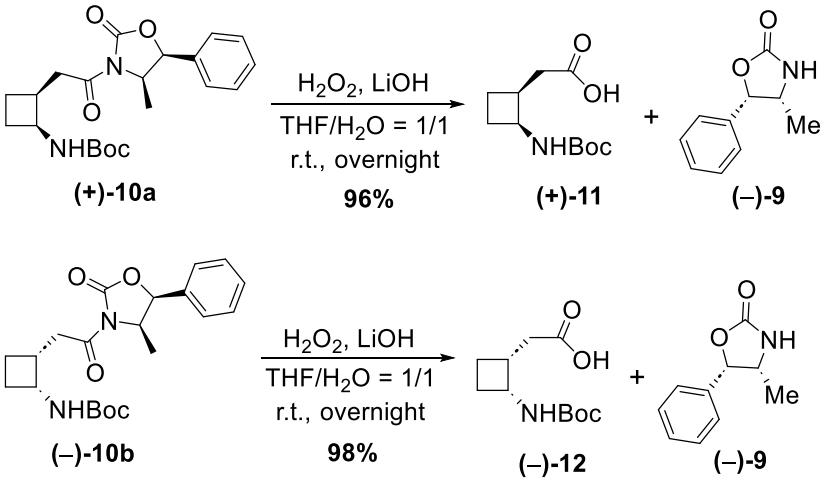

Scheme 16. The cleavage procedure to remove the chiral oxazolidinone (–)-**9**

1.2.2 Preparation of Boc-(*R*)-Ala-OBn **13** and Boc-(*S*)-Ala-OBn **14**

1.2.2.1 Preparation of Boc-(*R*)-Ala-OBn **13**

The preparation of Boc-(*R*)-Ala-OBn **13** began with commercial D-alanine (Scheme 17). Treatment with Boc_2O in the presence of NaOH at room temperature overnight gave a crude Boc-alanine which was mixed with benzyl alcohol, in the presence of DMAP and DCC at room

temperature overnight. After purification by column chromatography the fully protected Boc-(*R*)-Ala-OBn **13** was obtained with a yield of 60% for two steps.

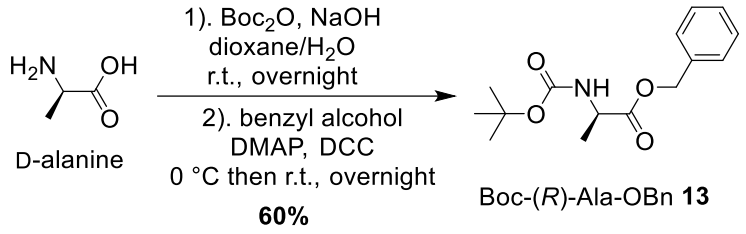

Scheme 17. Preparation of Boc-(*R*)-Ala-OBn **13**

1.2.2.2 Preparation of Boc-(*S*)-Ala-OBn **14**

The synthesis of Boc-(*S*)-Ala-OBn **14** began with commercial Boc-L-alanine. Treatment with benzyl alcohol, in the presence of DMAP and DCC at room temperature overnight. Followed by purification by column chromatography afforded Boc-(*S*)-Ala-OBn **14** in 97% yield (Scheme 18).

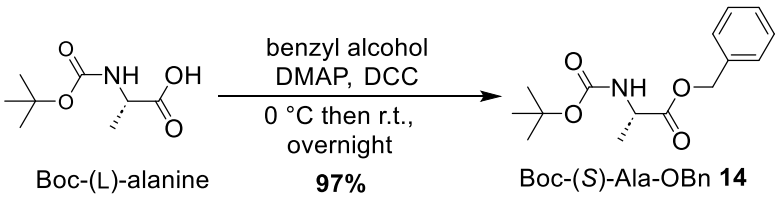

Scheme 18. Preparation of Boc-(*S*)-Ala-OBn **14**

1.2.3 Preparation of mixed γ/α-peptides

We initially proposed to prepare twelve γ/α hybrid peptides for the conformational studies (Figure 59). Boc-(*R,R*)-*cis*-^{3,4}CB-GABA **12** was picked as the γ-amino acid component and was combined with one or other enantiomer of alanine, in the form of Boc-(*R*)-Ala-OBn **13** or Boc-(*S*)-Ala-OBn **14**.

The twelve peptides are divided into two families depending on the configuration: *R*,*R*,*R* series and *R*,*R*,*S* series. For each series, different modifications on *C*-capped function: one as benzyl ester, and the other as benzyl amide. Peptides bearing a benzyl amide have an extra NH, that may be involved in their conformational behaviors.

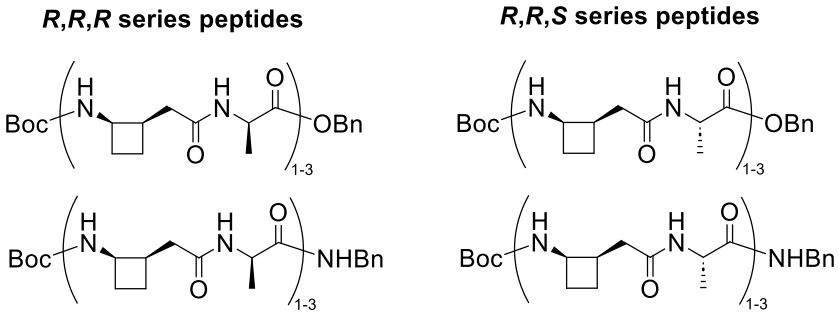

Figure 59. The *R*,*R*,*R* series and *R*,*R*,*S* series of mixed γ/α-peptides

1.2.3.1 The peptide synthesis strategy

To construct these small peptides, we employed solution phase peptide synthesis due to the advantage of being more flexible and amenable to modifications. Additionally, dipeptide was used as a motif to synthesize corresponding tetrapeptide and hexapeptide. HATU[O-(7-Azabenzotriazol-1-yl)-*N*,*N*,*N*',*N*'-tetramethyluroniumhexa-fluorophosphate] is a very efficient peptide coupling reagent with little racemization (Figure 60),[163,164] and on the basis of Monsour's work,[161] HATU was used as the coupling reagent in this chapter.

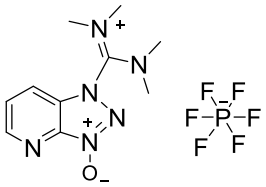

Figure 60. The chemical structure of HATU

1.2.3.2 Synthesis of *R*,*R*,*R* dipeptides **15** and **17**

The dipeptide Boc-(*R*,*R*)-*cis*-^{3,4}GABA-(*R*)-Ala-OBn **15** was prepared by the coupling of Boc-(*R*,*R*)-*cis*-^{3,4}CB-GABA **12** with Boc-(*R*)-Ala-OBn **13** (Scheme 19). Boc-(*R*,*R*)-*cis*-^{3,4}CB-GABA **12** was treated with DIPEA and HATU, during 10 minutes for activation of the carboxylic acid moiety. At the same time, Boc-(*R*)-Ala-OBn **13** was treated with TFA to deprotect the amine function and obtained the corresponding TFA salt. The TFA salt was then basified with a sufficient amount of DIPEA to reach a pH 9 solution. Then, the (*R*)-Ala-OBn solution was transferred to the activated **12** solution to afford the Boc-(*R,R*)-*cis*-^{3,4}GABA-(*R*)-Ala-OBn **15** in 93% yield after purification by column chromatography.

Hydrogenolysis of the dipeptide ester **15** was carried out with Pd/C catalyst under H_2 atmosphere at room temperature for 4 hours, giving carboxylic acid **16** in quantitative yield without purification. The carboxylic acid **16** was coupled with benzyl amine using HATU, in the presence of DIPEA at room temperature for 24 hours. After purification by column chromatography and preparative HPLC, the dipeptide amide, Boc-(*R*,*R*)-*cis*-^{3,4}GABA-(*R*)-Ala-NHBn **17** was obtained in 46% yield.

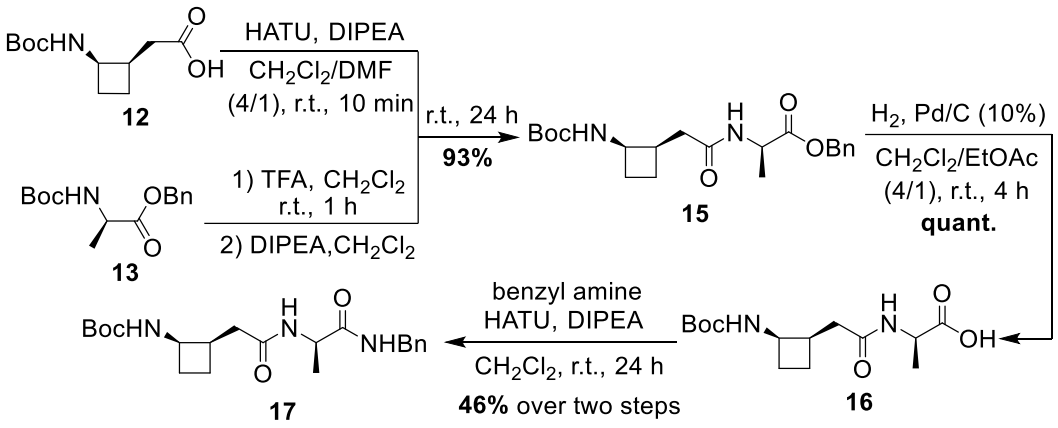

Scheme 19. Synthesis of *R,R,R* dipeptides **15** and **17**

1.2.3.3 Synthesis of *R,R,R* tetrapeptides **21** and **23**

The synthesis of tetrapeptide **21** was carried out by coupling carboxylic acid **16** with dipeptide ester **15** (Scheme 20). The dipeptide ester **15** was treated with TFA to deprotect the amine group leading to a TFA salt: DIPEA was then added to reach a pH 9 solution. The carboxylic acid **16** was treated with DIPEA, the above-described solution was then added, and finally HATU was introduced into the reaction mixture. The reaction was stirred at room temperature for 24 hours, to give the tetrapeptide ester, Boc-[(*R*,*R*)-*cis*-^{3,4}GABA-(*R*)-Ala]$_2$-OBn **21** in 73% yield after purification by column chromatography and preparative HPLC.

The tetrapeptide ester **21** was then submitted to hydrogenolysis under an H_2 atmosphere in the presence of Pd/C, to produce the carboxylic acid **22**. This compound was coupled with benzyl amine using HATU in the presence of DIPEA at room temperature for 24 hours, to give tetrapeptide amide, Boc-[(*R*,*R*)-*cis*-^{3,4}GABA-(*R*)-Ala]$_2$-NHBn **23** in 59% yield after purification by column chromatography.

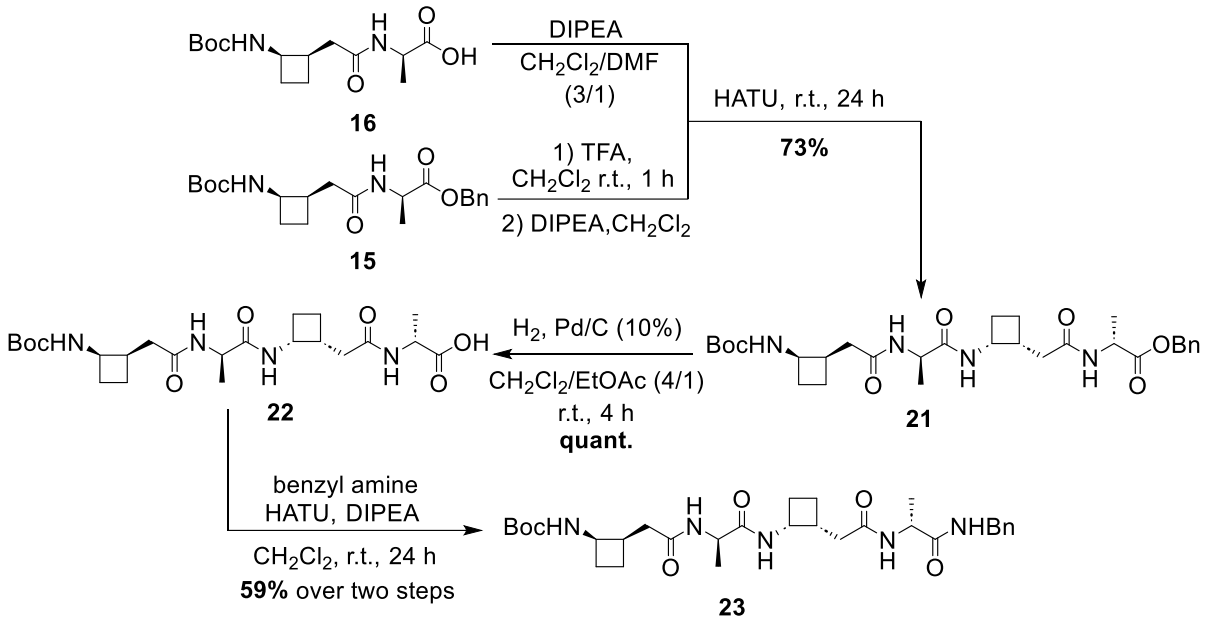

Scheme 20. Synthesis of *R*,*R*,*R* tetrapeptides **21** and **23**

1.2.3.4 Synthesis of *R*,*R*,*R* hexapeptide ester **27**

To synthesize the hexapeptide ester **27**, a peptide coupling reaction between carboxylic acid **16** and tetrapeptide ester **21** was performed (Scheme 21). The deprotection of the amino group of tetrapeptide ester **21** was carried out with TFA, and the resulting TFA salt was basified with enough DIPEA to reach a pH 9 solution. Next, the solution was introduced into a mixture containing carboxylic acid **16** and DIPEA, HATU was then added to the mixture. The reaction took 24 hours at room temperature to afford hexapeptide ester, Boc-[(*R*,*R*)-*cis*-^{3,4}GABA-(*R*)-Ala]$_3$-OBn **27** in 60% yield after purification by preparative HPLC.

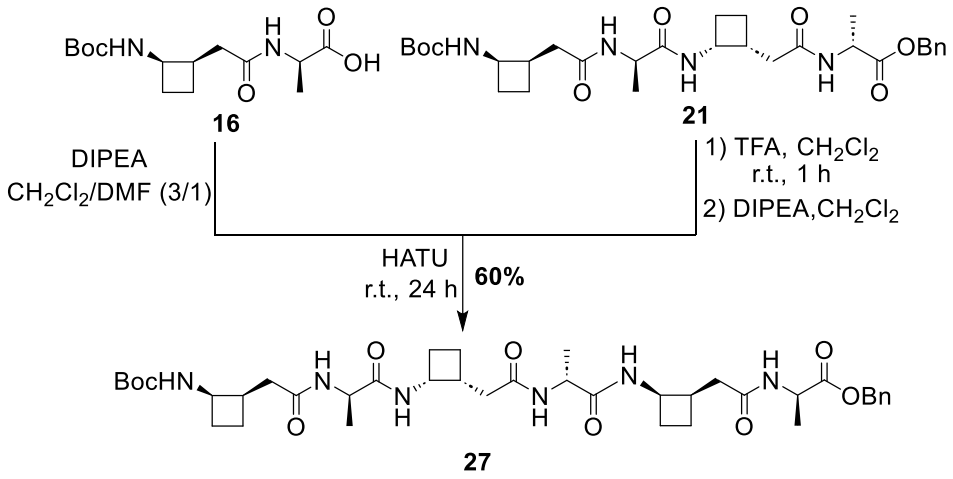

Scheme 21. Synthesis of *R*,*R*,*R* hexapeptide ester **27**

1.2.3.5 Synthesis of *R,R,R* hexapeptide amide **28**

Following the successful syntheses of di- and tetra-NHBn peptides, **17** and **23**, we attempted to replace the benzyl ester by a benzyl amide on hexapeptide ester **27**. However, due to the low solubility of hexapeptide **27**, we could not perform the hydrogenolysis in a solvent mixture of CH_2Cl_2/EtOAc (Scheme 22).

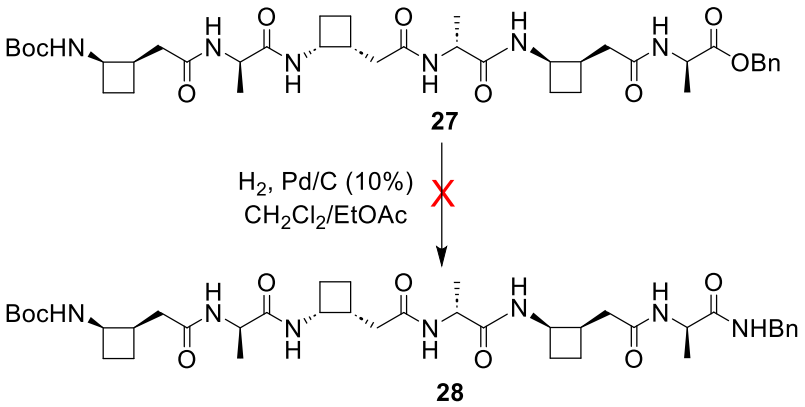

Scheme 22. Hydrogenolysis of the *R,R,R* hexapeptide ester **27**

To overcome the poor solubility of hexapeptide ester **27**, we used a more polar solvent, MeOH, for the hydrogenolysis. Although the benzyl group was successfully removed, we observed the rapid formation of a new hexapeptide methyl ester **31**, as shown in Scheme 23.

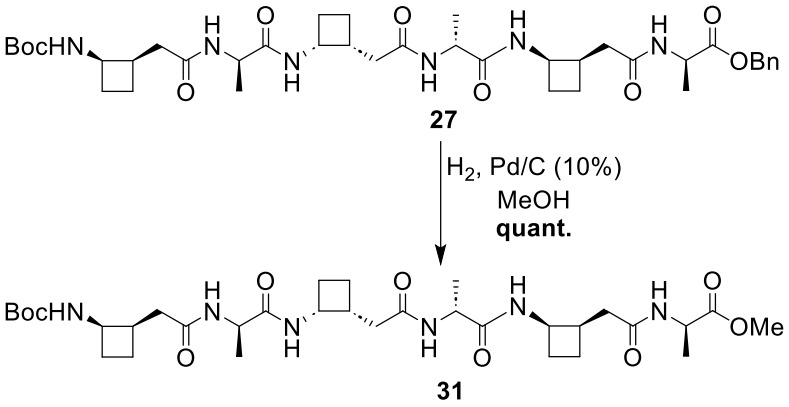

Scheme 23. The hexapeptide methyl ester **31** was generated in the hydrogenolysis

We therefore decided to change the dipeptide and tetrapeptide partners for the synthesis of the target hexapeptide. In this way, hexapeptide amide **28** was prepared by coupling carboxylic acid **16** with tetrapeptide amide **23** (Scheme 24).

The tetrapeptide **23** was treated with TFA and then the resulting TFA salt was basified with enough DIPEA to reach a pH 9 solution. The solution was introduced into a mixture containing carboxylic acid **16** and DIPEA, followed by the addition of HATU. The reaction took 24 hours at room temperature to afford the hexapeptide amide, Boc-[(*R*,*R*)-*cis*-^{3,4}GABA-(*R*)-Ala]$_3$-NHBn **28** in 61% yield after purification by preparative HPLC.

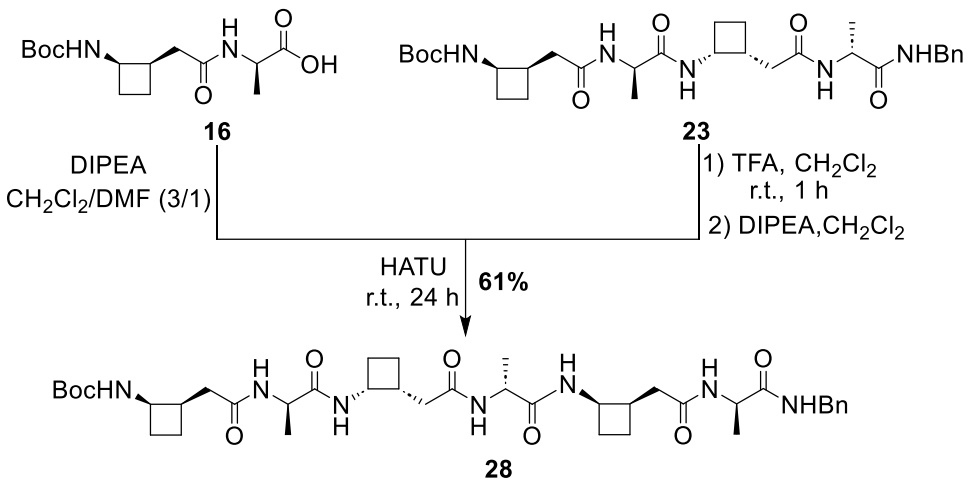

Scheme 24. Synthesis of the *R,R,R* hexapeptide amide **28**

1.2.3.6 Synthesis of *R,R,S* dipeptides **18** and **20**

Boc-(*R*,*R*)-*cis*-^{3,4}CB-GABA **12** was treated with DIPEA and HATU, during 10 minutes for activation of the carboxylic acid moiety. Boc-(*S*)-Ala-OBn **14** was treated with TFA to deprotect the amine function to give the corresponding TFA salt. The TFA salt was then treated with enough DIPEA to reach a pH 9 solution (Scheme 25). The (*S*)-Ala-OBn solution was transferred to the activated **12** solution and the reaction was stirred for 24 hours at room temperature to give the dipeptide ester, Boc-(*R*,*R*)-*cis*-^{3,4}GABA-(*S*)-Ala-OBn **18** in 93% yield after purification by column chromatography.

Hydrogenolysis of the dipeptide ester **18** was carried out with Pd/C under a H_2 atmosphere at room temperature for 4 hours, yielding the crude carboxylic acid **19** in quantitative yield. This compound was coupled with benzyl amine in the presence of HATU and DIPEA. The reaction took 24 hours and gave the dipeptide amide, Boc-(*R*,*R*)-*cis*-^{3,4}GABA-(*S*)-Ala-NHBn **20** in 46% yield after purification by column chromatography and preparative HPLC.

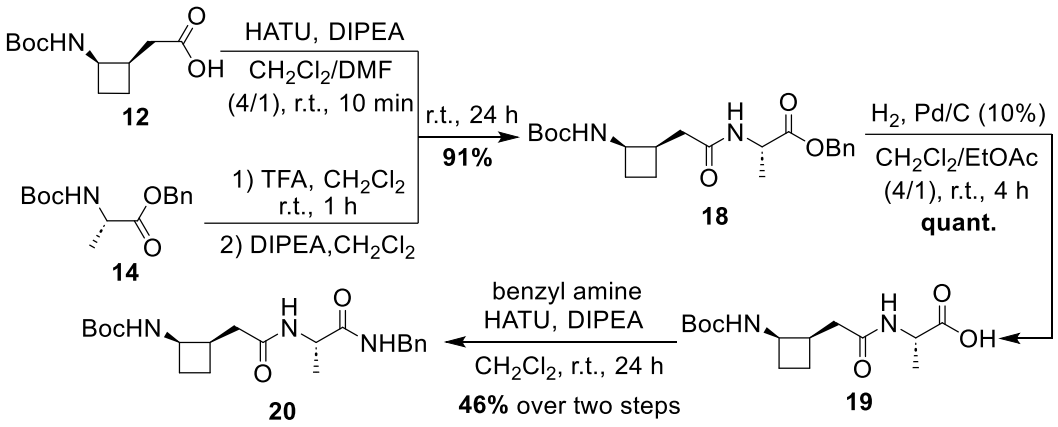

Scheme 25. Synthesis of *R,R,S* dipeptides **18** and **20**

1.2.3.7 Synthesis of *R,R,S* tetrapeptides **24** and **26**

The synthesis of tetrapeptide ester **24** was carried out by coupling carboxylic acid **19** with dipeptide ester **20** (Scheme 26). The dipeptide ester **18** was treated with TFA to deprotect the amine group at room temperature for 1 hour. The TFA salt was then treated with enough DIPEA to reach a pH 9 solution. The carboxylic acid **19** was treated with DIPEA, then the above-described solution was added, and finally HATU was introduced into the reaction mixture. After a 24 hours reaction and purification by column chromatography. Boc-[(*R*,*R*)-*cis*-^{3,4}GABA-(*S*)-Ala]$_2$-OBn **24** was obtained in 68% yield.

Hydrogenolysis of the tetrapeptide ester **24** using Pd/C under a H_2 atmosphere at room temperature for 4 hours, gave the crude carboxylic acid **25** in quantitative yield. This compound was coupled with benzyl amine using HATU in the presence of DIPEA at room temperature for 24 hours, to give tetrapeptide amide, Boc-[(*R*,*R*)-*cis*-^{3,4}GABA-(*S*)-Ala]$_2$-NHBn **26** in 88% yield after purification by column chromatography and preparative HPLC.

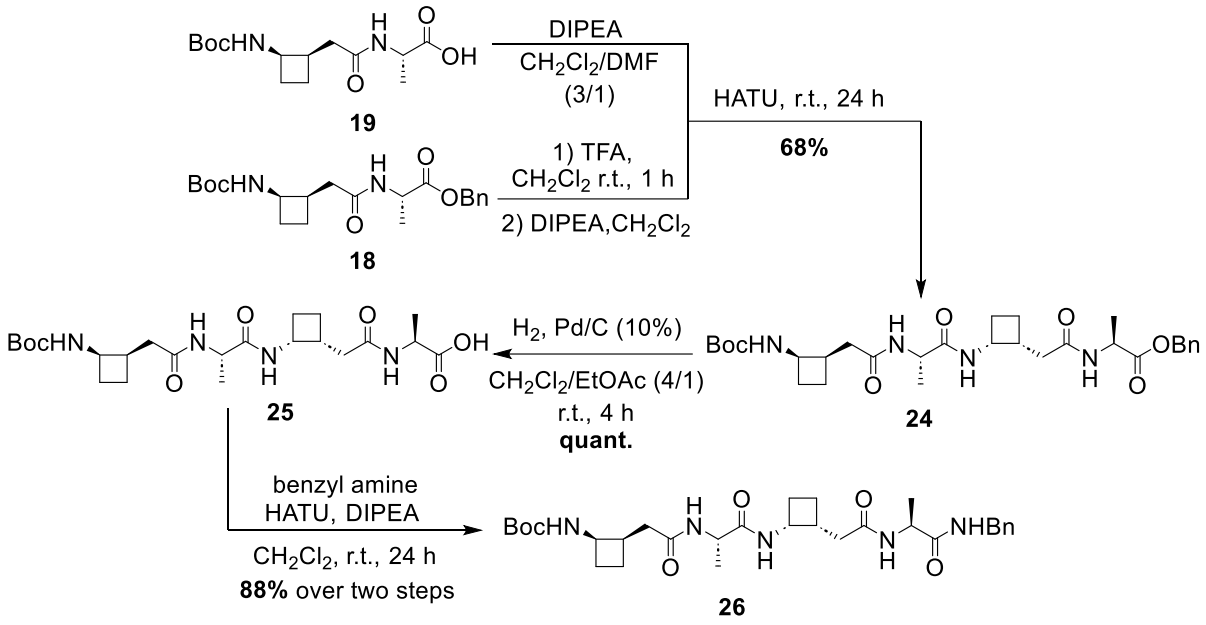

Scheme 26. Synthesis of *R,R,S* tetrapeptides **24** and **26**

1.2.3.8 Synthesis of *R,R,S* hexapeptide ester **29**

To synthesize hexapeptide ester **29**, a peptide coupling reaction between carboxylic acid **19** and tetrapeptide ester **24** was performed (Scheme 27). The deprotection of the amine group of tetrapeptide ester **24** was carried out with TFA at room temperature for 1 hour. The resulting TFA salt was basified with enough DIPEA to reach a pH 9 solution. The solution was injected into a mixture of carboxylic acid **19** and DIPEA, followed by the introduction of HATU. The reaction took 24 hours at room temperature to afford Boc-[(*R*,*R*)-*cis*-^{3,4}GABA-(*S*)-Ala]$_3$-OBn **29** in 55% yield after purification by column chromatography.

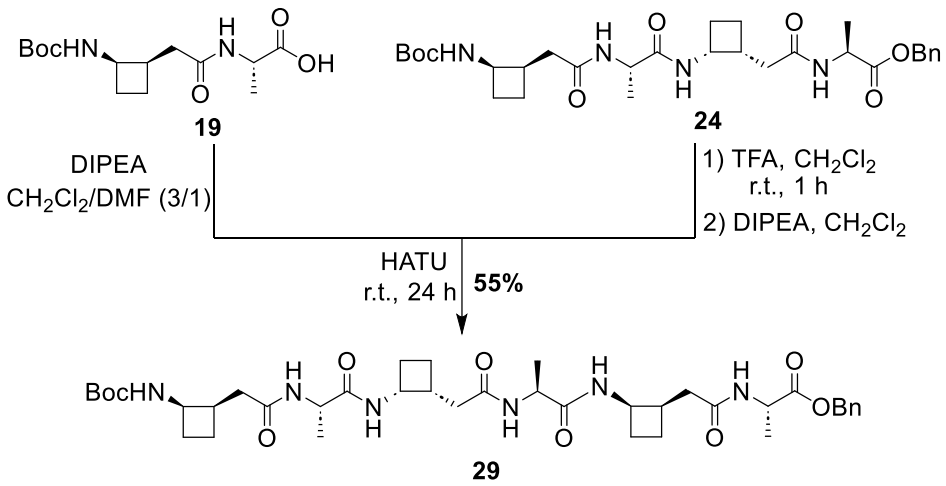

Scheme 27. Synthesis of *R,R,S* hexapeptide ester **29**

1.2.3.9 Synthesis of *R,R,S* hexapeptide amide **30**

The synthesis of hexapeptide amide **30** was achieved by coupling carboxylic acid **19** with tetrapeptide amide **26** (Scheme 28). The deprotection of the amine group of tetrapeptide amide **26** was carried out using TFA and the resulting TFA salt was basified with enough DIPEA to reach a pH 9 solution. The solution was introduced into a mixture of carboxylic acid **19** and DIPEA, followed by the addition of HATU. The reaction was stirred at room temperature for 24 hours afforded Boc-[(*R*,*R*)-*cis*-^{3,4}GABA-(*S*)-Ala]$_3$-NHBn **30** in 48% yield after purification by preparative HPLC.

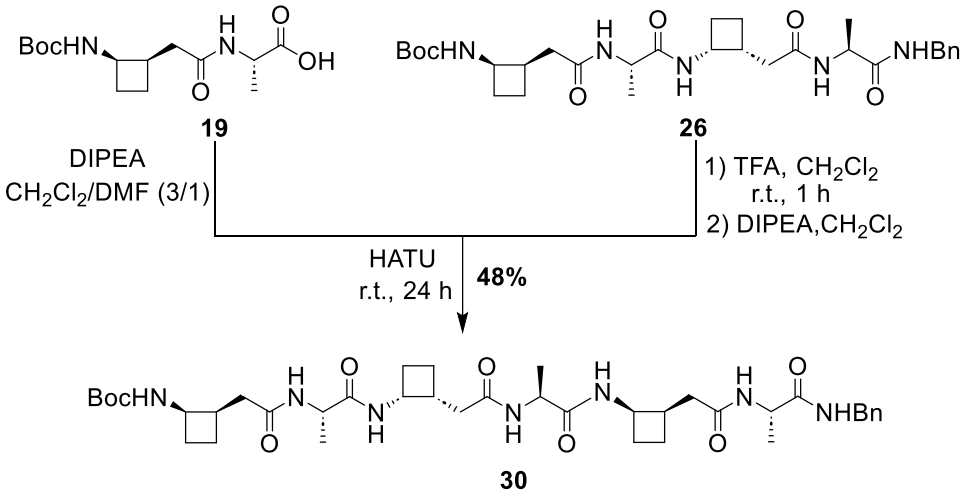

Scheme 28. Synthesis of *R,R,S* hexapeptide amide **30**

1.2.3.10 Epimerization and solubility issues

Epimerization usually occurs at the α-carbon during the activation of the carboxylic acid function. In our cases, slightly epimerization was observed during coupling reactions in synthesizing peptides **17**, **20**, **21** and **24** (Table 2). After a first purification by column chromatography, we observed the presence of the epimerized product in ^{1}H NMR spectrum. Then the sample was submitted to purification by preparative HPLC. Other samples were also checked by HPLC to confirm their absolute configuration for further conformational studies.

Entry	peptides	epimerization (%)
1	Boc-(*R*,*R*)-*cis*-^{3,4}GABA-(*R*)-Ala-NHBn **17**	12
2	Boc-(*R*,*R*)-*cis*-^{3,4}GABA-(*S*)-Ala-NHBn **20**	5
3	Boc-[(*R*,*R*)-*cis*-^{3,4}GABA-(*R*)-Ala]$_2$-OBn **21**	15
4	Boc-[(*R*,*R*)-*cis*-^{3,4}GABA-(*S*)-Ala]$_2$-OBn **24**	7

Table 2. The epimerization in the peptide coupling reaction

In the synthesis section, the structure identification of hexapeptides Boc-[(*R*,*R*)-*cis*-^{3,4}GABA-(*R*)-Ala]$_3$-OBn **27** and Boc-[(*R*,*R*)-*cis*-^{3,4}GABA-(*R*)-Ala]$_3$-NHBn **28** was challenging due to their poor solubility in $CDCl_3$ or pyridine-d_5, was then performed in DMSO-d_6. Therefore, solution state conformational studies of peptides **27** and **28** were not amenable to perform then have been canceled.

1.3 Conformational studies of γ/α-hybrid peptides

1.3.1 Methodologies in this section

1. **Molecular Modelling** studies were carried out in parallel with the spectroscopic assays below. The Hybrid Monte Carlo Multiple Minima (MCMM) conformational search, which was carried out in a chloroform media using Macromodel 04 from Schrodinger software and the force field with OPLS-2005. 10 000 conformers were generated by MCMM method. Low-energy conformers were retained and were sorted according to their conformer families. The calculations were performed without constraints from experimental data.

2. The **^{1}H** and **^{13}C** NMR assignments of each structure were established by a combination of 1D/2D NMR experiments: TOCSY, ^{1}H-^{1}H COSY, ^{1}H-^{13}C HSQC, ^{1}H-^{13}C HMBC, ^{1}H-^{15}N HSQC, ^{1}H-^{15}N HMBC, ^{1}H-^{1}H 2D NMR NOESY and ^{1}H-^{1}H 2D NMR ROESY.

3. **^{1}H NMR DMSO-d_6 titration** experiments were performed to establish extent of solvent accessibility of NH protons. DMSO is a polar solvent with a strong H-bond accepting ability that can form intermolecular H-bonds with NH protons in peptides, resulting in observable chemical shift changes in the NH signals of spectra. As DMSO is added progressively to the NMR tube, the environment around the molecule becoming more polar and DMSO solvates exposed the NH protons. The NH protons engaged in hydrogen bonding are less sensitive to the addition of DMSO-d_6, resulting in smaller changes in chemical shifts, while free NH protons experience more significant chemical shift changes.

All experiments were carried out at 300 K on a Bruker AV 400 MHz spectrometer. Each sample was dissolved in $CDCl_3$ (400 μL) at a concentration of 5 mM. DMSO-d_6 was added sequentially to the NMR tubes according to the concentration (%, v/v) required. After each addition and rapid agitation, the ^{1}H NMR spectrum was recorded. The difference between the starting and the final chemical shifts values $\Delta\delta$ was determined.

4. **^{1}H-^{1}H ROESY NMR** experiments were used to probe the three-dimensional geometry of the peptides in solution. For these 2D NMR experiments, the peptide concentration in deuterated solvent had to be high enough to avoid lengthy acquisition time, but low enough to exclude undesirable effects due to intermolecular contacts. The ^{1}H-^{1}H ROESY spectra were recorded on a Bruker AV 400 MHz spectrometer. Each sample was prepared in $CDCl_3$ or pyridine-d_5 at a concentration of 20 mM. The pulse sequence was roesyphpp. The experiments were performed by collecting 2048 points in f2 and 256 points in f1.

5. **Infrared (IR) in solution state experiments** were carried out to determine the presence and the type of H-bonds. Distinct amide environments can be identified for free and bonded N–H

when the amide stretching region (3200-3500 cm^{-1}) is examined. The stretching vibration for a free N–H is generally 3400-3500 cm^{-1} (blue region). When the amide proton is engaged in a H-bond, the N–H bond strength is weaker leading to a vibration frequency below 3400 cm^{-1} (red region).

6. **X-ray diffraction** of single crystals was performed when possible, to determine the three-dimensional structure of peptides in the lattice, and to establish their conformational preferences, in particular the role of intramolecular and intermolecular H-bonds in solid state.

1.3.2 Molecular Modelling

For each peptide, the list of conformation families was sorted in descending order of their abundance. The lowest energy for each conformation was recorded as kJ/mol. In the conformer nomenclature, 'f' was used to indicate a free NH; discreet, successive rings are separated by the symbol '-', as illustrated in Figure 61.

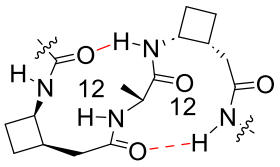

[f-f-12-12] conformer

Figure 61. Two examples of H-bonding patterns

1.3.2.1 Hybrid Monte Carlo Multiple Minima Calculations of *R*,*R*,*S* series peptides

*a. Hybrid MCMM conformational search of dipeptide **18***

The conformational search of dipeptide ester Boc-(*R*,*R*)-*cis*-^{3,4}GABA-(*S*)-Ala-OBn **18** with two amide NHs was performed with a 20 kJ/mol relative energy cut off. We obtained a total of 300 conformations, which were sorted into four different conformation families (Table 3).

Conformations	Relative abundance of each conformation	The lowest energy conformation
[f-9]	38.0%	–174.736
[10-f]	27.0%	–172.566
[f-f]	25.0%	–175.610
[7-f]	10.0%	–168.897

Table 3. Abundance and lowest energy of conformer families of *R*,*R*,*S* dipeptide ester **18**

The most abundant 38% is a [f-9] conformation implicating NH(2) in a 9 membered ring H-bond, and it has the second lowest energy. The second most abundant 27% is a [10-f] conformation implicating NH(1) in a C10 H-bond, with the third lowest energy. A [7-f] was found in 10% abundance. Rather surprising the lowest energy is a free conformation, in which both NHs were non hydrogen-bonded (Figure 62).

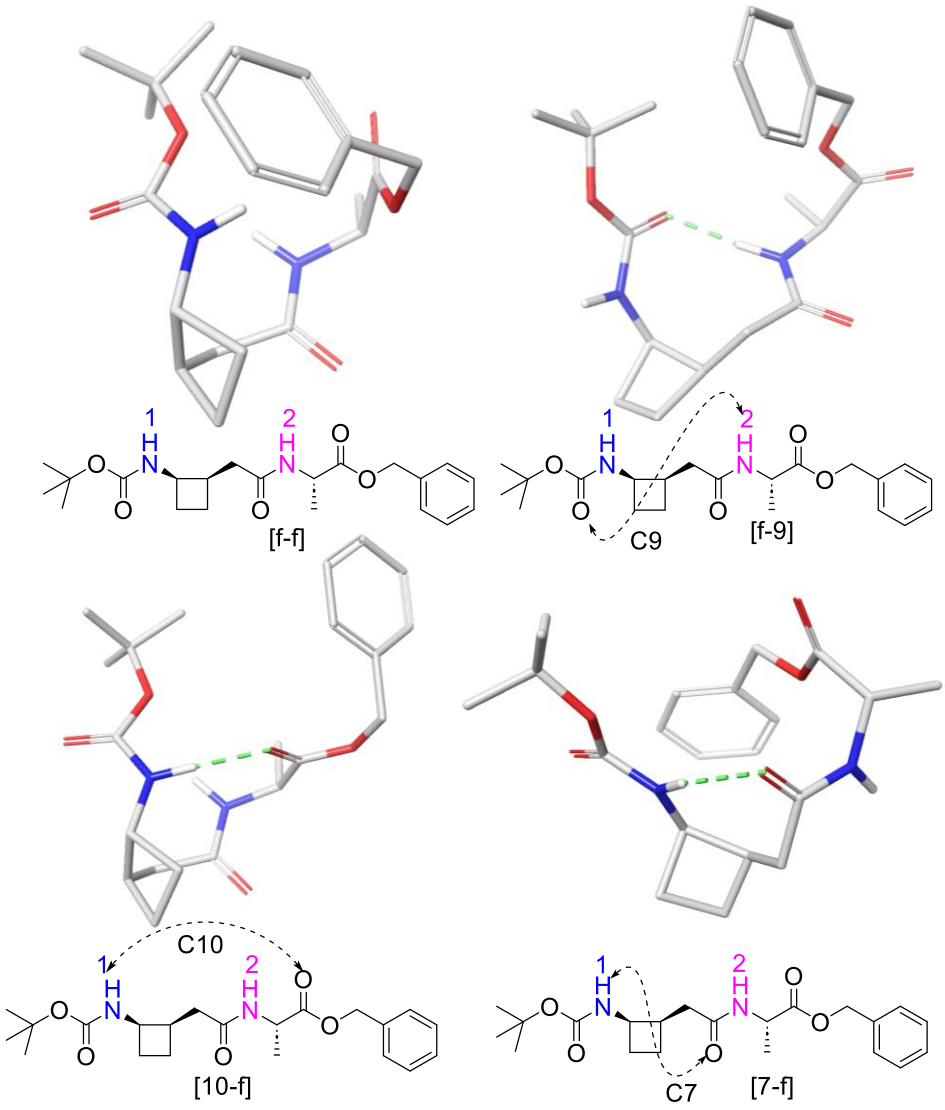

Figure 62. Four lowest energy conformation families found for *R*,*R*,*S* dipeptide ester **18** and their H-bonding patterns

*b. Hybrid MCMM conformational search of dipeptide **20***

The conformational search was carried out on dipeptide amide Boc-(*R*,*R*)-*cis*-^{3,4}GABA-(*S*)-Ala-NHBn **20**, which has three amide NHs. The calculation was performed with a 20 kJ/mol relative energy cut off, and afforded 298 conformations that were sorted into eight different conformation families (Table 4).

Conformations	Relative abundance of each conformation	The lowest energy conformation
[f-9-7]	37.0%	–254.066
[f-f-12]	18.0%	–254.415
[f-9-f]	11.0%	–257.024
[f-9-12]	10.0%	–256.813
[10-f]	10.0%	–250.837
[f-f-7]	7.0%	–259.530
[7-f-7]	6.0%	–249.913
[7-f-f]	1.0%	–248.251

Table 4. Abundance and lowest energy of conformer families of *R*,*R*,*S* dipeptide amide **20**

The most abundant 37% is a [f-9-7] conformation implicating NH(2) in a C9 H-bond, and NH(3) in a C7 H-bond, and it has the fifth lowest energy. The second most abundant 18% is a [f-f-12] conformation, in which NH(3) in a C12 H-bond. The lowest energy is a [f-f-7] conformation implicating NH(3) in a C7 H-bond and with 7% abundance, the second lowest energy is a [f-9-f] conformer and with 11% abundance (Figure 63).

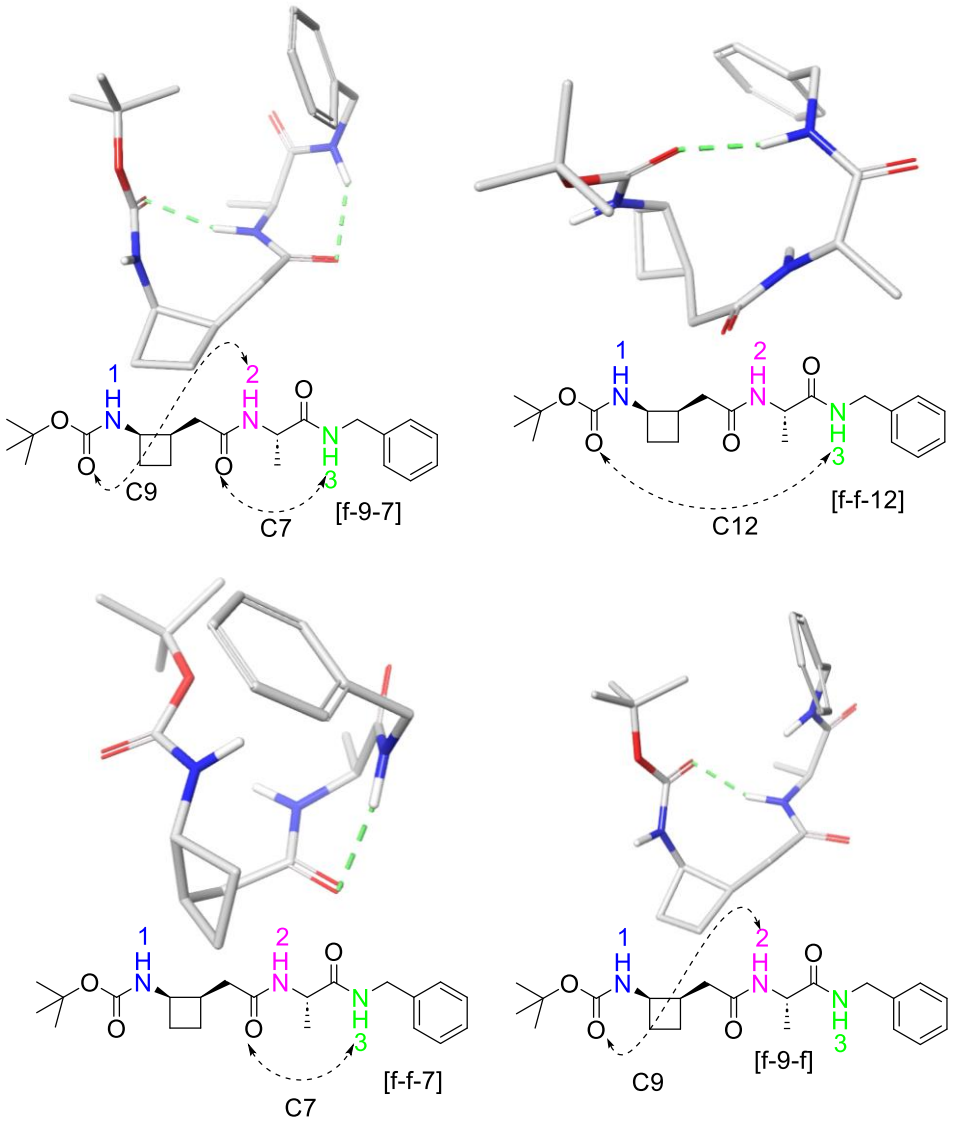

Figure 63. Two most abundant conformers (top) and two lowest energy conformation families (bottom) found for *R*,*R*,*S* dipeptide amide **20** and their H-bonding patterns

*c. Hybrid MCMM conformational search of tetrapeptide **24***

The conformational search was performed on the tetrapeptide ester Boc-[(*R*,*R*)-*cis*-^{3,4}GABA-(*S*)-Ala]$_2$-OBn **24** which has four amide NHs, with a 10 kJ/mol relative energy cut off. We obtained 258 conformations and divided into five different conformation families after classification (Table 5).

Conformations	Relative abundance of each conformation	The lowest energy conformation
[10-f-10-12]	44.0%	–347.191
[7-f-10-12]	31.0%	–345.493
[f-9-10-12]	14.0%	–339.990
[f-f-10-12]	10.0%	–339.753
[f-9-7-f]	1.0%	–337.337

Table 5. Abundance and lowest energy of conformer families of *R,R,S* tetrapeptide ester **24**

Notably, 99% of the structures featured a 12/10 helical conformation around the second γ-amino acid residue. The conformation family with the lowest energy and the highest abundance 44% appeared to be a right-handed 12/10-helix [10-f-10-12] as we anticipated. The second most abundant conformation 31% is a [7-f-10-12] structure with the second lowest energy (Figure 64).

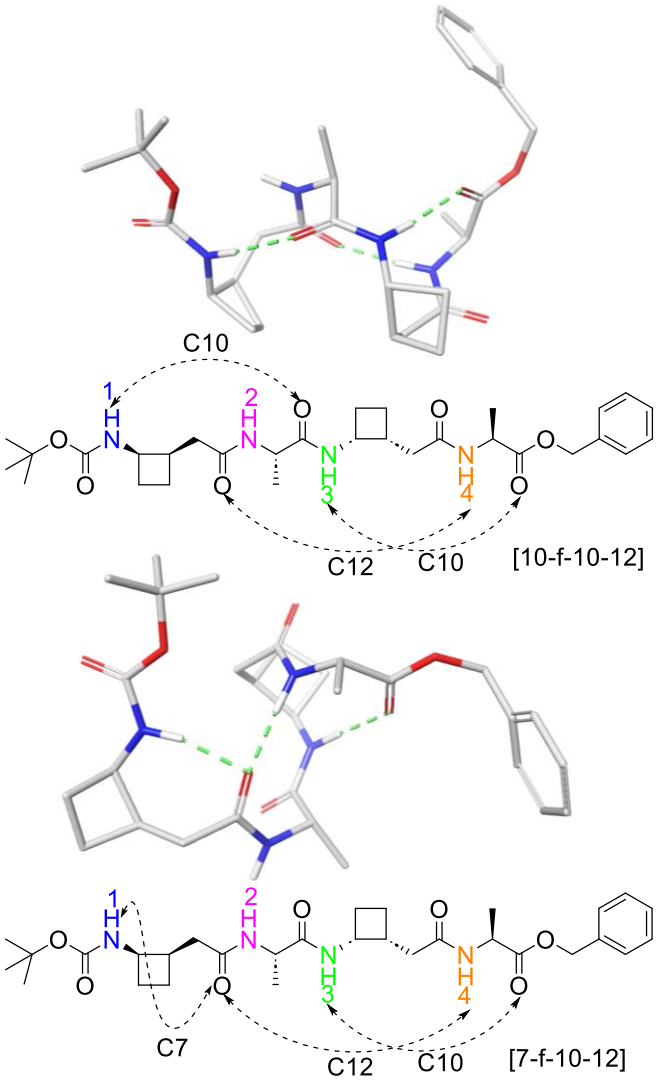

Figure 64. Two lowest energy conformation families found for *R,R,S* tetrapeptide ester **24** and their H-bonding patterns

*d. Hybrid MCMM conformational search of tetrapeptide **26***

The hybrid MCMM conformational search was performed on tetrapeptide amide Boc-[(*R*,*R*)-*cis*-^{3,4}GABA-(*S*)-Ala]$_2$-NHBn **26**, which has five amide NHs. The calculations were performed with a 10 kJ/mol relative energy cut off, which afforded 260 conformations that were sorted into six different conformation families (Table 6).

Conformations	Relative abundance of each conformation	The lowest energy conformation
[10-f-10-12-f]	44.0%	–427.475
[7-f-10-12-f]	35.0%	–426.464
[f-9-10-12-f]	8.0%	–420.052
[f-f-10-12-f]	8.0%	–419.917
[7-f-7-17-15]	4.0%	–423.704
[10-f-f-12-7]	1.0%	–422.192

Table 6. Abundance and lowest energy of conformer families of *R,R,S* tetrapeptide amide **26**

Five conformation families (96% abundance) in Table 6 evidenced that tetrapeptide **26** adopted a 12/10 helical shape around the second γ-amino acid residue. The most abundant conformation 44% is the right-handed 12/10-helix [10-f-10-12-f], which also has the lowest energy. The second most abundant conformation 35% is a [7-f-10-12-f] structure with the second lowest energy (Figure 65).

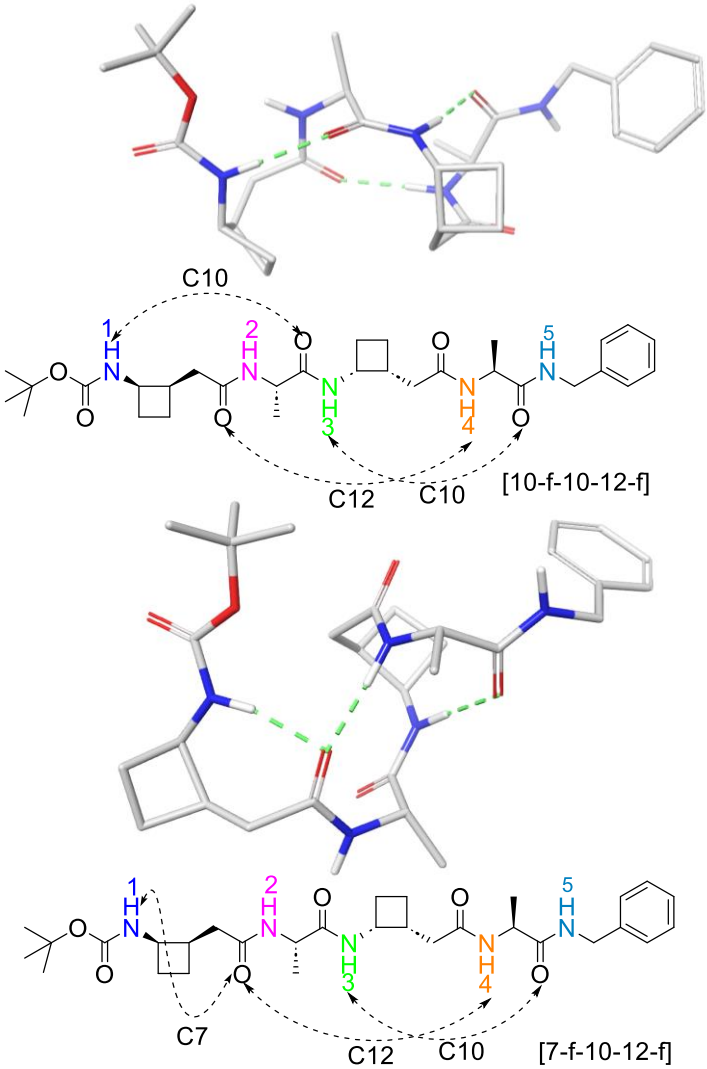

Figure 65. Two lowest energy conformation families found for *R,R,S* tetrapeptide amide **26** and their H-bonding patterns

*e. Hybrid MCMM conformational search of hexapeptide **29***

The conformational search was carried out on hexapeptide ester Boc-[(*R*,*R*)-*cis*-^{3,4}GABA-(*S*)-Ala]$_3$-OBn **29** which has six amide NHs. The calculations were performed with a 20 kJ/mol relative energy cut off, which afforded 533 conformations, sorted into six conformation families (Table 7).

Conformations	Relative abundance of each conformation	The lowest energy conformation
[7-f-10-12-10-12]	45.0%	–530.516
[f-f-10-12-10-12]	23.0%	–524.351
[10-f-10-12-10-12]	21.0%	–525.613
[f-9-10-12-10-12]	7.0%	–518.010
[10-f-12-10-f-12]	3.0%	–510.548
[18-13-7-9-10-12]	1.0%	–515.875

Table 7. Abundance and lowest energy of conformer families of *R,R,S* hexapeptide ester **29**

While the first γ-amino acid residue of hexapeptide ester **29** was engaged in different H-bond features – including C10, C9, C7 – or simply free, the rest of the sequences essentially adopted a 12/10 helical folding pattern. The most abundant conformation family 45% is a mixed 7/12/10-helix [7-f-10-12-10-12] which also had the lowest energy. The full right-handed 12/10 helical conformation [10-f-10-12-10-12] with 21% abundance had the second lowest energy. The second highest abundance is also a partial 12/10-helix in a family of [f-f-10-12-10-12] with the first NH being free and had the third lowest energy (Figure 66).

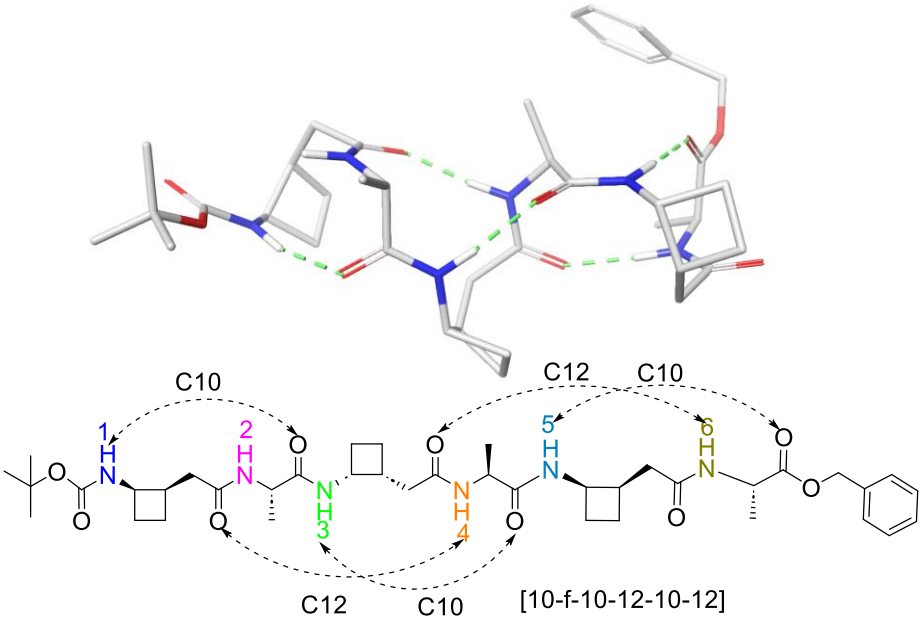

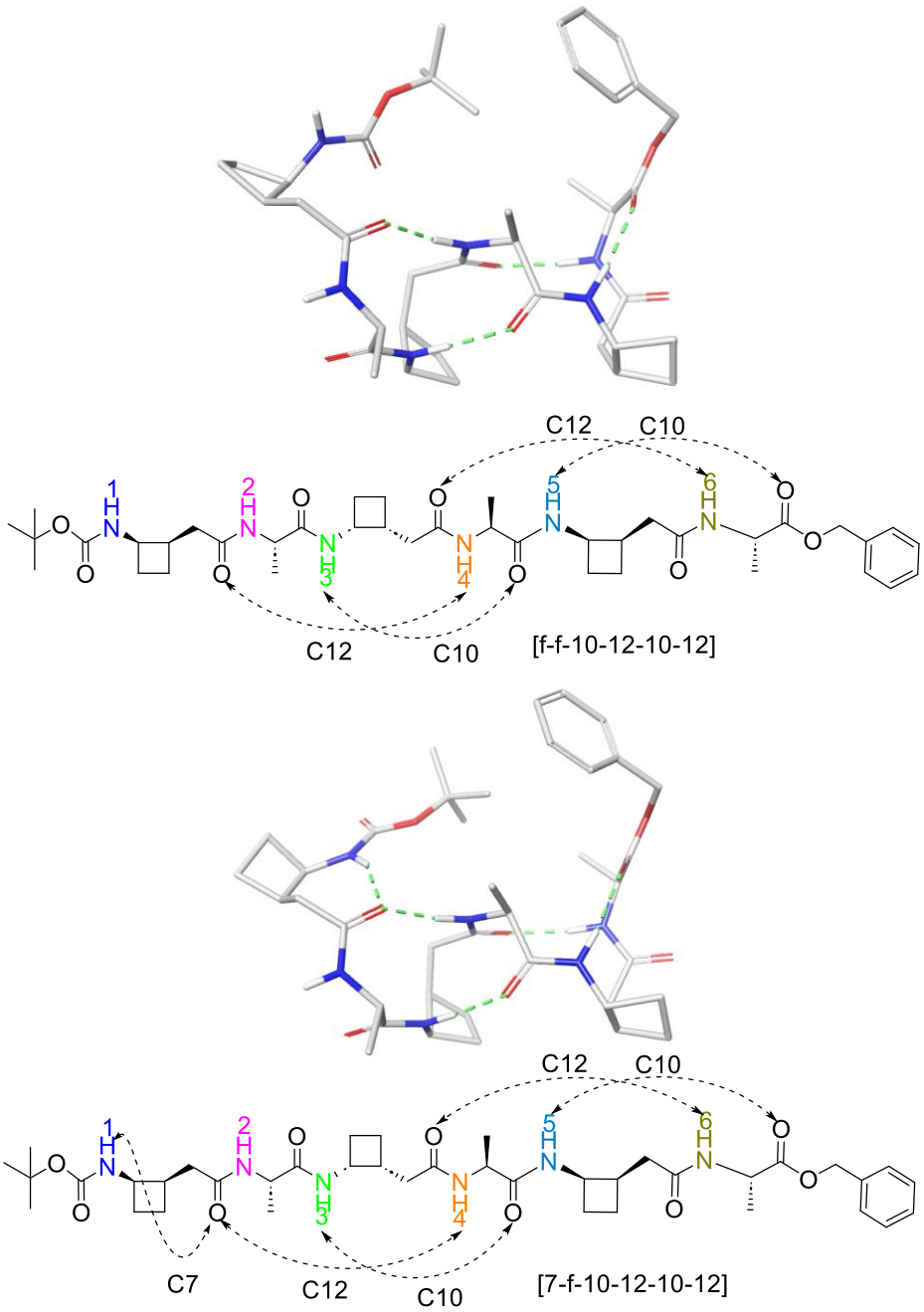

Figure 66. Three lowest energy conformation families found for *R,R,S* hexapeptide ester **29** and their H-bonding patterns

*f. Hybrid MCMM conformational search of hexapeptide **30***

The MCMM conformational search was conducted on hexapeptide amide Boc-[(*R*,*R*)-*cis*-^{3,4}GABA-(*S*)-Ala]$_3$-NHBn **30**, which has seven amide NHs. The calculations were performed with a 20 kJ/mol relative energy cut off and afforded 995 conformations. Results are shown below in Table 8, sorted into eleven different conformation families.

Conformations	Relative abundance of each conformation	The lowest energy conformation
[f-f-10-12-10-12-f]	38.0%	-599.554
[7-f-10-12-10-12-f]	29.0%	-604.683
[10-f-10-12-10-12-f]	14.0%	-605.466
[f-9-10-12-10-12-f]	10.5%	-597.840
[7-f-10-12-f-12-7]	3.0%	-599.167
[f-f-10-12-f-12-7]	2.0%	-598.186
[10-f-10-12-f-12-7]	1.0%	-596.231
[f-9-10-12-f-12-7]	1.0%	-593.680
[18-13-7-f-10-12-f]	0.5%	-593.460
[7-f-10-12-7-f-15]	0.5%	-598.821
[10-f-10-12-f-12-15]	0.5%	-595.768

Table 8. Abundance and lowest energy of conformer families of *R,R,S* hexapeptide amide **30**

In the case of hexapeptide **30**, we noticed that about 99% conformations suggested it adopt a 12/10 helical segment in the middle of the sequence. The most abundant 38% conformation [f-f-10-12-10-12-f] is a 12/10-helix with a single free NH at the *C*-terminal. The full right-handed 12/10-helix showed an abundance of 14% and had the lowest energy. The H-bond system [7-f-10-12-10-12-f] displayed a 7/12/10 mixed helix in 29% abundance and had the second lowest energy (Figure 67).

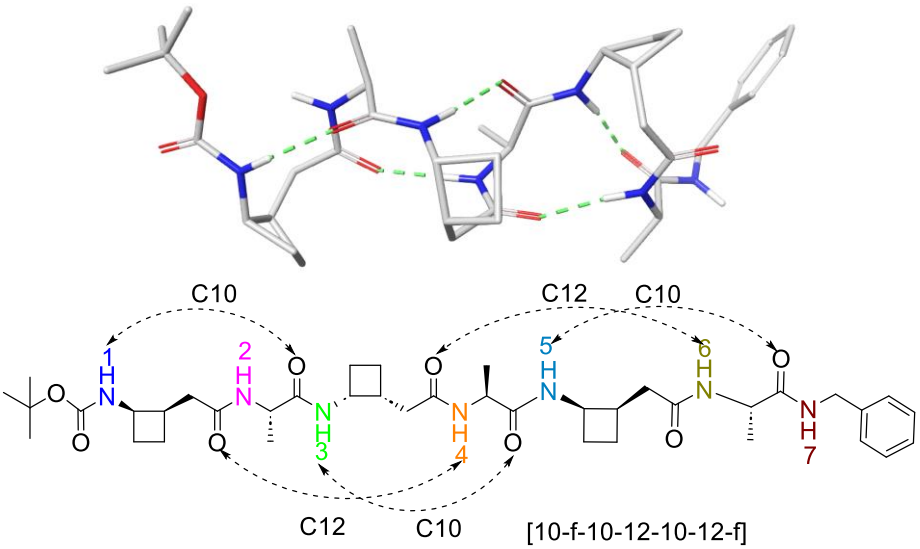

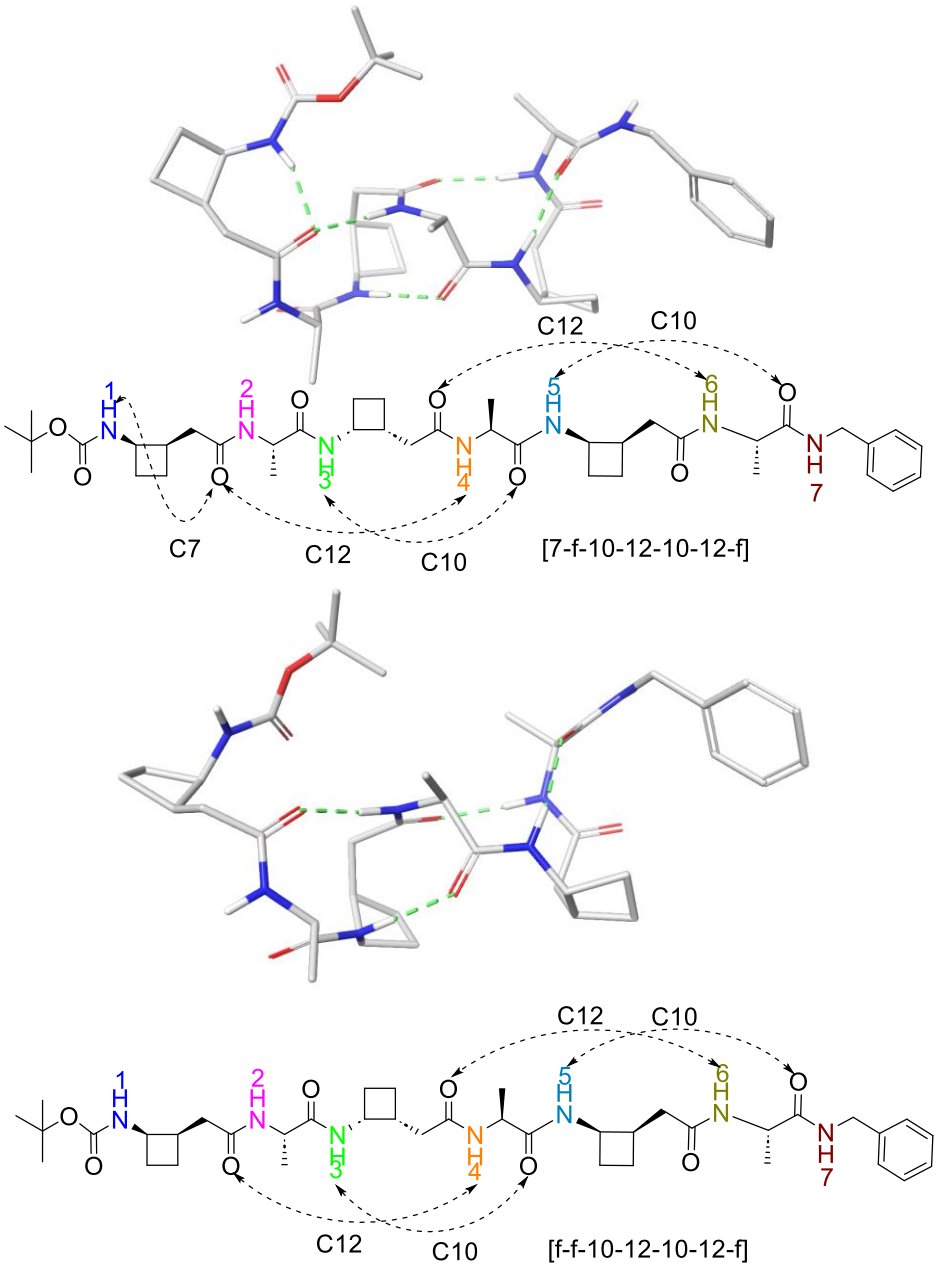

Figure 67. Three lowest energy conformation families found for *R,R,S* hexapeptide amide **30** and their H-bonding patterns

1.3.2.2 Hybrid Monte Carlo Multiple Minima Calculations of *R,R,R* series peptides

*a. Hybrid MCMM conformational search of dipeptide **15***

The conformational search of dipeptide ester Boc-(*R,R*)-*cis*-^{3,4}GABA-(*R*)-Ala-OBn **15** with two amide NHs was performed with a 20 kJ/mol relative energy cut off, 300 conformations were obtained and sorted into four different conformation families (Table 9).

Conformations	Relative abundance of each conformation	The lowest energy conformation
[f-9]	47.0%	–178.096
[f-f]	29.0%	–170.981
[7-f]	23.0%	–168.729
[10-f]	1.0%	–166.215

Table 9. Abundance and lowest energy of conformer families of *R*,*R*,*R* dipeptide ester **15**

The most abundant 47% is a [f-9] conformation implicating NH(2) in a C9 H-bond, and it has the lowest energy. The second most abundant 29% is a free conformation, in which both NHs are non hydrogen-bonded, and it has the second lowest energy. The third most abundant 23% is a [7-f] conformation, in which NH(1) in a C7 H-bond and NH(2) was free (Figure 68).

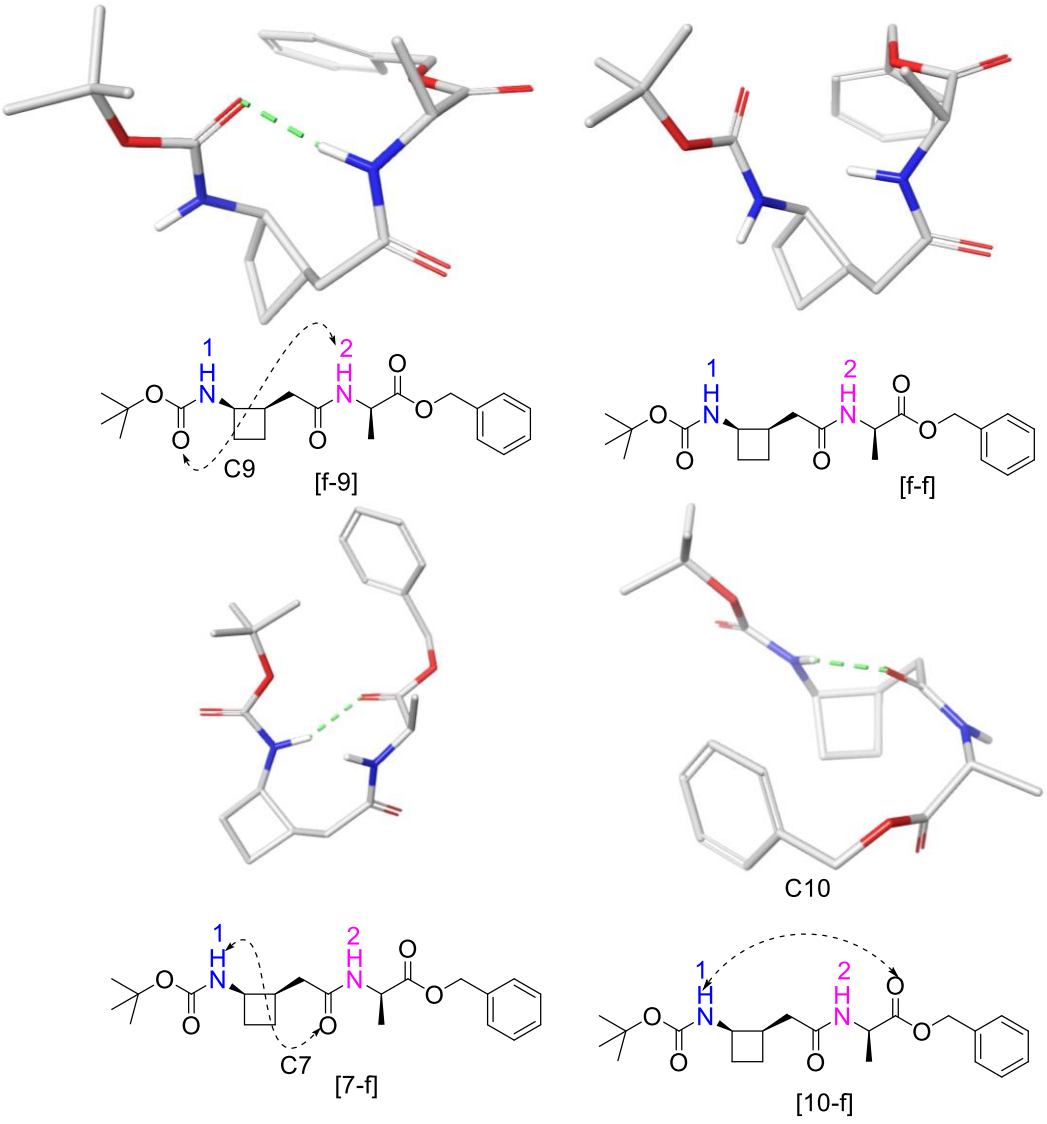

Figure 68. Four lowest energy conformation families found for *R*,*R*,*R* dipeptide ester **15** and their H-bonding patterns

*b. Hybrid MCMM conformational search of dipeptide **17***

The conformational search was carried out on dipeptide amide Boc-(*R*,*R*)-*cis*-^{3,4}GABA-(*R*)-Ala-NHBn **17**, which has three amide NHs. The calculation was performed with a 20 kJ/mol relative energy cut off and afforded 253 conformations that were sorted into seven different conformation families (Table 10).

Conformations	Relative abundance of each conformation	The lowest energy conformation
[f-9-12]	31.0%	–265.445
[f-f-7]	22.0%	–254.505
[f-9-7]	22.0%	–255.764
[7-f-7]	8.0%	–250.706
[f-9-f]	8.0%	–257.809
[f-f-f]	5.0%	–255.166
[f-f-12]	4.0%	–256.182

Table 10. Abundance and lowest energy of conformer families of *R*,*R*,*R* dipeptide amide **17**

The most abundant 31% is a [f-9-12] conformation and it has the lowest energy. The second most abundant 22% are [f-f-7] and [f-9-7] conformers which both of them showed NH(1) was free and NH(3) was engaged in local C7 H-bond. The second lowest energy is a [f-9-f] conformation with 8% abundance (Figure 69).

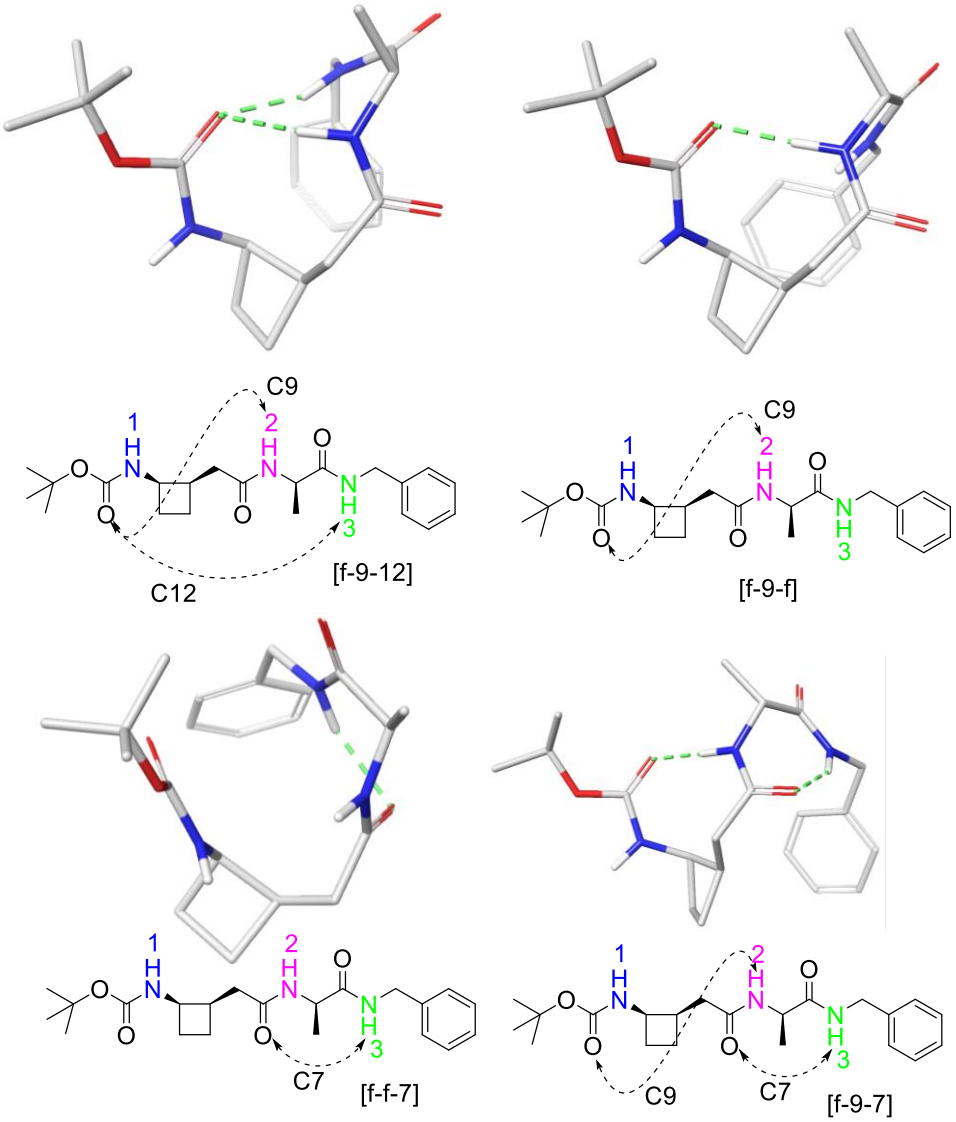

Figure 69. Four lowest energy conformation families found for *R*,*R*,*R* dipeptide amide **17** and their H-bonding patterns

*c. Hybrid MCMM conformational search of tetrapeptide **21***

The conformational search of tetrapeptide ester Boc-[(*R*,*R*)-*cis*-^{3,4}GABA-(*R*)-Ala]$_2$-OBn **21** with four amide NHs was performed with a 20 kJ/mol relative energy cut off. We obtained a total of 423 conformations, which were sorted into eleven different conformation families (Table 11).

Conformations	Relative abundance of each conformation	The lowest energy conformation
[f-f-12-12]	36.0%	–347.982
[f-9-f-12]	24.0%	–339.953
[7-f-10-12]	15.0%	–334.786
[7-f-7-17]	7.0%	–337.215
[7-f-7-12]	5.0%	–334.958
[7-f-f-12]	5.0%	–331.599
[f-9-12-12]	5.0%	–335.530
[f-9-7-12]	1.0%	–331.212
[f-f-f-12]	1.0%	–328.412
[f-9-10-12]	0.5%	–330.097
[f-f-7-9]	0.5%	–329.224

Table 11. Abundance and lowest energy of conformer families of *R,R,R* tetrapeptide ester **21**

At a first overall glance of the conformation families, the first γ-amino acid residue forms diverse H-bonding patterns, whereas 77% of conformers adopt a 12-membered ring system around the second γ-amino acid residue. The most abundant conformation 36% is a left-handed 12-helix [f-f-12-12] and it has the lowest energy. The second most abundant conformation 24% is a [f-9-f-12] structure with a second lowest energy (Figure 70).

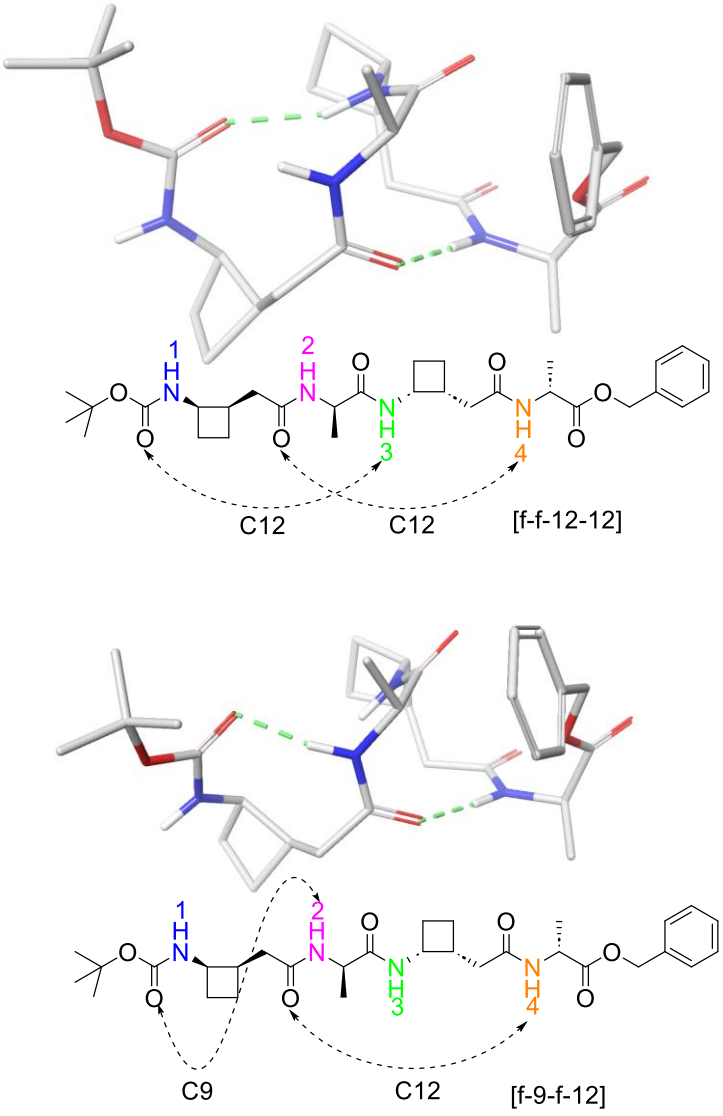

Figure 70. Two lowest energy conformation families found for *R,R,R* tetrapeptide ester **21** and their H-bonding patterns

*d. Hybrid MCMM conformational search of tetrapeptide **23***

The conformational search was carried out on tetrapeptide amide Boc-[(*R*,*R*)-*cis*-^{3,4}GABA-(*R*)-Ala]$_2$-NHBn **23**, which has five amide NHs. The calculations were performed with a 20 kJ/mol relative energy cut off, which gave 240 conformations that were sorted into fourteen different conformation families (Table 12).

Conformations	Relative abundance of each conformation	The lowest energy conformation
[f-f-12-12-12]	31.0%	–436.324
[f-9-f-12-12]	15.0%	–426.285
[f-9-f-12-7]	14.0%	–420.776
[f-f-12-12-7]	12.0%	–425.714
[f-f-12-12-15]	7.0%	–431.108
[7-f-7-17-15]	6.0%	–426.123
[f-9-12-12-15]	4.0%	–421.965
[f-f-12-12-f]	3.0%	–426.917
[f-f-7-17-15]	3.0%	–421.608
[f-9-12-12-12]	1.0%	–421.954
[f-f-12-f-15]	1.0%	–416.898
[f-9-f-12,15]	1.0%	–421.586
[f-9-f-12-f]	1.0%	–419.759
[7-f-7-17-20]	1.0%	–418.530

Table 12. Abundance and lowest energy of conformer families of *R,R,R* tetrapeptide amide **23**

We noticed seven conformation families, with around 70% abundance, in which tetrapeptide **23** adopted at least part of a 12 helical conformation. The most abundant conformation 31% with the lowest energy is the complete left-handed 12-helix [f-f-12-12-12]. The second most abundant conformation 15% is a [f-9-f-12-12] mixed helix, while the second lowest energy conformation is a [f-f-12-12-15] mixed helix, found with 7% abundance (Figure 71).

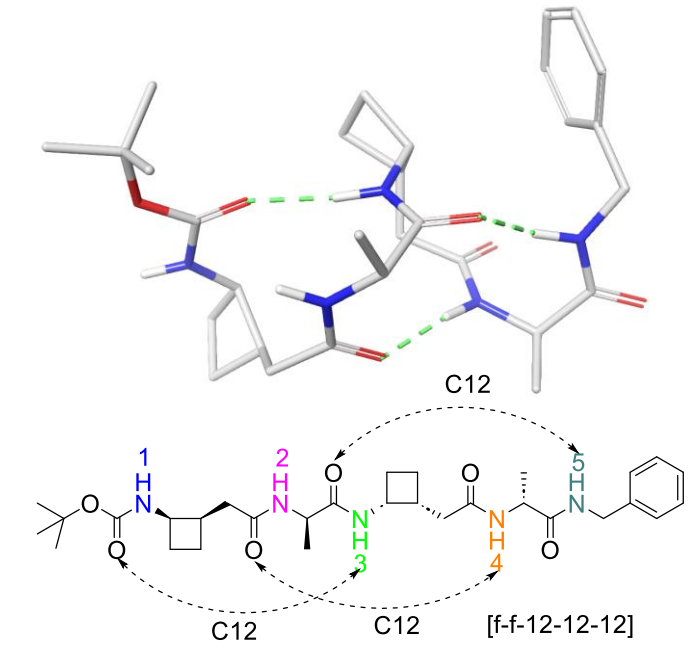
C12
C12
C12
[f-f-12-12-12]

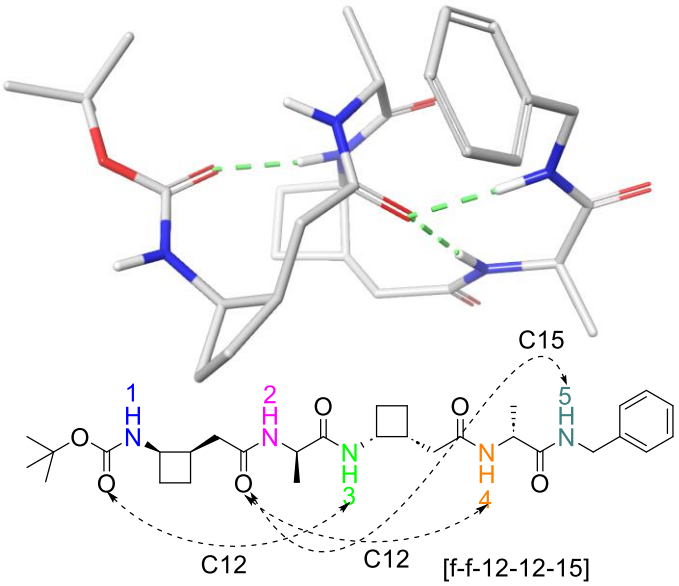
C15
C12
C12
[f-f-12-12-15]

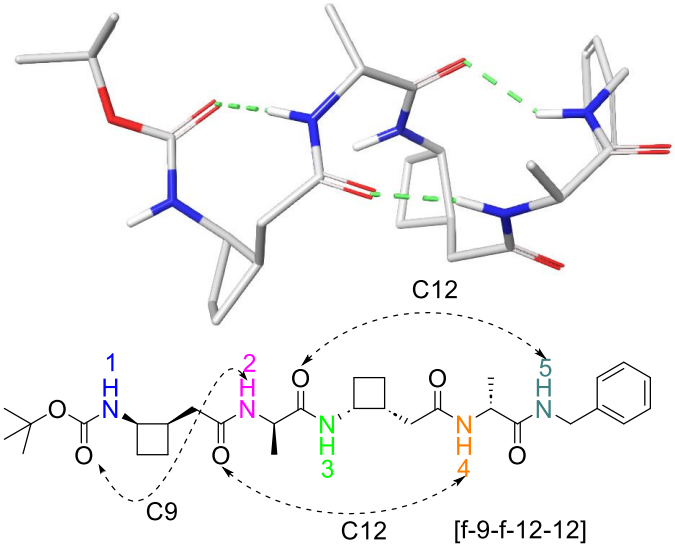
C12
C9
C12
[f-9-f-12-12]

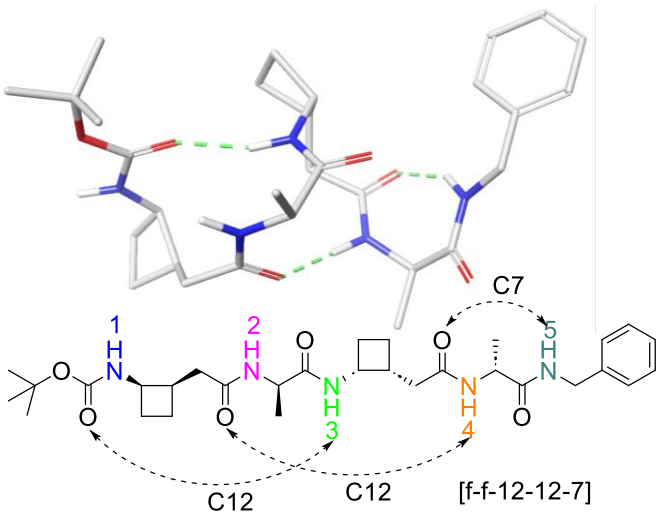

Figure 71. Four conformation family examples found for *R,R,R* tetrapeptide amide **23** and their H-bonding patterns

1.3.2.3 Discussion

The conformational search results of two series peptides showed, their dipeptides adopted different local interactions and non hydrogen-bonded conformers. The *R,R,S* peptides series appeared to be favorable towards the formation of right-handed 12/10-helix conformation, these torsion angel ranges were calculated from the lowest energy 12/10-helix conformation of peptides (**24**, **26**, **29** and **30**) (Table 13, top). The comparison of dihedrals with Hofmann's left-handed 12/10-helix conformer I (middle) is shown in Table 13. The observed torsion angels of *R,R,S* peptides are close to those of Hofmann's theoretical 12/10-helix model. The ability of cyclobutane motif accommodate the small value of θ may be related to its propensity for the 12/10-helix in the γ/α-peptide context, as suggested by Gellman's α/γ-peptides containing cyclic constraint APCH residues that adopt a left-handed 12/10-helix,[116] and its dihedral θ value is also relatively small (Table 13, bottom).

	Peptide residue	ϕ (°)	θ (°)	ζ (°)	ψ (°)
R,R,S peptides right-handed 12/10-helix	γ	+88 ± 6	+11 ± 2	+57 ± 3	–108 ± 8
	α	–65 ± 16			+155 ± 20
Hofmann's left-handed 12/10-helix	γ	–64 ± 1	–32 ± 1	–48 ± 1	+132 ± 5
	α	+68 ± 2			–148 ± 1
Gellman's left-handed 12/10-helix	γ	–90 ± 10	–7 ± 20	–71 ± 9	+140 ± 9
	α	+110 ± 20			–130 ± 10

Table 13. The dihedral angels of *R,R,S* peptides (top), Hofmann's 12/10-helix model (middle) and Gellman's 12/10-helix peptides (bottom)

The *R,R,R* peptides appeared to prefer to fold into a 12-helix conformation (Table 14, top), and the comparison of dihedral angels with Hofmann's 12-helix conformer I is shown (Table 14, middle). The observed torsion angels of *R,R,R* peptides are consistent with those of Hofmann's theoretical 12-helix model. An X-ray diffraction structure of a α/γ-peptide from Gellman adopted a right-handed 12-helix (Table 14, bottom) showed the dihedrals in opposite signs.

	Peptide residue	ϕ (°)	θ (°)	ζ (°)	ψ (°)
R,R,R peptides left-handed 12-helix	γ	+111 ± 16	–33 ± 3	–79 ± 4	+120 ± 10
	α	+80 ± 11			+37 ± 24
Hofmann's left-handed 12-helix	γ	+122 ± 1	–52 ± 1	–63 ± 1	+132 ± 5
	α	+70 ± 2			+29 ± 1
Gellman's right-handed 12-helix	γ	–129 ± 10	+56 ± 3	+55 ± 1	–120 ± 10
	α	–73 ± 18			–33 ± 3

Table 14. The dihedral angels of *R,R,R* peptides (top), Hofmann's 12-helix model (middle) and Gellman's 12-helix (bottom)

According to the precedent work for mixed 12/10-helices,[116,165] the difference in the conformational preferences between *R,R,S* and *R,R,R* peptides series could be explained by the signs of dihedrals ψ and ϕ. If successive ψ/ϕ(i)/ ψ/ϕ(i+1) pairs have the same sign, then the helix has all the H-bonds oriented in the same direction. If the dihedral pairs have opposite signs, then the H-bonding direction is alternated. In *R,R,S* peptides, the dihedral pairs were in opposite signs adopt 12/10-helix, and the *R,R,R* peptides showed the dihedral pairs were in the same sign adopt 12-helix conformation.

Interestingly, the absolute configuration of *cis*-[3,4]CB-GABA γ-residue in peptides appeared to match the conformation preference by changing the sign of torsion angel θ, the *R,R,S* peptides adopted a right-handed 12/10-helix showed the θ torsion angel as +11 ± 2°, the *R,R,R* peptides adopted a left-handed 12-helix showed the θ torsion angel as –33 ± 3°.

In addition, peptides bearing a benzyl amide have an extra NH appeared no influence in the *R,R,S* series, whereas the extra NH in *R,R,R* series contributed to stabilize the 12-helix conformation, or form a local C7 H-bond conformation.

1.3.3 Solution phase NMR studies

1.3.3.1 DMSO-d_6 titration experiments

Due to the low solubility in chloroform of the other peptides, DMSO-d_6 titration experiments were only performed on peptides **18**, **20** and **24** from *R*,*R*,*S* series, and **15**, **17** and **21** from the *R*,*R*,*R* series.

1.3.3.1.1 DMSO-d_6 titration experiments of *R*,*R*,*S* series peptides

*a. NH signal evolution of dipeptide **18***

Results of the DMSO-d_6 titration experiment on *R*,*R*,*S* dipeptide ester **18** are shown in Figure 72. After a total of 25% DMSO addition, two NH signals moved to downfield region ($\Delta\delta$ = 0.54 ppm for NH(1) and $\Delta\delta$ = 0.83 ppm for NH(2)), indicating both NH were partially solvent exposed, excluding strong intramolecular H-bond. These data are in agreement with several conformations (10-f, f-9, 7-f and f-f) present in solution, as suggested by molecular modelling.

	DMSO-d_6 (%, v/v)										
	0	*1*	*2*	*3*	*4*	*5*	*6*	*7*	*9*	*10*	Δδ
δNH1	5.27	5.35	5.42	5.51	5.57	5.62	5.67	5.70	5.76	5.81	0.54
δNH2	6.23	6.35	6.46	6.59	6.68	6.76	6.84	6.89	6.99	7.06	0.83

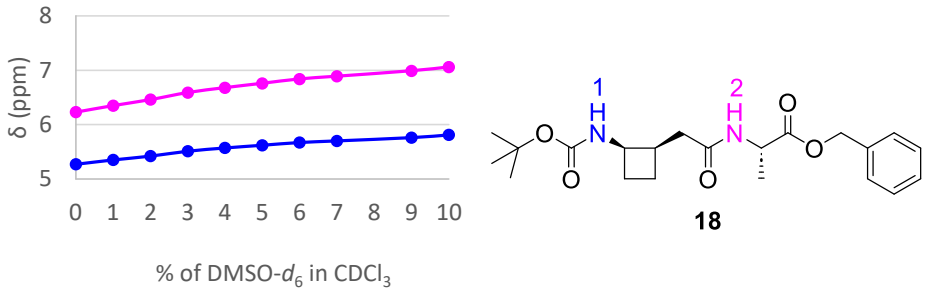

Figure 72. DMSO-d_6 titration of *R*,*R*,*S* dipeptide ester **18**

*b. NH signal evolution of dipeptide **20***

Results of the DMSO-d_6 titration experiment on *R*,*R*,*S* dipeptide amide **20** are shown in Figure 73. After a total of 25% DMSO addition, the three NH signals had moved to a downfield region, showed titration coefficients of $\Delta\delta$ = 0.69 ppm for NH(1), $\Delta\delta$ = 0.74 ppm for NH(2) and $\Delta\delta$ = 0.86 ppm for NH(3) indicating they were at least partially solvent exposed, were with no

particular strong H-bonding in evidence. These data are in agreement with several conformations present in solution, as suggested by molecular modelling.

	DMSO-d_6 (%, v/v)										
	0	*1*	*2*	*3*	*4*	*5*	*6*	*7*	*9*	*10*	Δδ
δNH1	5.17	5.37	5.48	5.58	5.64	5.69	5.72	5.75	5.81	5.86	0.69
δNH2	6.37	6.61	6.75	6.86	6.92	6.97	7.00	7.03	7.07	7.11	0.74
δNH3	6.59	6.88	7.05	7.17	7.22	7.29	7.32	7.36	7.41	7.45	0.86

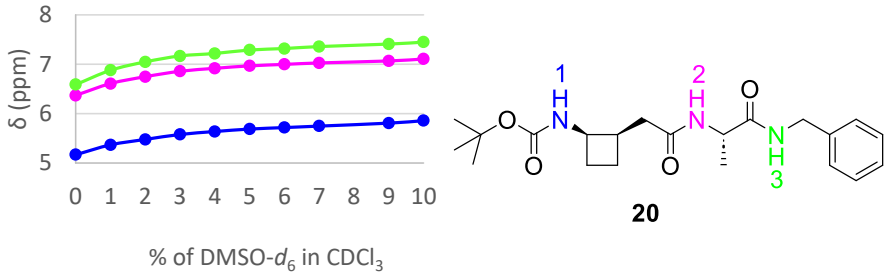

Figure 73. DMSO-d_6 titration of *R*,*R*,*S* dipeptide amide **20**

*c. NH signal evolution of tetrapeptide **24***

Results of the DMSO-d_6 titration experiment on *R*,*R*,*S* tetrapeptide ester **24** are shown in Figure 74. Titration of a $CDCl_3$ solution containing tetrapeptide **24** with DMSO-d_6 induced a downfield shift Δδ = 0.44 ppm for NH(1), suggesting partial solvent exposure. A slightly upfielded shifts for NH(15) and NH(22), reached low coefficients Δδ = –0.13 ppm for NH(3) and Δδ = –0.07 ppm for NH(4) suggesting they were engaged in strong intramolecular H-bonds. These results are compatible with a predominant 12/10-helix conformation present in solution, as suggested by conformational search, in which the NH(2) was non hydrogen-bonded. The NH(2) showed a titration coefficient of Δδ = 0.71 ppm indicating partially solvent exposure, could be engaged in a C9 H-bond, as also had been suggested by molecular modelling.

	DMSO-d_6 (%, v/v)										
	0	*1*	*2*	*3*	*4*	*5*	*6*	*7*	*9*	*10*	Δδ
δNH1	5.52	5.60	5.69	5.75	5.80	5.83	5.87	5.89	5.93	5.96	0.44
δNH2	6.49	6.64	6.79	6.91	6.99	7.04	7.09	7.14	7.18	7.20	0.71
δNH3	7.77	7.76	7.75	7.74	7.73	7.72	7.70	7.69	7.66	7.64	–0.13
δNH4	7.87	7.91	7.94	7.96	7.97	7.97	7.97	7.97	7.95	7.94	–0.07

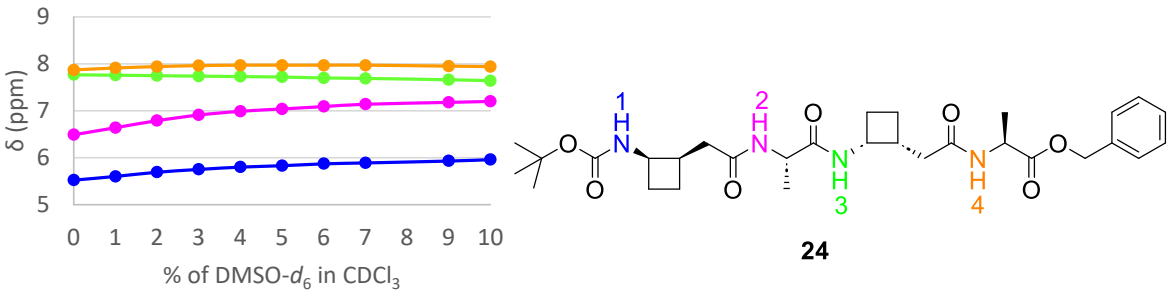

Figure 74. DMSO-d_6 titration of *R*,*R*,*S* tetrapeptide ester **24**

1.3.3.1.2 DMSO-d_6 titration experiments of *R*,*R*,*R* series peptides

*d. NH signal evolution of dipeptide **15***

Results of the DMSO-d_6 titration experiment on *R*,*R*,*R* dipeptide ester **15** are shown in Figure 75. After the addition of 25% of DMSO-d_6, both NH signals moved to a lower field and reached chemical shift changes, $\Delta\delta$ = 0.57 ppm for NH(1) and $\Delta\delta$ = 0.70 ppm for NH(2), pointing out both NH were partially solvent accessible and not strongly implicated in intramolecular H-bonding. These data are compatible with three main conformations (f-9, 7-f and f-f) present in solution, that were suggested by molecular modelling.

	DMSO-d_6 (%, v/v)										
	0	*1*	*2*	*3*	*4*	*5*	*6*	*7*	*9*	*10*	Δδ
δNH1	5.19	5.32	5.39	5.46	5.51	5.56	5.61	5.64	5.71	5.76	0.57
δNH2	6.34	6.49	6.58	6.66	6.73	6.78	6.85	6.90	6.98	7.04	0.70

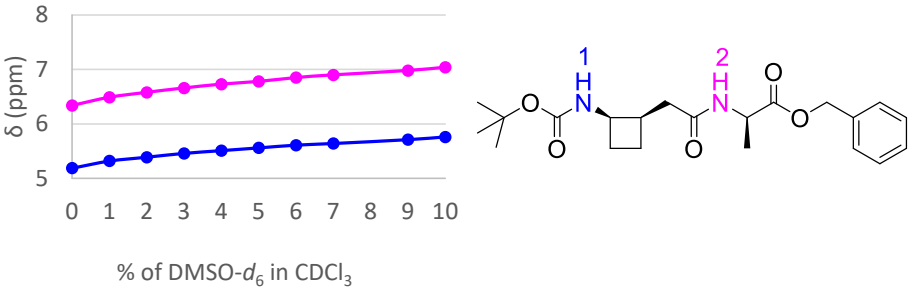

Figure 75. DMSO-d_6 titration of *R*,*R*,*R* dipeptide ester **15**

*e. NH signal evolution of dipeptide **17***

Results of the DMSO-d_6 titration experiment on *R*,*R*,*R* dipeptide amide **17** are shown in Figure 76. After 25% of DMSO was added, the three NH signals had moved to lower field and reached

coefficients of Δδ = 0.66 ppm for NH(1), Δδ = 0.60 ppm for NH(2) and Δδ = 0.72 ppm for NH(3) indicating they were moderate solvent accessible, not implicated in strong H-bonds. These data are in agreement with several conformations present in solution, as suggested by molecular modelling.

	DMSO-d_6 (%, v/v)										
	0	*1*	*2*	*3*	*4*	*5*	*6*	*7*	*9*	*10*	Δδ
δNH1	5.08	5.22	5.34	5.42	5.48	5.55	5.60	5.64	5.68	5.74	0.66
δNH2	6.40	6.55	6.67	6.76	6.82	6.88	6.92	6.94	6.97	7.00	0.60
δNH3	6.71	6.88	7.04	7.14	7.20	7.27	7.33	7.36	7.39	7.43	0.72

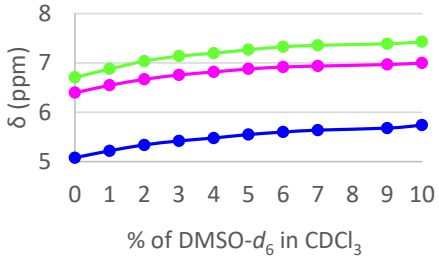

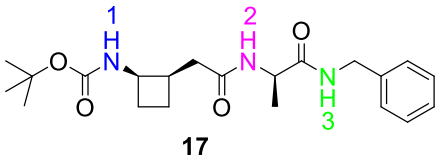

17

Figure 76. DMSO-d_6 titration of *R*,*R*,*R* dipeptide amide **17**

*e. NH signal evolution of tetrapeptide **21***

Results of the DMSO-d_6 titration experiment on *R*,*R*,*R* tetrapeptide ester **21** are shown in Figure 77. We observed that 25% of DMSO addition induced negligible downfield shift (Δδ = 0.12 ppm) for NH(3) suggesting no solvent exposure and it was involved in a strong intramolecular H-bonding, compatible with its implication in a 12-membered H-bond. Other three NH signals moved to lower field reached coefficients of Δδ = 0.54 ppm for NH(1), Δδ = 0.60 ppm for NH(2) and Δδ = 0.57 ppm for NH(4) indicating they were moderately solvent exposed. These data are compatible with several conformations present in solution, as suggested by molecular modelling.

	DMSO-d_6 (%, v/v)										
	0	*1*	*2*	*3*	*4*	*5*	*6*	*7*	*9*	*10*	Δδ
δNH1	5.24	5.36	5.46	5.50	5.55	5.60	5.64	5.69	5.74	5.78	0.54
δNH2	6.25	6.41	6.54	6.59	6.64	6.69	6.73	6.77	6.82	6.85	0.60
δNH3	7.58	7.64	7.68	7.69	7.71	7.72	7.72	7.72	7.71	7.70	0.12
δNH4	6.71	6.85	6.96	7.01	7.06	7.11	7.15	7.19	7.24	7.28	0.57

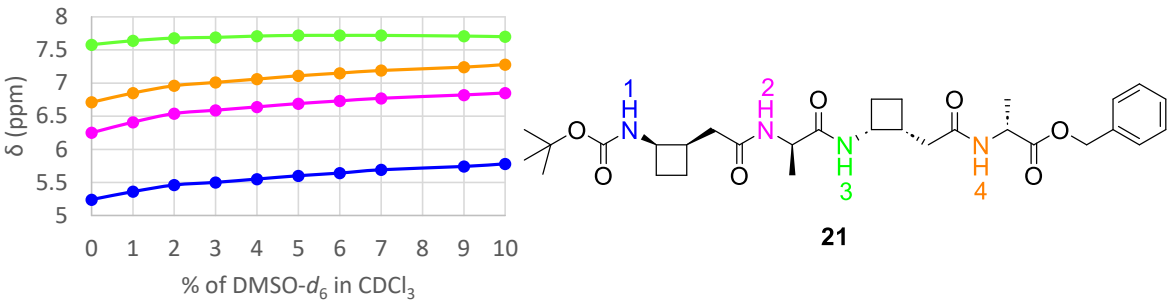

Figure 77. DMSO-d_6 titration of *R*,*R*,*R* tetrapeptide ester **21**

1.3.3.2 ^{1}H-^{1}H ROESY 2D NMR experiments

1.3.3.2.1 ^{1}H-^{1}H ROESY 2D NMR experiments in $CDCl_3$

2D NMR experiments in $CDCl_3$ were performed for peptides **15**, **17**, **18**, **20**, **21** and **24**. However, the other peptides **23**, **26**, **29** and **30** were too poorly soluble in $CDCl_3$ to be able to conduct ROESY experiments. Among all the observed ROE correlations, only the significant ones are presented in Figure 78 (solid arrows indicate strong correlations, and the dashed arrows indicate weaker ones).

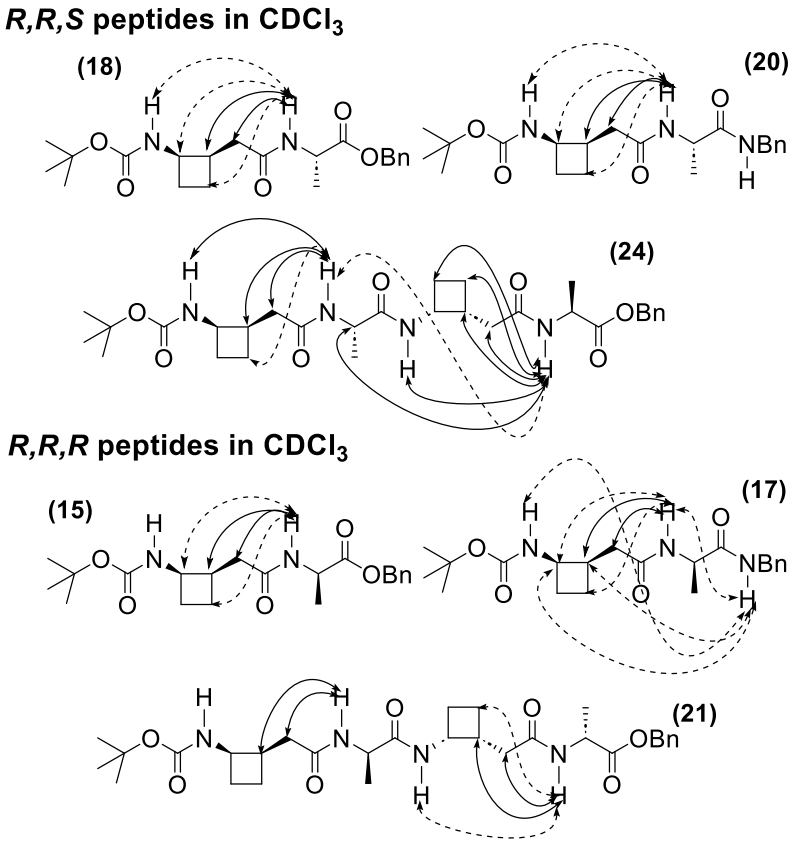

Figure 78. ROE correlations of several γ/α-hybrid peptides in $CDCl_3$

1.3.3.2.3 ^{1}H-^{1}H ROESY 2D NMR experiments of *R,R,S* series peptides in pyridine-d_5

We performed ^{1}H-^{1}H ROESY 2D NMR experiments of γ/α-hybrid peptides of the *R,R,S* series **18**, **20**, **24**, **26**, **29** and **30** in pyridine-d_5. Among the observed ROE correlations, the most significant ones are presented in Figure 79 (solid arrows indicate strong correlations, dashed arrows indicate weaker ones).

Upon comparing the consistent correlation maps of peptides **18**, **20** and **24** in $CDCl_3$ and in pyridine-d_5, we deduced that the conformational preferences of peptides did not appear to be influenced by the solvent switch.

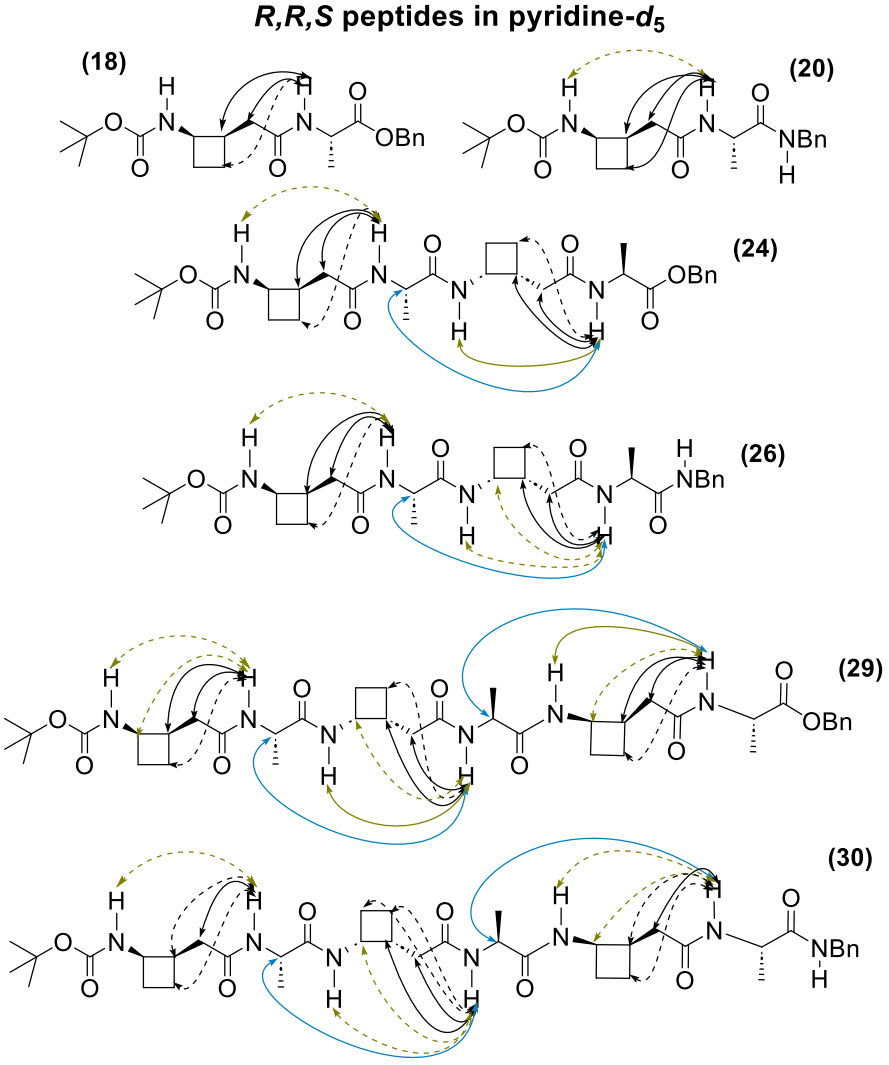

Figure 79. ROE correlations of *R,R,S* peptides in pyridine-d_5

The pale-yellow correlations showed interactions of the NH of each α-residue (i) with the NH and the Hγ of each γ-residue (i-1) which is indicative of C10 H-bonds. This correlation was reported previously in the literature for APCH derived α/γ-hybrid peptides that adopted a 12/10-helix conformation (Figure 80).[116] Other black correlations showed interactions of the

NH of each α-residue (i) with the Hα and Hβ of each γ-residue (i-1) indicating regular behavior. Without being diagnostic, such correlations are compatible with the presence of C10 H-bonds.

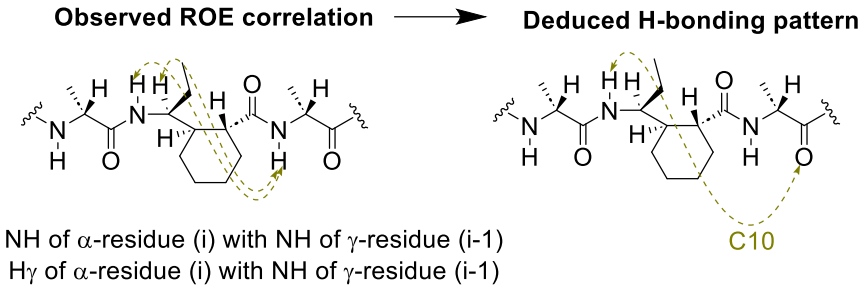

Figure 80. Previously observed ROE correlation indicative of a C10 H-bonded conformer

The blue arrows showed the ROE correlation of the NH of α-residue (i) with the Hα of α-residue (i-2) are in agreement with C12 H-bonds. This interaction was reported previously in the literature for α/γ-hybrid peptides containing C-linked carbo-γ-amino acids (Figure 81, top)[115] and the literature for APCH derived α/γ-hybrid peptides (Figure 81, bottom)[116] that showed a C12 H-bonded ring as part of a 12/10-helix conformation.

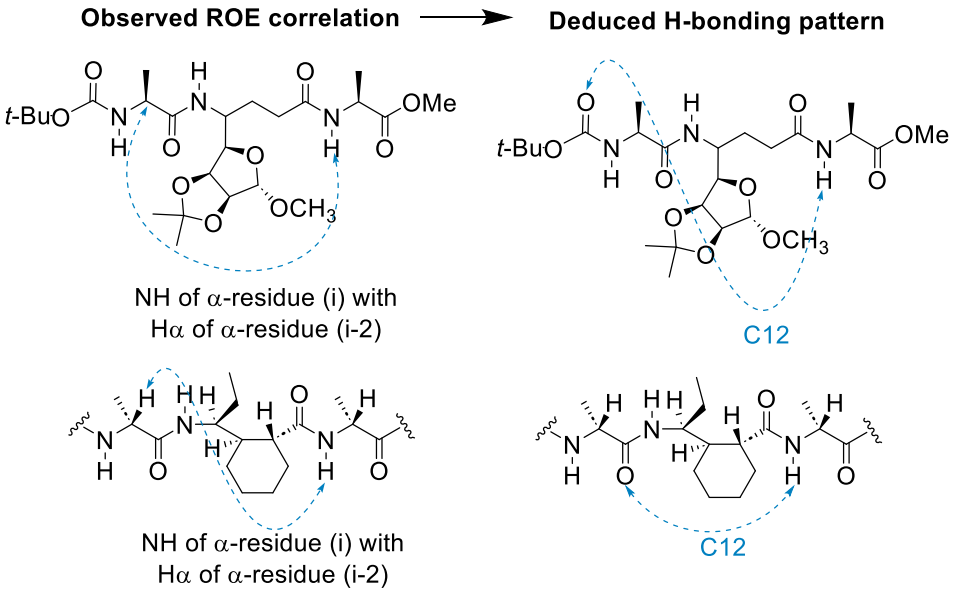

Figure 81. Previously observed ROE correlations indicative of a C12 H-bond in a 12/10-helix conformer

The dipeptides **18** and **20** show no clear-cut indication of C10 conformations in solution, in agreement with the molecular modelling. On the other hand, the correlation maps of *R,R,S* peptides **24**, **26**, **29** and **30** are consistent with the preference of a predominant 12/10-helix conformation in solution (Figure 82).

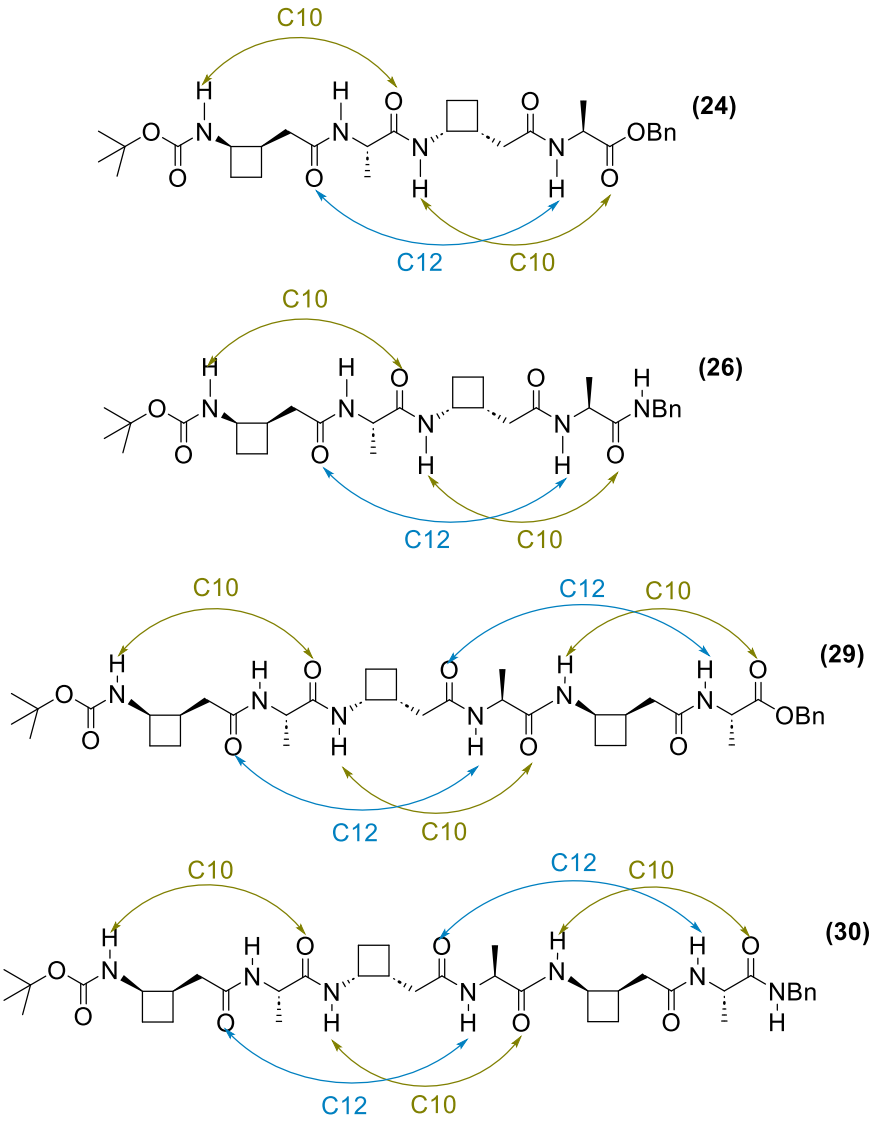

Figure 82. Alternating 12/10 helical conformation adopted by *R,R,S* peptides

1.3.3.2.3 ^{1}H-^{1}H ROESY 2D NMR experiments of *R,R,R* peptides in pyridine-d_5

2D ROESY NMR experiments of four *R,R,R* peptides **15**, **17**, **21** and **23** were performed in pyridine-d_5. Among the observed ROE correlations, only the significant ones are presented in Figure 83 (solid arrows indicate strong correlations, dashed arrows indicate weaker ones). Comparison with the ROESY correlations obtained for peptides **15**, **17** and **21** in $CDCl_3$, suggested no apparent influence of the solvent switch.

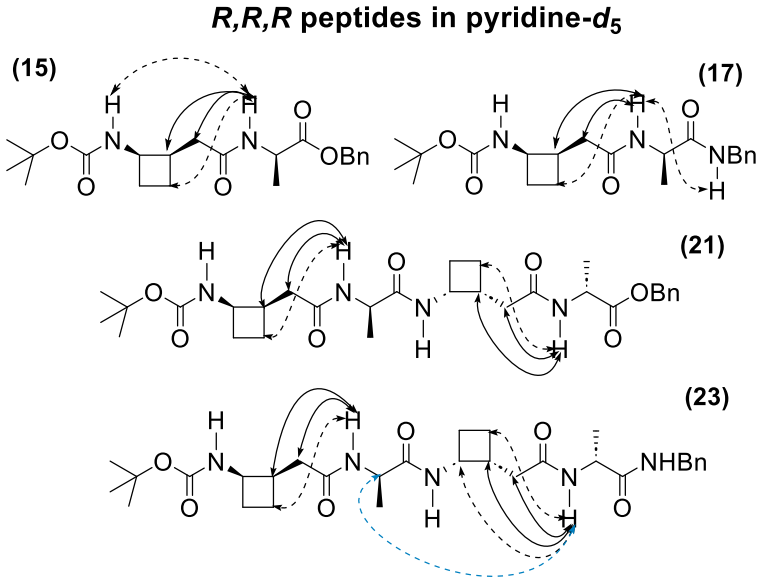

Figure 83. ROE correlations of *R,R,R* peptides in pyridine-d_5

These significant ROE correlations implicate the interactions of the NH of each α-residue (i) with the Hα and Hβ of each γ-residue (i-1). These correlations could be explained in terms of C10, C9, or C7 H-bonds, suggested regular behavior, without being diagnostic. In tetrapeptide **23**, the weak correlation of the NH of α-residue (i) with the Hα of α-residue (i-2) was in agreement with a C12 H-bonded ring. The correlation maps of *R,R,R* peptides **15**, **17**, **21** and **23** appeared to show no clear-cut in preference for a particular conformation in solution.

1.3.3.3 Discussion

DMSO-d_6 titration and 2D ROESY NMR experiments showed no clear-cut indication for a particular conformational preference for *R,R,R* series peptides, with no evidence for them to fold into a 12/10-helix, nor the 12-helix as suggested by molecular modelling.

In *R,R,S* series peptides, from NMR results, it is difficult to assign their particular conformational preference for short dipeptides **18** and **20**, as had been suggested by molecular modelling. However, the conformation landscape appeared to be clearer starting from tetrapeptides. DMSO-d_6 titration results suggested tetrapeptide **24** adopts a predominant 12/10-helix conformation, ROE NMR correlations of peptides **24**, **26**, **29** and **30** showed consistent correlation map and assignments suggesting their conformation for a 12/10-helix.

1.3.4 Solution phase infrared spectroscopy studies

In this section, we will describe the solution phase infrared studies of the ten selected γ/α-hybrid peptides. Depending on their solubility, solutions were prepared in a range of 1 mM to 5 mM concentration in chloroform.

1.3.4.1 Solution phase IR of *R,R,S* peptides

Each of the six *R,R,S* peptides **18**, **20**, **24**, **26**, **29** and **30** showed two bands in the NH stretch region. A sharp band located at 3442 cm^{-1} corresponded to free NHs, and a broad band from 3250 to 3360 cm^{-1} was indicative of hydrogen-bonded NHs (Figure 84).

The bands at 3250 to 3360 cm^{-1} of dipeptides **18** and **20** were broad and flat, and their intense bands at 3442 cm^{-1} may suggest their dominant feature was a free conformation. The tetrapeptide ester **24** showed a broad shoulder at around 3300 cm^{-1}, centered at 3330 cm^{-1}. This may be due to the NH protons of its first γ-amino acid residue was involved in different H-bonds, such as NH(2) was in a C9 H-bond, and the rest peptide residues in a 12/10-helix, as suggested by molecular modelling. The tetrapeptide amide **26** showed an intense at around 3300 cm^{-1} was more red-shifted than the broad band of tetrapeptide ester **24**, and free NH band of the former was more intense than the latter, this could be due to the extra NH of tetrapeptide amide **26** at *N*-terminal was free, and other NHs were in a 12-10 H-bonding system. The hexapeptides **29** and **30** showed intense bands at around 3295 cm^{-1}, consistent with a predominant 12/10-helix conformation. A tiny band at 3413 cm^{-1} of the hexapeptide amide **30** may implicating the *N*-terminal NH was engaged in a C5 H-bond.

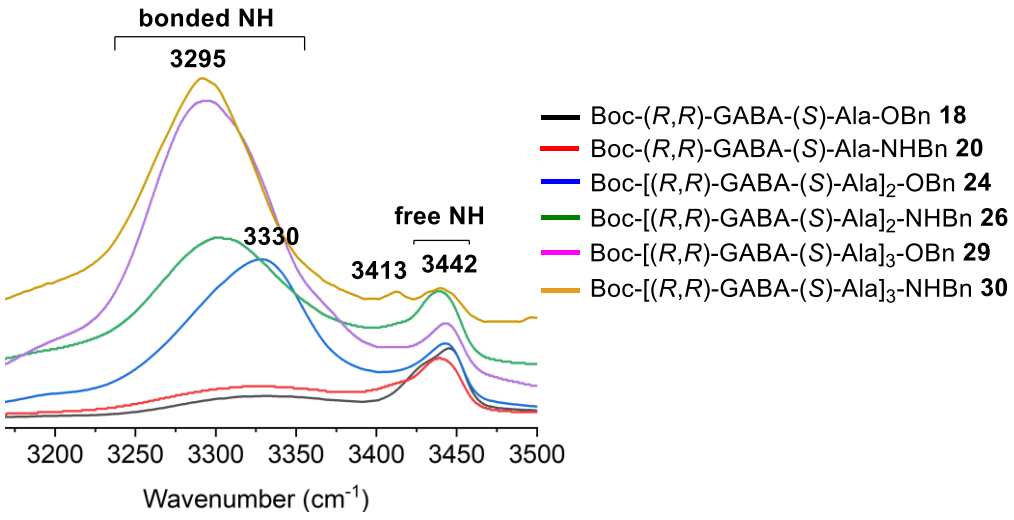

Figure 84. Superimposition of the IR spectra of *R,R,S* peptides in the N–H stretching region

1.3.4.2 Solution phase IR of *R,R,R* peptides

At first glance, the four *R,R,R* hybrid peptides **15**, **17**, **21** and **23** displayed the same general NH features in the stretch regions. A fairly sharp band located at 3443 cm^{-1} corresponded to free NHs, and a broad band from 3270 to 3360 cm^{-1} was indicative of hydrogen-bonded NHs (Figure 85).

In dipeptide **15**, one band at 3300 cm^{-1} indicating H-bonded NH, but the intense band at 3443 cm^{-1} may suggest its dominant feature was a free conformation. The bands from 3270 to 3360 cm^{-1} of dipeptides **17** and of tetrapeptide **21** are very broad, may suggested that multiple types of H-bonds were overlapped in this region, possibly including C9 H-bond (around 3340 cm^{-1})[166], C10 H-bond (around 3300 cm^{-1})[70] or C12 H-bond (3300-3330 cm^{-1}) [167,168], and it was challenging to assign their conformations. The IR spectrum of tetrapeptide **23** showed an intense band located at 3332 cm^{-1} may correspond to NH engaged in 12-membered H-bonds.

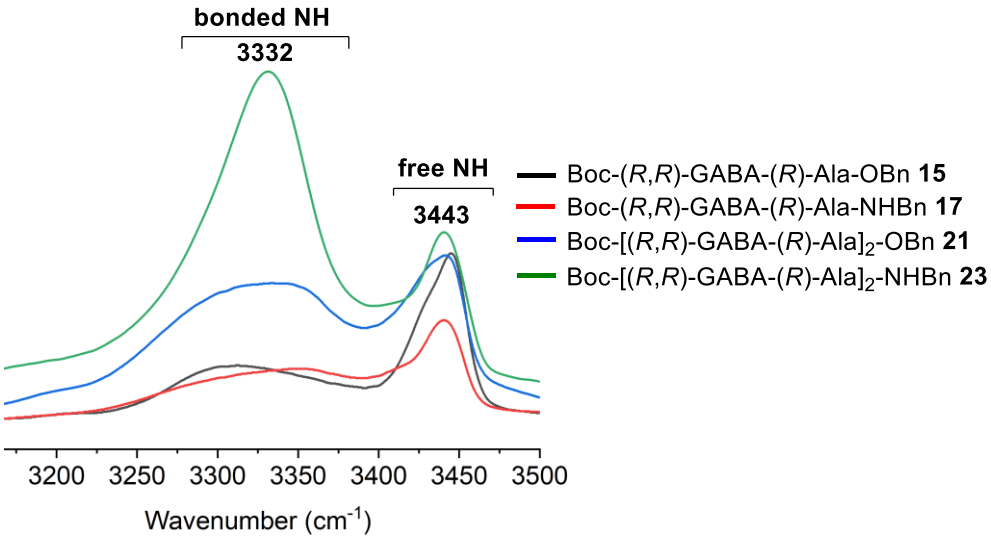

Figure 85. Superimposition of the IR spectra of *R,R,R* peptides in the N–H stretching region

1.3.5 X-ray diffraction experiments

We obtained single crystals of peptides **17**, **18**, **20** and **24**, their structural analyses were performed via X-ray diffraction.

1.3.5.1 X-ray diffraction of dipeptide **18**

A crystal structure of dipeptide Boc-(*R*,*R*)-*cis*-^{3,4}GABA-(*S*)-Ala-OBn **18** was obtained by slow evaporation of a dichloromethane solution at ambient temperature. The X-ray diffraction structure is shown in Figure 86. The structure shows only intermolecular H-bonds, in which

two amide NH form H-bonds with two carbonyl oxygens of a neighboring second molecule, respectively.

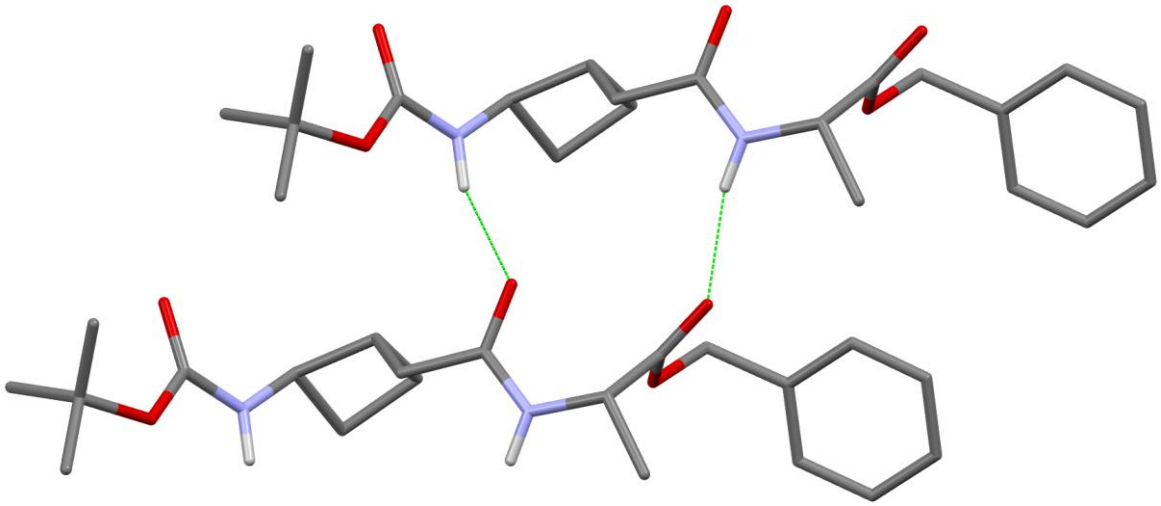

Figure 86. X-ray diffraction crystal structure of *R*,*R*,*S* dipeptide ester **18**

1.3.5.2 X-ray diffraction of dipeptide **20**

A crystal structure of dipeptide Boc-(*R*,*R*)-*cis*-^{3,4}GABA-(*S*)-Ala-NHBn **20** was obtained by slow evaporation of a methanol solution at ambient temperature, the X-ray diffraction structure is shown in Figure 87. The structure involves only intermolecular H-bonds, in which NH(1), NH(2) and NH(3) were engaged in H-bonds with carbonyl oxygens of a neighboring molecule, respectively.

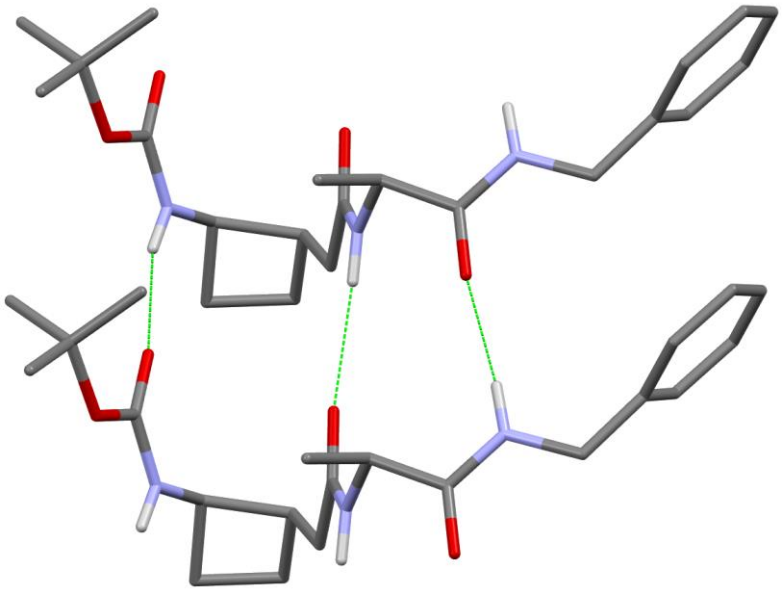

Figure 87. X-ray diffraction crystal structure of *R*,*R*,*S* dipeptide amide **20**

1.3.5.3 X-ray diffraction of tetrapeptide **24**

A crystal structure of tetrapeptide Boc-[(*R*,*R*)-*cis*-^{3,4}GABA-(*S*)-Ala]$_2$-OBn **24** was obtained by slow evaporation of an ethanol solution at ambient temperature, the X-ray diffraction structure is shown in Figure 88. The structure shows only intermolecular H-bonds, in which four NHs form H-bonds with carbonyl oxygens of a neighboring molecule, respectively.

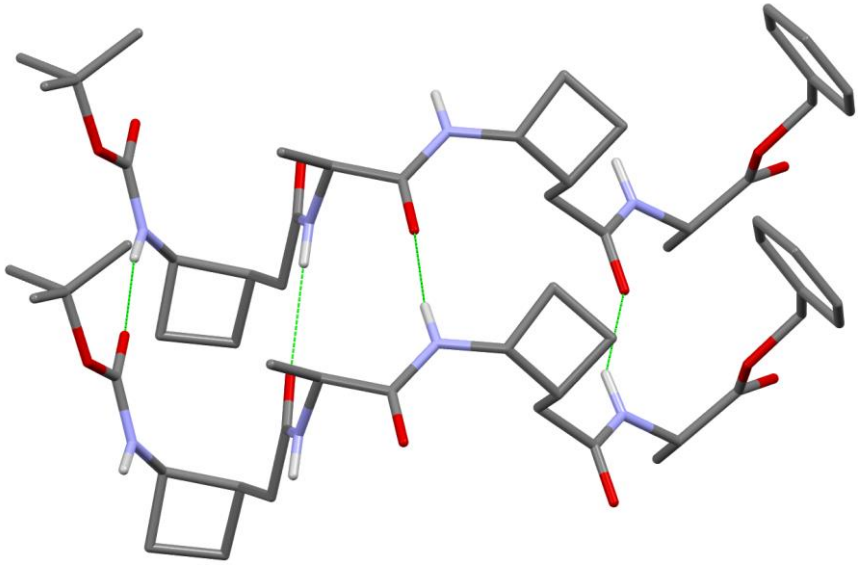

Figure 88. X-ray diffraction crystal structure of *R*,*R*,*S* tetrapeptide ester **24**

1.3.5.4 X-ray diffraction of dipeptide **17**

A crystal structure of dipeptide Boc-(*R*,*R*)-*cis*-^{3,4}GABA-(*R*)-Ala-NHBn **17** was obtained by slow evaporation of a dichloromethane solution at ambient temperature. The X-ray diffraction structure is shown in Figure 89, which displays only intermolecular H-bonds, three NHs form H-bonds with carbonyl oxygens of a neighboring molecule, respectively.

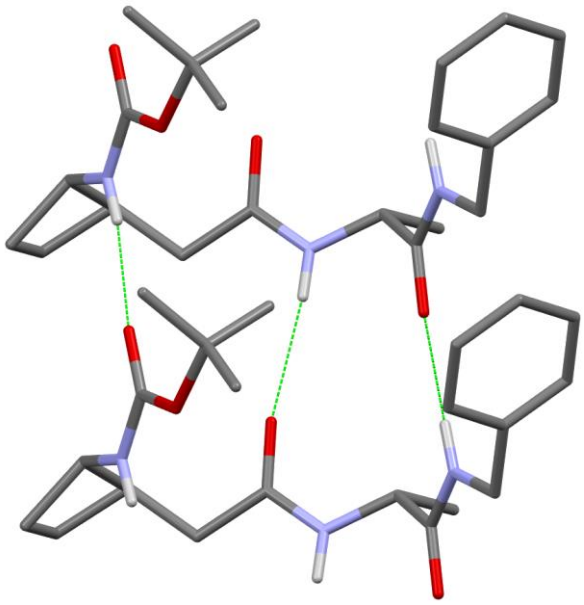

Figure 89. X-ray diffraction crystal structure of *R*,*R*,*R* dipeptide amide **17**

1.3.5.5 Discussion

In crystal structures, four peptides showed only intermolecular H-bonds, exhibiting sheet-like conformations. Compared to the dihedrals θ (+22°) of Boc-*cis*-^{3,4}CB-GABA-OBn, these crystal peptides appeared to maintain dihedral θ, no matter of the residues connected (Table 15).

	Peptide residue	ϕ (°)	θ (°)	ζ (°)	ψ (°)
Peptide **18**	γ	+93	+20	+170	–134
	α	–57			–41
Peptide **20**	γ	+99	+25	–85	+171
	α	–122			+122
Peptide **24**	γ	+103	+23	–81	+165
	α	–116			+127
	γ	+79	+22	+174	–119
	α	–123			+42
Peptide **17**	γ	+108	+22	–81	+165
	α	+143			–129
Boc-*cis*-^{3,4}CB-GABA-OBn	γ	+100	+22	+167	–153

Table 15. Dihedrals of the crystal structures of peptides and Boc-*cis*-^{3,4}CB-GABA-OBn

1.4 Conclusion and Perspectives

Collectively, twelve γ/α-hybrid peptides were successfully synthesized in solution phase using a convergent synthetic strategy in this chapter. The conformational behavior of γ/α-hybrid peptides alternating (*R*,*R*)-*cis*-^{3,4}CB-GABA and either (*R*) or (*S*)-alanine, both diastereomeric combinations *R,R,R* and *R,R,S* peptides were studied. The *R,R,R* peptides series did not receive enough data to support the conformational preference due to the lack of solubility of hexapeptides **27** and **28**. However, based on the data at hand, no evidence for a 12/10-helix. They showed no clear-cut preference for a particular conformation in solution. One crystal structure of dipeptide **17** was obtained, only intermolecular H-bonds were observed. The *R,R,S* peptides series appeared to be good examples for the formation of right-handed 12/10-helix, consistent with Hofmann's 12/10-helix model. Solution phase IR and NMR experimental results were in agreement with a 12/10-helix conformation in solution, as had been suggested by molecular modelling. In solid state, crystal structures of peptides **18**, **20** and **24** were obtained, showed only intermolecularly H-bonded, exhibiting sheet-like conformations.

This work provided a new case of γ/α-hybrid peptides that can fold into 12/10-helix conformation. The results of two diastereomeric combinations *R,R,R* and *R,R,S* peptides proved the importance of dihedrals cooperation of each residue for the helical structure formation. The conformational results of *R,R,S* peptides appeared to show that longer peptide

chain, more likely to fold into 12/10-helix conformation, further work may be interesting to extend the peptide chain of *R,R,S* series to octapeptides or decapeptides, and study their conformational behavior in longer peptides. The solubility of *R,R,R* series peptides hampered their conformational studies, to solve the solubility problem, it may be plausible to do modifications on the residues, and then study their conformational preference.

Chapter 2. Synthesis and conformational studies of cyclic α-amino acid Aatc and derivatives

Chapter 2. Synthesis and conformational studies of cyclic α-amino acid Aatc and derivatives

2.1 Introduction

2.1.1 The C5 interaction and the 2.0_5-helix conformation

As we saw in the general introduction, the intra-residue C5 interaction is one of the less common N–H···O=C H-bonds that accompany other non-covalent interactions in proteins, but may be important for the stabilization of secondary structures.[26] In principle, successive C5 H-bonds in a peptide backbone form may stabilize an extended conformation, but this structure is adopted by very few synthetic peptides that rely essentially on steric constraints to do so.[138,169] It is of note that oligomers of less voluminous α,α-disubstituted amino acids, such as Aib[170,171] or its carbocyclic analogues Acnc,[172–174] have a strong preference to adopt 3_{10}-helix structures (Figure 90).

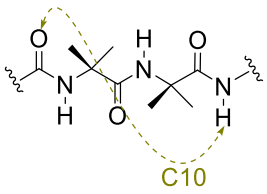

Figure 90. The H-bonding pattern of a 3_{10}-helix in Aib derivative

α,α-Disubstituted amino acids in which at least one (but usually both) of the alkyl or aryl hydrocarbon side chains have two or more carbons such as Deg, Dp_ng and Db_zg moieties, are the most propitious for the adoption of 2.0_5 helical conformations in homo-oligomers (Figure 91).[175]

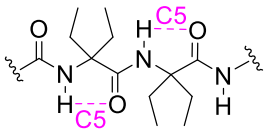

Figure 91. The H-bonding pattern of a 2.0_5-helix in Deg derivative

2.1.2 Cyclic α,α-disubstituted α-amino acid derivatives

For oligomers of cyclic Aib derivatives, the influence of a side chain hetero atom specifically at the γ-position (using the α-amino acid nomenclature) on the conformational preferences has been observed on several occasions.[176]

In 2007, the white group showed a crystal structure of a ribose-derived pentapeptide, in which a fully extended 2.0_5-helix was in evidence. Each C5 interaction was accompanied by a C6γ N–H···O(acetal) H-bond implicating the ring oxygen of each residue (Figure 92).[177]

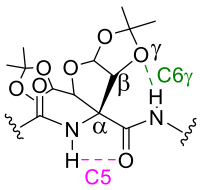

Figure 92. The H-bonding pattern of a ribose-derived amino acid

In 2010, the Aida group reported the conformational preference of a 4-aminopiperidine-4-carboxylic acid (Api) derived octapeptide. When protonated, the octapeptide showed a helical conformation. However, In basic solution the oligomers were devoid of H-bonds along the peptide backbone, and it was suggested that the free amine of piperidine group might form a C7δ H-bond with the backbone amide NH and hamper the helix formation, although no role was indicated for an intra-residue C5 H-bond (Figure 93).[178]

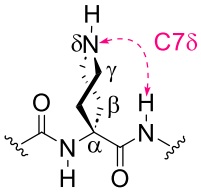

Figure 93. The H-bonding pattern of the Api derived peptide when in basic solution

In 2014, the Mangelinckx group presented the synthesis and conformational study of short peptides containing *N*-substituted 3-aminoazetidine-3-carboxylic acids [Aatc(R), R = *t*-Bu or *t*-Amyl]. The tripeptides Cbz-Aatc(*t*-Bu)-Ala-Ala-OMe (**A**) and Cbz-Ala-Aatc(*t*-Bu)-Ala-OMe (**B**) adopt the major conformation of a β-turn, a C10 H-bond formed between the carbonyl oxygen of the Cbz group and the third amide NH. It was also proposed, a sidechain to mainchain C6γ N–H···N H-bond was also present, which formed between amide NH of the alanine moiety and the nitrogen atom of the azetidine residue, and this C6γ H-bond stabilized the β-turn conformation (Figure 94).[179]

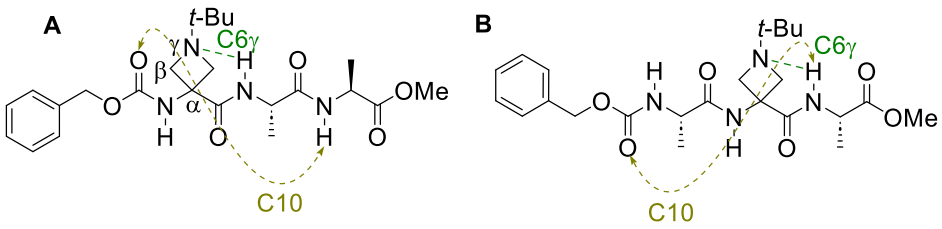

Figure 94. H-bonding patterns in the peptides **A** and **B**

In 2020, the host group conducted the conformational studies of cyclic α-amino acid derivatives containing the 3-aminothietane-3-carboxylic acid (Attc) residue. The sulfur atom from the Attc residue formed an inter-residue C6γ H-bond that stabilized a weak intra-residue C5 H-bond in the peptide backbone. The consecutive C5-C6γ H-bonding features exhibited an extended conformation in the monomer Cbz-Attc-NHMe and dimer Cbz-(Attc)$_2$-NHMe, as suggested by infrared both in gas and solution phases (Figure 95).

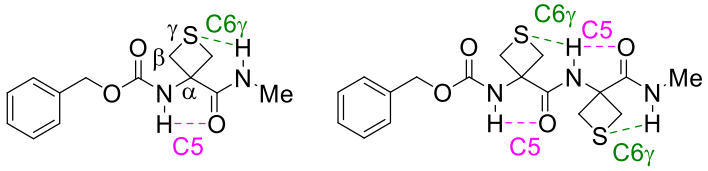

Figure 95. The H-bonding patterns of the extended conformation in Cbz-Attc-NHMe and Cbz-(Attc)$_2$-NHMe

In the trimer Cbz-(Attc)$_3$-NHMe, gas and solution phases infrared spectroscopy suggested a semi-extended form, in which a C5-C6γ H-bonding feature was replaced by a π_{am} interaction (Figure 96).

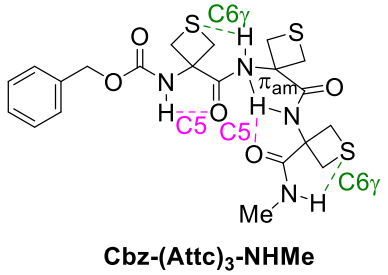

Figure 96. The H-bonding pattern of the semi-extended conformation in Cbz-(Attc)$_3$-NHMe

As a follow-up, in 2021, the strength of different N–H···X inter-residue H-bond for the stabilization of the C5 H-bond was studied in a series of 4-membered ring amino acids.[154] The Cbz-Aatc(Me)-NHMe (Figure 97) displayed an N–H···N H-bond that stabilized the C5 interaction in the backbone; the strength of the N–H···N C6γ H-bond was apparently stronger than that of the N–H···S C6γ H-bond in Cbz-Attc-NHMe (Figure 95).

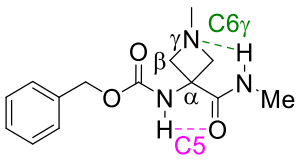

Figure 97. H-bonding pattern of the extended conformation in the Cbz-Aatc(Me)-NHMe **42**

2.1.3 Aim of this chapter

On the basis of these observations, we decide to examine short oligomers of the Aatc(Me) motif in the search for successive C5-C6γ H-bonding features to promote fully extended conformation that correspond to 2.0_5-helix structures (Figure 98).

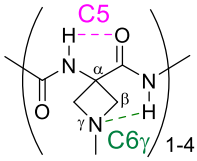

Aatc(Me) derivatives

Figure 98. Aatc(Me) derivatives for conformation studies in this chapter

2.2 Synthesis of Aatc(Me) derivatives **42**, **44**, **46** and **48**

In this section, a post-synthetic modification strategy[180] was employed for preparation of Aatc(Me) derived homo-oligomers, from monomer to tetramer, each derivative was required in free-amine form, with a simple methylamide cap at the *C*-terminal and a Cbz group at the *N*-terminal. The peptide synthesis was performed in solution phase, equimolar quantities of each Aatc-derived substrate were used in each chain-lengthening step, then deprotection was followed by final-step methylation of all the free-amine residues present in the oligomer.

2.2.1 Preparation of Cbz-Aatc(Boc)-NHMe **34**

Following the work of Dr. Zeynab Imani[9], our strategy for the synthesis of Cbz-Aatc(Boc)-NHMe **34** began with commercial H-Aatc(Boc)-OH **32** (Scheme 29). The free amine of the H-Aatc(Boc)-OH **32** was protected using 1.5 equivalents of benzyl chloroformate (0.5 eq. CbzCl was added every 24 hours) in the presence of 4.5 equivalents of sodium carbonate (Na_2CO_3) over three days at room temperature. After workup and purification by column chromatography Cbz-Aatc(Boc)-OH **33** was obtained in 93% yield.

Cbz-Aatc(Boc)-OH **33** was coupled with methylamine using isobutyl chloroformate (IBCF) in the presence of *N*-methylmorpholine (NMM). A large excess of methylamine (10 eq.) was employed to ensure the complete transformation of Cbz-Aatc(Boc)-OH **33**. The mixture was reacted for 1.5 hours at –20 °C. After purification by column chromatography Cbz-Aatc(Boc)-NHMe **34** was obtained in 85% yield.

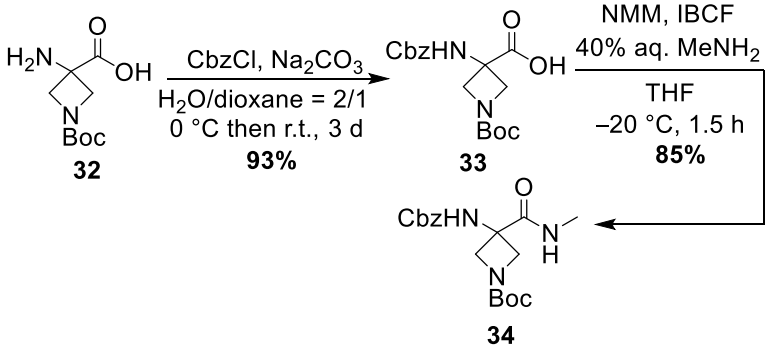

Scheme 29. Preparation of Cbz-Aatc(Boc)-NHMe **34**

2.2.2 Preparation of Cbz-[Aatc(Boc)]$_2$-NHMe **36**

Cbz-[Aatc(Boc)]$_2$-NHMe **36** was prepared via a coupling reaction between Cbz-Aatc(Boc)-OH **33** and H-Aatc(Boc)-NHMe **35** (Scheme 30). Cbz deprotection of Cbz-Aatc(Boc)-NHMe **34** was carried out by hydrogenolysis in the presence of Pd/C, under H_2 at room temperature for 30 minutes. The mixture was filtered through a celite pad and a PTFE membrane, to give the amine H-Aatc(Boc)-NHMe **35** as a white solid in quantitative yield.

Cbz-Aatc(Boc)-OH **33** was activated using IBCF and NMM, then was treated with the solution of the amine H-Aatc(Boc)-NHMe **35** in DMF at –30 °C. The reaction mixture was stirred overnight at –20 °C. After workup and purification by column chromatography afforded Cbz-[Aatc(Boc)]$_2$-NHMe **36** in 71% yield over two steps.

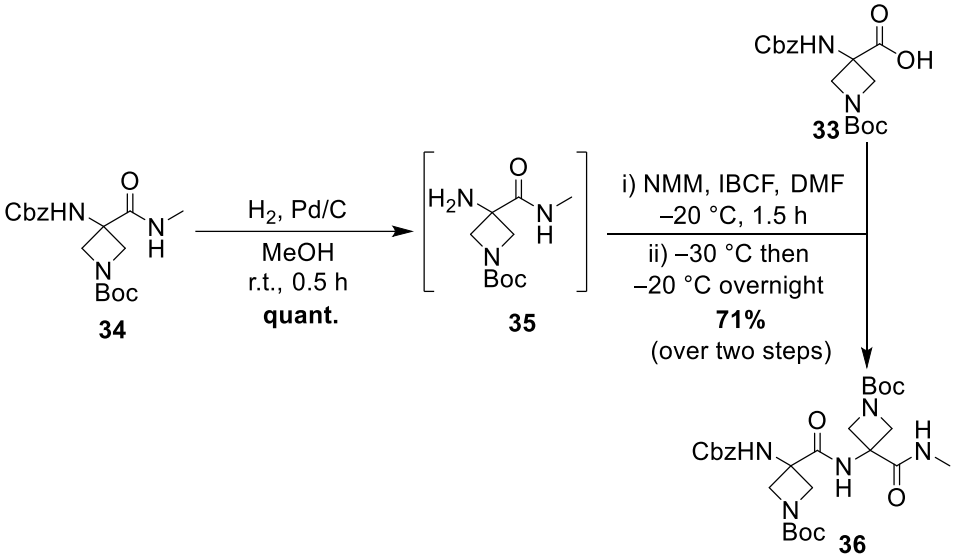

Scheme 30. Preparation of Cbz-[Aatc(Boc)]$_2$-NHMe **36**

2.2.3 Preparation of Cbz-[Aatc(Boc)]$_3$-NHMe **38**

The formation of Cbz-[Aatc(Boc)]$_3$-NHMe **38** was achieved by coupling Cbz-Aatc(Boc)-OH **33** with H-[Aatc(Boc)]$_2$-NHMe **37** (Scheme 31). The Cbz group of Cbz-[Aatc(Boc)]$_2$-NHMe **36** was removed using Pd/C under H_2 for 30 minutes at room temperature. The reaction mixture was filtered through a celite pad and a PTFE membrane. After solvent evaporation, the amine H-[Aatc(Boc)]$_2$-NHMe **37** was isolated as a white solid in a quantitative yield and was used without further purification.

Activation of the carboxylic function of Cbz-Aatc(Boc)-OH **33** was done using IBCF in the presence of NMM. This solution was mixed with a solution of the amine H-[Aatc(Boc)]$_2$-NHMe

37 in DMF at –30 °C; the reaction was stirred overnight at –20 °C. After workup and purification by column chromatography Cbz-[Aatc(Boc)]$_3$-NHMe **38** was obtained in 57% yield over two steps.

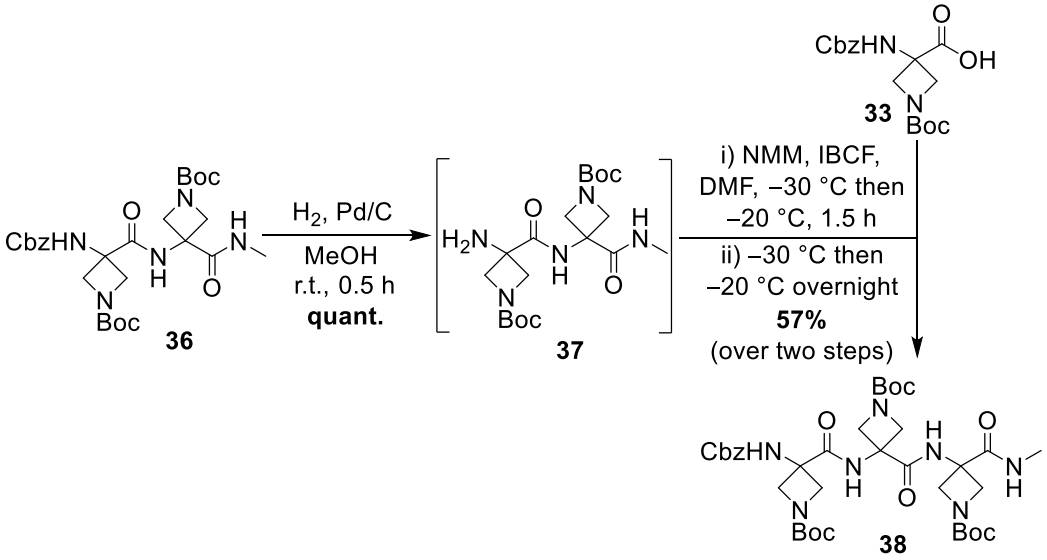

Scheme 31. Preparation of Cbz-[Aatc(Boc)]$_3$-NHMe **38**

2.2.4 Preparation of Cbz-[Aatc(Boc)]$_4$-NHMe **40**

The synthesis of Cbz-[Aatc(Boc)]$_4$-NHMe **40** was achieved via a coupling reaction between Cbz-Aatc(Boc)-OH **33** and H-[Aatc(Boc)]$_3$-NHMe **39**. (Scheme 32) Deprotection of Cbz-[Aatc(Boc)]$_3$-NHMe **38** was performed using Pd/C under H_2 for 30 minutes at room temperature. After filtration of the reaction mixture through a celite pad and a PTFE membrane then solvent evaporation, H-[Aatc(Boc)]$_3$-NHMe **39** was isolated in quantitative yield and was used without further purification.

Cbz-Aatc(Boc)-OH **33** was activated with IBCF in the presence of NMM, then the mixture was added to a solution of the amine H-[Aatc(Boc)]$_3$-NHMe **39** in DMF at –30 °C. The reaction mixture was stirred overnight at –20 °C to give Cbz-[Aatc(Boc)]$_4$-NHMe **40** in 60% yield over two steps after purification by column chromatography.

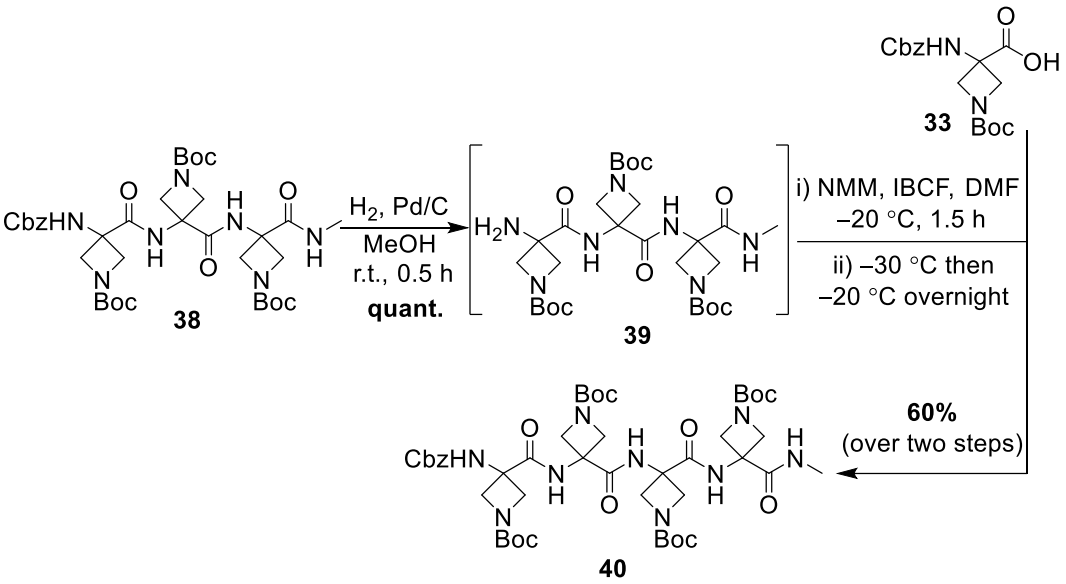

Scheme 32. Preparation of Cbz-[Aatc(Boc)]$_4$-NHMe **40**

2.2.5 Preparation of the target Aatc(Me) derivatives **42**, **44**, **46** and **48**

2.2.5.1 Preparation of Cbz-Aatc(Me)-NHMe **42**

To obtain the target monomer Cbz-Aatc(Me)-NHMe **42**, we performed two consecutive steps (Scheme 33). The Boc group of Cbz-Aatc(Boc)-NHMe **34** was removed by treatment with 4 M HCl in dioxane (50 equivalents), for 3 hours at room temperature. The hydrochloride salt **41** was obtained after evaporation of the solvent and the excess HCl.

Inspired by the strategy from literature[181], we performed with the reductive amination of hydrochloride salt **41** using aqueous formaldehyde (37%) in the presence of acetic acid and sodium cyanoborohydride. After purification by column chromatography Cbz-Aatc(Me)-NHMe **42** was obtained in 83% yield.

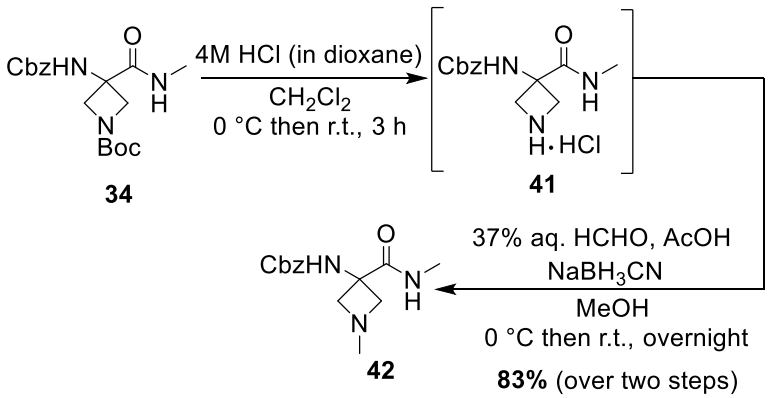

Scheme 33. Preparation of Cbz-Aatc(Me)-NHMe **42**

2.2.5.2 Preparation of Cbz-[Aatc(Me)]$_2$-NHMe **44**

To obtain Cbz-[Aatc(Me)]$_2$-NHMe **44**, both Boc groups first had to be removed from Cbz-[Aatc(Boc)]$_2$-NHMe **36**. The amount of 4 M HCl in dioxane was increased to 100 equivalents, Cbz-[Aatc(Boc)]$_2$-NHMe **36** was converted into its hydrochloride salt **43** in 4 hours in quantitative yield and was used without further purification (Scheme 34). In the reductive amination of hydrochloride salt **43**, 15 equivalents of formaldehyde, 10 equivalents of AcOH and 6 equivalents of $NaBH_3CN$ were used, and Cbz-[Aatc(Me)]$_2$-NHMe **44** was isolated with a 40% yield after purification (Table 16, entry 1).

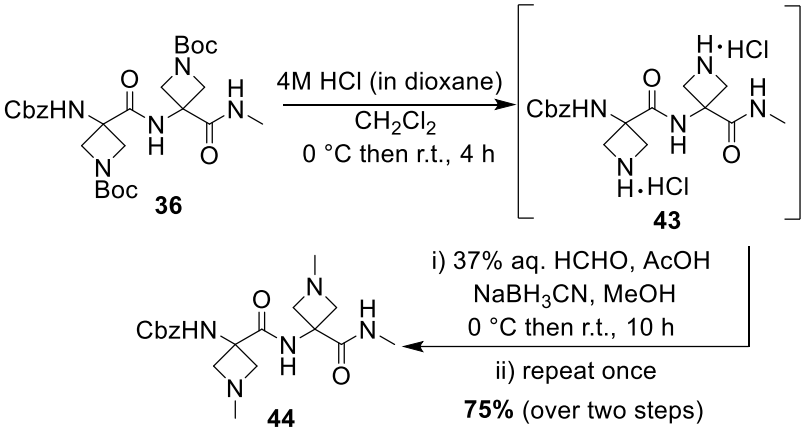

Scheme 34. Preparation of Cbz-[Aatc(Me)]$_2$-NHMe **44**

Entry	Aldehyde (eq.)	Acid (eq.)	Solvent	Reductant (eq.)	Yield (%)
1	HCHO (37% aq.) (15)	AcOH (10)	MeOH	$NaBH_3CN$ (6)	40
2	HCHO (37% aq.) (15)	AcOH (10)	MeOH	$NaBH(OAc)_3$ (6)	40
3	$(HCHO)_n$ (10)	AcOH (1 mL)	no	$NaBH_3CN$ (5)	46
4	HCHO (37% aq.) (2 × 10)	AcOH (2 × 5)	MeOH	$NaBH_3CN$ (2 × 3)	75

Table 16. Optimization of the preparation of Cbz-[Aatc(Me)]$_2$-NHMe **44**

To improve the yield of this transformation, optimization was carried out. The use of sodium triacetoxy borohydride [$NaBH(OAc)_3$, 6 equivalents] instead of $NaBH_3CN$ didn't give any improvement (Table 16, entry 2). Inspired by the work from Spring's group[182], paraformaldehyde was employed rather than formaldehyde (37% aq.), using AcOH (1 mL) and $NaBH_3CN$ (6 equivalents) led to a slightly higher yield of 46% (Table 16, entry 3). Encouraged by a strategy from Marcaurelle[183], we modified the addition of the reagents. 20 equivalents of formaldehyde (37% aq.), 10 equivalents of AcOH, and 6 equivalents of $NaBH_3CN$ were equally divided into two portions. The second portion was added 10 hours after the first one and kept stirring for 10 hours until the reaction was complete. In this manner, a total of 20

hours of reaction gave Cbz-[Aatc(Me)]$_2$-NHMe **44** a yield of 75% after purification by preparative HPLC (Table 16, entry 4).

2.2.5.3 Preparation of Cbz-[Aatc(Me)]$_3$-NHMe **46**

The hydrochloride salt **45** was prepared from Cbz-[Aatc(Boc)]$_3$-NHMe **38** using 150 equivalents of 4 M HCl in dioxane over 5 hours, giving hydrochloride salt **45** in quantitative yield, used without further purification (Scheme 35). Following the optimal conditions (Table 16, entry 4) for the preparation of Cbz-[Aatc(Me)]$_2$-NHMe **44**, we prepared Cbz-[Aatc(Me)]$_3$-NHMe **46** as follows. Three aliquots of 37% aq. formaldehyde (15 eq.), AcOH (6 eq.) and $NaBH_3CN$ (9 eq.) reagents were added to the reaction mixture at 10 hours intervals. A total of 30 hours of reaction time gave the desired Cbz-[Aatc(Me)]$_3$-NHMe **46** with a yield of 65% after purification by preparative HPLC.

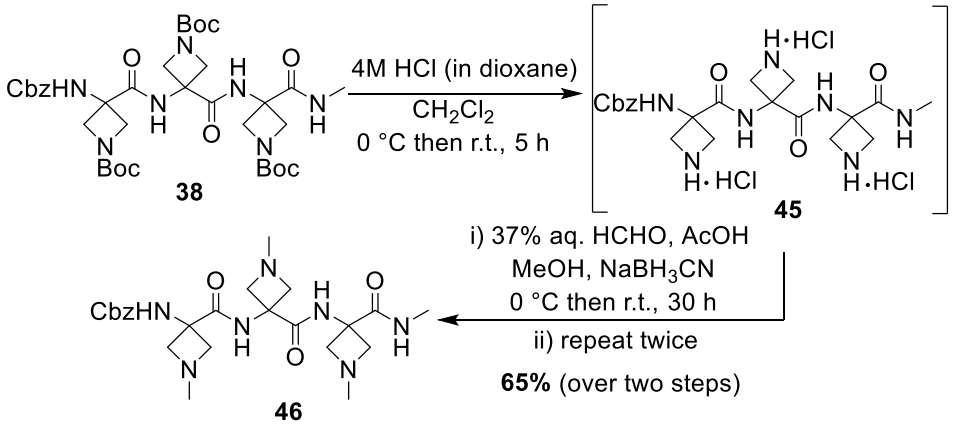

Scheme 35. Preparation of Cbz-[Aatc(Me)]$_3$-NHMe **46**

2.2.5.4 Preparation of Cbz-[Aatc(Me)]$_4$-NHMe **48**

For the quadruple deprotection of Cbz-[Aatc(Boc)]$_4$-NHMe **40**, we used 200 equivalents of 4 M HCl in dioxane. The reaction was completed in 15 hours, giving hydrochloride salt **47** in quantitative yield used without further purification (Scheme 36).

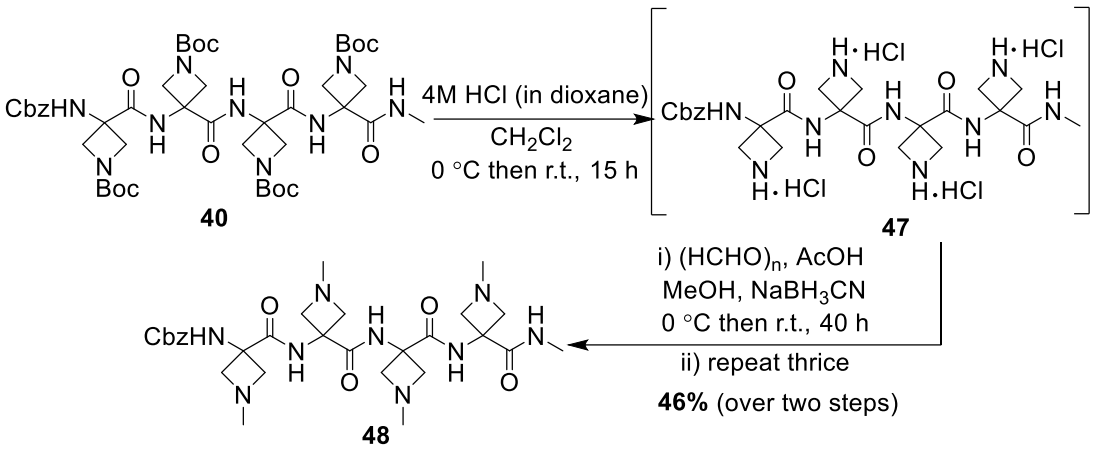

Scheme 36. Preparation of Cbz-[Aatc(Me)]$_4$-NHMe **48**

We again followed the optimal reductive amination conditions for the preparation of Cbz-[Aatc(Me)]$_4$-NHMe **48**. Aliquots of 37% aq. formaldehyde (15 eq.), AcOH (6 eq.) and $NaBH_3CN$ (9 eq.) reagents were added to the reaction mixture at 10 hours intervals. A total of 30 hours gave the Cbz-[Aatc(Me)]$_4$-NHMe **48** with a yield of only 10% (Table 17, entry 1).

In an effort to improve the yield, the reaction was carried out using paraformaldehyde (20 eq.), AcOH (1 mL) and $NaBH_3CN$ (10 eq.) (Table 17, entry 2), then again by increasing the amounts of reagents (paraformaldehyde to 40 equivalents and $NaBH_3CN$ to 20 equivalents) (Table 17, entry 3), but the yield of Cbz-[Aatc(Me)]$_4$-NHMe **48** did not improve at all. Finally, the protocol of adding four separate aliquots of paraformaldehyde (5 eq.), AcOH (6 eq.) and $NaBH_3CN$ (3 eq.) every 10 hours was examined. A total of 40 hours reaction yielded Cbz-[Aatc(Me)]$_4$-NHMe **48** in 46% after purification by preparative HPLC (Table 17, entry 4).

Entry	Aldehyde (eq.)	Acid (eq.)	Solvent	Reductant (eq.)	Yield (%)
1	HCHO (37% aq.) (3 × 15)	AcOH (3 × 6)	MeOH	$NaBH_3CN$ (3 × 9)	10
2	$(HCHO)_n$ (20)	AcOH (1 mL)	MeOH	$NaBH_3CN$ (10)	10
3	$(HCHO)_n$ (40)	AcOH (1 mL)	MeOH	$NaBH_3CN$ (20)	10
4	$(HCHO)_n$ (4 × 5)	AcOH (4 × 6)	MeOH	$NaBH_3CN$ (4 × 3)	46

Table 17. Optimization of the preparation of Cbz-[Aatc(Me)]$_4$-NHMe **48**

2.2.6 Stability and purity issues of Aatc(Me) derivatives

In this section, four Aatc(Me) derivatives **42**, **44**, **46** and **48** have been successfully prepared, each sample was stable enough stock in an open environment. The structure and assignment

of **42**, **44** and **46** were unambiguously identified by using standard 1D/2D NMR techniques and mass spectroscopy. However, for the tetramer **48**, chemical shift overlap prevented assignment of $C^{\beta}H_2$ protons of four azetidine residues, additionally, NH peaks were not well-defined and without clear assignment by standard 1D/2D NMR methods. The stability issue for tetramer **48** was in evidence, impurity was always detected by HPLC from the purified sample. More detail information of tetramer **48** will discuss later in section 2.4.

2.3 Conformational studies of Aatc(Me) derivatives **42**, **44** and **46**

In this section, we will describe the conformational studies of Cbz-Aatc(Me)-NHMe **42**, Cbz-[Aatc(Me)]$_2$-NHMe **44** and Cbz-[Aatc(Me)]$_3$-NHMe **46** (Figure 99). Conformational studies of Cbz-[Aatc(Me)]$_4$-NHMe **48** will discuss later in section 2.4.

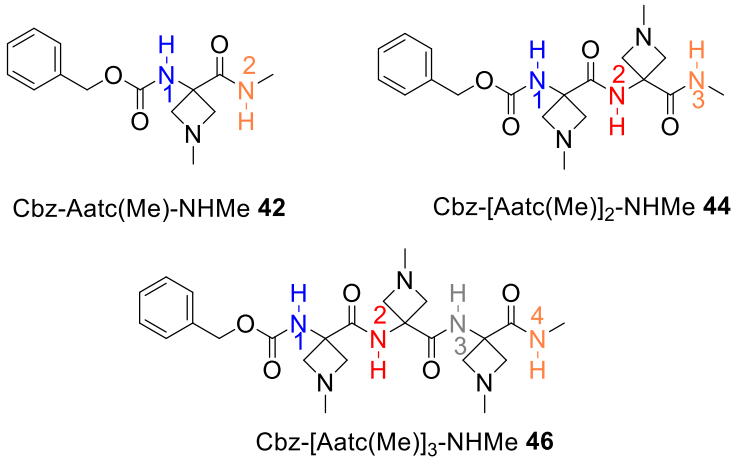

Figure 99. Three oligomers **42**, **44** and **46** for conformational studies in this section

2.3.1 Methodologies in this section

In this chapter, conformational studies were performed using quantum chemistry calculations, UV/IR spectroscopy in gas phase, IR spectroscopy in solution phase and 1D/2D NMR methods (DMSO-d_6 titration, temperature variation and 2D NOESY). The detailed description of several methods (IR spectroscopy in solution phase and DMSO-d_6 titration) has been described in section 1.3.1, chapter 1.

1. **Quantum chemistry calculations** were performed in gas and solution phase, respectively. The conformational exploration was done with the OPLS-2005 force field using the Monte-Carlo Multiple Minima (MCMM) procedures in the MacroModel suite (in Schrödinger). Geometry optimization was done using the Density functional theory (DFT)-D calculations. For each conformation of each compound, the theoretical IR spectrum was calculated as a reference for the IR spectrum in gas and solution phases.

This work was carried out by Prof. Michel Mons and Dr. Valérie Brenner in the LIDYL laboratory (CEA Saclay, Gif-sur-Yvette, France).

2. **UV/IR spectroscopy in gas phase** is particular useful for studying model peptides with weak interactions such as C5 interaction. In the gas phase conditions, vibrationally resolved spectra can be obtained for systems composed of several residues, comparison of the vibrationally resolved spectra with the theoretical IR spectra of low energy conformations allowed the assignment of the observed conformers to specific conformations, thereby providing a detailed description of the intramolecular H-bond system of each conformation.

This work was carried out by Prof. Michel Mons in the LIDYL laboratory (CEA Saclay, Gif-sur-Yvette, France).

3. **^{1}H NMR at variable temperature** experiments were performed to assess the H-bonding status of NH protons in each peptide. Increasing temperature induces the chemical shifts of NH signals to move to a higher field. The chemical shifts of H-bonded NH proton changes slightly but a free NH proton changes significantly.

4. **^{1}H-^{1}H NOESY NMR** experiments were used to probe the three-dimensional geometry of the peptides in solution, by studying through space magnetic interactions (polar couplings) that give rise to the NOE (Nuclear Overhauser Effect). The ^{1}H-^{1}H NOESY spectra were recorded on a Bruker AV 400 MHz spectrometer. Each sample was prepared in $CDCl_3$ at a concentration of 20 mM. The pulse sequence was noesygpph or roesyphpp. The experiments were performed by collecting 2048 points in f2 and 256 points in f1. The mixing times were 200 ms for compounds **42** and **44**, 600 ms for compound **46**.

2.3.2 Quantum chemistry calculations

For compound **42**, the conformational exploration was done with the OPLS-2005 force field using the Monte-Carlo Multiple Minima (MCMM) procedures in the MacroModel suite (in Schrödinger). Geometry optimization was done using the Density functional theory (DFT)-D calculations. The conformational landscape of compounds **44** and **46** were reconstructed based on compound **42**. The conformational analysis was carried out by building up a juxtaposition of local conformational preferences of compound **42**. These structures were then optimized at quantum chemistry level (DFT-D).

2.3.2.1 Lowest energy conformation of Cbz-Aatc(Me)-NHMe **42**

Theoretical calculations in gas phase suggested a predominant conformer of Cbz-Aatc(Me)-NHMe **42** as an extended conformation **A** (Figure 100, top). It showed an N–H···N inter-

residue C6γ H-bond implicating NH(2) and the azetidine nitrogen atom, and an N–H···O=C intra-residue C5 H-bond implicating NH(1) and the carbamate oxygen. These two H-bonds together constitute a C5–C6γ structural feature characterized by an extended planar backbone. Two folded conformers, free-π_{am} (π_{amide}) form **B** (middle) and free-C7 form **C** (Figure 100, bottom) were also found to be minor contributions. The free-π_{am} folded form in which the amide NH is close to the carbamate NH, thus making a π_{am} interaction, the C7 folded form was stabilized by a C7 H-bond linking the two ends of the molecule.

Theoretical calculations in solution phase showed three same conformational families within 5 kJ/mol of energy that could be populated: the fully extended C5-C6γ form (0 kJ/mol), together with a free-π_{am} (4.8 kJ/mol) form and a free-C7 (5.4 kJ/mol) form.

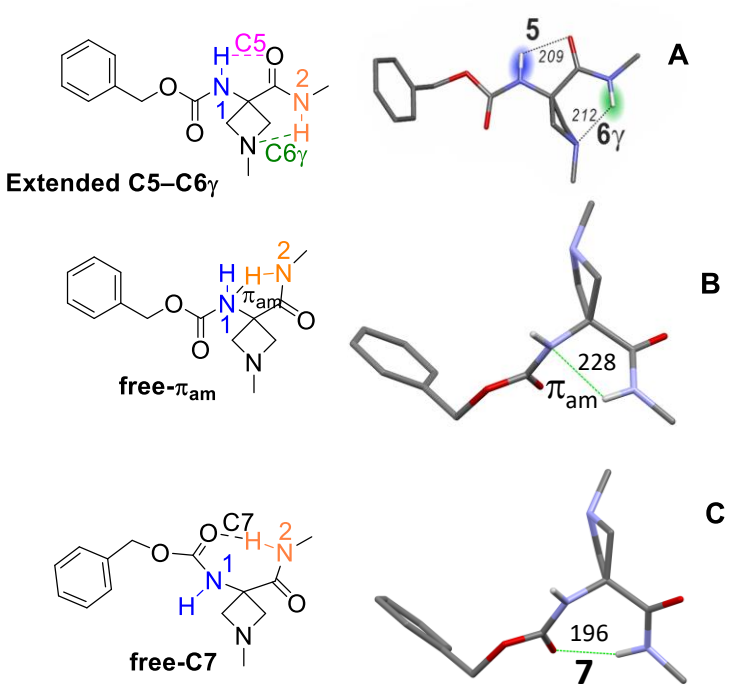

Figure 100. Extended conformation and H-bonding pattern (top), free-π_{am} conformation and H-bonding pattern (middle), free-C7 conformation and H-bonding pattern (bottom) of Cbz-Aatc(Me)-NHMe **42**

2.3.2.2 Lowest energy conformation of Cbz-[Aatc(Me)]$_2$-NHMe **44**

Theoretical calculations in gas phase identified a dominant conformation of Cbz-[Aatc(Me)]$_2$-NHMe **44** as an extended form **A**, result is shown in Figure 101 (top). It showed respective assignments to a C6γ H-bond implicating NH(3), and a C5 interaction implicating NH(1). In addition, NH(2) was engaged simultaneously in a C5 and C6γ H-bonds, featuring a three-

center H-bond of the type [C=O···H(N)···N]. The second most stable conformation was more energetic by ca. 10 kJ·mol^{-1} implicating a C5-C6γ H-bonding motif was replaced by a π_{am} interaction, as a semi-extended C5-C6γ/π_{am} form **B** (Figure 101, middle). The third structure formed a β-turn **C** (Figure 101, bottom), characterized by a C10 H-bond implicating NH(3).

Theoretical calculations showed that these types of conformations are found within 5 kJ/mol of energy that could be populated in solution: the fully extended C5-C6γ/C5-C6γ form (4.9 kJ/mol), together with a semi-extended C5-C6γ/π_{am} (0 kJ/mol) form and a β-turn (free-free-C10) (1.5 kJ/mol) form.

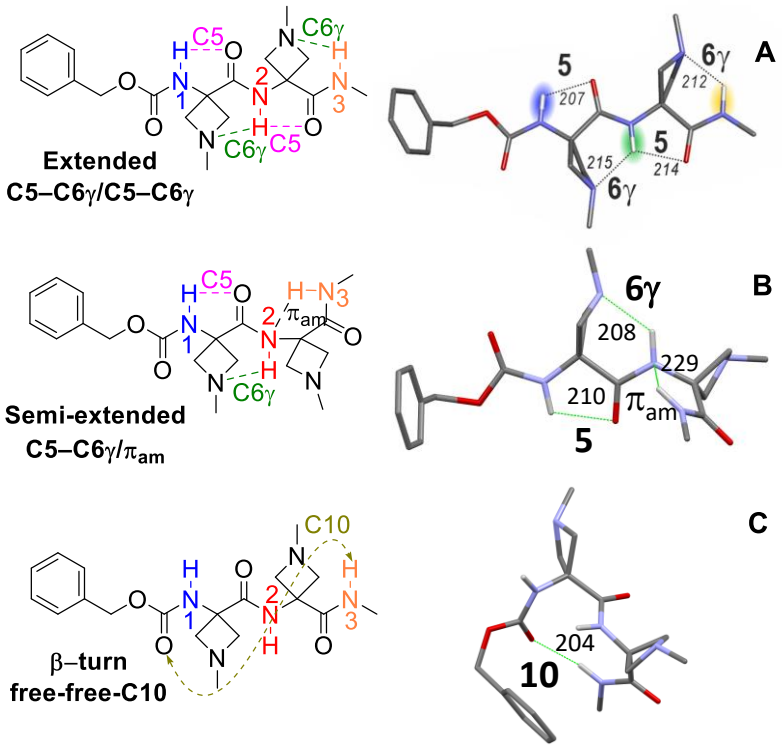

Figure 101. Fully extended conformation and H-bonding pattern (top), semi-extended conformation and H-bonding pattern (middle), β-turn conformation and H-bonding pattern (bottom) of Cbz-[Aatc(Me)]$_2$-NHMe **44**

2.3.2.3 Lowest energy conformation of Cbz-[Aatc(Me)]$_3$-NHMe **46**

Theoretical calculations in gas phase suggested three lowest energy conformations of Cbz-[Aatc(Me)]$_3$-NHMe **46** (Figure 102). The first conformation **A** showed three consecutive C5–C6γ H-bonding features exhibited a fully extended form (Figure 102, top). An N–H···N C6γ H-bond implicating NH(4), and an N–H···O=C C5 H-bond implicating NH(1). NH(2) and NH(3) were engaged simultaneously in a C5 and C6γ H-bonds, respectively. The second conformer **B** (Figure 102, middle) was a semi-extended form (C5-C6γ/π_{am}/C5-C6γ), in which the central

C5-C6γ H-bonding feature of the fully extended form was replaced by a π_{am} interaction, implicating NH(3) and N(2). The third conformer **C** (Figure 102, bottom) exhibited two parallel C10 H-bonds implicating NH(3) and NH(4), correspond to a 3_{10}-helix.

Theoretical calculations in solution showed same conformational families, two conformations were found within 5 kJ/mol of energy in solution: a semi-extended C5-C6γ/π_{am}/C5-C6γ (0 kJ/mol) form, and a free-free-C10-C10, 3_{10}-helix (3.1 kJ/mol) conformation. The fully extended C5-C6γ/C5-C6γ/C5-C6γ (10.1 kJ/mol) form was found in higher of energy.

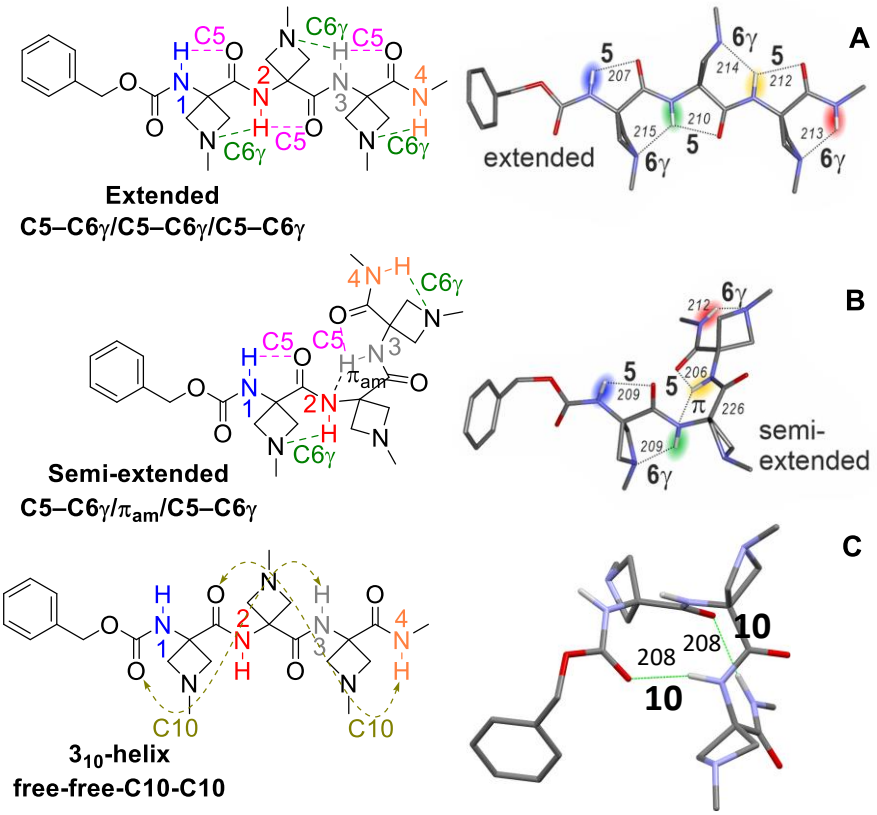

Figure 102. Fully extended conformation and H-bonding pattern (top), semi-extended conformation and H-bonding pattern (middle), 3_{10}-helix conformation and H-bonding pattern (bottom) of Cbz-[Aatc(Me)]$_3$-NHMe **46**

2.3.2.4 Discussion

Cbz-Aatc(Me)-NHMe **42**, Cbz-[Aatc(Me)]$_2$-NHMe **44** and Cbz-[Aatc(Me)]$_3$-NHMe **46** all showed the extended conformation with consecutive C5–C6γ H-bonding features in gas phase. Whereas in longer trimer **46**, the competition between extended and folded conformations was found to be more open, the semi-extended and 3_{10}-helix conformations were found to be low energy forms and challenged the fully extended conformation in gas phase calculations.

Conformations for these three Aatc(Me) derivatives in solution phase calculations, compared to that in gas phase, the relative stabilities of these families were found to vary significantly. The fully extended form appeared to be less and less favored as the number of residues increased (following the series **42**→**44**→**46**), while folded conformations were predicted to be more populated, with a slight preference for the turn/helical structures, in agreement with the larger dipole moment of these latter.

2.3.3 Gas phase studies

Molecules were vaporized using laser desorption and subsequently cooled down in a supersonic expansion, where the freezing of the vibrational degrees of freedom ensured a conformational distribution corresponding to that at room temperature. The UV spectra obtained by resonant two-photon ionization in the first near UV absorption region of the benzyl group were composed of narrow lines, from which the conformational populations were distinguished. Then IR absorption spectrum in the NH stretch region of each conformer was obtained by UV/IR laser spectroscopy. Interpretation of the data was made with help from the theoretical IR absorbances suggested by quantum chemistry calculations (See section 2.3.2).

This work was carried out by Prof. Michel Mons in the LIDYL laboratory (CEA Saclay, Gif-sur-Yvette, France).

2.3.3.1 Gas phase studies of Cbz-Aatc(Me)-NHMe **42**

The gas phase studies of Cbz-Aatc(Me)-NHMe **42** were already described.[154] The UV spectrum showed an intense UV band (labeled A) at 37587 cm^{-1}, accompanied by a second UV band (labeled A') located at 22 cm^{-1} higher in energy which was assigned to the same conformer as band A (Figure 103). Thus, the UV spectrum suggested the presence of only one conformer family for monomer Cbz-Aatc(Me)-NHMe **42**.

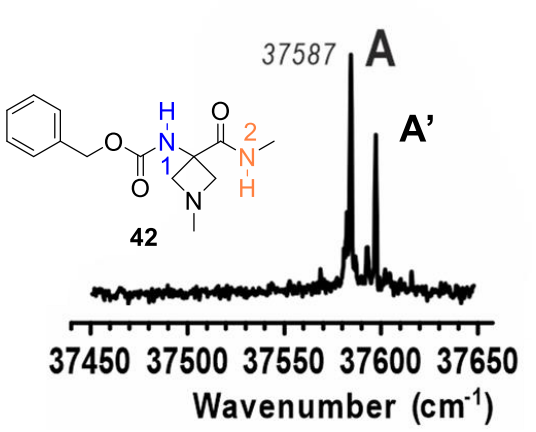

Figure 103. UV spectrum of Cbz-Aatc(Me)-NHMe **42** in gas phase

The IR spectrum was recorded on band A and showed two significant bands at 3331 cm^{-1} and 3401 cm^{-1} (Figure 104). The band at 3331 cm^{-1} was assigned to NH(2) in an N–H···N C6γ H-bond and the band at 3401 cm^{-1} was assigned to NH(1) in an N–H···O=C C5 interaction. This C5–C6γ structural feature is characterized by an extended planar backbone.

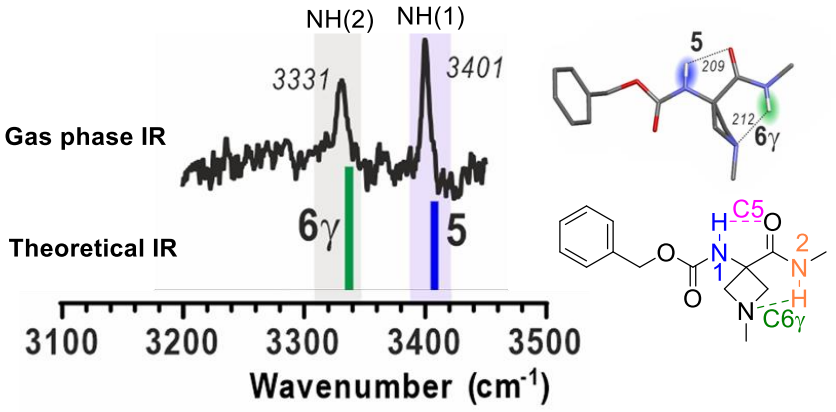

Figure 104. IR spectrum in gas phase and theoretical IR spectrum for the C5–C6γ conformer of Cbz-Aatc(Me)-NHMe **42**

2.3.3.2 Gas phase studies of Cbz-[Aatc(Me)]$_2$-NHMe **44**

The UV spectrum of Cbz-[Aatc(Me)]$_2$-NHMe **44** exhibited, in addition to an intense UV band (labeled A) at 37588 cm^{-1}, a small band (labeled A') nearby that was assigned to the same conformer as band A (Figure 105).

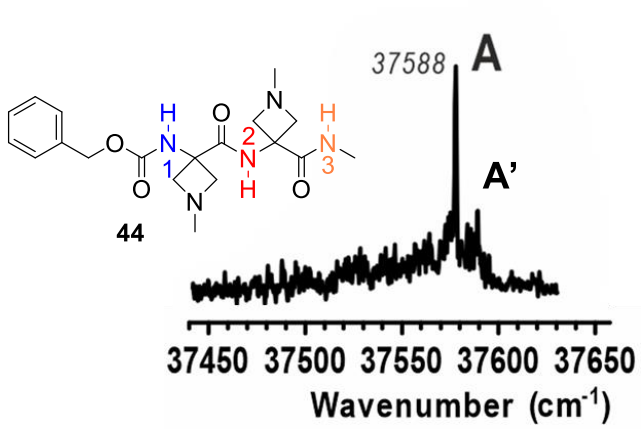

Figure 105. UV spectrum of Cbz-[Aatc(Me)]$_2$-NHMe **44** in gas phase

The IR spectrum was recorded on band A, showing three bands at 3198, 3336 and 3406 cm^{-1} (Figure 106). The two bands at 3336 and 3406 cm^{-1} were respectively assigned to an N–H···N C6γ H-bond implicating NH(3) and an N–H···O=C C5 interaction implicating NH(1). The third broad band appeared further to the red (at 3198 cm^{-1}), which suggested a stronger H-bonding in the conformation and provided a fair agreement with the bifurcated H-bond implicating NH(2) suggested by the theoretical IR spectrum. The NH(2) was engaged simultaneously in C5 and C6γ H-bonds, thereby implicated in a three-center H-bond of the type [C=O···H(N)···N]. These H-bonds exhibited a C5-C6γ/C5-C6γ, fully extended form.

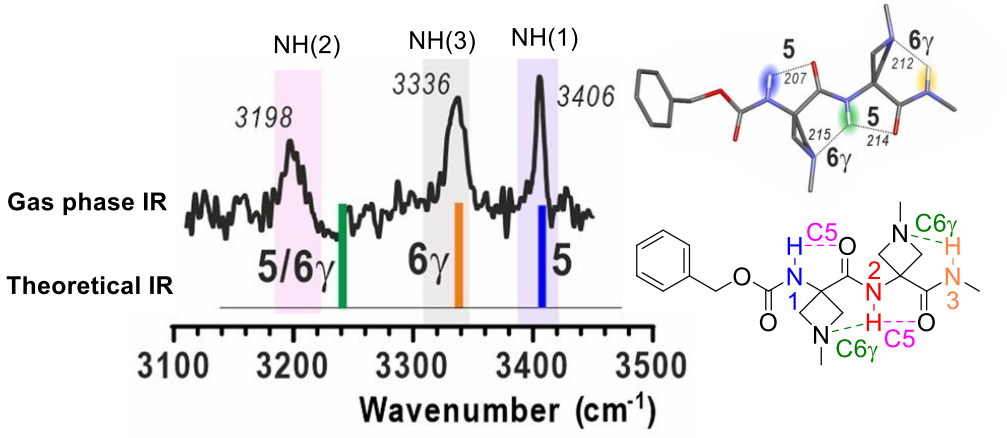

Figure 106. IR spectrum in gas phase and theoretical IR spectrum for the C5–C6γ/C5–C6γ conformer of Cbz-[Aatc(Me)]$_2$-NHMe **44**

2.3.3.3 Gas phase studies of Cbz-[Aatc(Me)]$_3$-NHMe **46**

The gas phase UV spectrum of Cbz-[Aatc(Me)]$_3$-NHMe **46** is shown in Figure 107. It showed an intense band (labelled A) at 37588 cm^{-1}, accompanied by a red-shifted shoulder (labeled X), which anticipated a more complex landscape implicating the presence of more than one conformation family.

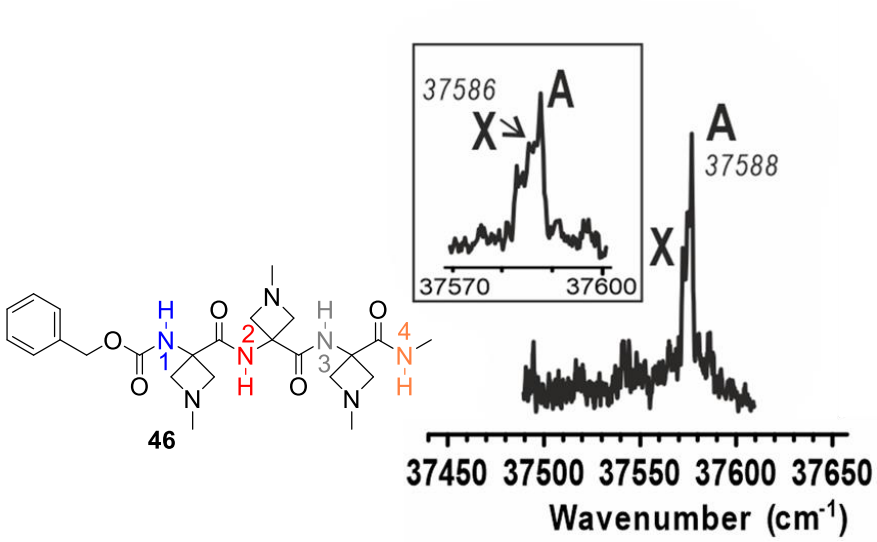

Figure 107. UV spectrum of Cbz-[Aatc(Me)]$_3$-NHMe **46** in gas phase

The IR spectrum was recorded on band A, and showed three bands at 3207, 3337 and 3403 cm^{-1} (Figure 108). The two bands at 3337 and 3403 cm^{-1} were assigned to an N–H···N C6γ H-bond implicating NH(4) and an N–H···O=C C5 interaction implicating NH(1), respectively. The third broad band appeared further to the red (at 3207 cm^{-1}), which made a fair agreement with the theoretical IR spectrum for the presence of two bifurcated H-bonds implicating NH(2) and NH(3). Both NH(2) and NH(3) were simultaneously involved in C5–C6γ H-bond systems, leading to the significant red shifts of their NH vibration frequencies. These H-bonds constituted a fully C5-C6γ/C5-C6γ/C5-C6γ extended conformer.

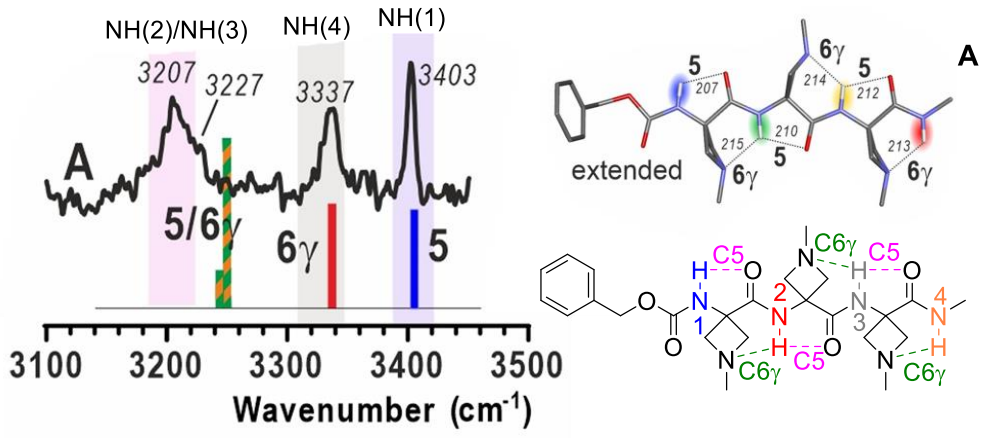

Figure 108. IR spectrum in gas phase of band A and theoretical IR spectrum for the fully extended conformer of Cbz-[Aatc(Me)]$_3$-NHMe **46**

The IR spectrum of band X of Cbz-[Aatc(Me)]$_3$-NHMe **46** showing five bands at 3207, 3263, 3325, 3382 and 3403 cm^{-1} (Figure 109). This IR spectrum was a hybrid with two components, one was the extended conformer A and the second was a different conformation (labeled B).

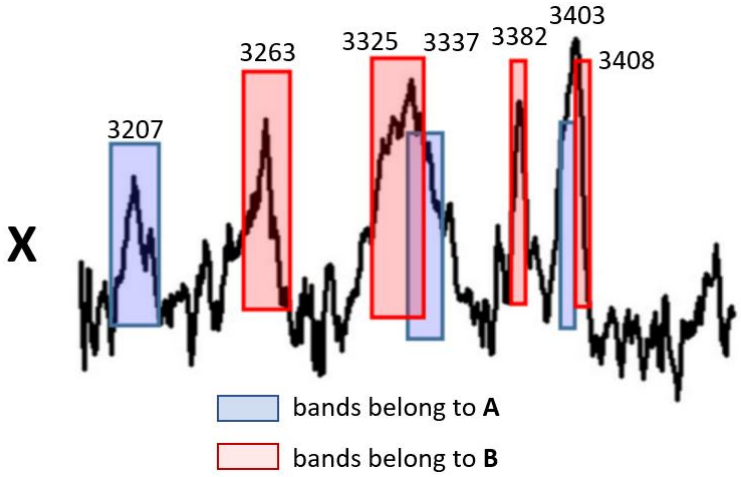

Figure 109. IR spectrum in gas phase of the band X of Cbz-[Aatc(Me)]$_3$-NHMe **46**

The IR spectrum of conformation B was reconstructed by subtraction and exhibited four bands at 3263, 3325, 3382 and 3408 cm^{-1}. Two bands at 3325 and 3408 cm^{-1} were assigned to NH(4) in a C6γ H-bond and NH(1) in a C5 H-bond, respectively (Figure 110). The other two bands at 3263 and 3382 cm^{-1} were found to significantly differ from those of NH(2) and NH(3) in the fully-extended form, suggesting a different conformation for the central part of the peptide chain. Comparison of the IR spectrum of conformation B with the theoretical IR spectrum of a semi-extended form provided a good agreement. This corresponds to the replacement of the C5-C6γ motifs in conformation A by a C6γ H-bond and a bifurcated π_{am}/C5 bond instead, for NH(2) (3263 cm^{-1}) and NH(3) (3382 cm^{-1}) respectively. These observations

demonstrated the presence of a second conformer B in trimer Cbz-[Aatc(Me)]$_3$-NHMe **46** as a C5-C6γ/π_{am}/C5-C6γ semi-extended form.

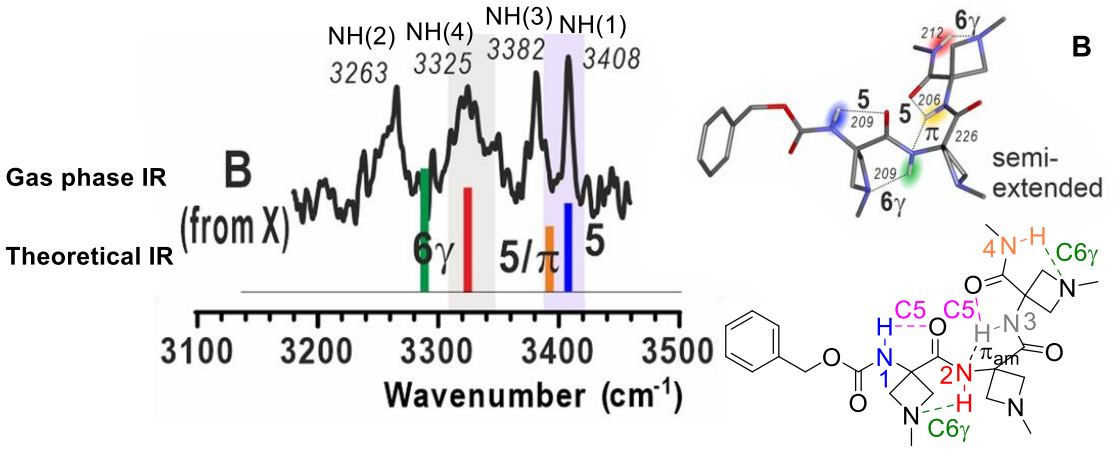

Figure 110. IR spectrum in gas phase of band B and theoretical IR spectrum for the semi-extended conformer of Cbz-[Aatc(Me)]$_3$-NHMe **46**

2.3.3.4 Discussion

In gas phase, the monomer Cbz-Aatc(Me)-NHMe **42** adopted an extended conformation with a C5-C6γ H-bonding feature, as suggested by theoretical calculations. This C5-C6γ H-bonding system appeared to propagate in the dimer Cbz-[Aatc(Me)]$_2$-NHMe **44**, which exhibited two consecutive C5-C6γ H-bonding systems linked by a three-centered C=O···H(N)···N H-bond. This H-bonding system also appeared to persist in the trimer Cbz-[Aatc(Me)]$_3$-NHMe **46**, which exhibited three consecutive C5-C6γ H-bonding systems. However, these H-bonding systems seem to start to be weaker in trimer **46**, and one of the C5-C6γ H-bonding systems was replaced by a π_{am} interaction causing a semi-extended form to appear as a second, minor conformation (Figure 111).

In previous work on 3-aminothietane-3-carboxylic acid (Attc) derivatives described that, a trimer Cbz-(Attc)$_3$-NHMe adopted only a semi-extended conformation in gas phase.[153] The trimer Cbz-[Aatc(Me)]$_3$-NHMe **46** in this work showed a major conformation as a fully extended form indicating the C5-C6γ H-bonding feature in the latter got better propagation.

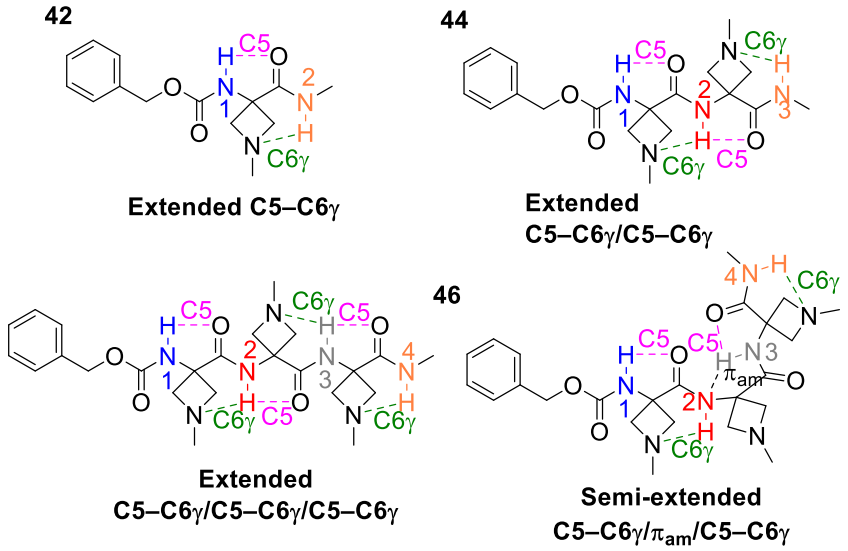

Figure 111. H-bonding patterns of three Aatc(Me) derivatives **42**, **44** and **46** in gas phase

2.3.4 Solution phase infrared spectroscopy studies

Infrared spectroscopy studies of Aatc derivatives **42**, **44** and **46** were performed in chloroform solution. At several low concentrations (0.5, 5, and 10 mM), the spectra showed no concentration-related effects in the NH stretch region (Figure 112), indicating the intramolecular nature of any non-covalent interactions and in particular H-bonding.

Interpretation of the data was made with help from the theoretical IR absorbances suggested by quantum chemistry calculations (See section 2.3.2).

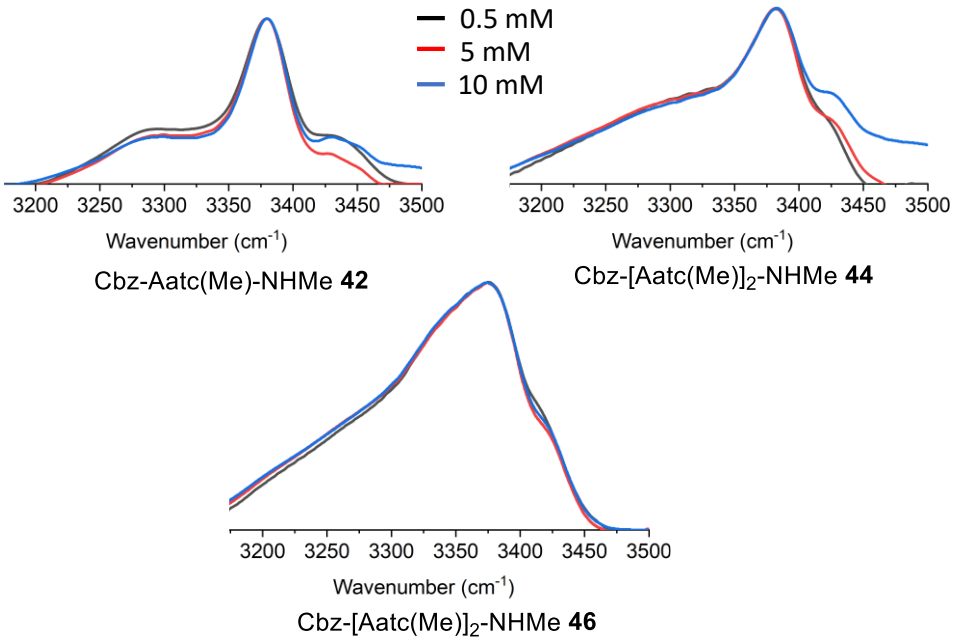

Figure 112. Solution phase IR spectra of three Aatc(Me) derivatives **42**, **44** and **46** at different concentrations

2.3.4.1 Solution phase IR of Cbz-Aatc(Me)-NHMe **42**

The infrared studies of Cbz-Aatc(Me)-NHMe **42** in solution were already described.[154] The infrared spectrum exhibited two main bands at 3380 and 3290 cm^{-1} (Figure 113, red line). The absorption band located at 3380 cm^{-1} was assigned to an C5 H-bond formed by NH(1), and the red-shifted band located at 3290 cm^{-1} was assigned to a C6γ H-bond implicating NH(2). Together, these data suggested a predominant stabilized C5–C6γ H-bond conformation, as had been observed in gas phase.

In addition, we observed two weak shoulders in the blue region, from 3430–3450 cm^{-1}, which could be assigned to minor free-π_{am} and free-C7 conformations supported by the theoretical IR spectra. The free-π_{am} conformation was composed of a π_{am} interaction between NH(2) and N(1), while NH(1) was non hydrogen-bonded. The free-C7 conformation was constituted of a seven-membered ring implicating NH(2) while NH(1) was non hydrogen-bonded.

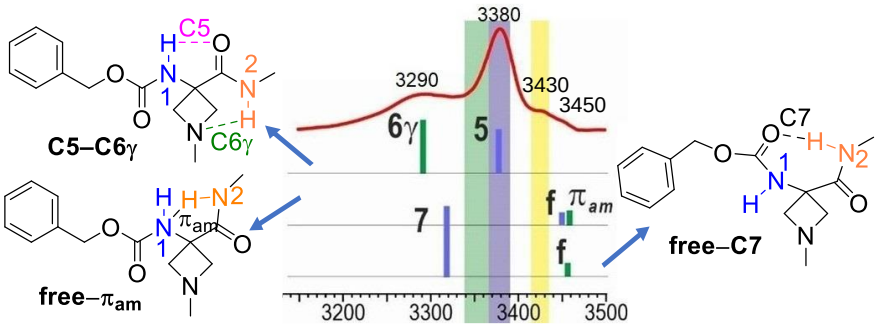

Figure 113. Infrared spectrum of Cbz-Aatc(Me)-NHMe **42** (red line, top) and three conformations (sticks, bottom) in solution suggested by the theoretical calculations and their H-bonding patterns

2.3.4.2 Solution phase IR of Cbz-[Aatc(Me)]$_2$-NHMe **44**

The infrared spectrum of Cbz-[Aatc(Me)]$_2$-NHMe **44** in solution exhibited three distinctive absorption bands. An intense band at 3380 cm^{-1}; a shoulder at 3430 cm^{-1} with a tail-off up to 3460 cm^{-1}; a broad band in the red, centered at 3280 cm^{-1} and extending down to 3150 cm^{-1} (Figure 114, red line).

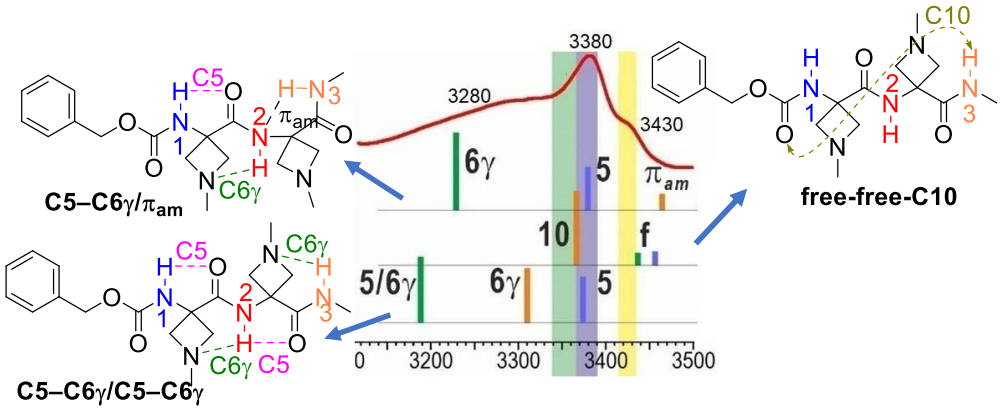

Figure 114. Infrared spectrum of Cbz-[Aatc(Me)]$_2$-NHMe **44** (red line, top) and three conformations (sticks, bottom) in solution suggested by the theoretical calculations and their H-bonding patterns

With the aid of the theoretical IR spectra, these data suggest that three types of conformation families are present in solution: a fully extended C5-C6γ/C5-C6γ form, a semi-extended C5-C6γ/π_{am} form and a β-turn (free-free-C10) form. The semi-folded C5-C6γ/π_{am} conformation present a C5 interaction implicating NH(1), which accounts for the presence of the 3380 cm^{-1} band (purple region), a C6γ H-bond implicating NH(2) contributes to the broad band at 3280 cm^{-1}, and a π_{am} interaction implicating NH(3) accounts for the presence of the 3430 cm^{-1} band (yellow region). The β-turn (free-free-C10) conformation has two non hydrogen-bonded NHs, NH(2) and NH(3) that contribute to the band at 3430 cm^{-1}. The C10 H-bond accounts for the

red shoulder of the 3380 cm^{-1} band (green region). The fully extended C5-C6γ/C5-C6γ conformation presents a C5 interaction implicating NH(1) that contributes to the 3380 cm^{-1} band, and a C6γ H-bond implicating NH(3) that contributes to the broad band at 3280 cm^{-1}. The C5-C6γ H-bonds implicating NH(2) may contribute to the absorptions of 3280 cm^{-1} regions, but without significant absorption in the 3200 cm^{-1} region, together with absorptions [the green (3350 cm^{-1}) and yellow region (3430 cm^{-1})] suggested that the fully extended form is a minor conformation.

2.3.4.3 Solution phase IR of Cbz-[Aatc(Me)]$_3$-NHMe **46**

The infrared spectrum of Cbz-[Aatc(Me)]$_3$-NHMe **46** in solution showed, a significant band at 3380m cm^{-1} (purple region), a red shoulder of the 3380m cm^{-1} band at 3330 cm^{-1}, a band at 3430 cm^{-1}, a broad band in the red region, centered at 3280 cm^{-1} and extending down to 3150 cm^{-1} (Figure 115).

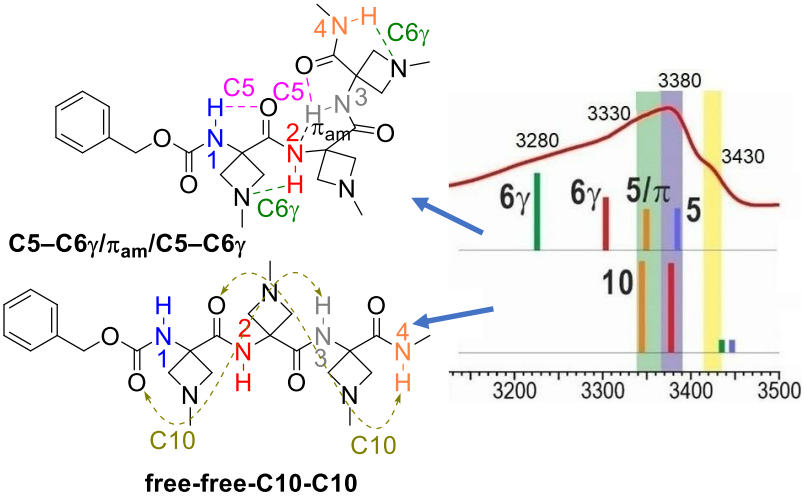

Figure 115. Infrared spectrum of Cbz-[Aatc(Me)]$_3$-NHMe **46** (red line, top) and two conformations (sticks, bottom) in solution suggested by the theoretical calculations and their H-bonding patterns

With the aid of the theoretical IR spectra, it was deduced that two types of conformations are present in solution: a semi-extended C5-C6γ/π_{am}/C5-C6γ form, and a free-free-C10-C10, 3_{10}-helix conformation. The semi-extended C5-C6γ/π_{am}/C5-C6γ conformation presents a C5 interaction implicating NH(1) accounts for the presence of 3380 cm^{-1} band (purple region), two C6γ H-bonds implicating NH(2) and NH(4) that contributes to the broad band from 3300 to 3280 cm^{-1}. The C5-π_{am} H-bonds implicating NH(3) account for the red shoulder at 3330 cm^{-1} (green region). The 3_{10}-helix conformation present two free NHs, NH(1) and NH(2) accounts

for the absorptions at 3430 cm^{-1} (yellow region), two C10 H-bonds formed by NH(3) and NH(4) that contribute to the bands of 3330 and 3380 cm^{-1}, respectively.

2.3.4.4 Discussion

On the basis of IR absorption data in solution phase, the monomer Cbz-Aatc(Me)-NHMe **42** showed a predominant extended C5-C6γ H-bonding conformation, had been observed in gas phase. However, minor contributions from free-C7 and free-π_{am} conformers appear in solution, that were not observed in gas phase. The C5-C6γ H-bonding system appeared to be present in the dimer Cbz-[Aatc(Me)]$_2$-NHMe **44**. However, the fully extended conformer with two consecutive C5-C6γ H-bonding systems was challenged by a semi-extended C5-C6γ/π_{am} form and a β-turn (free-free-C10) form. The C5-C6γ H-bonding system was still in present in the trimer Cbz-[Aatc(Me)]$_3$-NHMe **46** but essentially as a semi-extended C5-C6γ/π_{am}/C5-C6γ conformation. Furthermore, a 3_{10}-helix (free-free-C10-C10) conformation was also present for trimer **46**. It emerges from these studies that local C5-C6γ motifs are present on the conformational landscape of all three compounds, but that successive motifs, implicating bifurcated C5/C6γ H-bonding system, are less competitive than alternative partially folded structures.

2.3.5 Solution phase NMR studies

2.3.5.1 ^{1}H chemical shifts of NH signals

An expansion of the spectral window where the NH proton signals are located for Aatc(Me) derivatives **42**, **44** and **46** is shown in Figure 116. The signals of carbamate NH(1) of the Cbz-Aatc(Me)-NHMe **42**, Cbz-[Aatc(Me)]$_2$-NHMe **44** and Cbz-[Aatc(Me)]$_3$-NHMe **46** (δ = 6.35 ppm, δ = 6.14 ppm and δ = 6.38 ppm, respectively) were deshielded but were not in very downfield regions which may suggest their involvement in weak strength of H-bonds. The NH protons of each amide function in the Cbz-Aatc(Me)-NHMe **42** (δNH(2) = 8.24 ppm), Cbz-[Aatc(Me)]$_2$-NHMe **44** (δNH(2) = 9.07 ppm, δNH(3) = 7.94 ppm) and Cbz-[Aatc(Me)]$_3$-NHMe **46** (δNH(2) = 6.38 ppm, δNH(3) = 6.38 ppm and δNH(4) = 7.70 ppm) were all unshielded and located in more downfield regions, suggesting the involvement of each NH proton in an intramolecular H-bond, stronger than those NH(1) protons.

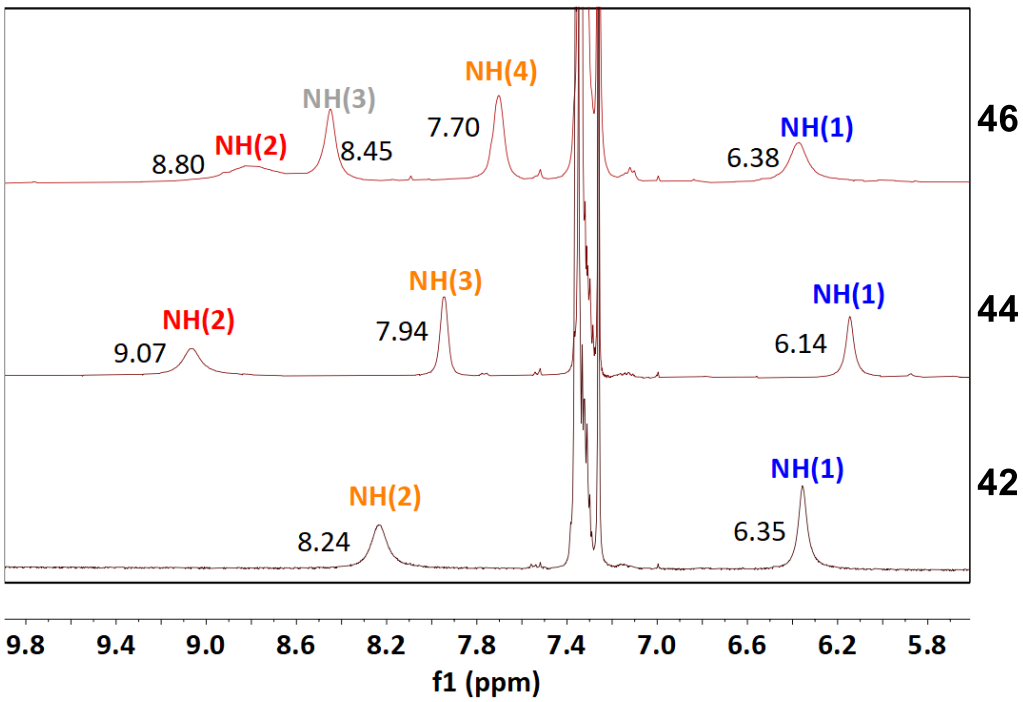

Figure 116. NH signals of Cbz-Aatc(Me)-NHMe **42** (bottom), Cbz-[Aatc(Me)]$_2$-NHMe **44** (middle) and Cbz-[Aatc(Me)]$_3$-NHMe **46** (top)

2.3.5.2 DMSO-d_6 titration experiments

*a. NH signal evolution of Cbz-Aatc(Me)-NHMe **42***

The DMSO-d_6 titration experiment was performed on Cbz-Aatc(Me)-NHMe **42**, and results are shown in Figure 117. After the total injection of 10% DMSO, NH(1) and NH(2) both showed small chemical shift changes, $\Delta\delta$ = 0.29 ppm and $\Delta\delta$ = –0.42 ppm, respectively. These results suggest that both NH(1) and NH(2) were intramolecularly H-bonded, consistent with a predominant C5-C6γ conformation. Other two conformers (free-C7 and free-π_{am}) suggested by infrared in solution have no evidence by DMSO-d_6 titration but not excluded.

	DMSO-d_6 (%, v/v)											
	0	*0.5*	*1*	*1.5*	*2*	*2.5*	*3*	*4*	*5*	*7.5*	*10*	Δδ
δNH1	6.33	6.36	6.38	6.40	6.42	6.44	6.47	6.49	6.52	6.57	6.62	0.29
δNH2	8.24	8.21	8.18	8.16	8.13	8.10	8.06	8.02	7.99	7.90	7.82	–0.42

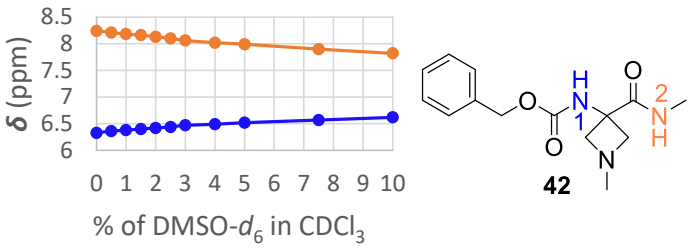

Figure 117. DMSO-d_6 titration of Cbz-Aatc(Me)-NHMe **42**

*b. NH signal evolution of Cbz-[Aatc(Me)]$_2$-NHMe **44***

The DMSO-d_6 titration experiment was performed on Cbz-[Aatc(Me)]$_2$-NHMe **44**, results are shown in Figure 118. 10% of DMSO-d_6 addition led to a downfield shift ($\Delta\delta$ = 0.58 ppm) for carbamate NH(1). Upfield shifts were observed for NH(2) and NH(3) ($\Delta\delta$ = –0.62 ppm and $\Delta\delta$ = –0.33 ppm), respectively. These values suggest each of these three NH protons was H-bonded, compatible with the co-existence of semi-extended C5-C6γ/π_{am} and fully extended C5-C6γ/C5-C6γ conformations. The lower value for NH(3) ($\Delta\delta$ = –0.33 ppm) compared to those of NH(2) ($\Delta\delta$ = –0.62 ppm) and NH(1) ($\Delta\delta$ = 0.58 ppm) indicating that NH(3) was less solvent accessible, may involve in a stronger H-bond, which may be due to the presence of the β-turn (free-free-C10) conformer implicating NH(3) in a C10 H-bond, NH(1) and NH(2) were free.

These results are compatible with the co-existence of three conformations (C5-C6γ/π_{am}, C5-C6γ/C5-C6γ and free-free-C10), as suggested by IR in solution.

	DMSO-d_6 (%, v/v)											
	0	*0.5*	*1*	*1.5*	*2*	*2.5*	*3*	*4*	*5*	*7.5*	*10*	Δδ
δNH1	6.12	6.16	6.20	6.23	6.27	6.30	6.34	6.40	6.46	6.59	6.70	0.58
δNH2	9.10	9.06	9.02	8.98	8.94	8.90	8.86	8.79	8.73	8.59	8.48	–0.62
δNH3	7.96	7.95	7.93	7.91	7.89	7.87	7.86	7.82	7.79	7.71	7.63	–0.33

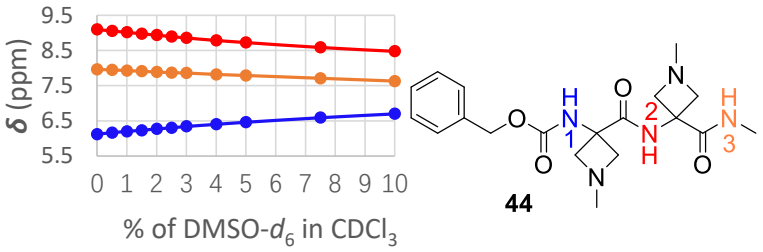

Figure 118. DMSO-d_6 titration of Cbz-[Aatc(Me)]$_2$-NHMe **44**

*c. NH signal evolution of Cbz-[Aatc(Me)]$_3$-NHMe **46***

Cbz-[Aatc(Me)]$_3$-NHMe **46** was submitted to the DMSO-d_6 titration experiment and results are shown in Figure 119. After the addition of 10% DMSO-d_6, carbamate NH(1) was significantly shifted to a downfield region ($\Delta\delta$ = 0.95 ppm) suggesting that NH(1) was more solvent accessible. Upfield shifts were observed for NH(2), NH(3) and NH(4) ($\Delta\delta$ = –0.51 ppm, $\Delta\delta$ = –0.58 ppm and $\Delta\delta$ = –0.60 ppm respectively) suggesting they were intramolecularly H-bonded. The higher coefficient of NH(1) may be attributed to the relative weakness of its C5 H-bond and the presence of a 3_{10}-helix conformation in which NH was free.

These results are compatible with two conformations in solution (a semi-extended C5-C6γ/π_{am}/C5-C6γ and a 3_{10}-helix) as had been suggested by IR in solution.

	DMSO-d_6 (%, v/v)											
	0	*0.5*	*1*	*1.5*	*2*	*2.5*	*3*	*4*	*5*	*7.5*	*10*	Δδ
δNH1	6.22	6.32	6.41	6.51	6.59	6.66	6.73	6.84	6.94	7.13	7.17	0.95
δNH2	8.85	8.80	8.73	8.68	8.63	8.58	8.55	8.49	8.44	8.38	8.34	–0.51
δNH3	8.48	8.43	8.38	8.33	8.29	8.25	8.21	8.15	8.09	7.98	7.90	–0.58
δNH4	7.79	7.75	7.70	7.65	7.60	7.56	7.52	7.45	7.40	7.27	7.19	–0.60

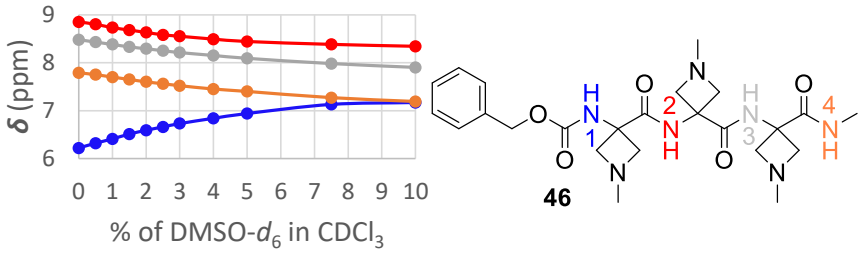

Figure 119. DMSO-d_6 titration of Cbz-[Aatc(Me)]$_3$-NHMe **46**

2.3.5.3 ^{1}H NMR experiments at variable temperatures

*a. NH signal evolution of Cbz-Aatc(Me)-NHMe **42***

The temperature variation experiment was carried out on the Cbz-Aatc(Me)-NHMe **42**, results are shown in Figure 120. When the temperature was increased from 300 K to 325 K, both NH protons showed low temperature coefficients, –2.8 ppb/K for NH(1) and –4.0 ppb/K for NH(2) indicating they were both H-bonded. These results are consistent with a predominant C5-C6γ H-bonded conformation, but not exclude contributions from the free-C7 and free-π_{am} conformer families as suggested by IR in solution.

	T (K)						
	300	*305*	*310*	*315*	*320*	*325*	**T.C. (ppb/K)**
δ NH1	6.35	6.34	6.32	6.31	6.29	6.28	–2.8
δ NH2	8.24	8.22	8.20	8.18	8.16	8.14	–4.0

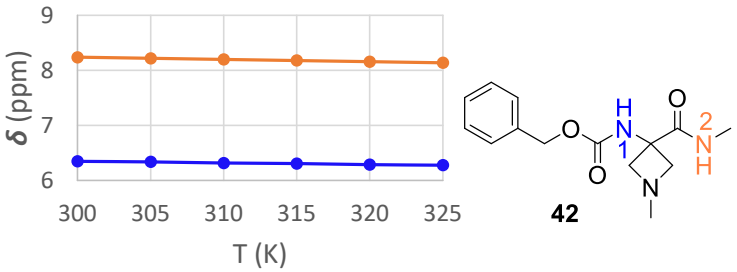

Figure 120. Temperature variation experiment of Cbz-Aatc(Me)-NHMe **42**

*b. NH signal evolution of Cbz-[Aatc(Me)]$_2$-NHMe **44***

The temperature variation experiment was performed on Cbz-[Aatc(Me)]$_2$-NHMe **44**, results are shown in Figure 121. When the temperature was increased from 300 K to 325 K, all three NH protons were shifted upfield with low temperature coefficients, –4.0 ppb/K for NH(1), –4.0 ppb/K for NH(2) and –3.2 ppb/K for NH(3) suggesting they were engaged in H-bonds. The data are consistent with the DMSO-d_6 titration results and are compatible with co-existence of semi-extended C5-C6γ/π_{am}, fully extended C5-C6γ/C5-C6γ. In particular, the temperature coefficient of NH(3) was slightly lower than those of NH(2) and NH(1), which would be expected for a contribution from a β-turn (free-free-C10) conformation, in which NH(1) and NH(2) were free, NH(3) was in a C10 H-bond.

These results are compatible with the co-existence of three conformations (C5-C6γ/π_{am}, C5-C6γ/C5-C6γ and β-turn) as suggested by IR in solution.

	T (K)						
	300	*305*	*310*	*315*	*320*	*325*	**T.C. (ppb/K)**
δ NH1	6.14	6.12	6.10	6.08	6.06	6.04	–4.0
δ NH2	9.07	9.05	9.03	9.01	8.99	8.97	–4.0
δ NH3	7.94	7.93	7.91	7.89	7.88	7.86	–3.2

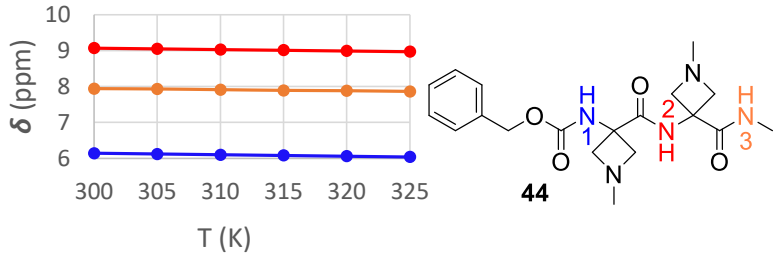

Figure 121. Temperature variation experiment of Cbz-[Aatc(Me)]$_2$-NHMe **44**

*c. NH signal evolution of Cbz-[Aatc(Me)]$_3$-NHMe **46***

The temperature variation experiment was performed on Cbz-[Aatc(Me)]$_3$-NHMe **46**, results are shown in Figure 122. Over a 25 K temperature range, a significant temperature coefficient for NH(1) (T.C. = –10.4 ppb/K) indicating that the NH(1) was more solvent exposed, may not strongly hydrogen-bonded. Low temperature coefficients for NH(2), NH(3) and NH(4), as –2.4 ppb/K, –0.4 ppb/K and 0 ppb/K, respectively, suggesting they were intramolecularly H-bonded, consistent with the DMSO-d_6 titration results.

The high coefficient of NH(1) may be attributed to the relative weakness of its C5 H-bond and the presence of a 3_{10}-helix conformation in which it was free. Therefore, these results are compatible with two main conformations in solution (a semi-extended C5-C6γ/π_{am}/C5-C6γ and a 3_{10}-helix) suggested by IR in solution.

	T (K)						
	300	*305*	*310*	*315*	*320*	*325*	**T.C. (ppb/K)**
δ NH1	6.38	6.31	6.25	6.20	6.15	6.12	–10.4
δ NH2	8.81	8.79	8.77	8.77	8.75	8.75	–2.4
δ NH3	8.45	8.45	8.45	8.45	8.45	8.44	–0.4
δ NH4	7.70	7.71	7.72	7.71	7.71	7.70	0

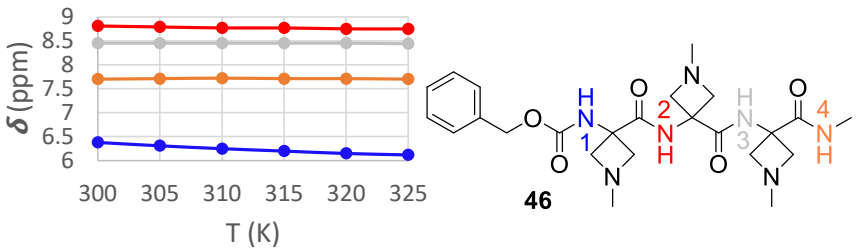

Figure 122. Temperature variation experiment of Cbz-[Aatc(Me)]$_3$-NHMe **46**

2.3.5.4 ^{1}H-^{1}H 2D NOESY studies

*a. NOESY experiment of Cbz-Aatc(Me)-NHMe **42***

From the ^{1}H-^{1}H NOESY experiment on the Cbz-Aatc(Me)-NHMe **42**, the correlation map for NH(1) and NH(2), and signal assignments are shown in Figure 123. A medium cross peak between NH(1) and the $C^\beta H^a$ protons, a strong cross peak between NH(2) and the $C^\beta H^b$ protons indicated that the distance between NH(2) and $C^\beta H^b$ protons is shorter than the distance between NH(1) and $C^\beta H^a$ protons. In addition, NH(2) had a weak correlations with $C^\beta H^a$ protons and a strong correlation with the neighboring methyl protons.

The correlation map showed local interactions, was in complete agreement with a dominant C5-C6γ extended conformation, as suggested by infrared spectroscopy studies in solution and 1D ^{1}H NMR experimental data.

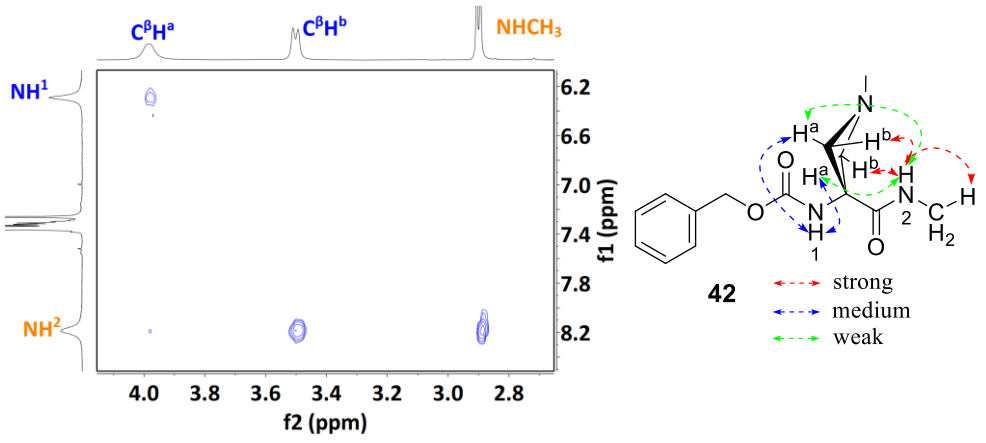

Figure 123. NOESY correlation map and signal assignments for Cbz-Aatc(Me)-NHMe **42**

*b. NOESY experiment of Cbz-[Aatc(Me)]$_2$-NHMe **44***

From the ^{1}H-^{1}H NOESY experiment on the Cbz-[Aatc(Me)]$_2$-NHMe **44**, the correlation map for NHs and signal assignments are shown in Figure 124. A medium cross peak was observed between NH(1) and the $C^{\beta}H^{a1}$ protons. NH(2) has moderate correlations with the $C^{\beta}H^{a2}$ protons and the $C^{\beta}H^{b1}$ protons. NH(3) showed strong correlation with the $C^{\beta}H^{b2}$ protons and weak correlation with both $C^{\beta}H^{a2}$ protons indicating the distance between the NH(3) and $C^{\beta}H^{b2}$ protons is shorter than the distance between the NH(2) and $C^{\beta}H^{b1}$ protons. These results are compatible with both a C5-C6γ/π_{am} semi-extended and a fully extended C5-C6γ/C5-C6γ conformations, as had been suggested by infrared in solution. The correlation map and signal assignments showed no evidence of the presence of a β-turn conformer.

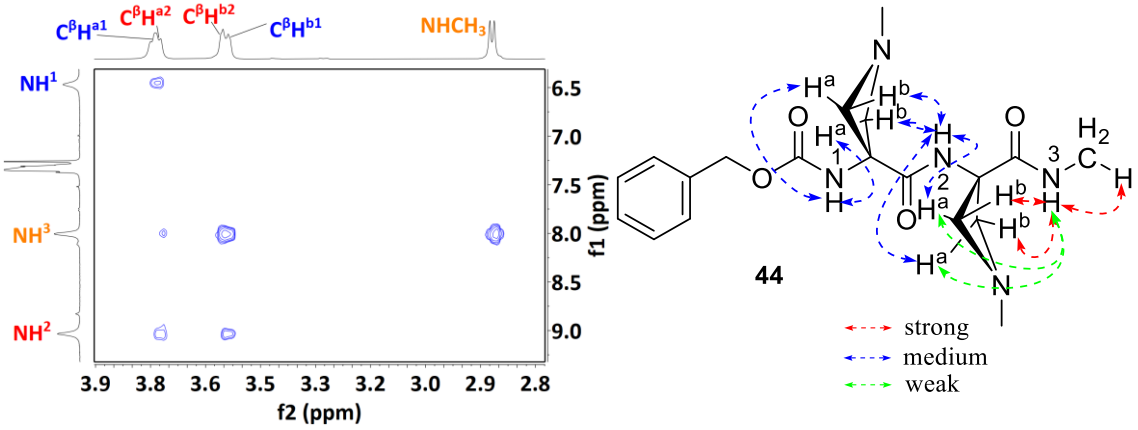

Figure 124. NOESY correlation map and signal assignments for Cbz-[Aatc(Me)]$_2$-NHMe **44**

*c. NOESY experiment of Cbz-[Aatc(Me)]$_3$-NHMe **46***

From the ^{1}H-^{1}H NOESY experiment on Cbz-[Aatc(Me)]$_3$-NHMe **46**, the correlation map of NHs and signal assignments are shown in Figure 125. NH(4) had a strong correlation with the $C^{\beta}H^{b3}$ protons and with the neighboring methyl protons, similarly to NH(2) of the Cbz-Aatc(Me)-NHMe **42** and NH(3) of the Cbz-[Aatc(Me)]$_2$-NHMe **44**. Medium cross peaks appeared between NH(1) and $C^{\beta}H^{a1}$ protons and $C^{\beta}H^{b1}$ protons. NH(3) present four moderate correlations with $C^{\beta}H^{a2}$, $C^{\beta}H^{b2}$, $C^{\beta}H^{a3}$ and $C^{\beta}H^{b3}$ protons. NH(2) of trimer **46** showed two weak correlations with $C^{\beta}H^{a2}$ protons and $C^{\beta}H^{b1}$ protons, whereas these correlations in the dimer **44** displayed medium intensity indicating that the C5-C6γ H-bonding system of the former may be challenged by alternative conformation, which are compatible with a semi-extended C5-C6γ/π_{am}/C5-C6γ conformation. Notably, a weak correlation between CH_2^{Cbz} protons and $C^{\beta}H^{a3}$ protons was observed, indicating the possible presence of a 3_{10}-helix conformation, as had been suggested by IR in solution.

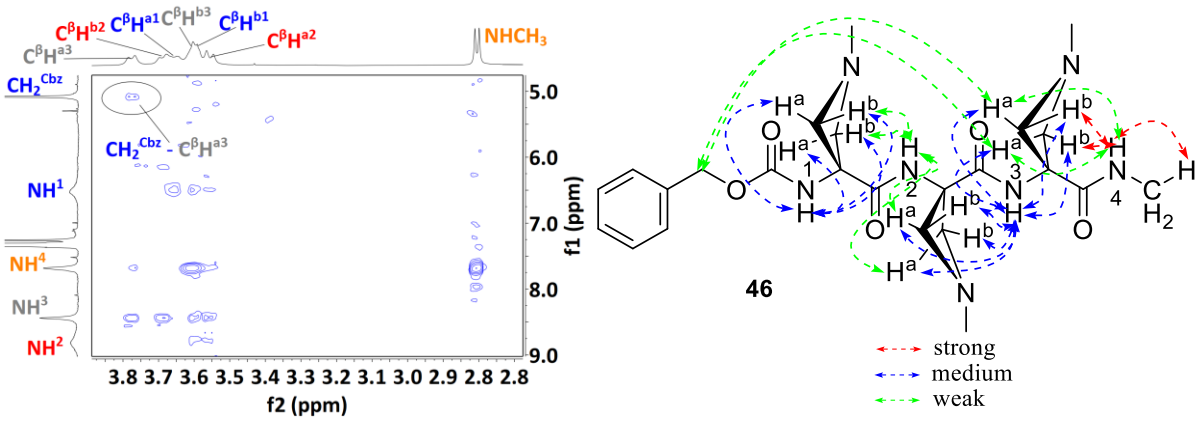

Figure 125. NOESY correlation map and signal assignments for Cbz-[Aatc(Me)]$_3$-NHMe **46**

2.3.6 Conclusions and Discussion

Collectively, the results from infrared and NMR studies in solution are in complete agreement that the monomer Cbz-Aatc(Me)-NHMe **42** adopts a predominant C5-C6γ extended conformation. The free-C7 and free-π_{am} conformers were detected by infrared but made only minor contributions (Figure 126).

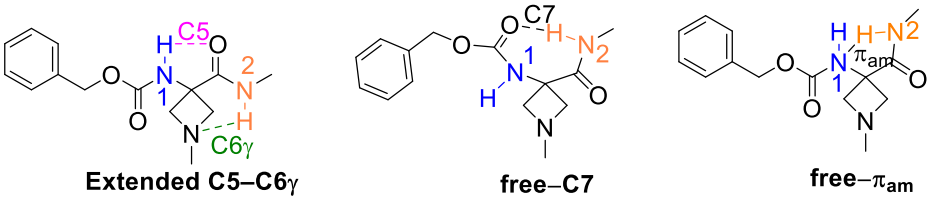

Figure 126. Three conformations present in Cbz-Aatc(Me)-NHMe **42** in solution

In solution, the dimer Cbz-[Aatc(Me)]$_2$-NHMe **44**, the C5-C6γ H-bonding motif was still in evidence suggested by infrared and by 1D/2D NMR. However, the fully extended C5-C6γ/C5-C6γ conformation was accompanied by a semi-extended C5-C6γ/π_{am} conformation and by a β-turn conformation, as had been suggested by infrared spectroscopy (Figure 127).

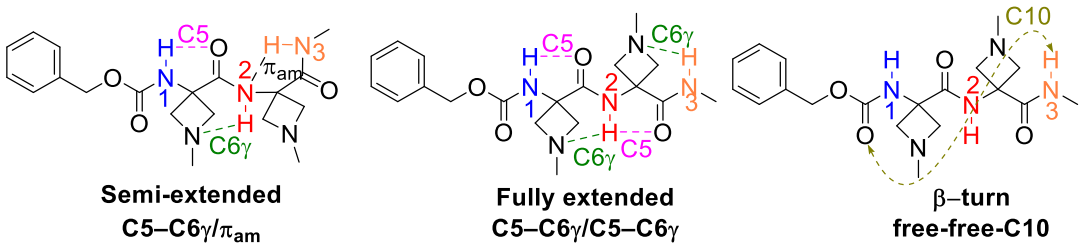

Figure 127. Three conformations present in Cbz-[Aatc(Me)]$_2$-NHMe **44** in solution

In the trimer Cbz-[Aatc(Me)]$_3$-NHMe **46**, results obtained from 1D/2D NMR studies (^{1}H chemical shifts of NH protons, DMSO-d_6 titration, temperature variation experiments and NOESY) agreed that the C5-C6γ was in evidence but the fully extended C5-C6γ/C5-C6γ/C5-C6γ conformer is not competitive and replaced by semi-extended C5-C6γ/π_{am}/C5-C6γ and 3_{10}-helix conformations, as had been observed by infrared in solution (Figure 128).

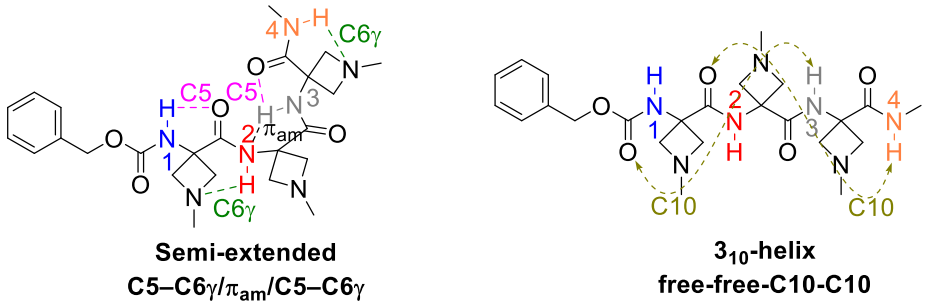

Figure 128. Two conformations present in Cbz-[Aatc(Me)]$_3$-NHMe **46** in solution

Therefore, in solution, the C5-C6γ H-bonding motifs are present on the conformational landscape of all three compounds, but the consecutive C5-C6γ motifs are less competitive than alternative partially folded structures. These findings may suggest that the longer the Aatc(Me) oligomer chain, the more likely it will fold into a 3_{10}-helix conformation.

In gas phase, Cbz-Aatc(Me)-NHMe **42**, Cbz-[Aatc(Me)]$_2$-NHMe **44** and Cbz-[Aatc(Me)]$_3$-NHMe **46** appeared to more favour to persist the extended conformation compared to in solution phase. The successive locally planar C5-C6γ motifs override the options to fold into more compact structures, resulting in a dominant extended backbone conformation of the 2.0_5-helix. These architectures are globally stabilized through a succession of cooperative intra-residue C5 backbone and inter-residue N–H···N C6γ H-bonds. Overall, the conformation landscape of each compound, no C5 conformation was observed without the support of a C6γ H-bond, suggest that the N–H···N C6γ interaction play an essential role in stabilizing the weak C5 H-bond.

2.4 Conformational studies of Cbz-[Aatc(Me)]$_4$-NHMe **48**

2.4.1 Gas phase studies

Gas phase study of the tetramer Cbz-[Aatc(Me)]$_4$-NHMe **48** was attempted. However, a massive fragmentation process was observed, as testified by the mass spectrum (Figure 129). It was recorded with the UV laser tuned on the main transition of dimer **44** and trimer **46** at 37588 cm^{-1}. No parent ion (m/z = 613) could be observed: the largest (and most intense) mass

channel observed was m/z = 228. The UV spectrum recorded by R2PI on this mass channel was flat in a large region between 36500 and 37650 cm^{-1}, suggesting the presence of an UV chromophore possessing a more red-shifted absorption than the benzyl ring of Cbz, potentially a doubly substituted phenyl ring, which might be formed during the laser-desorption process.

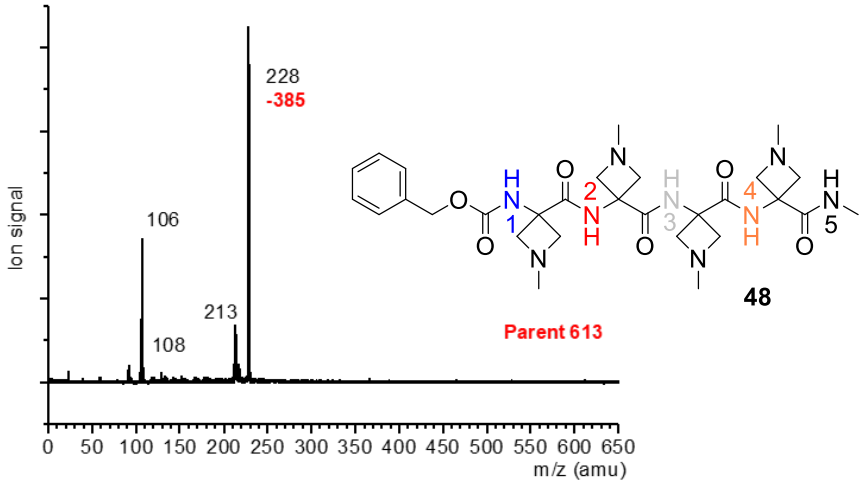

Figure 129. Mass spectrum of Cbz-[Aatc(Me)]$_4$-NHMe **48**, was recorded with the UV laser tuned on the main transition of dimer **44** and trimer **46** at 37588 cm^{-1}

2.4.2 Solution phase IR studies

The infrared spectrum of Cbz-[Aatc(Me)]$_4$-NHMe **48** in solution showed, a broad band at 3329 cm^{-1} and extending down to 3150 cm^{-1}. Two other shoulders located at 3380 and 3430 cm^{-1} (Figure 130, green line). With comparison to other three derivatives **42**, **44** and **4**6, the bands at 3329 and 3380 cm^{-1} may contribute to C10 H-bonds implicating NH(3), NH(4) and NH(5), NH(1) and NH(2) account for the absorptions at 3430 cm^{-1}. These data are compatible with a 3_{10}-helix conformation present in solution.

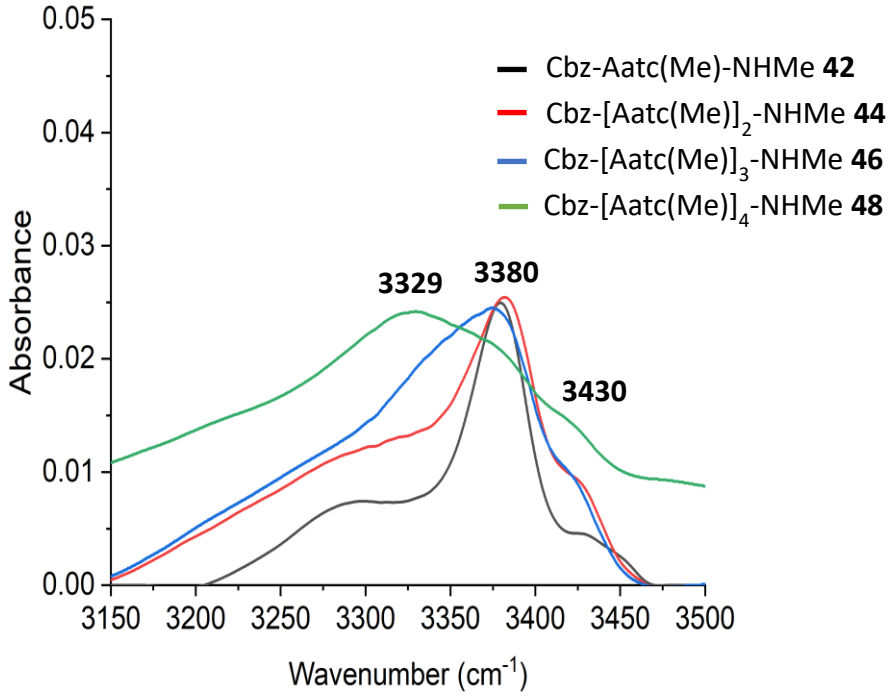

Figure 130. Infrared spectra in solution of four Aatc(Me) derivatives **42**, **44**, **46** and **48** at 5 mM concentration

2.4.3 ^{1}H NMR spectrum

The ^{1}H NMR spectrum of Cbz-[Aatc(Me)]$_4$-NHMe **48** is shown in Figure 131. We observed one NH signal was overlapped with the aromatic peak, and this NH proton was assigned to NH(5), confirmed by COSY spectrum that it correlated with methyl proton. One NH signal at 6.78 ppm may correspond to NH(1), other three NH signals located in lower field region suggesting they were H-bonded, but without clear assignment checked by standard 1D/2D NMR techniques. These NH signals appeared as broad peaks, indicative of an exchange process or interconversion between several conformations. The assignment of C$^{\beta}$H$_2$ protons of four azetidine residues for tetramer **48** was not clear as well due to the peaks were overlapped. In this case, other 1D/2D NMR experiments for conformation studies were challenging to perform.

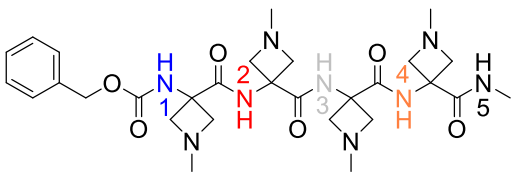

48

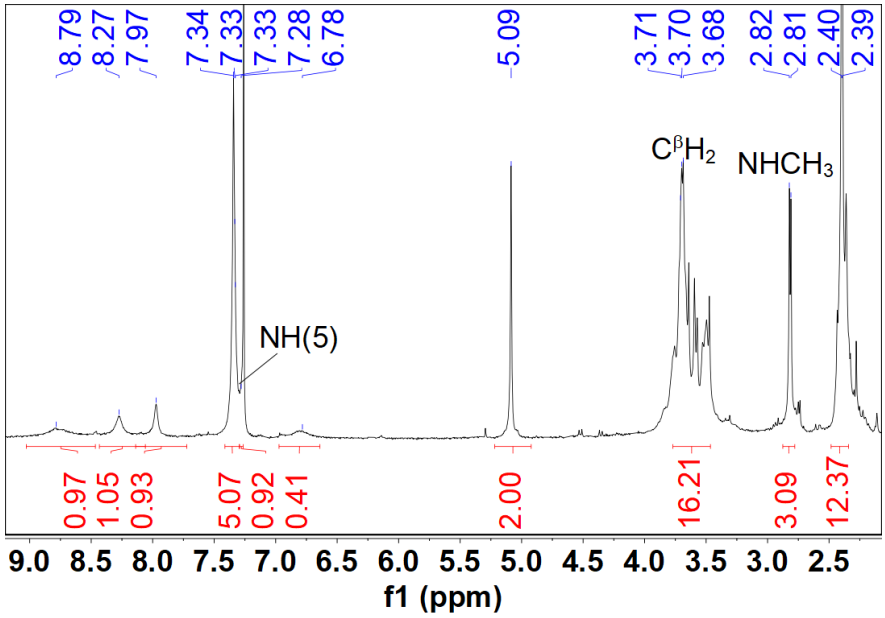

Figure 131. ^{1}H NMR spectrum of Cbz-[Aatc(Me)]$_4$-NHMe **48**

2.4.4 Discussion

Due to the undesired fragmentation process, Cbz-[Aatc(Me)]$_4$-NHMe **48** did not manage to perform further gas phase studies. In solution, the challenging assignments and exchange process or interconversion issues between several conformations in solution, further 1D/2D NMR studies did not perform. However, on the basis of limited data of tetramer **48**, compared with other three Aatc(Me) derivatives **42**, **44** and **46**, the ^{1}H NMR chemical shift of NH protons and IR in solution results are compatible with a 3_{10}-helix conformation present in solution, may evidence that the longer the Aatc(Me) oligomer chain, the more likely it will be a folded conformation.

2.5 Conclusion and Perspectives

In this chapter, a post-synthetic modification strategy has proven successful for the preparation of the Aatc(Me) oligomer series. While the achievement bears a resemblance to classical final-stage deprotection of peptides, it was more challenging, since deprotection was followed by final-step methylation of all the free-amine residues present in the oligomer. This accomplishment provides a new contribution to the emerging area of controlled post-synthetic modification of peptides and expands the repertoire of building blocks of azetidine-3-carboxylic acid, which is of recognized interest for biological applications and drug design.[184,185]

The demonstration of the fully extended C5-C6γ/C5-C6γ/C5-C6γ conformer of compound **46** in gas phase is the first example of a 2.0_5-helix whose stability relies on cooperative hydrogen bonding rather than steric effects. In solution, the fully extended 2.0_5-helix gives way to folded conformations, one of which is the classical 3_{10}-helix, but the other of which is a semi-extended conformer in which two separate C5-C6γ motifs prevail. This suggests that a local C5-C6γ motif may be sufficiently robust to serve as a localized planar "spacer" feature in larger peptides with more diverse primary sequences, and as such contributes a useful tool for the design of peptide architecture.

Chapter 3. Synthesis and conformational studies of Aatc and Attc oxide derivatives

Chapter 3. Synthesis and conformational studies of Aatc and Attc oxide derivatives

3.1 Introduction

In peptides and proteins, the oxygen atom act as H-bond acceptor primarily through the carbonyl functional group, which forms H-bond with amide proton in the backbone. However, there are other instances where oxygen can act as H-bond acceptor for conformational contribution.

3.1.1 Acetyl oxygen

α,α-Disubstituted α-amino acid derived oligopeptides have demonstrated a propensity to adopt 3_{10}- and α-helix conformations, specifically, α-aminoisobutyric acid (Aib) due to the bulky nature of the Aib side chain, which restricts conformational flexibility and favors the formation of helical structures. Whereas many cyclic α,α-disubstituted α-amino acids with acetal moieties have shown other conformational preferences.

In 1998, the Toniolo group reported the conformational preferences of Hms(Ipr) (*O*,*O*-isopropylidene-α-hydroxymethylserine) derived homopeptides. Unlike the typical 3_{10}-helix conformation formed by Ac_6c (1-amino cyclohexane carboxylicacid) peptides, these peptides were destabilized by intramolecular H-bonds between side chain acetal -O- and main chain NH. In the crystal structures, Boc-$[HmS(Ipr)]_2$-OMe (**A**) showed a six-membered ring, intramolecular H-bond (C6γ) formed between $N–H^{i+1}$ and $-O-^{i}$. The homo-tripeptide Cbz-$[HmS(Ipr)]_3$-OMe (**B**) displayed two intramolecular H-bonds (a C5 intra-residue and a C6γ). The 3_{10}-helix conformation was exhibited in the tetrapeptide Cbz-$[HmS(Ipr)]_4$-OMe (**C**), two C10 H-bonds, and a C6γ H-bond formed from the side chain (Figure 132).[176]

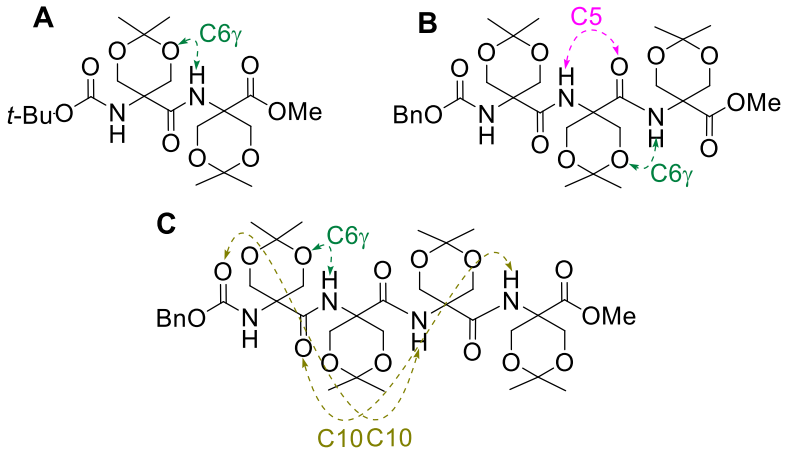

Figure 132. H-bonding patterns of Hms(Ipr) derived homo-peptides in crystal structures

In 2015, Tanaka described the conformational preferences of a series of homopeptides derived from (*R*,*R*)-Ac$_6$c^{35dBu}, in which two chiral acetal moieties located at 3,5 positions of the cyclohexane, aim to help the formation of H-bonds with side chains. Three homo-peptides were characterized by infrared in solution, suggested that only C6δ H-bonds between peptide NH and acetal -O- (ether) of the same residue were observed (Figure 133). In crystal structures, homo-dipeptide (**B**) and homo-tripeptide (the crystal structure of homo-tripeptide is a COOH at *C*-terminal of **C**) both have shown consecutive C6δ H-bonds.[93]

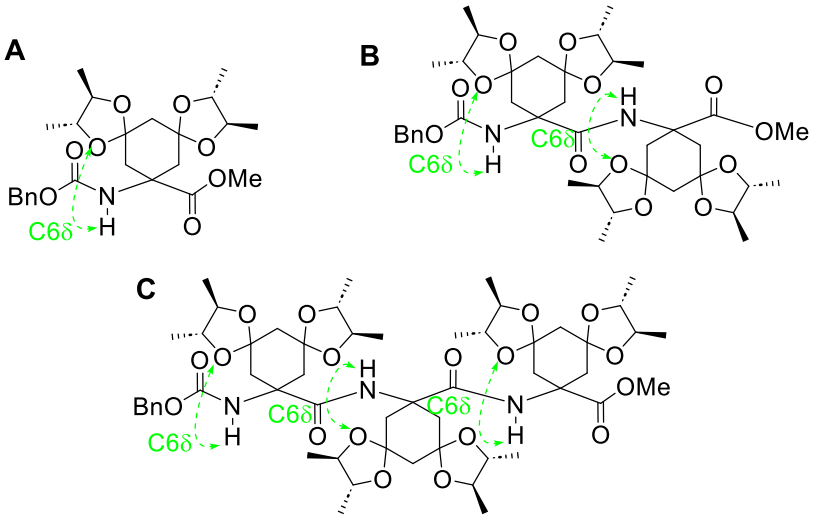

Figure 133. H-bonding patterns of (*R*,*R*)-Ac$_6$c^{35dBu} homopeptides in solution

3.1.2 *N*-oxides

N-oxides are known for their high polarity, which stems from the charges of nitrogen and oxygen, and from the electronegativity difference between the nitrogen and oxygen atoms. The oxygen atom of the *N*-oxide functional group is an excellent hydrogen-bond acceptor due

to its negative charge, which allows it to form H-bonds and can contribute to the stabilization of molecular conformations.

In 1993, the O'Neil group described the oxidation of *N*-benzyl L-proline amide to the corresponding *N*-oxide. Generally, *N*-oxides are unstable and easy convert to more stable and low-polarity products by arrangement.[186,187] The chiral proline *N*-oxide produced in this work showed remarkable stability may correspond to intramolecular H-bonding, suggested by NMR and crystal structure (Scheme 37).[188]

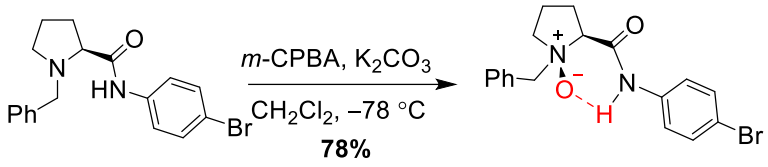

Scheme 37. The chiral proline *N*-oxide was stabilized by an intramolecular N–H···O H-bond

In 1995, O'Neil described the oxidation of a series of *N*-alkylated proline and azetidine derivatives, which bear H-bond donors in both *N*-substituent and carboxyamide residues to investigate the oxygen H-bonding capability of amine oxide. Verified by ^{1}H NMR, both NH signals of the *N*-oxide peptides were in more downfield than their precursors, indicating both NH protons were intramolecularly H-bonded to the oxygen of the amine oxide. The stability of these *N*-oxides was contributed to intramolecular H-bonds, even though the azetidine oxide was decomposed in flash chromatography on silica (Scheme 38).[189]

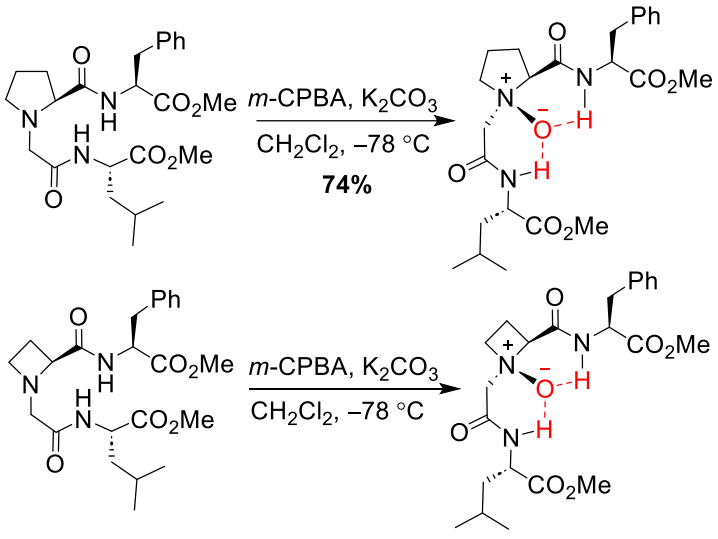

Scheme 38. Proline *N*-oxide and azetidine *N*-oxide as strong H-bond acceptors forming intramolecular H-bonds

3.1.3 *S*-oxides

Sulfide can be partially oxidized to a sulfoxide or completely oxidized to sulfone in oxidizing conditions. The oxygen atom in sulfoxide or sulfone can act as a hydrogen bond acceptor for conformational contribution.

In 1998, Craik reported the oxidation of methionine Amyloid β-peptide Aβ(1-40) into the Aβ(1-40)Met(O) with induced its conformation change. The Aβ(1-40) is known to adopt a helical conformation within the membrane-spanning amyloid precursor proteins (APPs), to a random coil form in water, then to transform into a β-sheet structure which aggregates. But Aβ(1-40)Met(O) destabilized the helical conformation, possibly due to the oxygen of the methionine sulfoxide as H-bonding acceptor forming H-bond with the main chain amide NH proton. These results were suggested by ^{1}H NMR and NOE correlation studies and supported by theoretical calculations.[190]

In 2001, Burgess described the oxidation of a cyclic thioether inducing the generation of a β-turn conformation. In this peptide, the distance between NH and O=S facilitated the formation of a NH^{i+2}···O=S H-bond. This result was suggested by NMR studies and supported by theoretical calculations. With the partial oxidation of cyclic thioether to sulfoxide (*cis* and *trans*), only the *cis*-sulfoxide formed an N–H^{i+2}···O=S H-bond and exhibited a β-turn conformation (Scheme 39).[191]

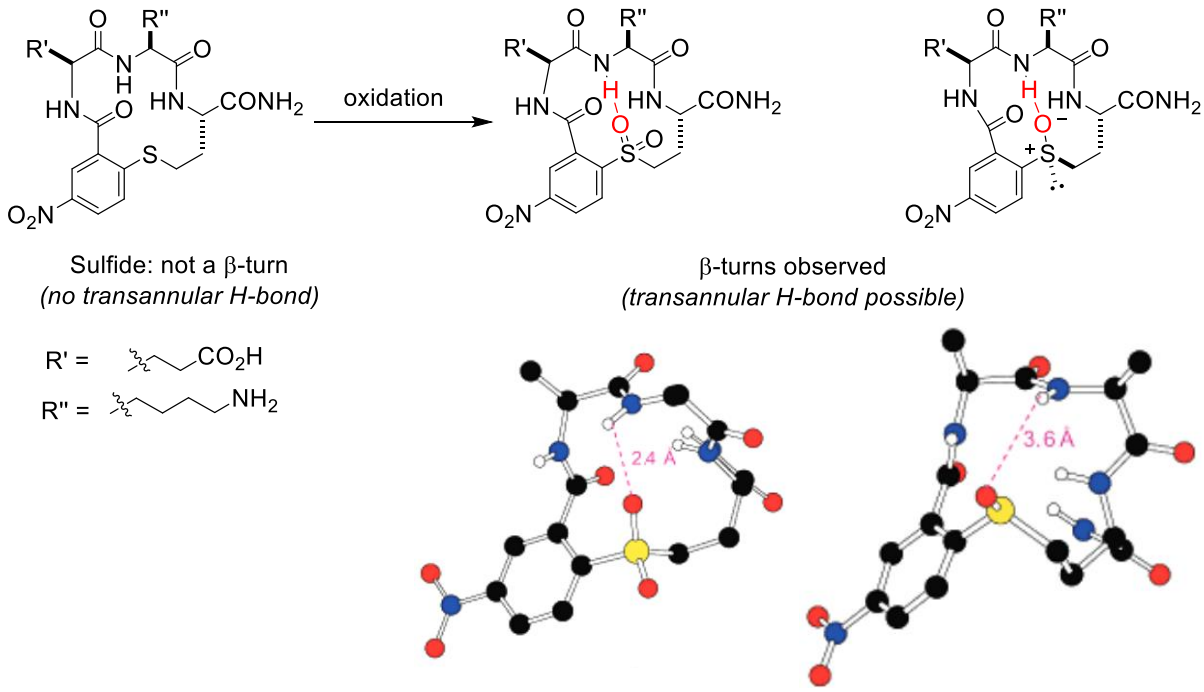

Scheme 39. The H-bonding pattern of cyclic sulfone and sulfoxide (top) and β-turn conformations simulated by QMD (bottom) (These two conformation images were reproduced from the literature)[191]

3.1.4 Aim of this chapter

The intra-residue C5 H-bond, is relatively weak in strength but contributes significantly to peptides and proteins stabilization. Normally, the C5 H-bond is formed along with other inter-residue H-bonds to stabilize a conformation.

In 2020, the Aitken group reported the stabilization of a C5 H-bond by supportive N–H···X interaction. In the Cbz-Attc-NHMe **54** (Figure 134, left), a C5 H-bond was supported by an N–H···S C6γ H-bond. The C6γ H-bond implicating the sulfur atom of the thietane moiety showed the capability to intramolecularly H-bonded to the amide NH and stabilized the weak C5 interaction in the backbone, exhibiting an extended conformation. The Cbz-Aatc(Me)-NHMe **42** (Figure 134, right) also exhibited a predominant C5-C6γ H-bonding feature, suggested by infrared studies in gas and solution phases and NMR studies. The nitrogen atom of azetidine moiety formed a six-membered H-bonding ring with amide NH and stabilized the weak C5 H-bond in the backbone.[154]

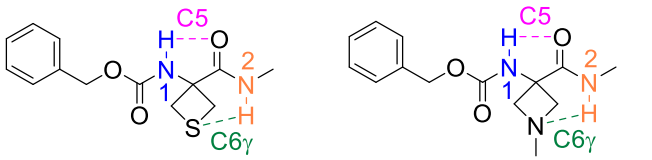

Cbz-Attc-NHMe **54** Cbz-Aatc(Me)-NHMe **42**

Figure 134. The stabilization of a C5 H-bond in Cbz-Attc-NHMe **54** (left) and Cbz-Aatc(Me)-NHMe **42** (right)

On the basis of these findings, we aim to investigate the conformational preferences of oxidized Aatc and Attc derivatives, Cbz-Aatc(Me,O)-NHMe, Cbz-Attc(O)-NHMe and Cbz-Attc(O,O)-NHMe.

The influence of generated oxygen atom in the conformation will be assessed. Introducing the oxygen atom may disrupt the C5-C6γ extended conformation, and could lead to a C6δ H-bond, or a C7δ H-bond that may stabilize the C5 H-bond and result in a new conformation. Alternately, the presence of the oxygen atom may not disturb C5-C6γ extended conformation in some cases (Figure 135).

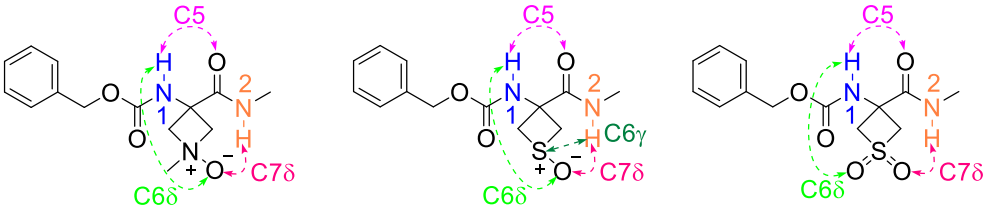

Cbz-Aatc(Me,O)-NHMe Cbz-Attc(O)-NHMe Cbz-Attc(O,O)-NHMe

Figure 135. Possible H-bonds in the oxidized structures

3.2 Synthesis of Cbz-Aatc(Me,O)-NHMe *trans* **49**

3.2.1 Synthesis of Cbz-Aatc(Me,O)-NHMe *trans* **49**

Inspired by the method of O'Neil,[188] the oxidation of Aatc(Me) derivative **42** was performed using 1 equivalent of 3-chloroperoxybenzoic acid (*m*-CPBA) as the oxidant, in the presence of 2 equivalents of potassium carbonate as the base (Scheme 40), at –78 °C for 3 hours. Purification by column chromatography Cbz-Aatc(Me,O)-NHMe *trans* **49** was obtained in 83% yield, as a white solid and the only product. Identification of the structure was determined by X-ray diffraction analysis (See section 3.4.6). Additionally, the sample of Cbz-Aatc(Me,O)-NHMe *trans* **49** was stored at room temperature for a couple of months without any degradation.

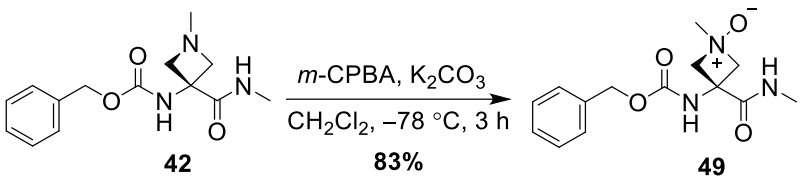

Scheme 40. The oxidation of Cbz-Aatc(Me)-NHMe **42** with *m*-CPBA

3.2.2 Thermal stability experiments of Cbz-Aatc(Me,O)-NHMe *trans* **49**

Couty described the formation and rearrangement of azetidine *N*-oxides to isoxazolidines at room temperature (Scheme 41). The oxidation was carried out using 1.5 equivalents of *m*-CPBA in the presence of 3 equivalents of sodium carbonate at room temperature for 2 hours. The azetidine *N*-oxides were thermally unstable and rearranged to isoxazolidines directly.[192]

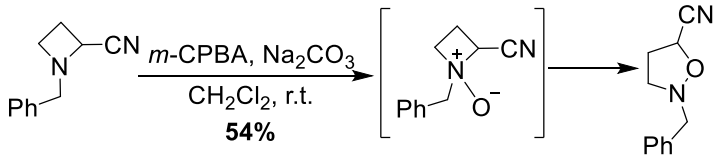

Scheme 41. Rearrangement of azetidine *N*-oxides to isoxazolidines

Compared with Couty's azetidine *N*-oxides, Cbz-Aatc(Me,O)-NHMe *trans* **49** showed remarkable stability. To evaluate the stability of Cbz-Aatc(Me,O)-NHMe *trans* **49**, we conducted a series of thermal stability experiments by refluxing the compound **49** in different chlorinated solvents (CH_2Cl_2, $CHCl_3$ and 1,2-dichloroethane) of increasing boiling point for three hours. The reaction mixture was checked by TLC and ^{1}H NMR, and results are shown in Table 18.

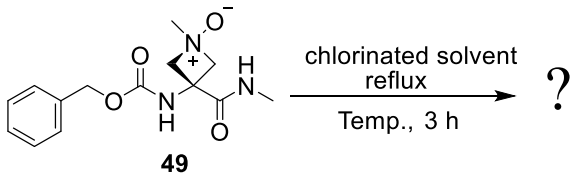

49

Entry	Solvent	Temperature (°C)	**49** (yield[a], %)
1	CH_2Cl_2	40	100
2	$CHCl_3$	61	100
3	1,2-DCE	84	0

a: isolated yield.

Table 18. Thermal stability experiment of Cbz-Aatc(Me,O)-NHMe *trans* **49**

The thermal stability experiments running in dichloromethane and in chloroform, respective showed no degradation of Cbz-Aatc(Me,O)-NHMe *trans* **49** checked by TLC and ^{1}H NMR, and starting material was fully recovered (Table 18, entries 1 and 2). 1,2-dichloroethane (1,2-DCE) was then used as a higher boiling point solvent. After three hours of reflux, the colorless solution had turned pale yellow. The reaction mixture was checked by TLC, and all Cbz-Aatc(Me,O)-NHMe *trans* **49** had been consumed (Table 18, entry 3). After purification by column chromatography, we obtained deoxygenated compound Cbz-Aatc(Me)-NHMe **42** with a yield of 25%, with no observation of rearranged product.

The remarkable stability of Cbz-Aatc(Me,O)-NHMe *trans* **49** in thermal experiments, could possibly be due to an intramolecular N–H···O–N H-bond within the molecule.

3.3 Synthesis of Cbz-Attc(O)-NHMe **55**, **56** and Cbz-Attc(O,O)-NHMe **57**

3.3.1 Preparation of Cbz-Attc-NHMe **54**

Cbz-Attc-NHMe **54** was prepared as described in the literature,[153] from commercially available thietane-3-one **50** and completed over four steps (Scheme 42). Inspired by Kozikowski's work,[193] thietane-3-one **50** was treated with potassium cyanide and ammonium carbonate to perform a Bucherer-Bergs reaction, and gave hydantoin **51** in 82 % crude yield. After successive saponification and acidification, free amino acid (Attc) **52** was obtained. Reaction with CbzOSu afforded crude Cbz-Attc **53**, which was treated with IBCF in the presence of NMM, and coupled with methylamine (40% aq.). After purification by column

chromatography, Cbz-Attc-NHMe **54** was obtained as a white solid, with an overall yield of 36% for the last three steps.

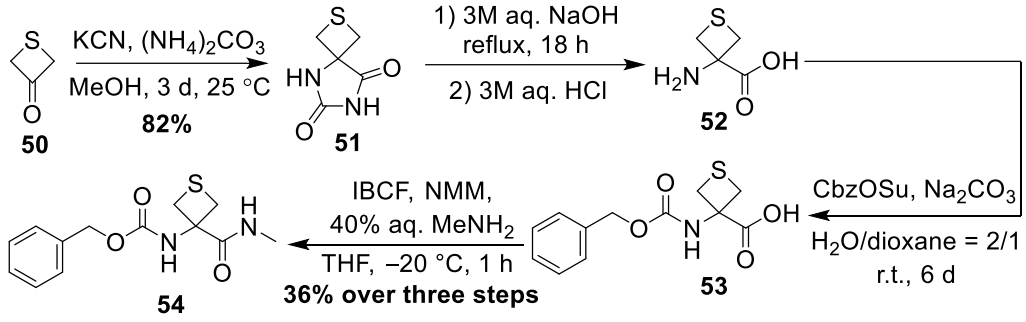

Scheme 42. Preparation of Cbz-Attc-NHMe **54**

3.3.2 Preparation of Cbz-Attc(O)-NHMe *trans* **55** and *cis* **56**

Two oxidizing conditions were performed on the oxidation of Cbz-Attc-NHMe **54**.

a. H_2O_2-AcOH as the oxidant

Taking inspiration from Volynskii's work[194], oxidation of Cbz-Attc-NHMe **54** was conducted using H_2O_2-AcOH as the oxidant. The reaction worked efficiently at 10 °C and gave sulfoxide in 90% yield after purification by column chromatography. Two isomers were separated, and the ratio of Cbz-Attc(O)-NHMe *trans* **55** to Cbz-Attc(O)-NHMe *cis* **56** was determined as 1:2 (by ^{1}H NMR, before the separation) (Scheme 43). The structures were determined by X-ray diffraction analysis (See section 3.4.6).

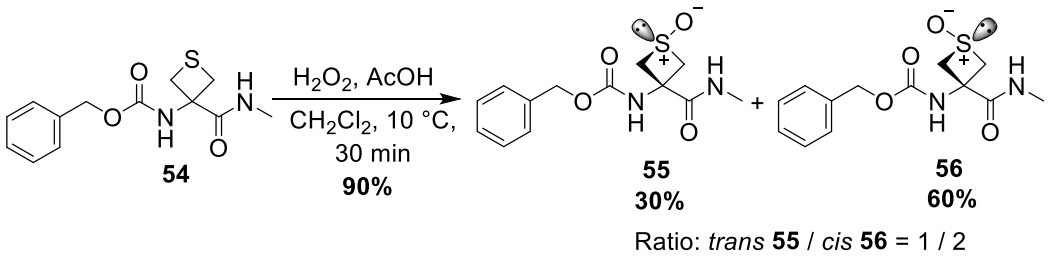

Scheme 43. Oxidation of Cbz-Attc-NHMe **54** with H_2O_2-AcOH

b. m-CPBA as the oxidant

Oxidation of Cbz-Attc-NHMe **54** was also performed using *m*-CPBA as the oxidant (Scheme 44). Cbz-Attc-NHMe **54** was mixed with 1 equivalent of *m*-CPBA, and 2 equivalents of K_2CO_3

for three hours at –78 °C. After purification by column chromatography sulfoxide was obtained in 80% yield. Now, the ratio between Cbz-Attc(O)-NHMe *trans* **55** and Cbz-Attc(O)-NHMe *cis* **56** was determined as 2:1.

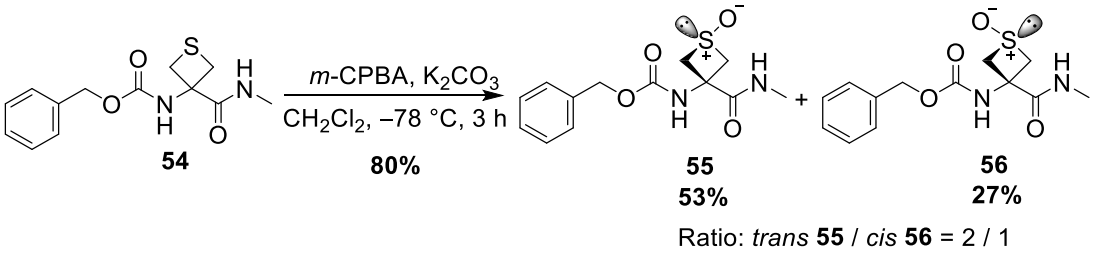

Scheme 44. Oxidation of Cbz-Attc-NHMe **54** with *m*-CPBA

3.3.3 Preparation of Cbz-Attc(O,O)-NHMe **57**

In order to obtain sulfone Cbz-Attc(O,O)-NHMe **57**, oxidation of Cbz-Attc-NHMe **54** was carried out using 2 equivalents of *m*-CPBA and 2 equivalents of K_2CO_3, for two hours at 0 °C. Sulfone **57** was obtained in 92% yield after purification by column chromatography (Scheme 45).

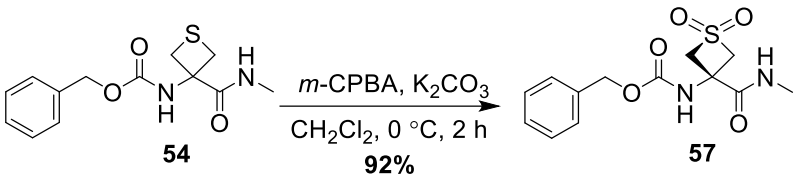

Scheme 45. Complete oxidation of Cbz-Attc-NHMe **54** with *m*-CPBA

3.4 Conformational studies of oxide derivatives **49**, **55**, **56** and **57**

In this section, we will describe the conformational studies on the *N*-oxide Cbz-Aatc(Me,O)-NHMe *trans* **49** and the three *S*-oxides [Cbz-Attc(O)-NHMe *trans* **55**, Cbz-Attc(O)-NHMe *cis* **56** and Cbz-Attc(O,O)-NHMe **57**] (Figure 136). The investigations were performed using quantum chemistry calculations, UV/IR spectroscopy in gas phase, IR spectroscopy in solution phase and 1D/2D NMR methods (DMSO-d_6 titration, temperature variation and 2D NOESY). The detailed description of these methods has been described in section 1.3.1 of chapter 1 and in section 2.3.1 of chapter 2.

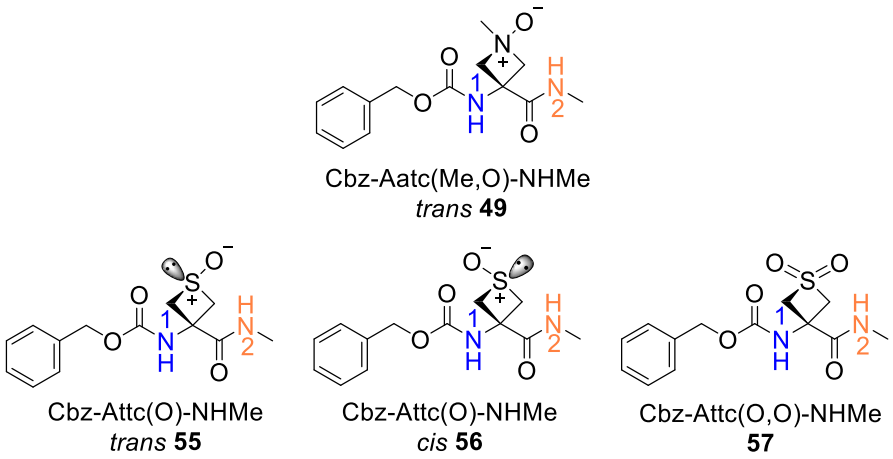

Figure 136. Four oxides for conformational studies in this section

3.4.1 Quantum chemistry calculations

This work was carried out by Prof. Michel Mons and Dr. Valérie Brenner in the LIDYL laboratory (CEA Saclay, Gif-sur-Yvette, France).

3.4.1.1 Lowest energy conformation of Cbz-Aatc(Me,O)-NHMe *trans* **49**

Differing from our expectation, only a dehydrogenated alanine structure was detected from IR spectroscopy experiment in gas phase. It is not very interesting to perform further theoretical calculations, therefore, the calculation of lowest energy conformation of Cbz-Aatc(Me,O)-NHMe *trans* **49** did not perform (Scheme 46).

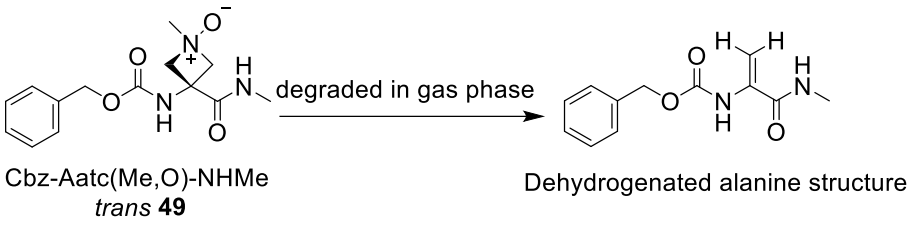

Scheme 46. Cbz-Aatc(Me,O)-NHMe *trans* **49** was degraded in gas phase

3.4.1.2 Lowest energy conformation of Cbz-Attc(O)-NHMe *trans* **55**

Theoretical calculations identified the lowest energy conformation of Cbz-Attc(O)-NHMe *trans* **55** as an extended conformer, depicted in Figure 137.

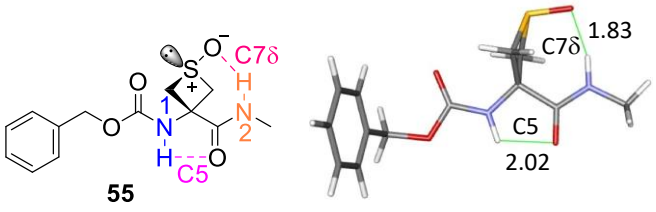

Figure 137. Lowest energy conformation (right) and H-bonding pattern (left) of Cbz-Attc(O)-NHMe *trans* **55**

The lowest energy conformation of Cbz-Attc(O)-NHMe *trans* **55** displayed two H-bonding interactions: a C7δ, N–H···O–S H-bond implicating NH(2) and a C5, N–H···O=C H-bond implicating NH(1). These two H-bonds together constitute a C5–C7δ structural feature characterized by an extended planar backbone.

3.4.1.3 Lowest energy conformation of Cbz-Attc(O)-NHMe *cis* **56**

Three conformer families were observed in theoretical calculations of Cbz-Attc(O)-NHMe *cis* **56**, as shown below in Figure 138.

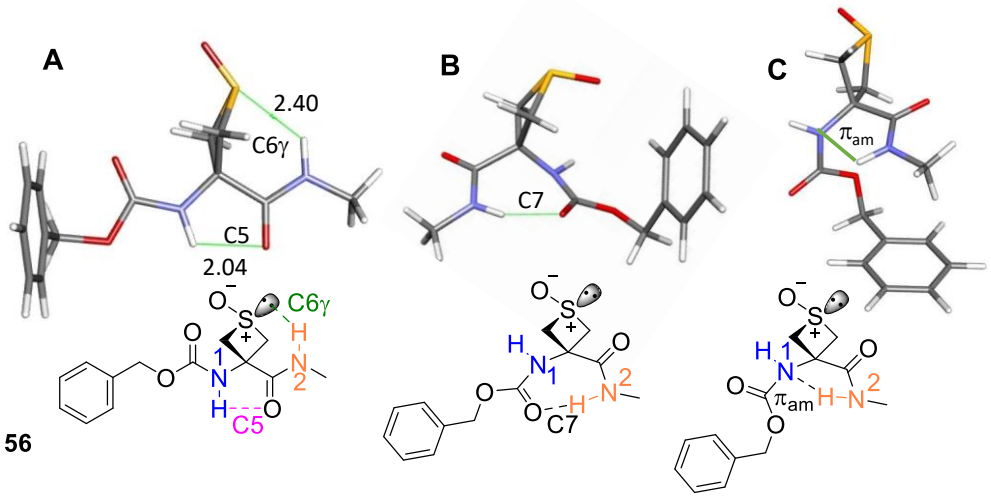

Figure 138. Lowest energy conformations (top) and H-bonding patterns (bottom) of Cbz-Attc(O)-NHMe *cis* **56**

The first conformer family **A** of Cbz-Attc(O)-NHMe *cis* **56** had an extended form featuring a C5-C6γ H-bonding motif, in which the C6γ H-bond was formed between NH(2) and the lone pair of the S atom from the side chain, and the C5 H-bond was established between NH(1) and the carbonyl oxygen of the backbone amide (Figure 138, left); The second conformer family **B** exhibited a C7 N–H···O=C H-bond, formed between NH(2) and the carbamate carbonyl in the backbone, while NH(1) was in free state (non hydrogen-bonded) (Figure 138,

center); The third conformer family **C** showed an N–H···N π_{am} interaction implicating NH(2) and N(1), while NH(1) was free (non hydrogen-bonded) (Figure 138, right). The first conformer family **A** exhibited an extended feature, while the two other conformer families **B** and **C** without the support of the C6γ and C5 H-bonds, were favored folded conformations.

3.4.1.4 Lowest energy conformation of Cbz-Attc(O,O)-NHMe **57**

Three conformer families were obtained from theoretical calculations on Cbz-Attc(O,O)-NHMe **57** (Figure 139).

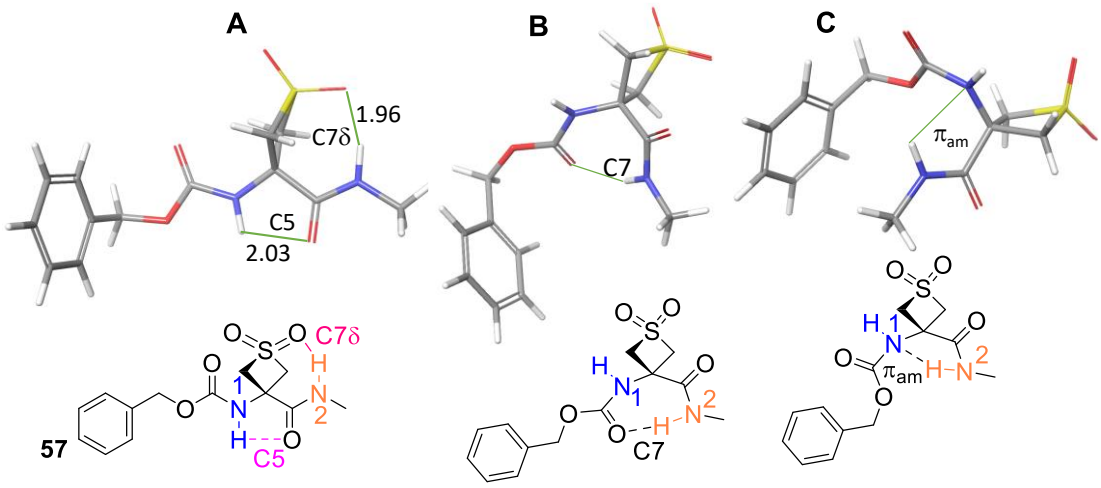

Figure 139. Lowest energy conformations (top) and H-bonding patterns (bottom) of Cbz-Attc(O,O)-NHMe **57**

The first conformer family **A** adopted an extended form featuring a C7δ H-bond together with a C5 H-bond. The C7δ H-bonding implicated one oxygen atom from the sulfone and amide NH(2), the C5 H-bond implicated carbonyl oxygen and carbamate NH(1) (Figure 139, left). The second conformer family **B** displayed a C7, N–H···O=C H-bond implicating amide NH(2) and carbonyl oxygen of the carbamate, and NH(1) was free (no H-bond involved) in this case (Figure 139, center). In the third conformation **C**, carbamate NH(1) was in a free state, while NH(2) formed an N–H···N H-bonding feature with N(1) through a π_{am} interaction (Figure 139, right). Alike the Cbz-Attc(O)-NHMe *cis* **56**, Cbz-Attc(O,O)-NHMe **57** adopted an extended C5-C7δ conformer **A** and two folded conformers **B** and **C** (free-C7 and free-π_{am}).

3.4.1.5 Discussion

Comparing the extended conformation of Cbz-Attc-NHMe **54**[153] and Cbz-Attc(O)-NHMe *trans* **55**, the distance of N–H···O–S (1.83 Å) of the latter is shorter than the distance of N–H···S (2.41 Å) of the former (Figure 140) suggesting stronger strength of a C7δ than a C6γ H-bond. In a same way, the distance of N–H···O=C of the latter (2.02) is shorter than of the former (2.05), suggesting that the C5 H-bond is stronger in Cbz-Attc(O)-NHMe *trans* **55**.

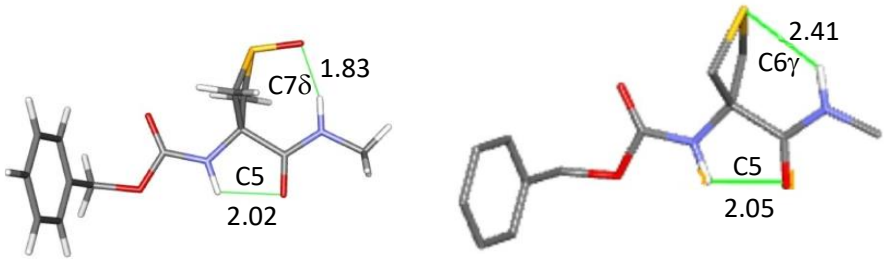

Figure 140. The lowest energy conformation of Cbz-Attc(O)-NHMe *trans* **55** (left) and Cbz-Attc-NHMe **54** (right)[153]

Comparison of Cbz-Attc-NHMe **54** and Cbz-Attc(O)-NHMe *cis* **56**, highlighted a similar geometry with a C5-C6γ feature for both compounds. The comparable hydrogen bond distances in both molecules suggest that the strength of the H-bonds is comparable (Figure 141).

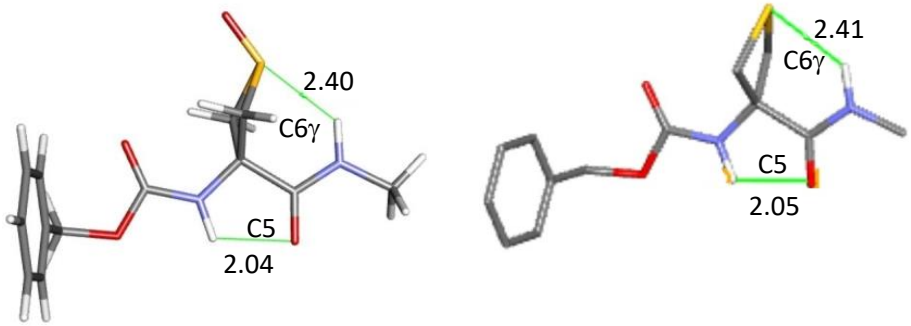

Figure 141. The C5-C6γ H-bonding feature of Cbz-Attc-NHMe **54** (left)[153] and Cbz-Attc(O)-NHMe *cis* **56** (right)

For Cbz-Attc(O)-NHMe *cis* **56** and Cbz-Attc(O,O)-NHMe **57**, three lowest energy conformer families were identified. Both Cbz-Attc(O)-NHMe *cis* **56** and Cbz-Attc(O,O)-NHMe **57** showed an extended conformation but with minor contribution, as C5-C6γ and C5-C7δ, respectively. This may be due to the additional oxygen atom at carbamate side weaken the H-bonding acceptor ability for sulfur atom in compound *cis* **56** and for oxygen atom in compound **57**. In

the case of without enough support from side chain interaction, both compounds **56** and **57** favored major folded conformers, the free-C7 and free-π_{am} forms (Figure 142).

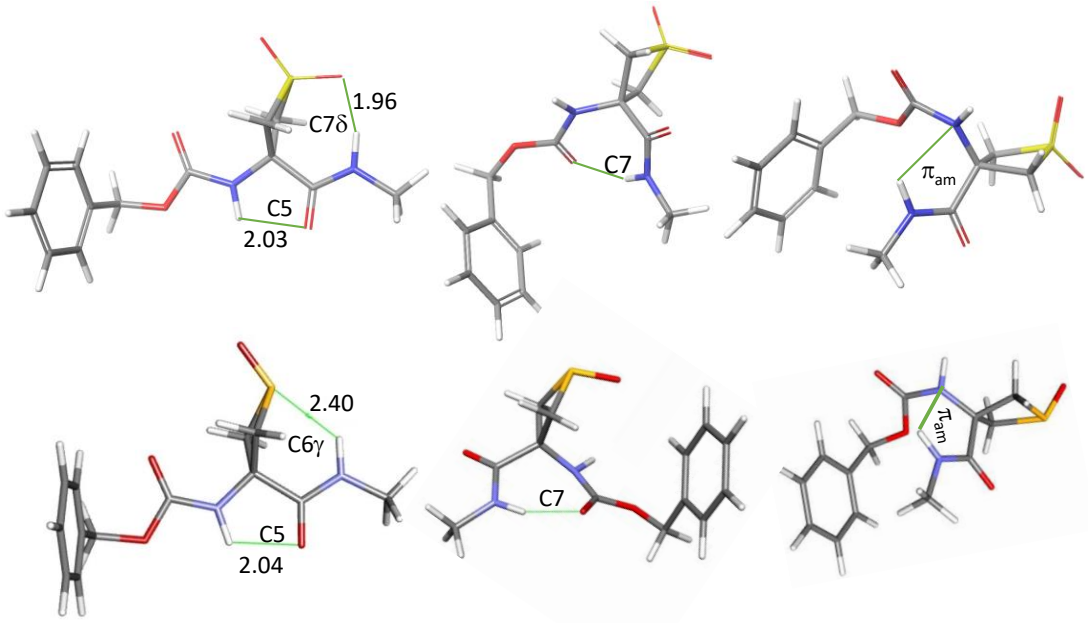

Figure 142. The conformations of Cbz-Attc(O)-NHMe *cis* **56** (top) and Cbz-Attc(O,O)-NHMe **57** (bottom)

3.4.2 Gas phase studies

In this section, we will describe the infrared spectroscopy studies in gas phase of Cbz-Aatc(Me,O)-NHMe *trans* **49**, Cbz-Attc(O)-NHMe *trans* **55**, Cbz-Attc(O)-NHMe *cis* **56** and Cbz-Attc(O,O)-NHMe **57**. The comparison compound for *N*-oxide **49** was Cbz-Aatc(Me)-NHMe **42**; and the comparison for *S*-oxides **55**, **56** and **57** was Cbz-Attc-NHMe **54**.

Interpretation of the data was made with help from the theoretical IR absorbances suggested by quantum chemistry calculations (See section 3.4.1).

This work was carried out by Prof. Michel Mons in the LIDYL laboratory (CEA Saclay, Gif-sur-Yvette, France).

3.4.2.1 Gas phase studies of Cbz-Aatc(Me,O)-NHMe *trans* **49**

The UV/IR absorption spectrum in gas phase was recorded for Cbz-Aatc(Me,O)-NHMe *trans* **49**, and results are shown in Figure 143.

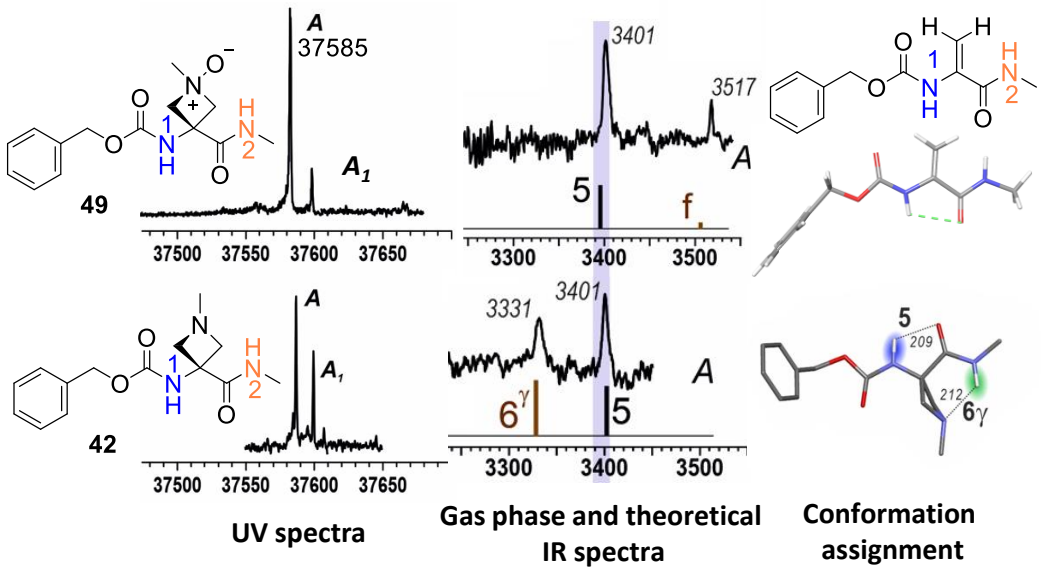

Figure 143. Gas phase UV (left), IR spectra (center) and conformation assignment (right) of Cbz-Aatc(Me,O)-NHMe *trans* **49** (top) and Cbz-Aatc(Me)-NHMe **42** (bottom)

The UV spectrum of Cbz-Aatc(Me,O)-NHMe *trans* **49** showed an intense band (labeled A) at 37585 cm^{-1}, and a second UV band (labeled A_1) located at 22 cm^{-1} higher in energy which was assigned to the same conformer as band A (Figure 143, top, left). The UV spectrum is similar with Aatc(Me) derivative **42** (Figure 143, bottom, left).

The IR spectrum (Figure 143, top, center) of Cbz-Aatc(Me,O)-NHMe *trans* **49** recorded for band A conformer showed two bands: one at 3401 cm^{-1}, which was assigned to NH(1) in the expected C5 conformation, consistent with the gas phase IR spectrum of the C5-C6γ conformation of Aatc(Me) derivative **42** (Figure 143, bottom, center); The second band at 3517 cm^{-1}, however, could only arise from a free NH(2) and not from a C7δ H-bonded conformer. The explanation for this was obtained by mass spectroscopy of band A, which revealed a dehydro-alanine structure (Figure 143, top, right).

The degradation of Cbz-Aatc(Me,O)-NHMe *trans* **49** to dehydro-alanine derivative could be due to the high temperature used in gas phase UV/IR experiments. This phenomenon was also observed in the high-resolution mass spectrum of Cbz-Aatc(Me,O)-NHMe *trans* **49** (Figure 144). It was recorded with an electrospray ionization source in positive mode and heated at 180 °C. Two peaks [294.1441 (M+H) and 316.1260 (M+Na)] for *trans* **49** were

observed, and two peaks [235.1068 (M+H) and 257.0896 (M+Na)] for dehydro-alanine derivative were also in evidence.

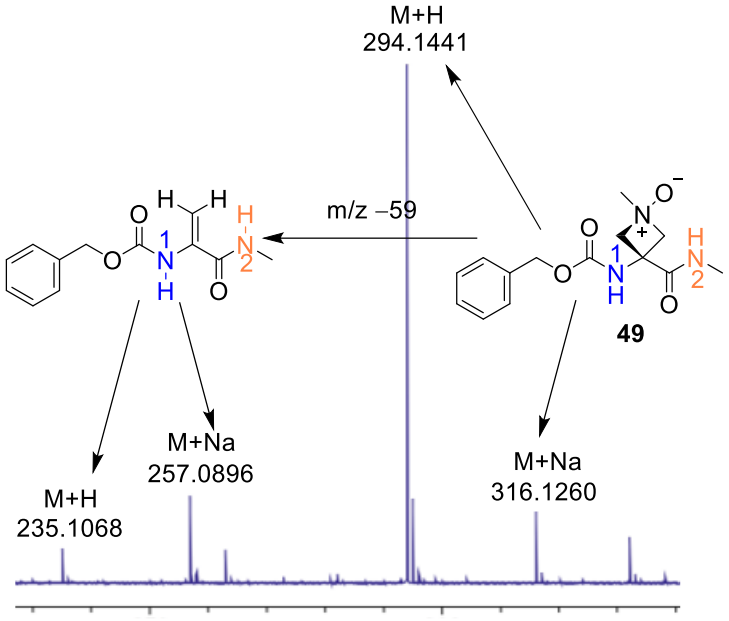

Figure 144. Partially high-resolution mass spectrum of Cbz-Aatc(Me,O)-NHMe *trans* **49**

3.4.2.2 Gas phase studies of Cbz-Attc(O)-NHMe *trans* **55**

The UV/IR spectroscopy study in gas phase was performed on the *S*-oxide Cbz-Attc(O)-NHMe mixture (the ratio of *trans* **55**/*cis* **56** was around 3/2), results are shown in Figure 145.

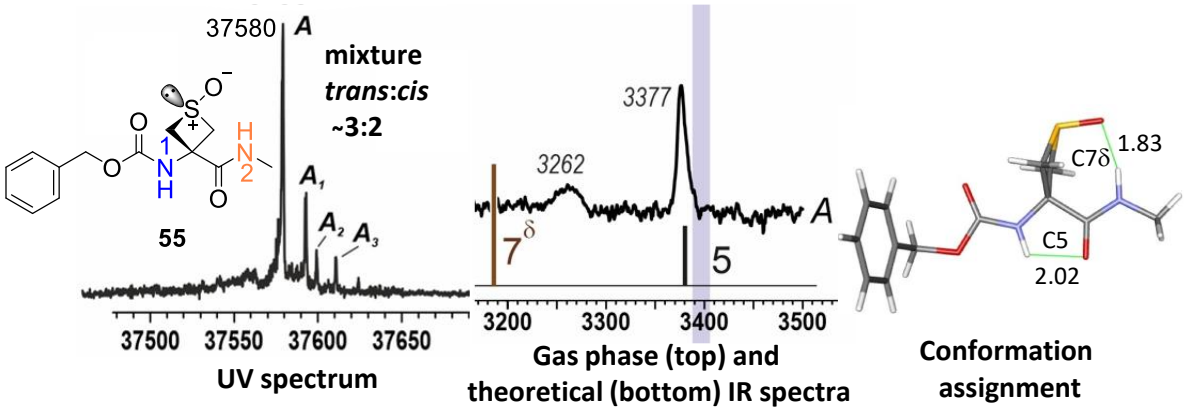

Figure 145. Gas phase UV (left), IR spectra (center) and conformation assignment (right) of Cbz-Attc(O)-NHMe mixture (*trans* **55**/*cis* **56** = 3/2) from band A

An intense UV band (labeled A) was observed at around 37580 cm^{-1} (Figure 145, left), accompanied by several small bands located in a higher energy region, those small bands

were assigned to the same conformer as band A. These results indicated the presence of only one conformer family, even in a mixture of Cbz-Attc(O)-NHMe (*trans* **55**/*cis* **56**, 3/2).

The IR spectrum of the Cbz-Attc(O)-NHMe mixture was recorded for band A and showed two absorption bands (Figure 145, center). One significant band at 3377 cm^{-1} was assigned to NH(1) in a C5 H-bonded conformer, which is compatible with the predicted IR spectrum. The second band is situated in a red-shifted region at 3262 cm^{-1}, which was assigned to NH(2) engaged in an N–H···O-S C7δ H-bond (Figure 145, right). The C5-C7δ form was the only conformation that could be observed in gas phase for the Cbz-Attc(O)-NHMe mixture (*trans* **55**/*cis* **56**, around 3/2), and must derive from Cbz-Attc(O)-NHMe *trans* **55**. No spectroscopic data were detected at all from Cbz-Attc(O)-NHMe *cis* **56**.

3.4.2.3 Gas phase studies of Cbz-Attc(O)-NHMe *cis* **56**

To further probe the gas phase behavior of compound *cis* **56**, the UV/IR spectroscopy study was repeated using a sample of Cbz-Attc(O)-NHMe mixture (*trans* **55**/*cis* **56** = 5/95), results are shown in Figure 146.

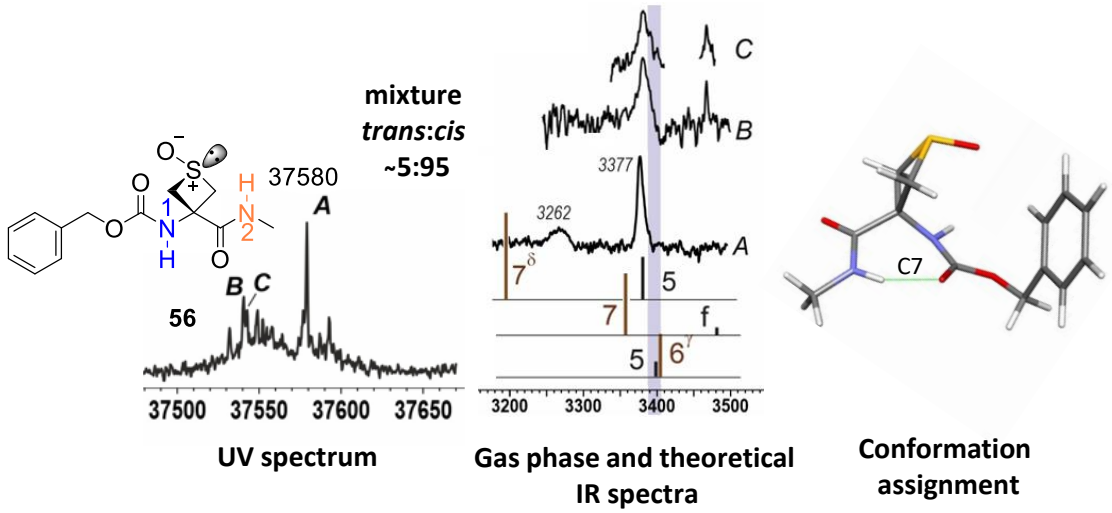

Figure 146. Gas phase UV (left), IR spectra (center) and conformation assignment (right) of Cbz-Attc(O)-NHMe mixture (*trans* **55**/*cis* **56**~ 5/95)

An intense UV band (labeled A) was observed at 37580 cm^{-1}, accompanied by several small bands (including two labeled B and C) located in the lower energy region (Figure 146, left). The Infrared spectrum was recorded for bands A, B and C.

The IR spectrum of band A (37580 cm^{-1}) was that of the extended conformer. The presence of *trans* **55** in the sample explains the appearance of its spectrum in gas phase (Figure 146, center).

The IR spectra of bands B and C were best assigned to a free-C7 conformation of Cbz-Attc(O)-NHMe *cis* **56** in low intensity (Figure 146, center), according to their frequency values are consistent with that of Cbz-Ac4c-NHMe in a same conformer.[154] The free-C7 form showed a C7 N–H···O=C H-bond implicating NH(2) formed in the backbone, and carbamate NH(1) was free (non hydrogen-bonded) (Figure 146, right). This conformer had been suggested as a low-energy conformer by theoretical studies, and there was no spectroscopic evidence for the other two conformations (C5-C6γ and free-π_{am}) of Cbz-Attc(O)-NHMe *cis* **56**, which were also suggested by calculations.

The fact is that even with high ratio of Cbz-Attc(O)-NHMe *cis* **56** sample, resulted in a minor free-C7 conformer was detected. This could be due to the conversion of *cis* **56** into *trans* **55** at high temperature for the stabilization reason, or it also could be due to the limitation of gas phase spectroscopy for the compound *cis* **56**.

3.4.2.4 Gas phase studies of Cbz-Attc(O,O)-NHMe **57**

The UV/IR spectra were recorded in gas phase for Cbz-Attc(O,O)-NHMe **57**, results are shown in Figure 147.

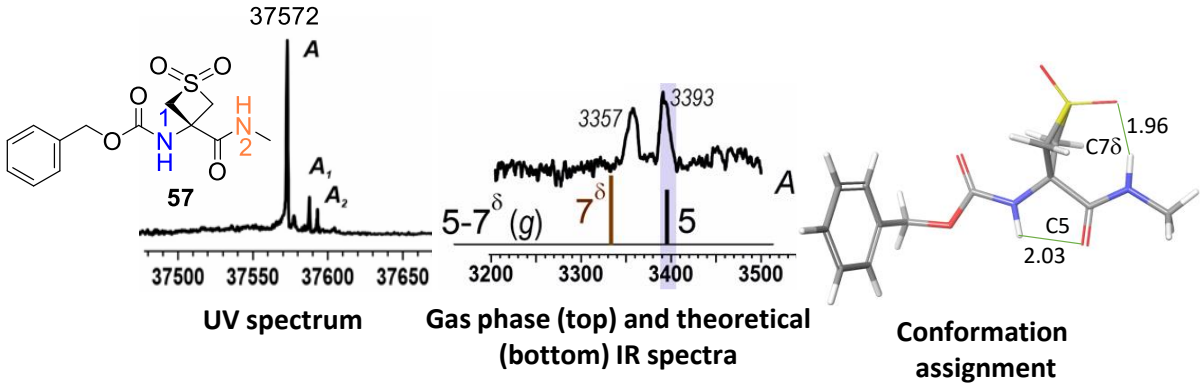

Figure 147. Gas phase UV (left), IR spectra (center) and conformation assignment (right) of Cbz-Attc(O,O)-NHMe **57**

The UV spectrum of Cbz-Attc(O,O)-NHMe **57** showed an intense UV band (labeled A) at 37572 cm^{-1}, accompanied by two small UV bands (labeled A_1 and A_2) located at higher frequency (Figure 147, left). These bands were assigned to the same conformer as band A, since identical

IR spectra were obtained for these three bands. The presence of only one conformation family was deduced.

The IR spectrum of band A was recorded (Figure 147, center), it was assigned to an extended conformation on the basis of a band at 3393 cm^{-1} for NH(1) engaged in a C5 H-bond, and another red-shifted band located at 3357 cm^{-1}, for NH(2) engaged in an N–H···O=S C7δ H-bonding system (Figure 147, right).

In the gas phase study of Cbz-Attc(O,O)-NHMe **57**, the C5-C7δ conformer was the only one detected, we found no evidence for the free-C7 or free-π_{am} conformers that had been suggested by theoretical calculations.

3.4.2.5 Discussion

Comparison of the IR spectra of Cbz-Attc-NHMe **54** and Cbz-Attc(O)-NHMe *trans* **55** showed that, NH(1) band (at 3377 cm^{-1}) of the latter was more red-shifted than that of the former (at 3398 cm^{-1}) indicating that the strength of C5 H-bond is stronger in Cbz-Attc(O)-NHMe *trans* **55**. In the same way, the NH(2) of Cbz-Attc(O)-NHMe *trans* **55** at 3262 cm^{-1} in a C7δ H-bond is stronger than the NH(2) Cbz-Attc-NHMe **54** at 3360 cm^{-1} in a C6γ H-bond (Figure 148).

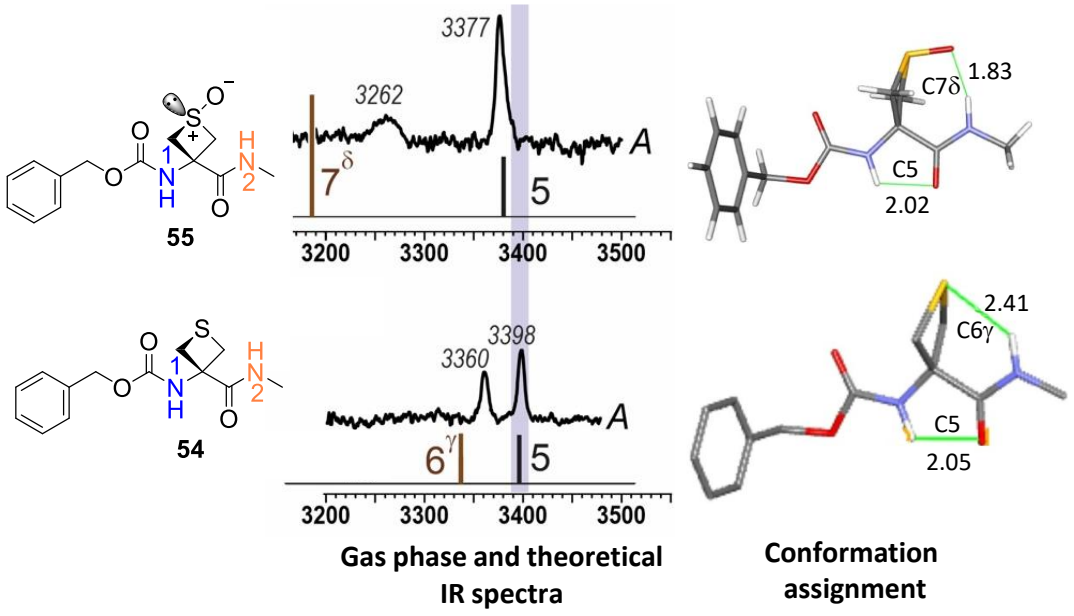

Figure 148. The gas phase IR spectra of Cbz-Attc(O)-NHMe *trans* **55** (top) and Cbz-Attc-NHMe **54** (bottom)

In comparison with Cbz-Attc(O)-NHMe *trans* **55**, both NH stretch bands of Cbz-Attc(O,O)-NHMe **57** were more blue-shifted, suggesting that the C5-C7δ H-bonding system in the latter is weaker (Figure 149).

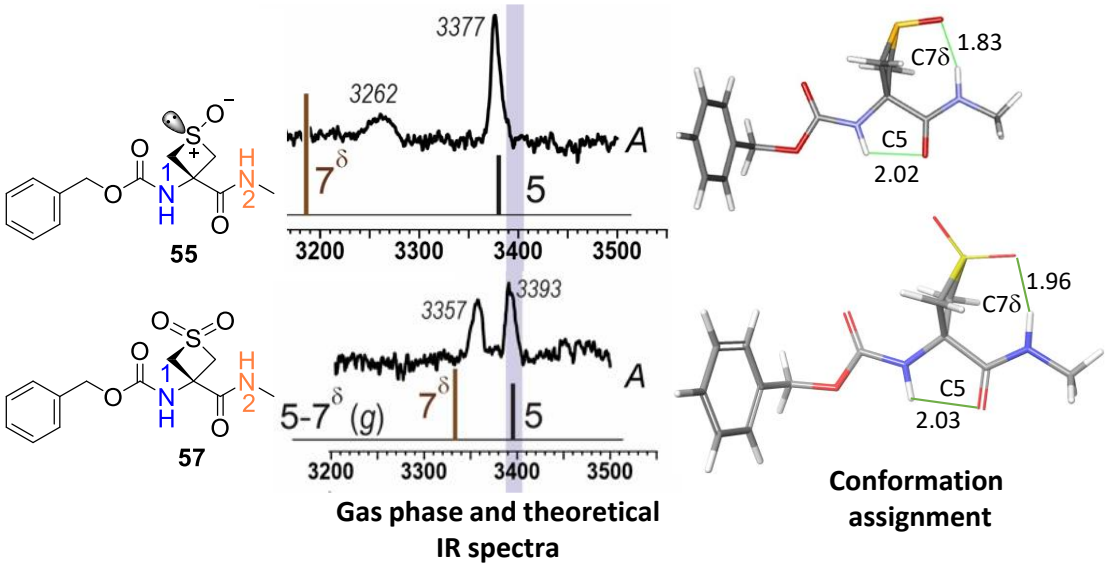

Figure 149. The gas phase IR spectra of Cbz-Attc(O)-NHMe *trans* **55** (top) and Cbz-Attc(O,O)-NHMe **57** (bottom)

3.4.3 Solution phase infrared spectroscopy studies

Infrared spectroscopy studies of compounds **49**, **55**, **56** and **57** were performed in chloroform, spectra were recorded at several concentrations (2, 5, 10 and 30 mM). They showed no concentration-related effects in the NH stretch region (Figure 150), indicating the intramolecular nature of any non-covalent interactions and in particular H-bonding.

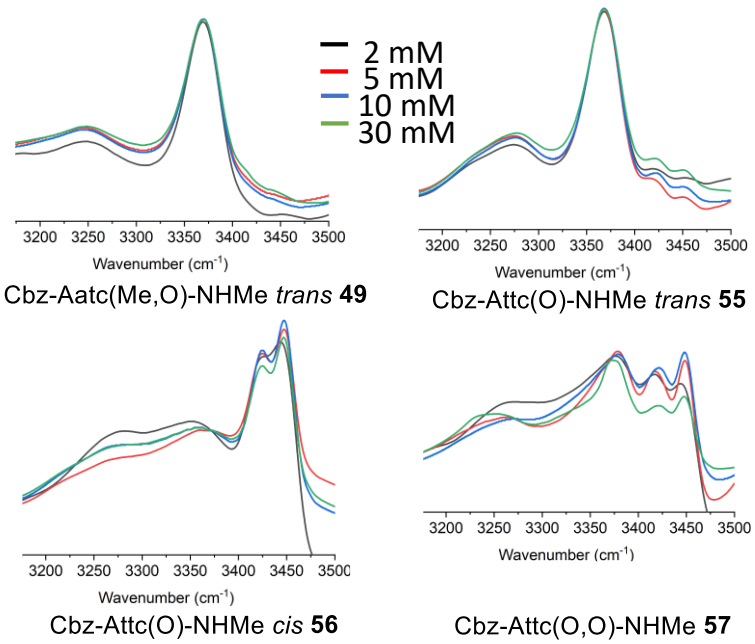

Figure 150. Solution phase IR spectra of four oxides at different concentrations

3.4.3.1 Solution phase IR of Cbz-Aatc(Me,O)-NHMe *trans* **49**

The absorption spectrum of Cbz-Aatc(Me,O)-NHMe *trans* **49** is shown in Figure 151. It showed an intense band located at 3369 cm^{-1} and a very broad band located at 3245 cm^{-1}. The intense band at 3369 cm^{-1} was assigned to NH(1) in a C5 H-bonded conformation, the broad red-shifted band at 3245 cm^{-1} was assigned to NH(2) implicated in a C7δ H-bond. Thus, it is suggested that Cbz-Aatc(Me,O)-NHMe *trans* **49** adopts a single conformation in solution, as an extended form composed of a C5 and a C7δ H-bond.

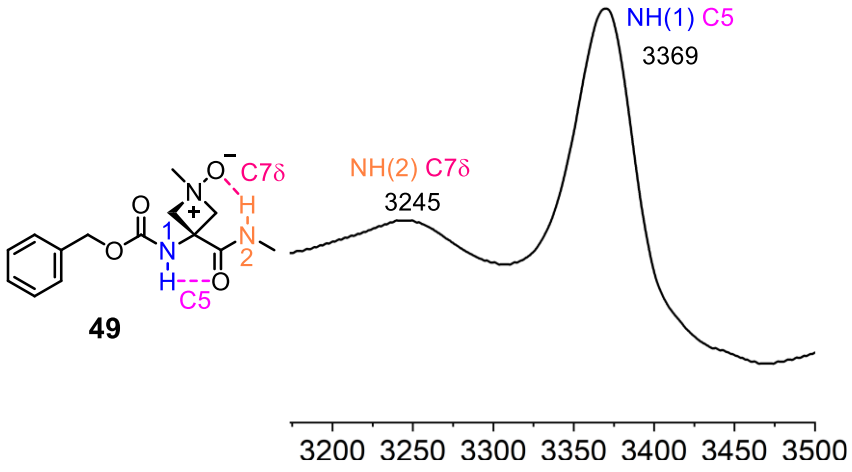

Figure 151. Solution phase IR spectra (5 mM) of Cbz-Aatc(Me,O)-NHMe *trans* **49**

3.4.3.2 Solution phase IR of Cbz-Attc(O)-NHMe *trans* **55**

Figure 152 shows the solution phase IR spectrum of Cbz-Attc(O)-NHMe *trans* **55**. The spectrum showed two major bands at 3274 and 3368 cm^{-1}. In agreement with the gas phase study, it is suggested that the band at 3368 cm^{-1} is due to NH(1) implicated in a C5 H-bond, and the broad band at 3276 cm^{-1} is due to NH(2) implicated in a C7δ H-bond. The C5-C7δ H-bonding motif adopts principally the same C5-C7δ extended form as that assigned to the gas phase conformer. Two small shoulders located in blue region around 3421 and 3452 cm^{-1}, suggested minor conformations exist in solution. They were assigned to a free-π_{am} and/or a free-C7 conformer, according to similar NH frequency values were previously indicated for free-π_{am} and/or free-C7 conformers in Cbz-Attc-NHMe **54**.[195]

Thus, Cbz-Attc(O)-NHMe *trans* **55** showed two conformations in solution: a dominant C5-C7δ extended form, free-π_{am} and/or a free-C7 conformers as minor contributors.

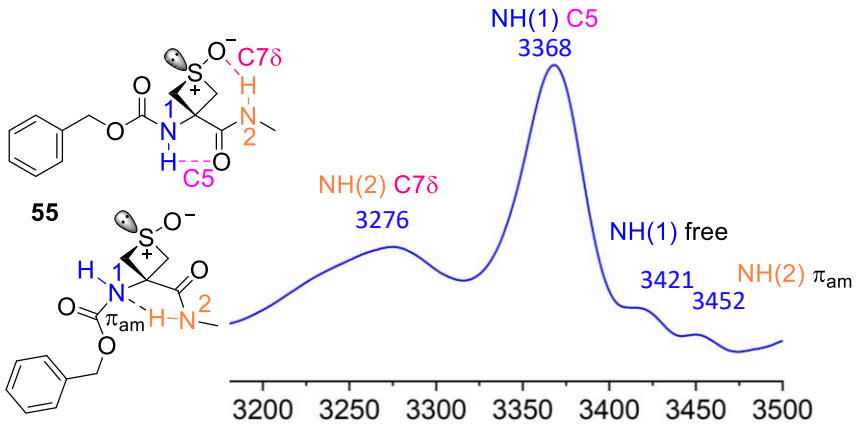

Figure 152. Solution phase IR spectrum (5 mM) of Cbz-Attc(O)-NHMe *trans* **55**

3.4.3.3 Solution phase IR of Cbz-Attc(O)-NHMe *cis* **56**

Figure 153 shows the solution phase IR spectrum of Cbz-Attc(O)-NHMe *cis* **56** with two intense bands located in blue region at 3424 and 3447 cm^{-1}, they were attributed to a free NH and a π_{am} interaction, exhibiting as a free-π_{am} conformer. Besides these two significant bands, a broad absorption shoulder at 3267 cm^{-1} was also observed, which was assigned to NH(2) implicated in a C7 N–H···O=C H-bond formed in the backbone and NH(1) was free located at 3447 cm^{-1} together constituted a free-C7 conformer. A broad band located at 3368 cm^{-1} may be due to NH(1) and NH(2) implicated in C5 and C6γ H-bonds, respectively, according to similar NH frequency values were previously indicated for C5-C6γ conformer of Cbz-Attc-NHMe **54**,[195] the C5-C6γ H-bonding motif adopts an extended conformer. Collectively, Cbz-

Attc(O)-NHMe *cis* **56** seems to display three conformer families that were suggested by theoretical calculations.

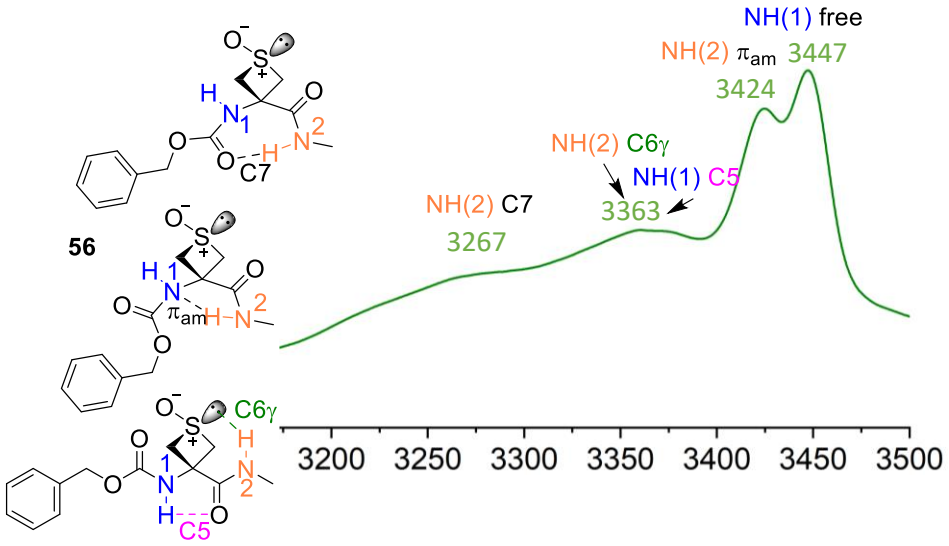

Figure 153. Solution phase IR spectrum (5 mM) of Cbz-Attc(O)-NHMe *cis* **56**

3.4.3.4 Solution phase IR of Cbz-Attc(O,O)-NHMe **57**

Figure 154 shows the solution phase IR spectrum of Cbz-Attc(O,O)-NHMe **57**, four significant bands located at 3262, 3378, 3418 and 3449 cm^{-1}.

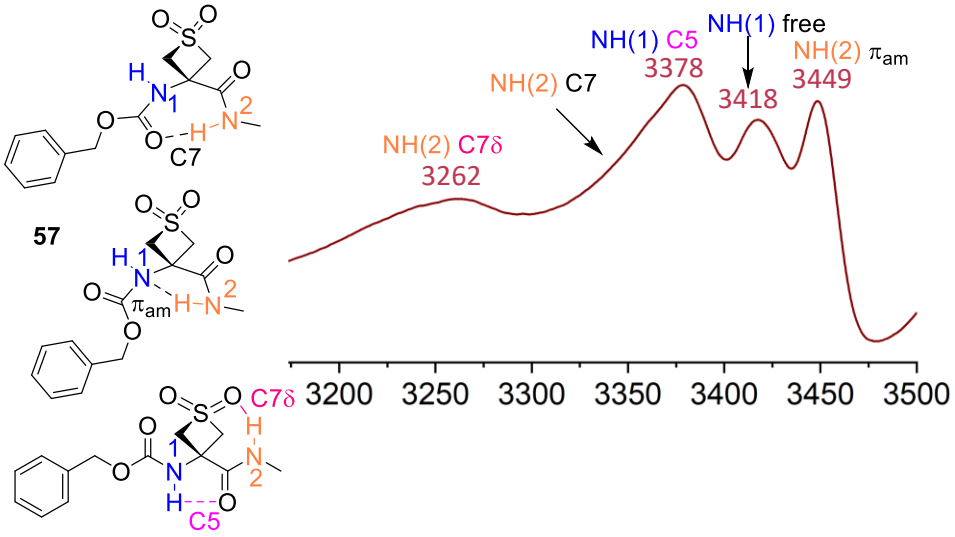

Figure 154. Solution phase IR spectrum (5 mM) of Cbz-Attc(O,O)-NHMe **57**

The broad band at 3262 cm^{-1} was assigned to NH(2) implicated in a C7δ H-bond, and the intense band at 3378 cm^{-1} is due to NH(1) in a C5 H-bond, together supporting an extended

C5-C7δ conformer. Two other significant bands in blue region were similar to those observed for Cbz-Attc(O)-NHMe *cis* **56** (Figure 153), located at around 3418 and 3449 cm^{-1} and were contributed to a free NH(1) and a π_{am} interaction from NH(2), exhibited a second conformation in free-π_{am} feature. In the region from 3378 to 3262 cm^{-1}, a slight shoulder is present, which could be a C7 N–H···O=C H-bonding contributed from NH(2) and with a free NH(1) at 3449 cm^{-1} adopt a free-C7 conformation in the backbone, as a possible minor conformation. Hence, Cbz-Attc(O,O)-NHMe **57** may displayed three conformer families, as suggested by theoretical calculations.

3.4.3.5 Discussion

Comparing the IR spectra of Cbz-Aatc(Me,O)-NHMe *trans* **49** with Cbz-Aatc(Me)-NHMe **42**, the more red-shifted band of NH(1) of the former (3369 cm^{-1}) than NH(1) of the latter (3378 cm^{-1}) indicating the stronger C5 H-bond in Cbz-Aatc(Me,O)-NHMe *trans* **49**. The same observation was made for NH(2) of *trans* **49** (3245 cm^{-1}) in a C7δ H-bond that is stronger than NH(2) of compound **42** (3287 cm^{-1}) in a C6γ H-bond. The stronger C5 in Cbz-Aatc(Me,O)-NHMe *trans* **49** could be due to the increased H-bond strength of C7δ than C6γ.

In comparison to the IR spectrum of Cbz-Attc-NHMe **54**, the more red-shifted band of NH(2) of Cbz-Attc(O)-NHMe *trans* **55** (3276 cm^{-1}) than NH(2) of Cbz-Attc-NHMe **54** (3375 cm^{-1})[153] indicating the stronger C7δ H-bond in the former. These increased H-bond strength resulted in a stronger C5 H-bond in Cbz-Attc(O)-NHMe *trans* **55**.

Cbz-Attc(O)-NHMe *trans* **55** has exhibited at least two conformations in solution, a predominant C5-C7δ extended form, accompanied by minor contributions of free-π_{am} and/or free-C7 conformers. In Cbz-Attc(O)-NHMe *cis* **56**, the free-π_{am} became the primary form due to the oxygen atom orientation prevents the formation of a C7δ H-bond, thus favoring the folding conformation. In Cbz-Attc(O,O)-NHMe **57**, one oxygen atom is oriented towards the methylamide allowing a C7δ H-bond formation alike Cbz-Attc(O)-NHMe *trans* **55**. Nonetheless, the C5-C7δ H-bonding form in sulfone **57** was not dominant, which could be attributed to the presence of an additional oxygen atom at carbamate side, which weakened the H-bonding acceptor ability of the oxygen atom to form a robust C7δ H-bond.

Compared to Cbz-Attc-NHMe **54**, who adopted a dominant C5-C6γ extended conformation, this extended conformer in Cbz-Attc(O)-NHMe *cis* **56** was a minor contributor. This may be due to the generated oxygen atom weakened H-bonding acceptor ability of the sulfur atom to form a robust C6γ H-bond.

3.4.4 Solution phase NMR studies

3.4.4.1 ^{1}H chemical shifts of NH signals

*a. ^{1}H chemical shifts of NH signals of Aatc derivatives **42** and **49***

An expansion of the spectral window where the NH proton signals are located for Cbz-Aatc(Me)-NHMe **42** (bottom) and Cbz-Aatc(Me,O)-NHMe *trans* **49** (top) is shown in Figure 155. Cbz-Aatc(Me)-NHMe **42** (Figure 155, bottom) was shown in section 2.3.5.1, exhibited a C5-C6γ extended form, characterized by chemical shifts of carbamate NH(1) at δ = 6.36 ppm and amide NH(2) at δ = 8.24 ppm were due to their implication in a C5 and a C6γ H-bond, respectively.

In comparison, Cbz-Aatc(Me,O)-NHMe *trans* **49** (Figure 155, top) showed a remarkable downfield NH(2) signal at δ = 11.60 ppm suggesting a very strong H-bonding of N(2)H···O-N. The carbamate NH(1) (δ = 6.76 ppm) signal was also deshielded compared to NH(1) in Cbz-Aatc(Me)-NHMe **42**, suggesting that the C5 interaction in Cbz-Aatc(Me,O)-NHMe *trans* **49** is stronger.

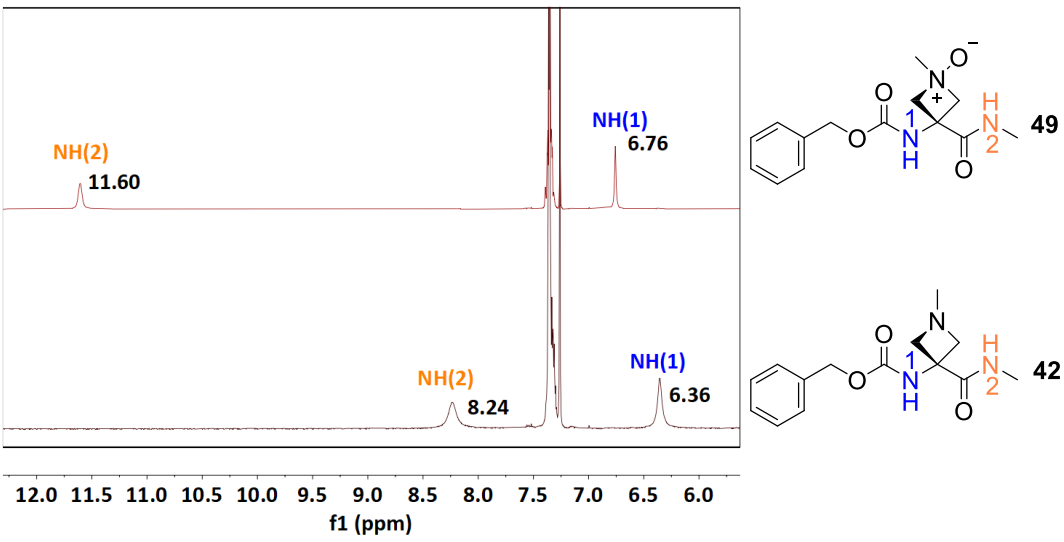

Figure 155. NH signals of compounds Cbz-Aatc(Me)-NHMe **42** (bottom) and Cbz-Aatc(Me,O)-NHMe *trans* **49** (top)

*b. ^{1}H chemical shifts of NH signals of Attc derivatives **54**, **55**, **56** and **57***

An expansion of the spectral window where the NH proton signals are located for Cbz-Attc-NHMe **54**, Cbz-Attc(O)-NHMe *trans* **55**, Cbz-Attc(O)-NHMe *cis* **56**, and Cbz-Attc(O,O)-NHMe **57** is shown in Figure 156. Cbz-Attc-NHMe **54** (Figure 156, bottom) was shown previously to

exhibit a predominant C5-C6γ pattern as an extended form in solution[196]. The signal at δ = 6.44 ppm is assigned to NH(1) involved in a C5 H-bond, and the deshielded signal at δ = 7.96 ppm for NH(2) in a C6γ H-bond.

Compared with the NH signals of Cbz-Attc-NHMe **54**, Cbz-Attc(O)-NHMe *trans* **55** (Figure 156, lower middle) showed both NH signals (NH(1) δ = 6.69 ppm and NH(2) δ = 8.78 ppm) were moved to more downfield regions. These observations are compatible with a strong C7δ H-bond formed between NH(2) and the oxygen atom of the side chain, and an intra-residue backbone C5 H-bond involving NH(1). This C5-C7δ H-bonding feature displayed an extended conformer, is in full agreement with infrared results in solution.

When comparing the NH signals of Cbz-Attc-NHMe **54** and Cbz-Attc(O)-NHMe *trans* **55**, it is observed that all NH signals of Cbz-Attc(O)-NHMe *cis* **56** (Figure 156, top middle) (NH(1) δ = 5.73 ppm and NH(2) δ = 6.41 ppm) and Cbz-Attc(O,O)-NHMe **57** (Figure 156, top) (NH(1) δ = 5.80 ppm and NH(2) δ = 6.80 ppm) in more upfield. These phenomena could be compatible with not H-bonded NHs or with weaker H-bonds in *cis* **56** and sulfone **57**, as suggested by infrared studies in solution.

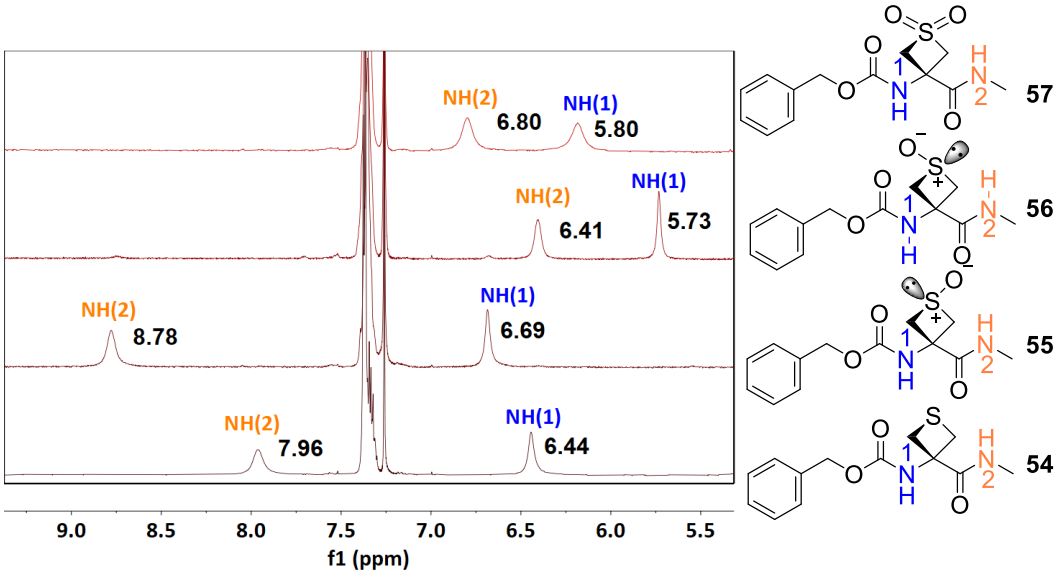

Figure 156. NH signals of Cbz-Attc-NHMe **54** (bottom), Cbz-Attc(O)-NHMe *trans* **55** (lower middle), Cbz-Attc(O)-NHMe *cis* **56** (top middle) and Cbz-Attc(O,O)-NHMe **57** (top)

3.4.4.2 ^{1}H chemical shifts of $C^{\beta}H^{a}$ and $C^{\beta}H^{b}$

The assignments of $C^{\beta}H^{a}$ (carbamate side) and $C^{\beta}H^{b}$ (methyl amide side) protons of each compound were based on their NOESY (See section 3.4.4.5) correlations intensities with the

neighboring NH protons. The chemical shifts of $C^{\beta}H^{a}$ and $C^{\beta}H^{b}$ of compounds **49**, **55**, **56** and **57** are shown in Table 19. For Cbz-Aatc(Me,O)-NHMe *trans* **49** and Cbz-Attc(O)-NHMe *trans* **55**, $C^{\beta}H^{a}$ signal was more downfield shifted than $C^{\beta}H^{b}$ signal, but for Cbz-Attc(O)-NHMe *cis* **56** and Cbz-Attc(O,O)-NHMe **57** the $C^{\beta}H^{b}$ signal was more downfielded than $C^{\beta}H^{a}$ signal. Based on these findings, it is possible that *N*-oxide *trans* **49** and *S*-oxide *trans* **55** have similar conformational preference. Similarly, Cbz-Attc(O)-NHMe *cis* **56** and Cbz-Attc(O,O)-NHMe **57** may adopt similar conformation.

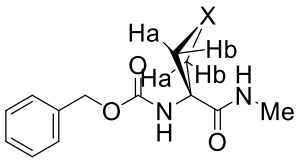

	Cbz-Aatc(Me,O)-NHMe *trans* **49**	Cbz-Attc(O)-NHMe *trans* **55**	Cbz-Attc(O)-NHMe *cis* **56**	Cbz-Attc(O,O)-NHMe **57**
δ $C^{b}H^{a}$ (ppm)	5.38	4.53	3.22	4.33
δ $C^{b}H^{b}$ (ppm)	4.22	3.31	4.20	4.71

Table 19. Chemical shifts of $C^{\beta}H^{a}$ and $C^{\beta}H^{b}$ for four oxide derivatives **49**, **55**, **56** and **57**

3.4.4.3 DMSO-d_6 titration experiments

*a. NH signal evolution of Cbz-Aatc(Me,O)-NHMe trans **49***

DMSO-d_6 titration experiment was first performed on the Cbz-Aatc(Me,O)-NHMe *trans* **49**, and results are shown in Figure 157. After a total injection of 10% DMSO, both NH signals showed only very low chemical shift changes [$\Delta\delta$ = –0.11 ppm for NH(1) and –0.21 ppm for NH(2)]. These results suggested no solvent exposure in solution for both NH protons, commensurate with them being intramolecularly H-bonded and consistent with a C5-C7δ conformation, as had suggested by infrared in solution.

	DMSO-d_6 (%, v/v)											
	0	*0.5*	*1*	*1.5*	*2*	*2.5*	*3*	*4*	*5*	*7.5*	*10*	$\Delta\delta$
δ NH1	6.71	6.71	6.70	6.69	6.68	6.67	6.66	6.65	6.64	6.62	6.60	–0.11
δ NH2	11.74	11.74	11.72	11.71	11.70	11.69	11.67	11.65	11.64	11.59	11.53	–0.21

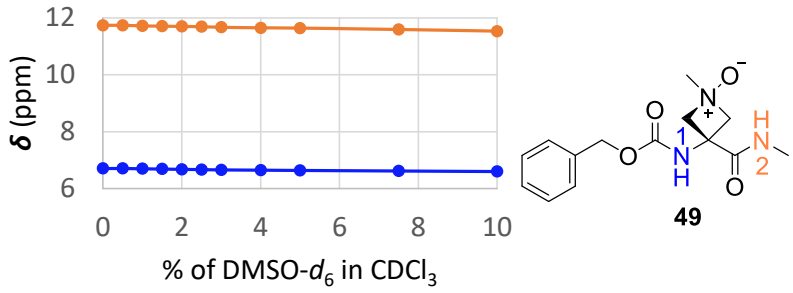

Figure 157. DMSO-d_6 titration of Cbz-Aatc(Me,O)-NHMe *trans* **49**

*b. NH signal evolution of Cbz-Attc(O)-NHMe trans **55***

The results of DMSO-d_6 titration of Cbz-Attc(O)-NHMe *trans* **55** are shown in Figure 158. After 10% of DMSO-d_6 was added in a NMR tube containing *trans* **55** in $CDCl_3$, it was clearly seen that the chemical shifts of two NH signals were significantly affected. A downfield shift of NH(1) signal, ($\Delta\delta$ = 0.76 ppm) was observed, which indicated not extensive solvent accessible for NH(1), may be involved in a H-bond. A large upfield shift ($\Delta\delta$ = –1.62 ppm) of NH(2) pointing to extensive solvent exposure, indicated that the NH(2) was not hydrogen-bonded. These data indicate possibly no intramolecular H-bond in solution, which is contradictory with a predominant C5-C7δ conformation suggested by infrared spectroscopy and ^{1}H NMR chemical shifts. This may be because the sulfoxide function of Cbz-Attc(O)-NHMe *trans* **55** can interact with DMSO by van der Waals interactions and induced the extensive solvent exposure.[197]

	DMSO-d_6 (%, v/v)											
	0	*0.5*	*1*	*1.5*	*2*	*2.5*	*3*	*4*	*5*	*7.5*	*10*	$\Delta\delta$
δ NH1	6.68	6.79	6.90	6.97	7.04	7.10	7.15	7.23	7.25	7.33	7.44	0.76
δ NH2	8.79	8.56	8.34	8.18	8.04	7.91	7.80	7.64	7.56	7.37	7.17	–1.62

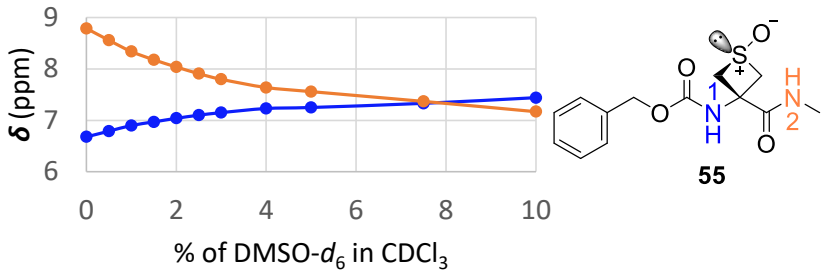

Figure 158. DMSO-d_6 titration of Cbz-Attc(O)-NHMe *trans* **55**

*c. NH signal evolution of Cbz-Attc(O)-NHMe cis **56***

Titration of a $CDCl_3$ solution containing Cbz-Attc(O)-NHMe *cis* **56** with DMSO-d_6 was carried out and results are shown in Figure 159. A significant downfield shift of the NH(1) signal was noted ($\Delta\delta$ = 2.14 ppm for 10% added DMSO-d_6), suggesting an extensive solvent exposure for NH(1), and that NH(1) was not hydrogen-bonded. A small downfield shift was observed for NH(2) signal ($\Delta\delta$ = 0.37 ppm for 10% added DMSO-d_6), suggesting its implication in an intramolecular H-bonding. These results are compatible with the co-existence of two major conformations (free-C7, free-π_{am}) as suggested by IR in solution, but no evidence for a C5-C6γ conformer.

	DMSO-d_6 (%, v/v)											
	0	*0.5*	*1*	*1.5*	*2*	*2.5*	*3*	*4*	*5*	*7.5*	*10*	$\Delta\delta$
δ NH1	5.64	6.62	7.04	7.30	7.44	7.54	7.61	7.67	7.72	7.77	7.78	2.14
δ NH2	6.40	6.50	6.55	6.58	6.61	6.63	6.65	6.67	6.70	6.74	6.77	0.37

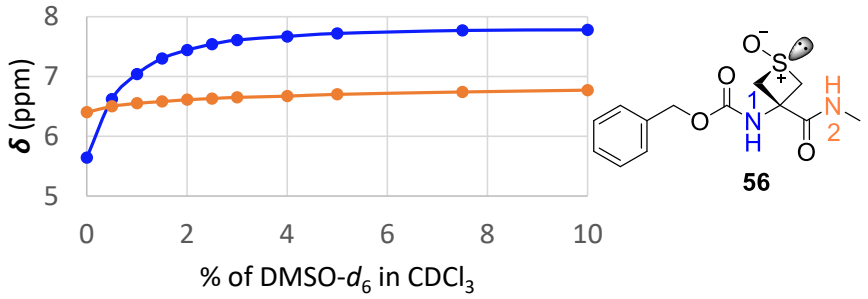

Figure 159. DMSO-d_6 titration of Cbz-Attc(O)-NHMe *cis* **56**

*d. NH signal evolution of Cbz-Attc(O,O)-NHMe **57***

The DMSO-d_6 titration experiment was performed on Cbz-Attc(O,O)-NHMe **57**, and results are shown in Figure 160. NH(1) signal was significantly shifted to a downfield region ($\Delta\delta$ = 2.22 ppm), pointing to extensive solvent exposure of this proton without implication in any H-bonding. A low downfield shift ($\Delta\delta$ = 0.12 ppm) for the NH(2), suggesting it was engaged in an intramolecular H-bonding.

These data can be compatible with NH(1) was free and NH(2) was involved in intramolecular H-bonding, as in the free-C7 and free-π_{am} conformations. The results are in agreement with the results obtained from infrared studies in solution phase suggesting that Cbz-Attc(O,O)-NHMe **57** exhibited two conformer families (a free-C7, a free-π_{am}), but no evidence for a C5-C7δ conformer.

	DMSO-d_6 (%, v/v)											
	0	*0.5*	*1*	*1.5*	*2*	*2.5*	*3*	*4*	*5*	*7.5*	*10*	Δδ
δ NH1	6.02	7.48	7.78	7.95	8.07	8.14	8.19	8.23	8.25	8.25	8.24	2.22
δ NH2	6.80	6.76	6.76	6.76	6.77	6.78	6.79	6.81	6.83	6.88	6.92	0.12

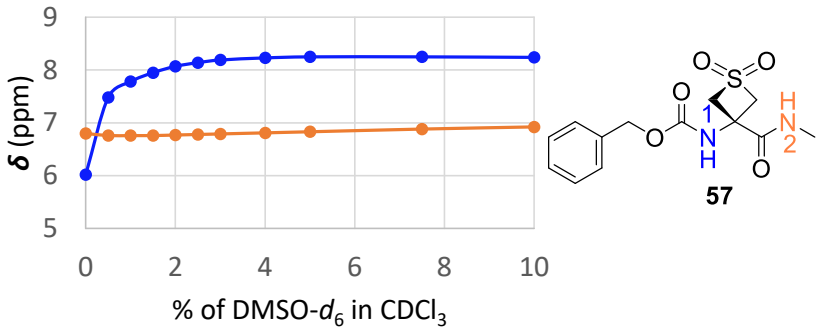

Figure 160. DMSO-d_6 titration by Cbz-Attc(O,O)-NHMe **57**

3.4.4.4 ^{1}H NMR experiments at variable temperatures

*a. NH signal evolution of Cbz-Aatc(Me,O)-NHMe trans **49***

The temperature variation experiment carried out on Cbz-Aatc(Me,O)-NHMe *trans* **49**, with the temperature increased from 300 K to 325 K, induced NH(1) and NH(2) signals to be very slightly downfield shifted ($\Delta\delta$ = 0.01 ppm and $\Delta\delta$ = 0.04 ppm, respectively) (Figure 161). The low temperature coefficients for both NH signals, 0.4 ppb/K for NH(1) and 1.6 ppb/K for NH(2) suggesting that they were intramolecularly H-bonded. These results are compatible with a C5-C7δ H-bonded system in the molecule suggested by IR in solution and ^{1}H NMR chemical shifts and are in agreement with the DMSO titration results.

	T (K)						
	300	*305*	*310*	*315*	*320*	*325*	**T.C. (ppb/K)**
δ NH1	6.72	6.72	6.72	6.72	6.72	6.73	0.4
δ NH2	11.72	11.73	11.73	11.74	11.75	11.76	1.6

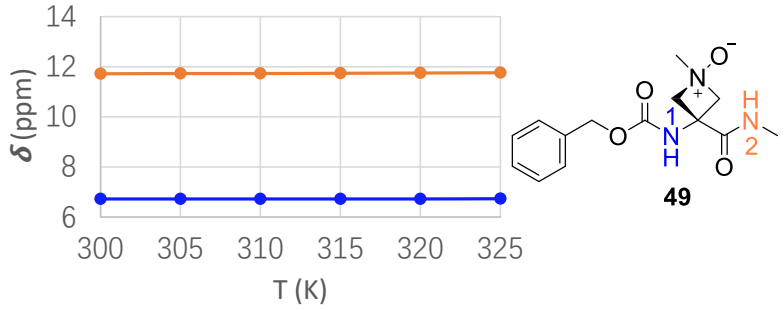

Figure 161. Temperature variation experiment of Cbz-Aatc(Me,O)-NHMe *trans* **49**

*b. NH signal evolution of Cbz-Attc(O)-NHMe trans **55***

In the temperature variation experiment on Cbz-Attc(O)-NHMe *trans* **55**, both NH protons shifted upfield were observed when the temperature increased from 300 to 325 K (Figure 162). The temperature coefficients (T.C.) were modest: –2.4 ppb/K for NH(1) and –4.4 ppb/K for NH(2) suggesting that both of them were intramolecularly H-bonded, which is compatible with a dominant C5-C7δ conformation presented in the molecule suggested by infrared spectroscopy and ^{1}H NMR chemical shifts. These higher temperature coefficients for Cbz-Attc(O)-NHMe *trans* **55** than for Cbz-Aatc(Me,O)-NHMe *trans* **49** may suggest less strong H-bonds in the C5-C7δ H-bonding system of the Cbz-Attc(O)-NHMe *trans* **55**.

	T (K)						
	300	*305*	*310*	*315*	*320*	*325*	**T.C. (ppb/K)**
δ NH1	6.69	6.67	6.66	6.65	6.64	6.63	–2.4
δ NH2	8.80	8.78	8.76	8.74	8.71	8.69	–4.4

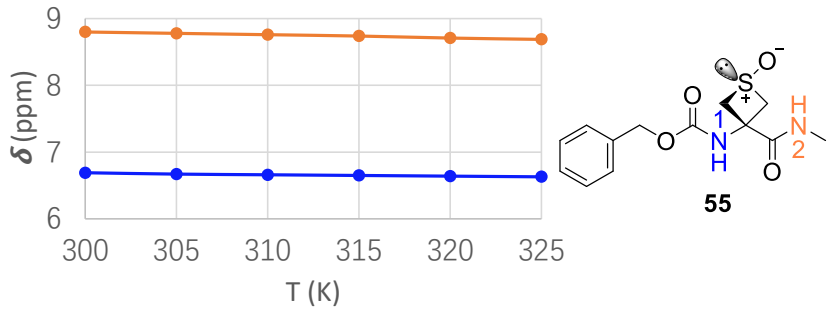

Figure 162. Temperature variation experiment of Cbz-Attc(O)-NHMe *trans* **55**

*c. NH signal evolution of Cbz-Attc(O)-NHMe cis **56***

The temperature variation experiment performed on the Cbz-Attc(O)-NHMe *cis* **56** revealed (Figure 163), over a 25 K temperature range, a non-negligible temperature coefficient for NH(1) (–5.2 ppb/K) indicating it was not H-bonded. The NH(2) showed a slightly upfielded shift with a low-temperature coefficient (–2.0 ppb/K) implicating it was intramolecularly H-bonded. These data are similar to that of DMSO-d_6 titration experiment results showing that NH(1) was more solvent exposed than NH(2), and are compatible with two major conformations (free-C7, free-π_{am}) presented in solution suggested by IR in solution, but no evidence for a C5-C6γ conformer.

	***T* (K)**						
	300	*305*	*310*	*315*	*320*	*325*	**T.C. (ppb/K)**
δ NH1	5.63	5.60	5.57	5.54	5.52	5.50	–5.2
δ NH2	6.40	6.39	6.38	6.37	6.36	6.35	–2.0

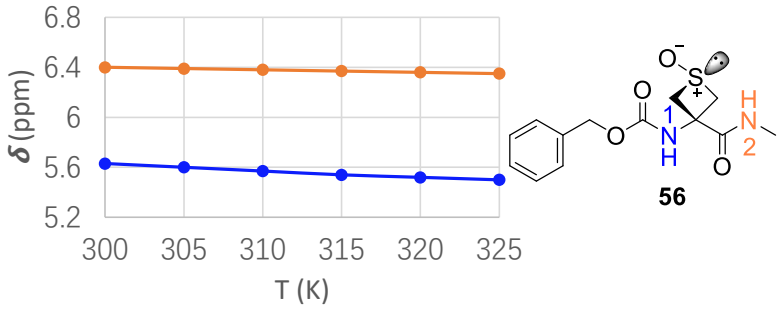

Figure 163. Temperature variation experiment of Cbz-Attc(O)-NHMe *cis* **56**

*d. NH signal evolution of Cbz-Attc(O,O)-NHMe **57***

The temperature variation experiment was carried out on Cbz-Attc(O,O)-NHMe **57**, and results are shown in Figure 164. Both NH signals moved to higher field with temperature increase. Over a 25 K temperature range, a non-negligible temperature coefficient for NH(1) (–5.6 ppb/K) indicating it was not H-bonded, and a low temperature coefficient for NH(2) (–1.6 ppb/K) pointing to its implication in an intramolecular H-bonding. The results are similar to that of DMSO-d_6 titration experiment results showing that NH(1) was more solvent accessible than NH(2), which are compatible with two major conformations (free-C7, free-π_{am}) that co-existed in solution, as suggested by infrared spectroscopy in solution, but no evidence for a C5-C7δ conformer.

	T (K)						
	300	*305*	*310*	*315*	*320*	*325*	**T.C. (ppb/K)**
δ NH1	6.04	6.01	5.98	5.95	5.92	5.90	–5.6
δ NH2	6.81	6.79	6.78	6.78	6.77	6.77	–1.6

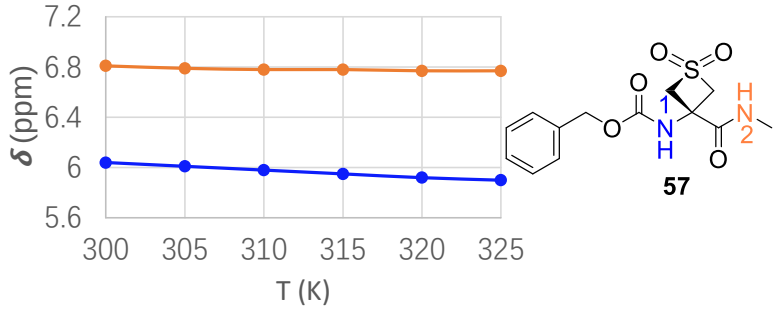

Figure 164. Temperature variation experiment of Cbz-Attc(O,O)-NHMe **57**

3.4.4.5 ^{1}H-^{1}H 2D NOESY NMR studies

*a. NOESY experiment of Cbz-Aatc(Me,O)-NHMe trans **49***

From the ^{1}H-^{1}H NOESY experiment on the Cbz-Aatc(Me,O)-NHMe *trans* **49**, the correlation map (focus on NH(1)/NH(2)) and signal assignments are shown in Figure 165. A medium cross peak between NH(1) and the $C^{\beta}H^{a}$ protons, and a weak cross peak between NH(1) and the $C^{\beta}H^{b}$ protons were observed. Strong cross peaks were observed between NH(2) and the $C^{\beta}H^{b}$ protons, and between NH(2) and the neighboring methyl protons. This correlation map is in complete agreement with a C5-C7δ extended conformation suggested by IR in solution and ^{1}H NMR chemical shifts.

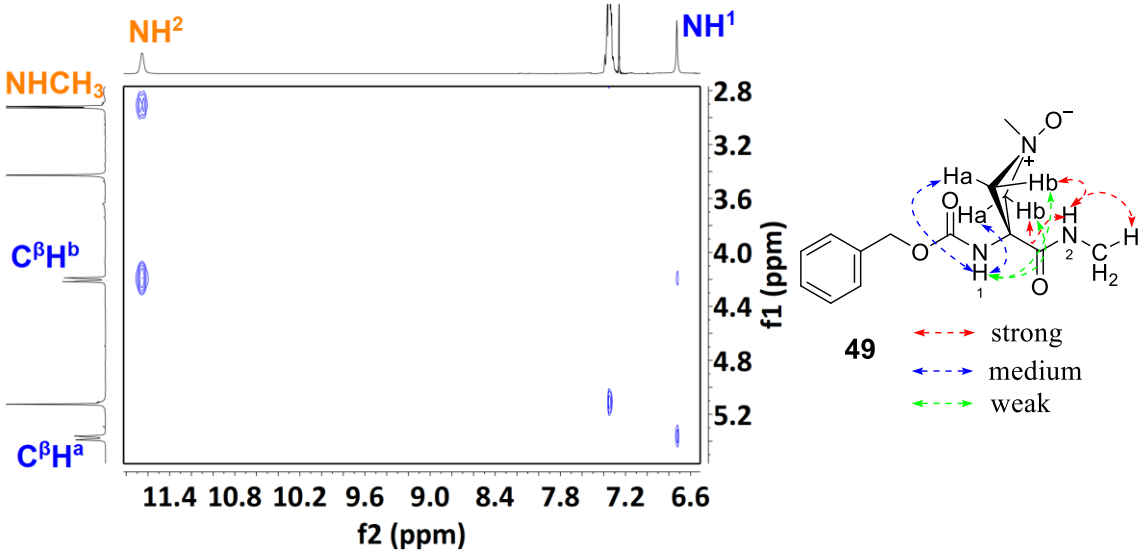

Figure 165. NOESY correlation map and signal assignments for Cbz-Aatc(Me,O)-NHMe *trans* **49**

*b. NOESY experiment of the Cbz-Attc(O)-NHMe trans **55***

From the ^{1}H-^{1}H NOESY experiment on Cbz-Attc(O)-NHMe *trans* **55**, the correlation map and signal assignments are shown in Figure 166. A medium cross peak between NH(1) and the $C^{\beta}H^{a}$ protons, and a weak cross peak between NH(1) and the $C^{\beta}H^{b}$ protons were observed. Strong cross peaks were observed between NH(2) and the $C^{\beta}H^{b}$ protons, and between NH(2) and the neighboring methyl protons. The correlation map resembles to that of Cbz-Aatc(Me,O)-NHMe *trans* **49** and was entirely in agreement with the predominance of an extended C5-C7δ conformation of Cbz-Attc(O)-NHMe *trans* **55** in solution.

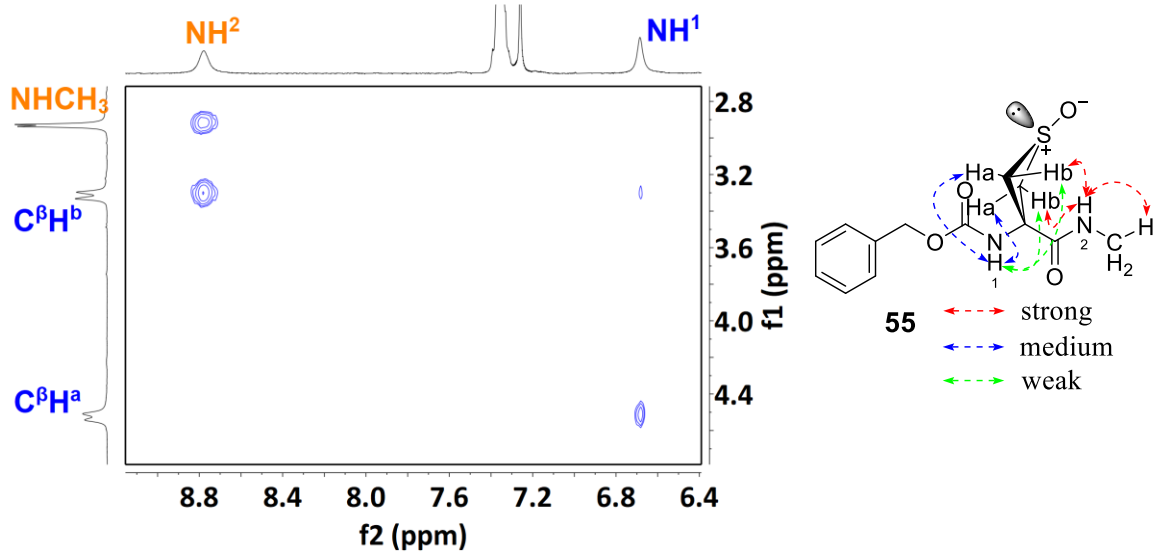

Figure 166. NOESY correlation map and signal assignments for Cbz-Attc(O)-NHMe *trans* **55**

*c. NOESY experiment of Cbz-Attc(O)-NHMe cis **56***

From the ^{1}H-^{1}H NOESY experiment on Cbz-Attc(O)-NHMe *cis* **56**, the correlation map and signal assignments are shown in Figure 167. NH(1) showed a strong correlation with the $C^{\beta}H^{a}$ protons and a weak correlation with the $C^{\beta}H^{b}$ protons. A weak cross peak was observed between NH(2) and the $C^{\beta}H^{b}$ protons, and NH(2) correlated strongly with the neighbouring methyl protons. The correlation map and signal assignments are compatible with the free-C7 and free-π_{am} conformations presented in solution, as suggested by IR in solution, but no evidence of the C5-C6γ conformer.

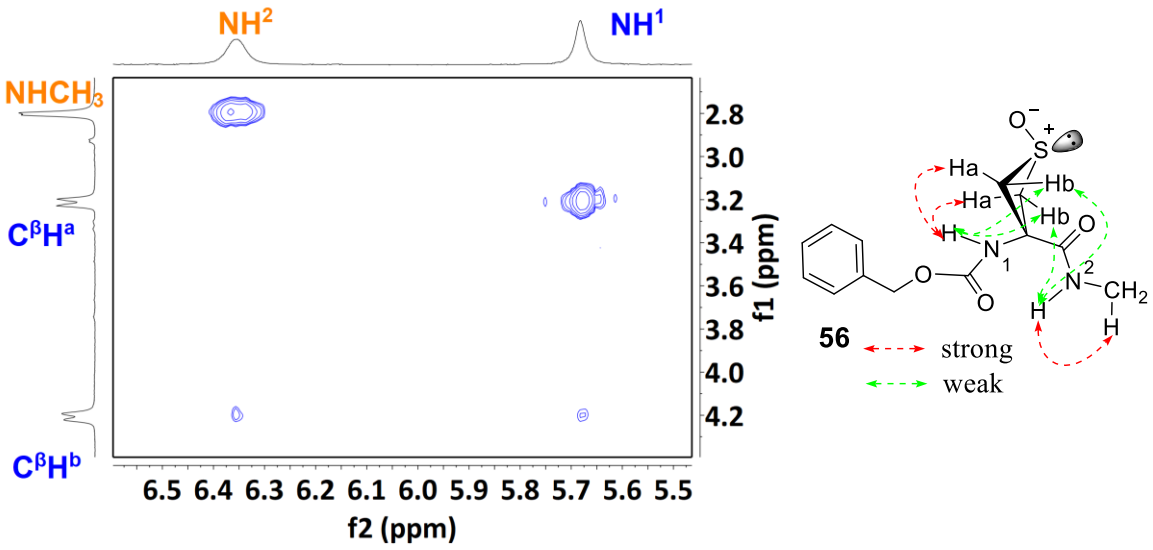

Figure 167. NOESY correlation map and signal assignments for Cbz-Attc(O)-NHMe *cis* **56**

*d. NOESY experiment of Cbz-Attc(O,O)-NHMe **57***

From the ^{1}H-^{1}H NOESY experiment on the Cbz-Attc(O,O)-NHMe **57**, the correlation map and signal assignments are shown in figure 168. They partly resembles that of the Cbz-Attc(O)-NHMe *cis* **57**. A strong cross peak was observed between NH(1) and the $C^{\beta}H^{a}$ protons. NH(2) showed weak correlation with the $C^{\beta}H^{b}$ protons, and strong correlation with neighbouring methyl protons. The correlation map and signal assignments are compatible with free-C7 and free-π_{am} conformations presented in solution, as suggested by IR in solution, but no evidence for the presence of the C5-C7δ conformer.

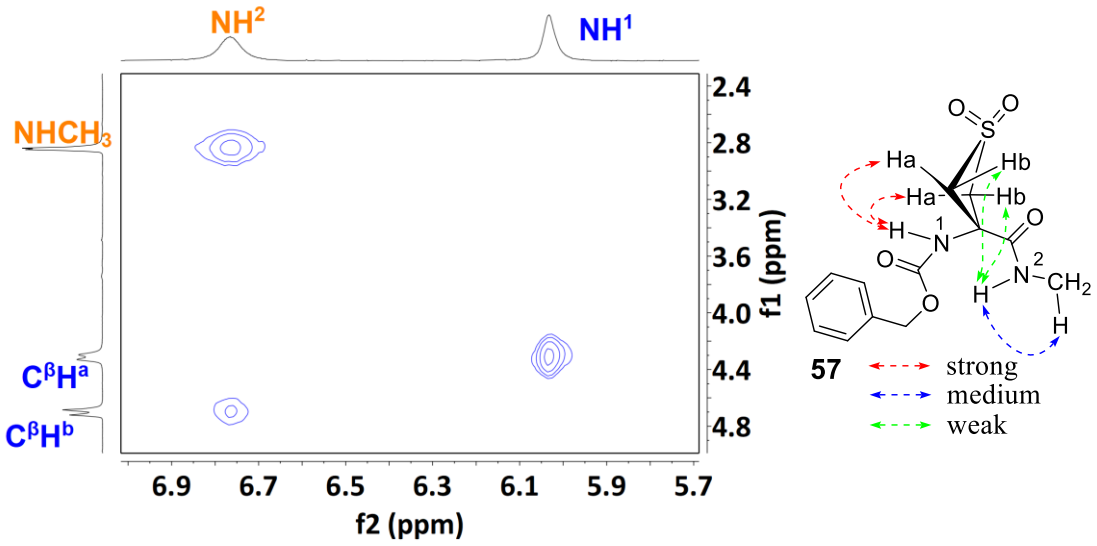

Figure 168. NOESY correlation map and signal assignments for Cbz-Attc(O,O)-NHMe **57**

3.4.5 Discussion and Conclusions

Based on the conformational analysis in solution, it appeared that the predominant conformation for Cbz-Aatc(Me,O)-NHMe *trans* **49** and Cbz-Attc(O)-NHMe *trans* **55** is a C5-C7δ extended conformation. Both NH signals of *N*-oxide *trans* **49** were more deshielded than that of *S*-oxide *trans* **55**, suggesting that the inter-residue N–H···O–N C7δ H-bond in *N*-oxide *trans* **49** is stronger than the inter-residue N–H···O–S C7δ H-bond in *S*-oxide *trans* **55**. The Cbz-Attc(O,O)-NHMe **57** also showed a C5-C7δ conformation but seems to be a minor player, as suggested by solution phase IR and NMR studies. These results suggest that the strength of the C7δ H-bond in these three oxides derivatives: *N*-oxide *trans* **49** > *S*-oxide *trans* **55** > sulfone **57** (Figure 169).

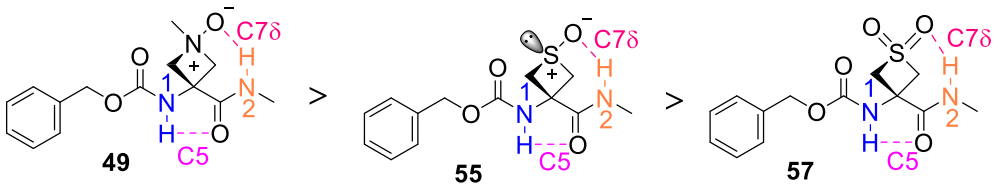

Figure 169. The strength of the C7δ H-bond in Cbz-Aatc(Me,O)-NHMe *trans* **49**, Cbz-Attc(O)-NHMe *trans* **55** and Cbz-Attc(O,O)-NHMe **57**

In the Cbz-Attc(O)-NHMe *cis* **56**, the orientation of the S-O on the carbamate side hampered the formation of a C7δ H-bond. The sulfur atom of *cis* **56** formed a C6γ H-bond and exhibited a C5-C6γ extended conformation similar to that of Cbz-Attc-NHMe **VIII**, but the extended conformer in the former is a minor contributor suggesting that the strength of the inter-residue N–H···S C6γ in *cis* **56** is weaker than in Cbz-Attc-NHMe **54** (Figure 170).

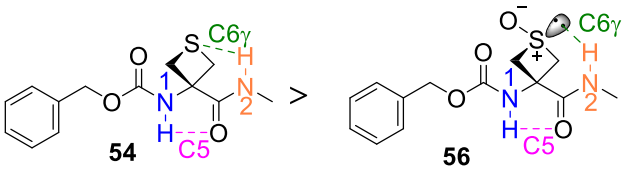

Figure 170. The strength of the C6γ H-bond in Cbz-Attc(O)-NHMe *cis* **56** and Cbz-Attc-NHMe **54**

Collectively, the results of 1D/2D NMR studies (^{1}H chemical shifts of NH signals, DMSO-d_6 titration, temperature variation and NOE NMR experiments) were fully agreed with Cbz-Aatc(Me,O)-NHMe *trans* **49** adopting a predominant C5-C7δ extended conformation, consistent with the result obtained from infrared in solution (Figure 171).

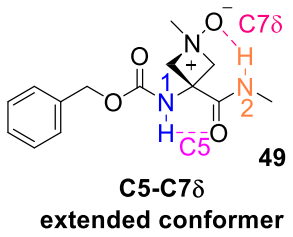

Figure 171. Cbz-Aatc(Me,O)-NHMe *trans* **49** exhibited a predominant C5-C7δ extended conformation in solution

The results from ^{1}H chemical shifts and NOE correlation map of Cbz-Attc(O)-NHMe *trans* **55** are consistent with that of Cbz-Aatc(Me,O)-NHMe *trans* **49**, suggesting that the former also adopted a predominant C5-C7δ extended conformation, as predicted by theoretical calculations and observed in gas phase IR. However, the minor contributions of free-π_{am} and/or free-C7 conformations suggested by infrared in solution was not clearly observe from NMR experiments (Figure 172).

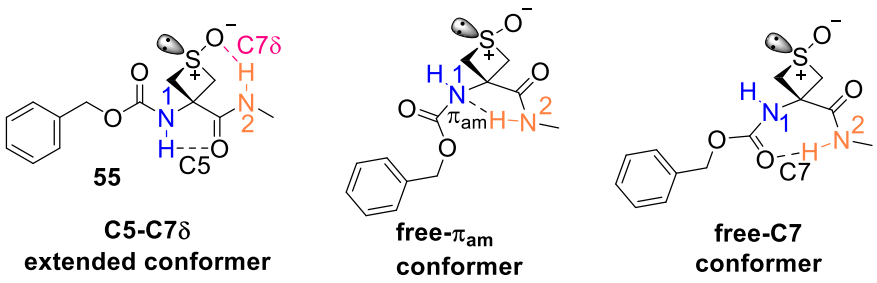

Figure 172. Cbz-Attc(O)-NHMe *trans* **55** exhibited a predominant C5-C7δ extended conformation with minor free-π_{am} and/or free-C7 conformers in solution

DMSO-d_6 titration and temperature variation results indicated that in Cbz-Attc(O)-NHMe *cis* **56**, NH(1) was not H-bonded and NH(2) was H-bonded, which is compatible with major free-C7 and free-π_{am} conformations predicted by theoretical calculations. In addition, the NOE correlation map and signal assignments also suggested a folded conformation. The C5-C6γ conformer suggested by infrared in solution was not highlighted by NMR experimental results, pointing out this conformer was a minor contributor (Figure 173).

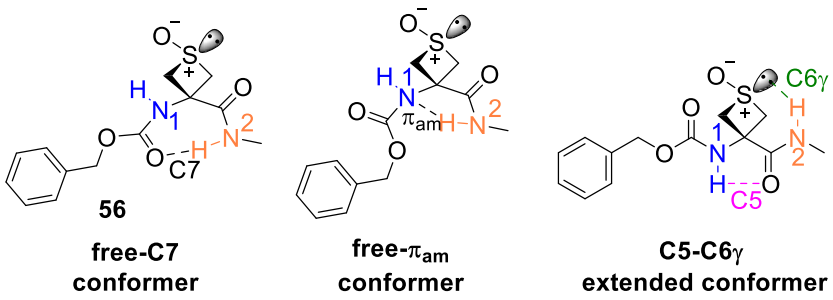

Figure 173. Cbz-Attc(O)-NHMe *cis* **56** exhibited three conformations in solution

The conformational results for Cbz-Attc(O,O)-NHMe **57** are similar to those of Cbz-Attc(O)-NHMe *cis* **56**, the NOE correlation map and signal assignments of the former were strongly suggested its adoption of a folded conformation, consistent with two folded conformers (free-C7 and free-π_{am}) suggested by infrared in solution. The C5-C7δ conformer observed in infrared in solution was not well revealed by NMR experimental results indicating this conformer was a minor player (Figure 174).

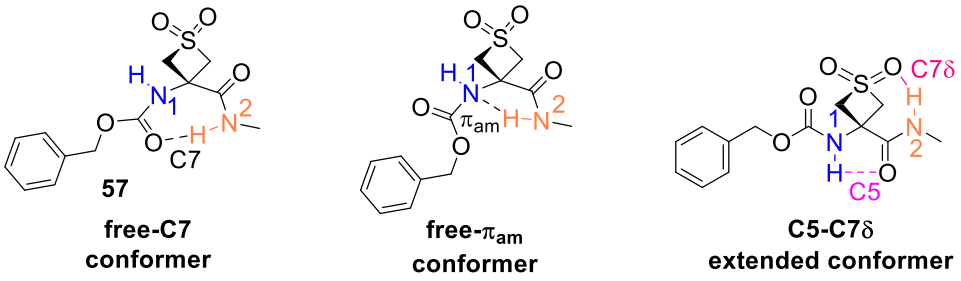

Figure 174. Cbz-Attc(O,O)-NHMe **57** exhibited three conformations in solution

3.4.6 X-ray diffraction experiments

We obtained single crystals of Cbz-Aatc(Me,O)-NHMe *trans* **49**, Cbz-Attc(O)-NHMe *trans* **55** and Cbz-Attc(O,O)-NHMe **57**, which then performed their structural analysis via X-ray diffraction.

3.4.6.1 X-ray diffraction of Cbz-Aatc(Me,O)-NHMe *trans* **49**

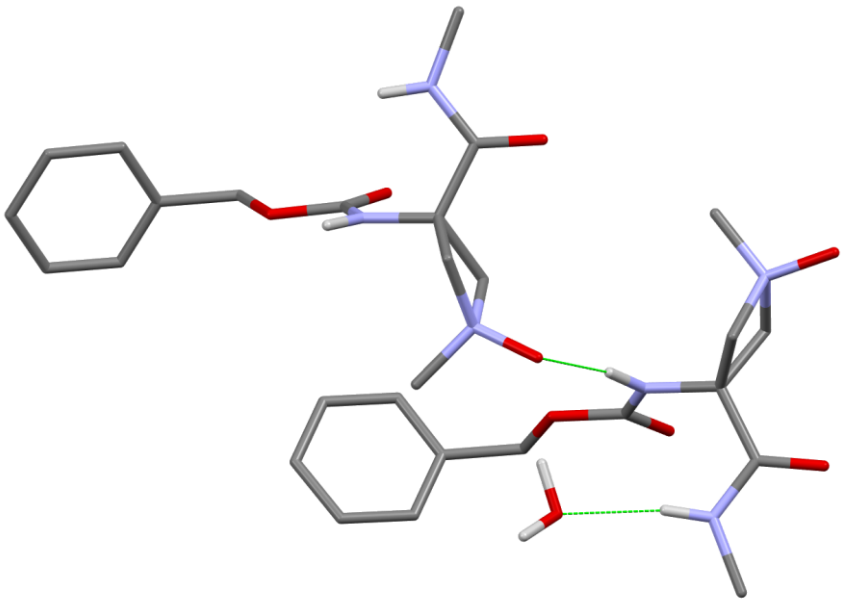

Figure 175. X-ray diffraction crystal structure of Cbz-Aatc(Me,O)-NHMe *trans* **49**

A crystal of Cbz-Aatc(Me,O)-NHMe *trans* **49** was obtained by slow evaporation of a methanol solution at ambient temperature. The X-ray diffraction structure is shown in Figure 175, it shows only intermolecular H-bonds, in which NH(2) H-bonded with oxygen atom of H_2O molecule and NH(1) intermolecularly H-bonded to oxygen atom (O–N) of a second *N*-oxide *trans* **49** molecule.

3.4.6.2 X-ray diffraction of Cbz-Attc(O)-NHMe *trans* **55**

A crystal of Cbz-Attc(O)-NHMe *trans* **55** was obtained by slow evaporation of a chloroform solution at ambient temperature. The X-ray diffraction structure is shown in Figure 176, it shows only intermolecular H-bonds. NH(2) was engaged in an intermolecular H-bond with the carbonyl oxygen of methyl amide of a second *trans* **55** molecule, and NH(1) formed H-bond with oxygen atom (O–S) of a third *trans* **55** molecule.

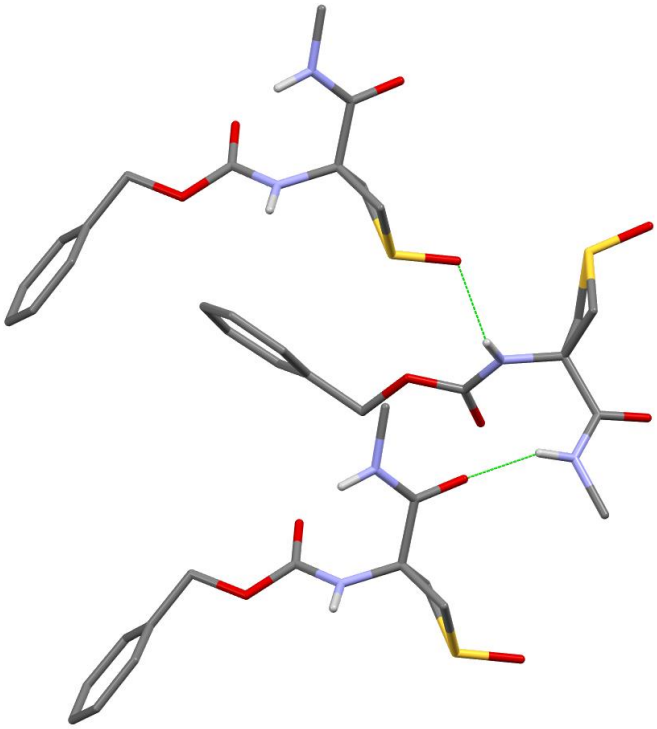

Figure 176. X-ray diffraction crystal structure of Cbz-Attc(O)-NHMe *trans* **55**

3.4.6.3 X-ray diffraction of Cbz-Attc(O,O)-NHMe **57**

A crystal of Cbz-Attc(O,O)-NHMe **57** was obtained by slow evaporation of a methanol solution at ambient temperature. The X-ray diffraction structure is shown in Figure 177, it shows only intermolecular H-bonds. NH(1) and NH(2) were engaged in H-bond with oxygen atoms of carbonyl and of O=S=O of a second Cbz-Attc(O,O)-NHMe **57** molecule, respectively.

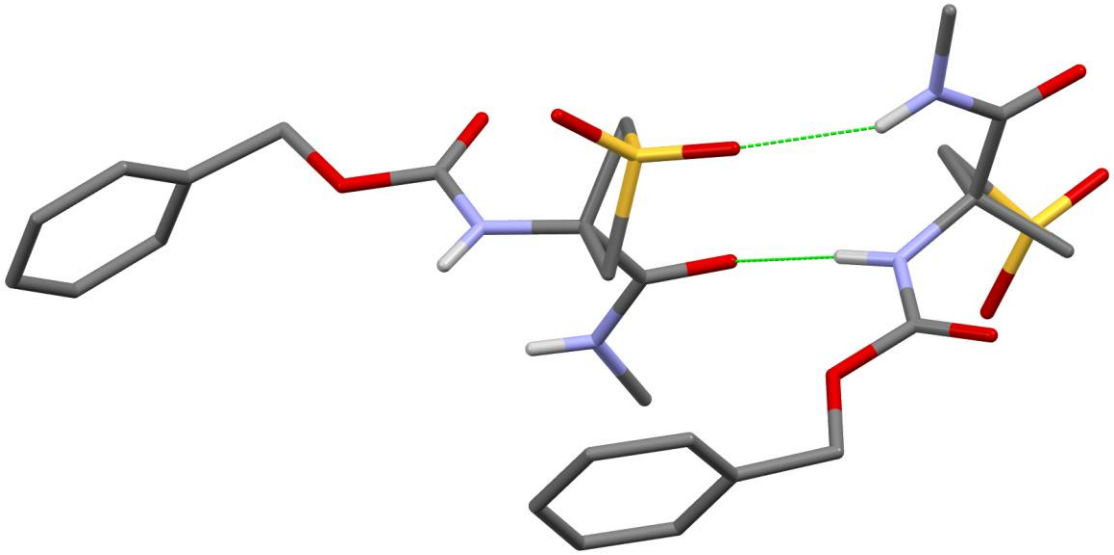

Figure 177. X-ray diffraction crystal structure of Cbz-Attc(O,O)-NHMe **57**

3.4.6.4 Conclusion

The crystal structures of Cbz-Aatc(Me,O)-NHMe *trans* **49**, Cbz-Attc(O)-NHMe *trans* **55** and Cbz-Attc(O,O)-NHMe **57** have shown only the formation of intermolecular H-bonds, no observation of intramolecular H-bond at all. But the oxygen atom of the *N*-oxide and *S*-oxide still showed the ability to act as an H-bond acceptor in participating in intermolecular H-bonding. More importantly, these crystal structures played a crucial role in identifying the structures and configurations of these molecules.

3.5 Conclusion and Perspectives

In this chapter, Cbz-Aatc(Me,O)-NHMe *trans* **49**, Cbz-Attc(O)-NHMe *trans* **55**, Cbz-Attc(O)-NHMe *cis* **56** and Cbz-Attc(O,O)-NHMe **57** were successfully synthesized via common oxidizing conditions. The *N*-oxide *trans* **49** showed remarkable stability, and its structure was identified by X-ray diffraction. The oxidation of Cbz-Attc-NHMe **54** can easily control to partially convert

to *S*-oxide **55** and **56**, and completely convert to sulfone **57**, and the *trans* stereochemistry of *S*-oxide **55** was confirmed by crystal structure.

Conformational results have shown that the oxygen atom of *N*-oxide in Cbz-Aatc(Me,O)-NHMe *trans* **49** and of *S*-oxide in Cbz-Attc(O)-NHMe *trans* **55** act as a good H-bond acceptor. The generated oxygen atom from side chain formed a strong C7δ H-bond that successfully stabilized a weak intra-residue C5 H-bond in the peptide backbone, exhibited an extended conformation. These findings provided new cases for the stabilization of the weak C5 H-bond.

In previous studies, Cbz-Aatc(Me)-NHMe **42** and Cbz-Attc-NHMe **54** have shown the adoption of a dominant C5-C6γ extended conformation. By lengthening the peptide chain, their peptides were more likely to a folded conformation rather than an extended conformation. In comparison to the C6γ H-bond in Cbz-Aatc(Me)-NHMe **54** and in Cbz-Attc-NHMe **54**, Cbz-Aatc(Me,O)-NHMe *trans* **49** and Cbz-Attc(O)-NHMe *trans* **55** both revealed a stronger C7δ H-bond that was more helpful to the stabilization of the weak C5 H-bond. Therefore, Cbz-Aatc(Me,O)-NHMe *trans* **49** and Cbz-Attc(O)-NHMe *trans* **55** can be good candidates for further investigations to explore the strength of the C7δ H-bonding in longer peptides, to have a better understanding of the capability of an oxygen atom in the side chain as H-bond acceptor.

Chapter 4. Conformational studies of cyclic constraint amino acid ACBC derivatives

Chapter 4. Conformational studies of cyclic constraint amino acid ACBC derivatives

4.1 Introduction

4.1.1 Presentation of ACBC

2-Aminocyclobutane-1-carboxylic acid (ACBC) exists in four stereoisomeric forms due to two chiral centers on its cyclobutane ring (Figure 178).

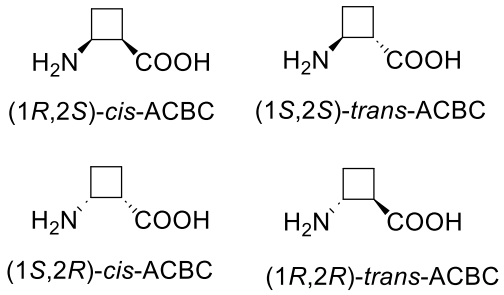

Figure 178. Four stereoisomeric forms of ACBC

Cyclobutanes are valuable building blocks in organic synthesis for the preparation of multi-functionalized molecules and biologically active products,[198,199] and ACBC derivative is one of the interesting functionalized cyclobutane molecules.[200,201]

The most common synthetic approach for preparing ACBC derivatives is via a [2+2] cycloaddition reaction, achieved by thermal, photochemical, or metal-catalyzed conditions.

In 1963, Kelly described a synthetic method targeting ACBC derivative, in which *N*,*N*-dimethyl isobutenylamine was reacted with methyl acrylate for 2 hours at 170 °C with a yield of 75% (Scheme 47).[202]

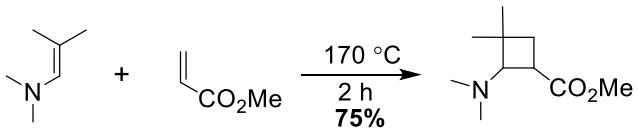

Scheme 47. Preparation of ACBC derivative by thermal method

In 2011, the Aitken group reported a [2+2] cycloaddition to prepare ACBC derivatives. The reaction was carried out using ethylene and Boc-uracil in acetone, and the mixture was irradiated with a mercury lamp at room temperature for 4 hours giving cyclobutane compound. After ring-opening and chiral resolution steps, the enantiopure *cis*-ACBC

derivatives were obtained. The *trans*-ACBC derivatives required one more epimerization step to be isolated (Scheme 48).[203]

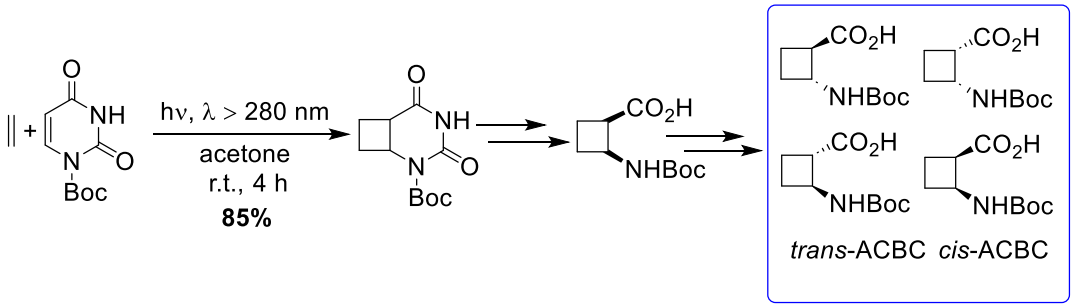

Scheme 48. Preparation of ACBC derivative by photochemical method

In 2018, the Feng group developed a strategy for synthesizing ACBC derivatives via metal-catalyzed asymmetric [2+2] cycloaddition. The reaction was carried out using alkylidene malonate and *N*-allenamide, catalyzed by $Mg(OTf)_2$ giving the cyclobutane product in 99% yield with 87% ee (Scheme 49).[204]

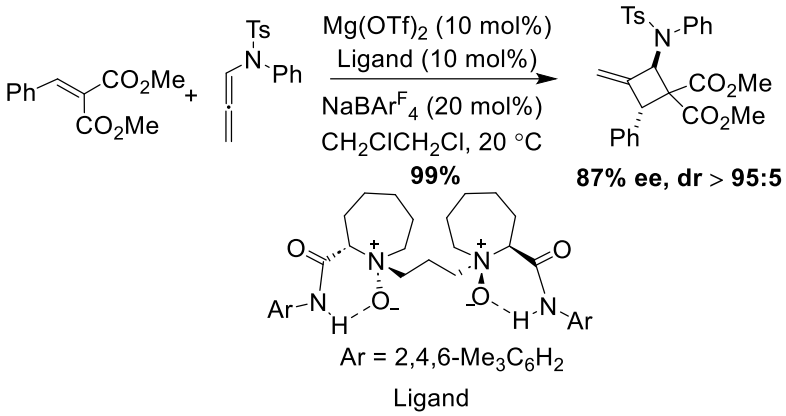

Scheme 49. Preparation of ACBC derivative by metal-catalyzed method

In 2023, the Frongia group reported a novel protocol for synthesizing ACBC derivatives via a tandem coupling/aza-Michael addition, which provided diastereoselective access to *trans*-ACBC derivatives. The reaction was carried out using cyclobutene-1- carboxylic acid reacting with 2 equivalents of benzo[d]oxazol-2(3H)-ones in CH_2Cl_2, in the presence of DMAP and DIC for 40 hours at room temperature. This produced a separable mixture of *trans* and *cis* diastereomers **A** and **A'** (dr = 93:7) in 72% yield (Scheme 50).[205]

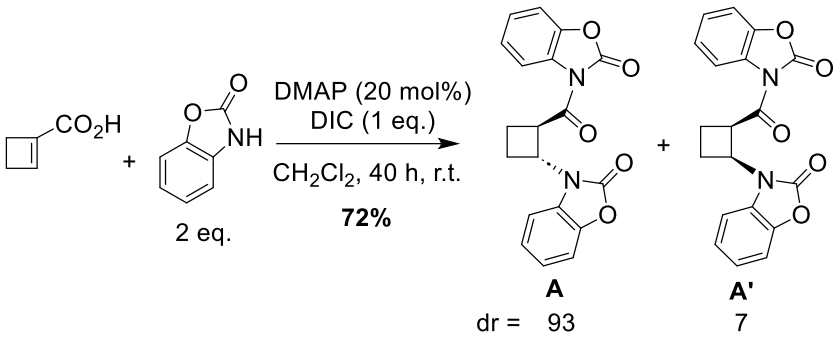

Scheme 50. Preparation of ACBC derivatives by tandem coupling/aza-Michael addition

Furthermore, the benzoxazolinone moiety at the *C*-terminus of the ACBC is a good leaving group that can be substituted by other nucleophiles resulting in diverse *N*-benzoxazolinone protected ACBC derivatives (Scheme 51).

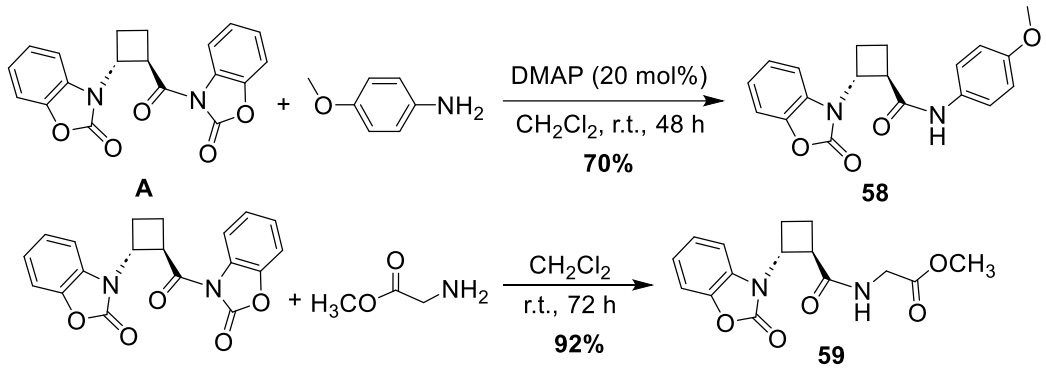

Scheme 51. Preparation of *trans*-ACBC derivatives **58** and **59**

4.1.2 The conformational preference of *trans*-ACBC derivative in homopeptides

trans-ACBC derivative has shown the capability to adopt a well-defined secondary structure in homo-oligomers, attributed to the unique structural features that enable them to form short-range hydrogen bonds.

In 2015, the Aitken group described the local folding propensity of a single residue derivative of *trans*-ACBC, suggesting its adoption of a predominant C8 H-bonded conformation characterized by infrared spectroscopy in gas phase. The author deduced that the rigidity of the cyclobutane and the orientations of the substituents, lead to a closer distance between the amide group and the carbamate moiety that facilitates the formation of the C8 H-bond (Figure 179).[206]

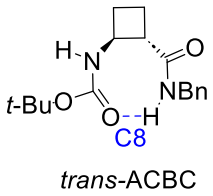

Figure 179. Local folding propensity of *trans*-ACBC derivative

In 2009, the Ortuno research group showed the conformational preference of *trans*-ACBC-derived dipeptides. The formation of an eight-membered H-bonding ring was noted for (*trans*, *trans*) and (*trans*, *cis*) combinations, whereas the methyl moiety of the C-terminus in these cases seems to hindered further C8 H-bond formation of *trans*-ACBC (Figure 180).[207]

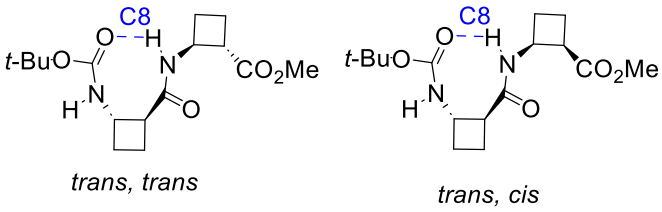

Figure 180. Stereochemistry of the ACBC governs the conformation in dipeptides

In 2012, the Ortuno group continued investigating the conformational preferences of *trans*-ACBC derivatives. A dipeptide capped with a methyl amide at the *C*-terminal, present two consequential C8 H-bonds. When the peptide chain was extended to a tetrapeptide, the formation of three consecutive C8 H-bonds was observed, suggested by ^{1}H NMR spectroscopy and theoretical calculations (Figure 181).[89]

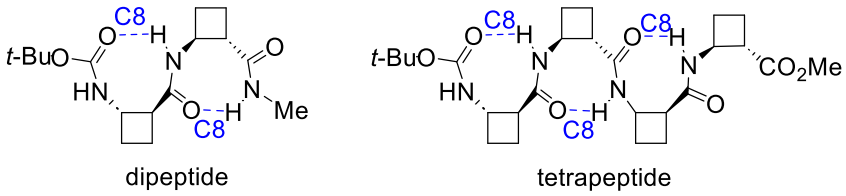

Figure 181. The conformational preferences of *trans*-ACBC derived di- and tetrapeptides

In 2010, the Aitken group investigated the structural feature of *trans*-ACBC in longer oligomers. They demonstrated that the hexamer and octamer of *trans*-ACBC have a preference to fold into a well-defined 12-helix conformation both in solution and in the solid state, supported by theoretical calculations. When *trans*-ACBC derivatives are in short oligomers, their structural features enable them to form short-range H-bonds and adopt C8 H-bonded conformations. In longer oligomers of *trans*-ACBC, formation of long-range H-bonds was favored (Figure 182).[90]

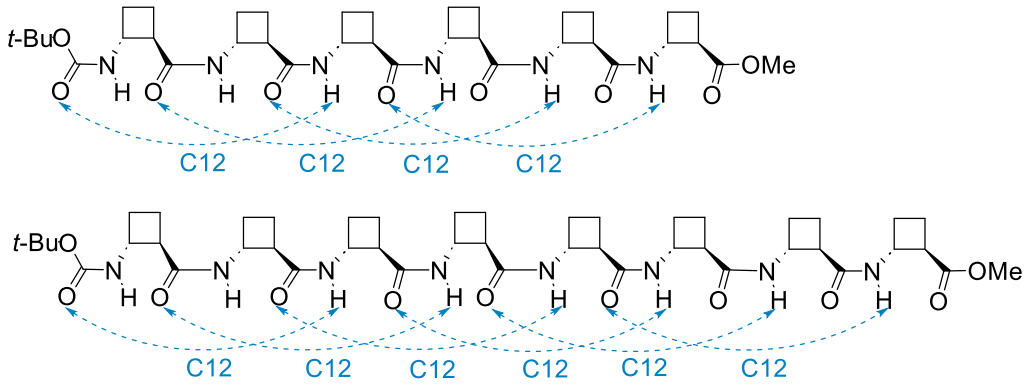

Figure 182. The conformational preferences of *trans*-ACBC derived hexa- and octapeptides

4.1.3 The conformational preference of *trans*-ACBC derivative in hybrid peptides

Based on the structural feature of *trans*-ACBC that possesses a high constraint backbone, in 2015, the Aitken group described a β/γ-hybrid peptide constituted of *trans*-ACBC motif alternating with unsubstituted GABA, γ-amino acid. The *trans*-ACBC remained capable of forming a C8 H-bond, and the unconstrained γ-amino acid, due to its local flexibility, formed a C9 H-bond, alternating C9/C8 H-bonding network exhibited a 9/8-ribbon. These results were suggested by theoretical calculations and confirmed by infrared spectroscopy in solution and NMR studies (Figure 183).[166]

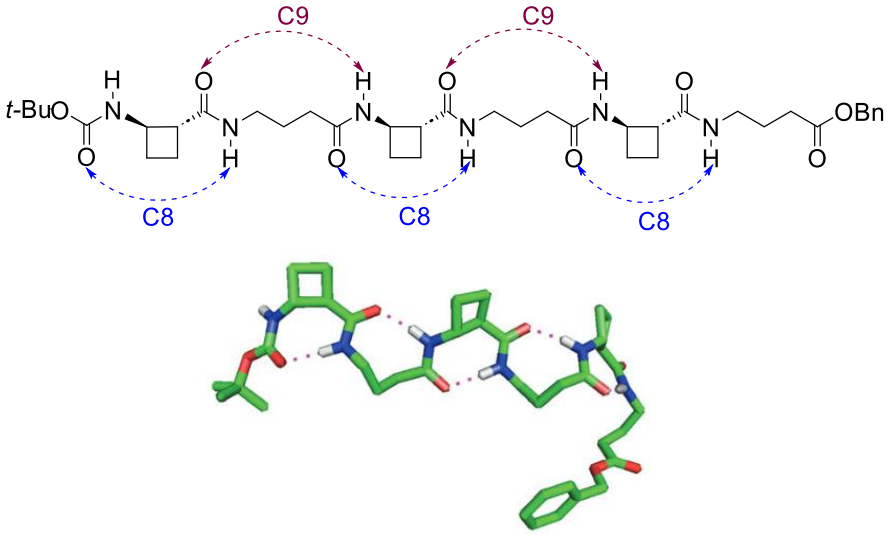

Figure 183. H-bonding pattern (top) of *trans*-ACBC and GABA derived β/γ-hexapeptide and a 9/8 ribbon conformer (bottom) image was reproduced from the literature[166]

In 2016, the Aitken group reported other β/γ-hybrid peptides of *trans*-ACBC and γ^4-amino acids in alternation and successfully targeted a 13-helix conformation. The *trans*-ACBC and the singly substituted (R)-γ^4-Phe and (R)-γ^4-Leu provided sufficient steric imposition to induce

the 13-helix conformation, which was verified by IR in solution, CD experiment and NMR studies, and supported by theoretical calculations (Figure 184).[208]

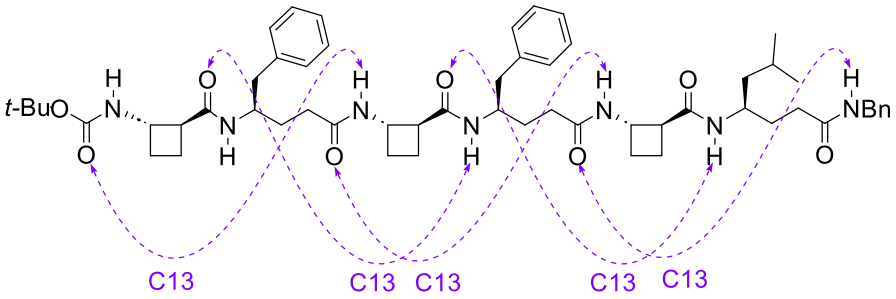

Figure 184. H-bonding pattern of a β/γ-hybrid peptide adopted 13-helix conformation

4.1.4 Aim of this chapter

As previously mentioned, the constraint backbone of *trans*-ACBC derivative enables the formation of short-ranged H-bond and mainly adopts C8 H-bonded conformation in short oligomers. In most cases, Boc and Cbz were popular moieties used for *N*-capping. In comparison to these common protection groups, the benzoxazolinone moiety of *trans*-ACBC derivatives, which was developed by the Frongia group is unusual and less flexible.[205]

Therefore, it is intriguing to investigate their conformational preferences and evaluate the influence of *N*-carbamate substituent on these preferences, particularly with respect to the retention of the C8 feature. To achieve this goal, *trans*-ACBC derivatives **58** and **59** were selected as model compounds for the conformational studies in this chapter, in collaboration with the Frongia group (Figure 185).

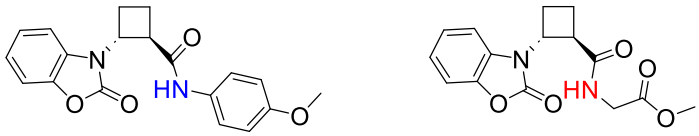

58 **59**

Figure 185. Two *trans*-ACBC derivatives **58** and **59** for the conformational studies in this chapter

4.2 Conformational studies of *trans*-ACBC derivatives **58** and **59**

In this chapter, conformational studies were performed using molecular modelling, IR spectroscopy in solution phase and DMSO-d_6 titration experiments. The detailed description of these methods has been described in section 1.3.1, chapter 1.

4.2.1 Molecular Modelling

A hybrid Monte Carlo Molecular Mechanics (MCMM) conformational search was carried out on each compound in a chloroform medium using Macromodel version 10.6 (Schrödinger, LLC, New YORK, 2014) and the OPLS 2005 force field without restraints. From the first 1000 generated conformers, those within a 50 kJ·mol^{-1} relative energy were retained and sorted according to their conformer families.

4.2.1.1 Lowest energy conformations of *trans*-ACBC derivative **58**

The conformational search performed on *trans*-ACBC derivative **58** afforded 186 conformations, which revealed two low energy conformers which are shown in Figure 186. The C8 conformer family with the lowest energy displayed a C8 H-bond, the abundance is given in 4%. The second lowest energy family is the most abundant with 96% and the conformations with a free NH.

Conformations	Relative abundance of each conformation	The lowest energy conformation
[8]	4%	84.565
free	96%	100.555

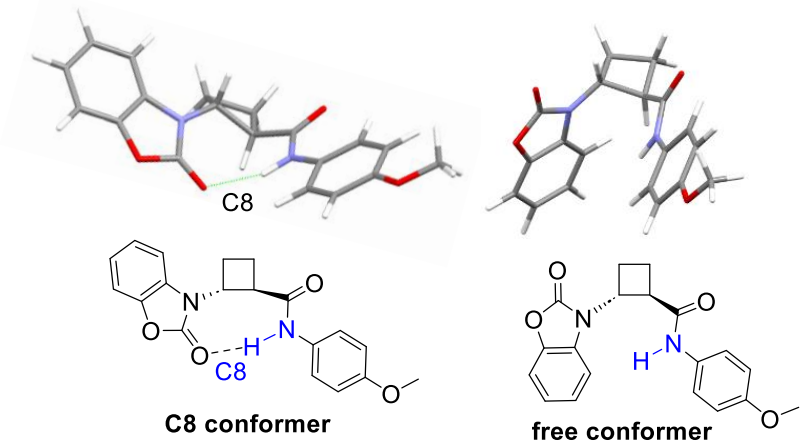

Figure 186. Two conformation families (top) and H-bonding patterns (bottom) of *trans*-ACBC derivative **58**

4.2.1.2 Lowest energy conformations of *trans*-ACBC derivative **59**

The conformational search performed on *trans*-ACBC derivative **59** afforded 597 conformations, which revealed three conformations that are shown in Figure 187. The conformer family with the lowest energy showed a C8 H-bond, but with an abundance of 8%. The C5 conformer family showed that the NH in a C5 interaction implicating the glycine

residue, in an abundance of 12%. The most abundant conformer family is given in 81% and revealed that the NH was not hydrogen-bonded.

Conformations	Relative abundance of each conformation	The lowest energy conformation
[8]	8%	–24.740
[5]	12%	–15.996
free	81%	–11.568

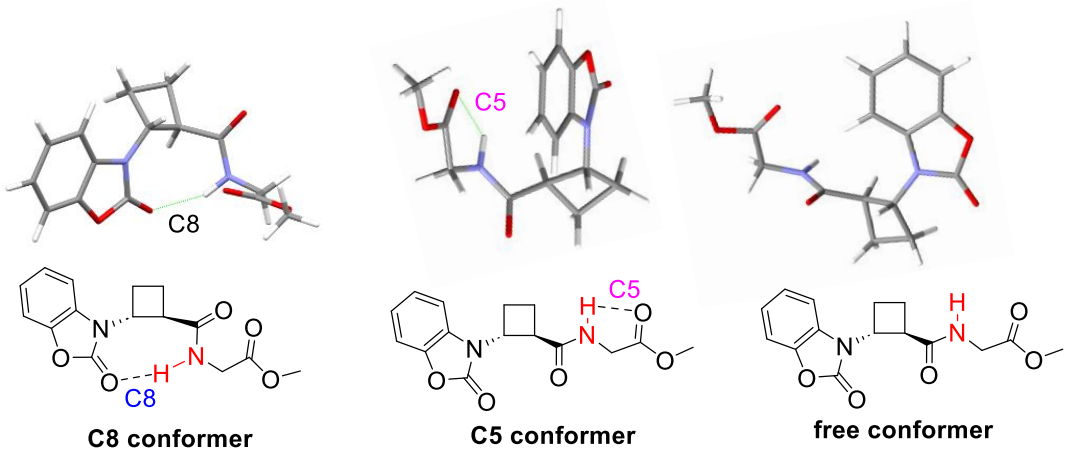

Figure 187. Three conformation families (top) and H-bonding patterns (bottom) of *trans*-ACBC derivative **59**

4.2.1.3 Discussion

The *N*-benzoxazolinone capped *trans*-ACBC derivatives **58** and **59** exhibited a low propensity to form a robust C8 H-bond and favor conformation with a free NH compared to *trans*-ACBC derivatives with more common *N*-capping groups such as Boc and Cbz. This phenomenon could be due to the influence of the bulkiness of the benzoxazolinone moiety and the less flexibility. In addition to a C8 and a free conformer family, derivative **59** also exhibited an intra-residue C5 H-bonded conformer implicating the glycine residue. The C5 H-bond is present in this structure without other interaction support, which is not observed in the structures described in Chapters 2 and 3.

4.2.2 Solution phase IR studies of *trans*-ACBC derivatives **58** and **59**

Infrared spectroscopy studies of *trans*-ACBC derivatives **58** and **59** were performed in chloroform solution at several concentrations (0.5, 1, 5, and 10 mM), the spectra showed slightly concentration-related effects in the NH stretch region, which the proportion of conformations was changed by different concentrations.

Each conformation obtained from molecular modelling was submitted to the simulation of IR spectrum in solution. This simulation work was carried out by Prof. Michel Mons in the LIDYL laboratory (CEA Saclay, Gif-sur-Yvette, France).

4.2.2.1 Solution phase IR of *trans*-ACBC derivative **58**

The solution state IR spectrum of *trans*-ACBC derivative **58** showed a broad, red-shifted NH stretch absorbance in the range of 3275-3375 cm^{-1}, centered at 3316 $cm^{-}1$, was assigned to the NH in a C8 H-bonded conformer. The appearance of a sharper band at 3428 cm^{-1} points to the presence of a second conformer with a free, non hydrogen-bonded NH. (Figure 188). These two bands are consistent with the simulated IR spectra. The discrepancy between the experimental bands and theoretical sticks may be due to the solvent effect in solution. Therefore, *trans*-ACBC derivative **58** presented two conformations in solution, supported by theoretical calculations.

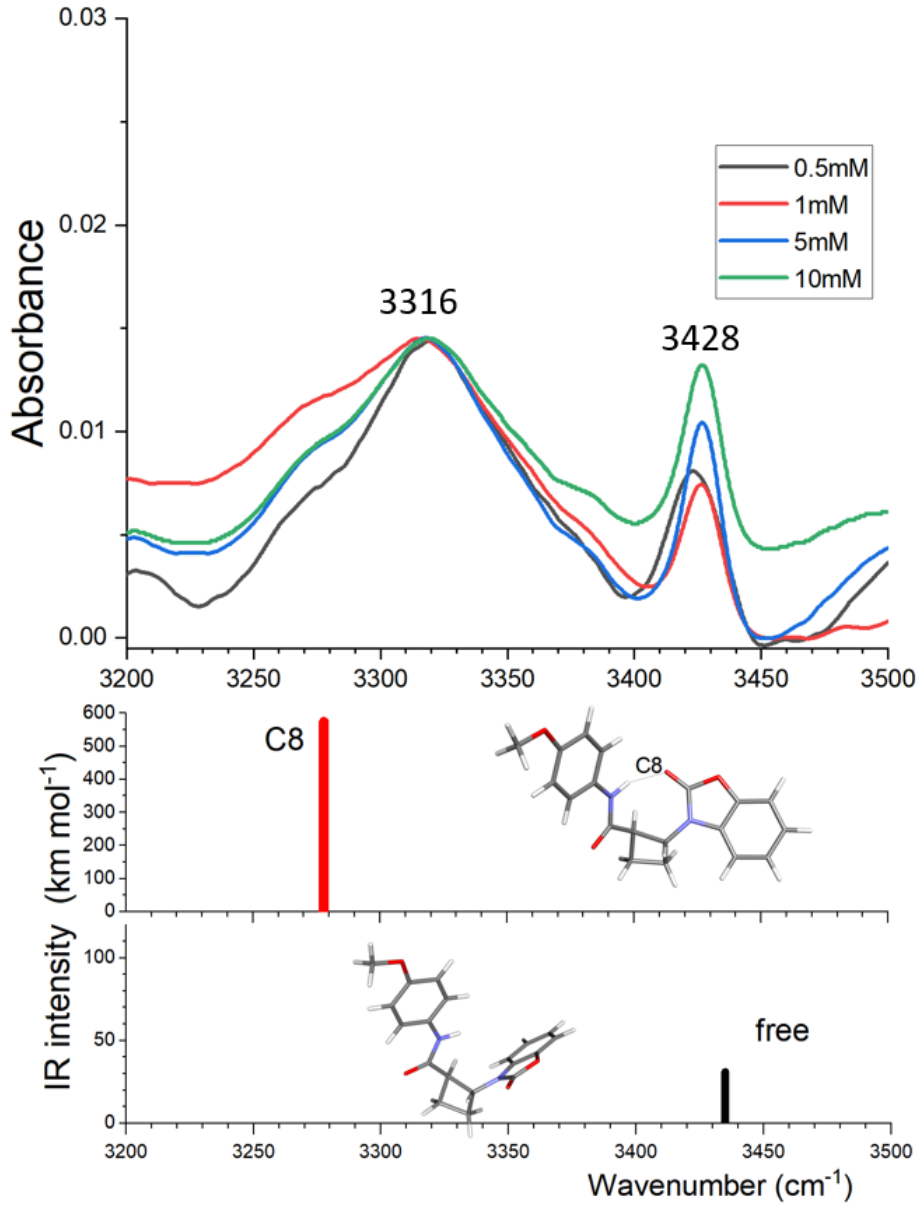

Figure 188. Upper panel: IR spectra of *trans*-ACBC derivative **58** in chloroform solution at several low concentrations; lower panels: theoretical (stick) IR spectra of minimized conformations in chloroform solution

4.2.2.2 Solution phase IR of *trans*-ACBC derivative **59**

The IR spectrum of *trans*-ACBC derivative **59** showed three bands (Figure 189). A broad, red-shifted band centered at 3338 cm^{-1} was assigned to NH implicated in a C8 H-bond. Two blue bands located at 3425 and 3450 cm^{-1}, were assigned to conformers having a 5-membered ring H-bond (C5) implicating the NH of the glycine residue and a free NH, respectively. These three bands are consistent with the theoretical IR spectrum simulated for each conformer.

Therefore, *trans*-ACBC derivative **59** presented three conformations in solution supported by theoretical calculations.

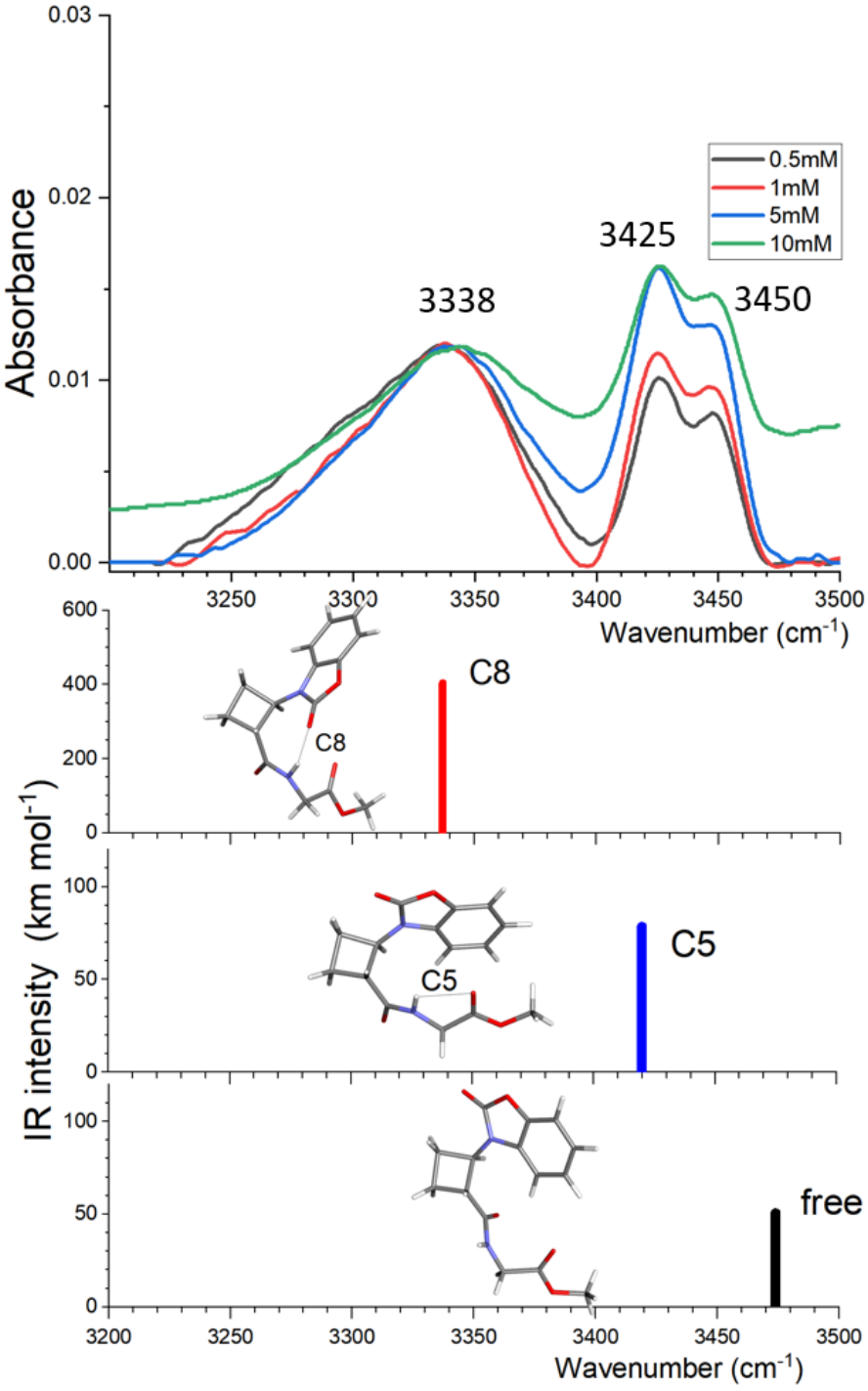

Figure 189. Upper panel: IR spectra of *trans*-ACBC derivative **59** in chloroform solution at several low concentrations; lower panels: theoretical (stick) IR spectra of minimized conformations in chloroform solution

4.2.2.3 Discussion

trans-ACBC derivatives **58** and **59** have shown more than one significant bands by IR spectroscopy experiments, indicating that the C8 H-bonded conformer is not the only contributor in solution. In addition, as the concentration increases, the proportion of the C8 decreased and the one of free conformer increased, indicating that the C8 H-bonded conformer is not very robust, and a higher concentration favors a free conformation.

4.2.3 DMSO-d_6 titration experiments

*a. NH signal evolution of trans-ACBC derivative **58***

Firstly, we noted that the NH signal of *trans*-ACBC derivative **58** has a chemical shift of 8.25 ppm in pure $CDCl_3$ at a 5 mM concentration. With increasing the concentration of DMSO-d_6, the NH signal was moved to a lower field and reached a downfield shift ($\Delta\delta$ = 0.75 ppm) which indicated no extensively solvent exposure, the NH may be involved in a C8 intramolecular H-bond (Figure 190). In previous research observations, *trans*-ACBC derivatives exhibiting strong C8 H-bonding conformations. In the DMSO-d_6 titration experiments for 50% concentration of DMSO, the resulting $\Delta\delta$ for a β/γ hybrid peptide Boc-*t*ACBC-GABA-OBn (described in Figure 183) was 0.18 ppm.[14]

In comparison with the $\Delta\delta$ (0.18 ppm) of the Boc-*t*ACBC-GABA-OBn, the higher $\Delta\delta$ value (0.75 ppm) of *trans*-ACBC derivative **58,** suggesting not only a C8 H-bonded conformation but also other conformation may be present in solution. These results are compatible with two conformations (C8 and free) present in solution, as suggested by infrared spectroscopy.

	DMSO-d_6 (%, v/v)											
	0	*1*	*2*	*3*	*4*	*6*	*8*	*10*	*14*	*20*	*50*	**Δδ**
δNH	8.25	8.46	8.62	8.73	8.61	8.95	9.01	9.05	9.09	9.09	9.00	0.75

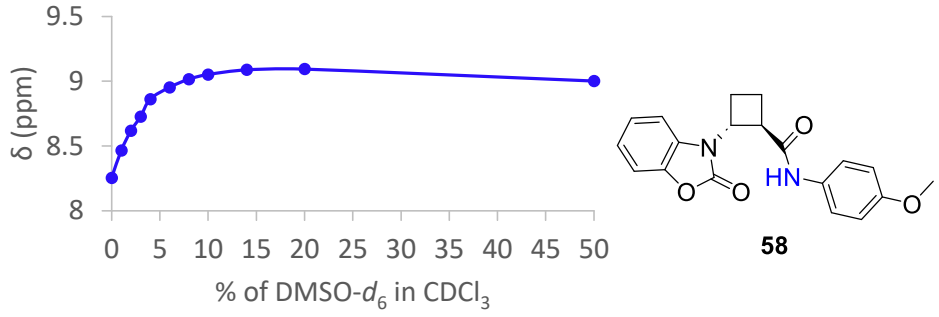

Figure 190. DMSO-d_6 titration of *trans*-ACBC derivative **58**

*b. NH signal evolution of trans-ACBC derivative **59***

Titration of a $CDCl_3$ solution containing *trans*-ACBC derivative **59** (5 mM) with DMSO-d_6 was carried out and results are shown in Figure 191. After the addition of 50% DMSO-d_6, a downfield shift of the NH signal ($\Delta\delta$ = 0.98 ppm) was observed. Compared to the data mentioned in the reference above, this significant value of the *trans*-ACBC derivative **59**, suggesting not only a C8 H-bonded conformation, but also other conformations that may be present in solution. These results are compatible with three conformations (a C8, a C5 and a free) that co-existed in solution, as suggested by infrared spectroscopy.

	DMSO-d_6 (%, v/v)											
	0	*1*	*2*	*3*	*4*	*6*	*8*	*10*	*14*	*20*	*50*	$\Delta\delta$
δNH	6.54	6.74	6.92	7.08	7.19	7.28	7.35	7.43	7.48	7.53	7.52	0.98

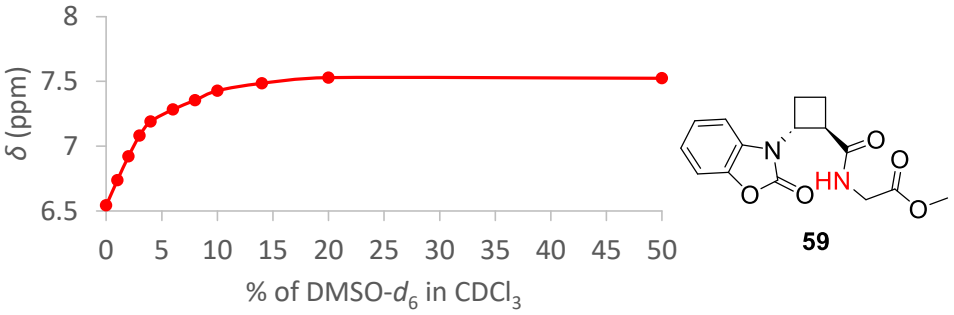

Figure 191. DMSO-d_6 titration of *trans*-ACBC derivative **59**

4.2.4 X-ray diffraction experiments

A single crystal of *trans*-ACBC derivative **58** was obtained by slow evaporation of an ethyl acetate solution at ambient temperature. The X-ray diffraction structure is shown in Figure 192. The X-ray diffraction structure of *trans*-ACBC derivative **58** shows only intermolecular H-bond. The NH was intermolecularly H-bonded with the carbonyl oxygen of the benzoxazolinone group from a second molecule.

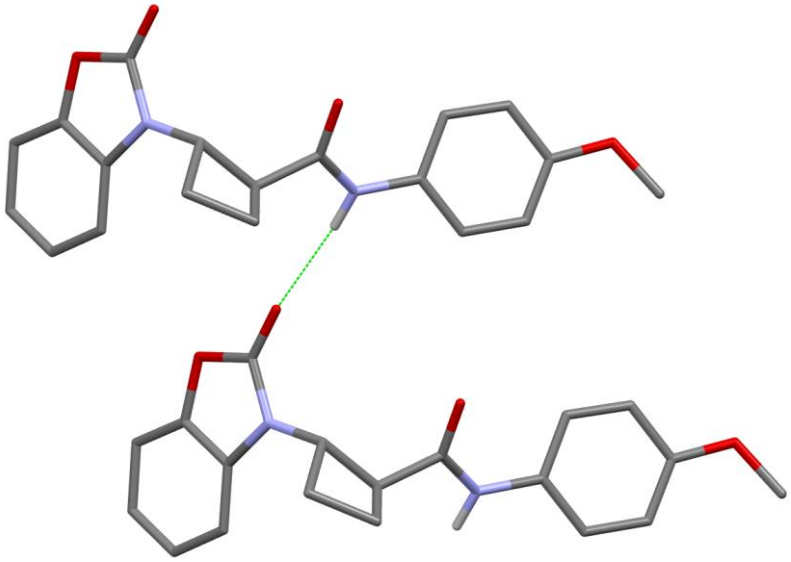

Figure 192. X-ray diffraction crystal structure of *trans*-ACBC derivative **58**

4.3 Conclusion and Perspectives

In this chapter, the conformational landscape of two *trans*-ACBC derivatives **58** and **59** was studied in solution by molecular modelling, infrared spectroscopy and 1D NMR DMSO-d_6 titration experiments. In derivative **58**, two conformations were observed: a C8 and a free conformer (Figure 193, top). In derivative **59**, three conformations were observed: a C8, a C5 and a free conformer (Figure 193, bottom).

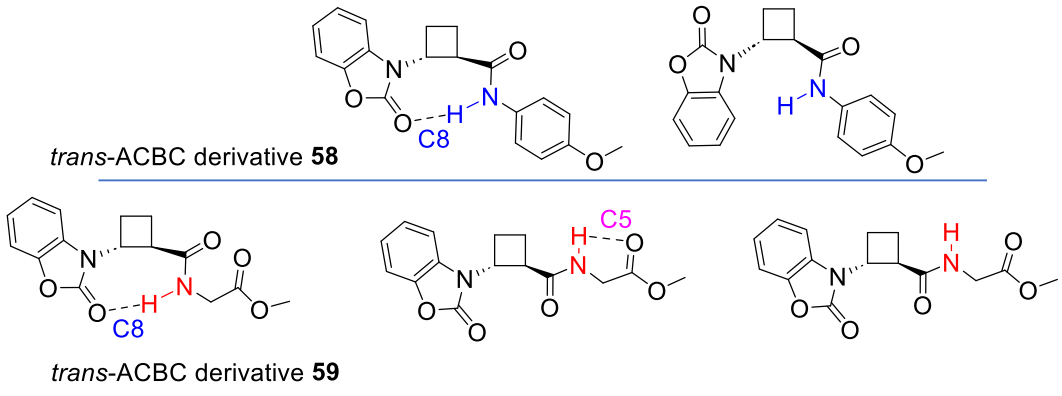

Figure 193. Conformation families adopted by *trans*-ACBC derivatives **58** and **59** in solution

trans-ACBC derivatives **58** and **59** both have exhibited at least two conformations in solution indicating that the *C*-capped moieties, methoxybenzyl and glycine residue are not the main factors interfering with the C8 feature formation, the interference comes from the *N*-capped benzoxazolinone moiety. These results demonstrated that the bulky and less flexible

benzoxazolinone motif is not a suitable *N*-capping group to induce C8 H-bonded conformation in the *trans*-ACBC derivative.

The phenomenon that *N*-benzoxazolinone *trans*-ACBC derivative did not adopt a robust C8 H-bonded conformation was not observed with other *N*-carbamate *trans*-ACBC derivatives, which triggered one interest in the scope investigation of the *N*-capping group for the maintenance of C8 H-bonded conformation. Other interests in modifying the benzoxazolinone moiety of *trans*-ACBC derivatives to strengthen the C8 conformation in solution. In addition, study conformational preference of peptides imparted by the heterocyclic *N*-capping *trans*-ACBC derivatives would be also interesting.

GENERAL CONCLUSION

& PERSPECTIVES

General Conclusion & Perspectives

The objective of this thesis was to gain a comprehensive understanding of the different types of H-bonding and their contributions to conformation. To investigate long–range backbone–backbone H-bonding, a series of γ/α-hybrid peptides composed of *cis*-^{3,4}CB-GABA and alanine were synthesized. Short–range backbone–backbone C5 H-bonding and the side chain–backbone N–H···N C6γ H-bonding were studied using Aatc(Me) derivatives. Additionally, to estimate the role of oxygen atom of oxidized derivatives in stabilizing C5 interaction, Aatc(Me,O), Attc(O) and Attc(O,O) were prepared. Finally, the conformational behavior of two *trans*-ACBC derivatives was also investigated to evaluate the local conformation feature.

In the first chapter, we focused on the conformational studies of **γ/α-hybrid peptides** incorporating **(*R*,*R*)-*cis*-^{3,4}CB-GABA** and either **(*R*)-** or **(*S*)-alanine**. Relevant γ/α-hybrid peptides were successfully synthesized in solution using a convergent synthetic strategy, efficiently resulting in di-, tetra- and hexapeptides. To account for the dihedral cooperations for helical formation, both enantiomers of alanine were used, resulting in *R,R,R* series and *R,R,S* series peptides. In addition, peptides with benzyl ester and benzyl amide at *C*-terminal moiety were prepared to evaluate the contribution of the extra NH for the conformational behaviors. Therefore, a total of twelve peptides were synthesized.

The conformational behavior of these peptides was carried out in chloroform and pyridine solutions using an array of spectroscopic techniques (DMSO-d_6 titration, ^{1}H-^{1}H ROESY 2D NMR, IR) and theoretical calculations (Hybrid Monte Carlo Multiple Minima conformational search). These investigations revealed that the *R,R,R* series γ/α-peptides showed no clear-cut indication for a particular conformational preference, and no evidence for them to fold into a 12/10-helix conformation. The *R,R,S* series γ/α-peptides appeared to adopt a 12/10-helix conformation, as suggested by 1D/2D NMR experiments, infrared in solution and molecular modelling. This work provided a new case of γ/α-hybrid peptides that can fold into 12/10-helix conformation.

The second chapter was dedicated to the conformational studies of **Aatc(Me)** derivatives. The post-synthetic modification strategy was employed to prepared Aatc(Me) derivatives ranging from monomer to di-, tri- and tetramer. Each Aatc(Boc) substrate was first deprotected and then methylated at all free amine residues present in the oligomer, resulting in moderate to good yields of methylated products. The conformational behavior of these Aatc(Me) derivatives (mono-, di- and trimer) was explored in chloroform solution using spectroscopic techniques (UV/IR in gas phase, IR in solution, DMSO-d_6 titration, temperature variation, ^{1}H-^{1}H NOESY 2D NMR) and quantum chemistry calculations. These investigations showed the concomitant existence of an inter-residue N–H···N, side chain–backbone C6γ H-bonding and

an intra-residue N–H···O=C, C5 interaction for these Aatc(Me) derivatives. Successive C5-C6γ H-bonding systems exhibited extended conformation.

In the monomer Cbz-Aatc(Me)-NHMe, this extended C5-C6γ conformation was identified by theoretical calculations and was suggested by both gas and solution phase studies. The consecutive C5-C6γ H-bonding motifs also appeared to exhibit a fully extended C5-C6γ/C5-C6γ conformation of the dimer Cbz-[Aatc(Me)]$_2$-NHMe identified by theoretical calculations, which is in agreement with infrared in gas phase results. These two C5-C6γ motifs are linked by a 3-center C=O···H(N)···N interaction. However, infrared in solution results showed the fully extended C5-C6γ/C5-C6γ conformation was accompanied by a semi-extended C5-C6γ/π_{am} conformation and by a β-turn conformation. The semi-extended C5-C6γ/π_{am} conformation, in which a C5-C6γ H-bonding feature was replaced by a π_{am} interaction. Other NMR spectroscopic results were compatible with the conformational landscape of the dimer in solution. The lowest energy conformations of the trimer Cbz-[Aatc(Me)]$_3$-NHMe, as calculated theoretically in gas phase, showed primarily a fully extended C5-C6γ/C5-C6γ/C5-C6γ form and a semi-extended C5-C6γ/π_{am}/C5-C6γ form, consistent with infrared in gas phase results. In solution, infrared studies suggested that the fully extended C5-C6γ/C5-C6γ/C5-C6γ conformer is not competitive and was replaced by semi-extended C5-C6γ/π_{am}/C5-C6γ and 3_{10}-helix conformations. The semi-extended C5-C6γ/π_{am}/C5-C6γ form was present, suggested by 1D/2D NMR studies (^{1}H chemical shifts of NH signals, DMSO-d_6 titration, temperature variation experiments and NOESY 2D NMR). The presence of the newcomer 3_{10}-helix conformation was evidenced by ^{1}H-^{1}H NOESY 2D NMR, where long-range correlation between CH_2 of Cbz group and $C^{\beta}H^{a}$ of the third azetidine residue was observed. Overall, from monomer to trimer, the C5-C6γ H-bonding features were present on the conformational landscape of all three compounds, but the consecutive C5-C6γ motifs are less competitive than alternative partially folded structures. The conformational studies for tetramer Cbz-[Aatc(Me)]$_4$-NHMe were also attempted, undesired fragmentation process in gas phase of the sample hampered further gas phase studies. In solution, infrared spectroscopy experiment was performed and may suggested that 3_{10}-helix conformation present in solution. These conformational results from monomer to tetramer, may indicate that the longer the Aatc(Me) oligomer chain, the more likely it will be a folded conformation.

In the third chapter, the conformational behaviors of four **oxidized derivatives,** including ***trans*-Cbz-Aatc(Me,O)-NHMe**, ***trans*-Cbz-Attc(O)-NHMe**, ***cis*-Cbz-Attc(O)-NHMe** and **Cbz-Attc(O,O)-NHMe**, have been investigated. The high temperature used for the infrared in gas phase caused the degradation of Cbz-Aatc(Me,O)-NHMe to a dehydrogenated alanine structure, and theoretical calculations were not performed on this structure. However, in solution, infrared spectroscopic results showed a predominant C5-C7δ extended conformation, in which an inter-residue N–H···O–N C7δ H-bonding was formed from side

chain, together with an N–H···O=C C5 interaction formed in the peptide backbone. 1D/2D NMR (^{1}H chemical shifts of NH signals, DMSO-d_6 titration, temperature variation and ^{1}H-^{1}H NOESY 2D NMR experiments) results were in complete agreement with the C5-C7δ extended conformation presented in Cbz-Aatc(Me,O)-NHMe. In solid state, the crystal structure of Cbz-Aatc(Me,O)-NHMe only showed intermolecular H-bond implicating the oxygen atom of the azetidine moiety and an amide NH from a second molecule. The theoretical calculations for *trans*-Cbz-Attc(O)-NHMe showed a predominant C5-C7δ extended conformation, in which an inter-residue N–H···O–S C7δ H-bonding was formed from side chain, together with an N–H···O=C C5 interaction formed in the peptide backbone, as suggested by infrared in gas and solution phases and NMR studies. In solution, apart from a dominant C5-C7δ extended form, minor contributions of an N–H···N π_{am} interaction form and/or a free-C7 conformer present as well. In solid state, the crystal structure of *trans*-Cbz-Attc(O)-NHMe showed intermolecular H-bond implicating the oxygen atom of the thietane residue and an amide NH from a second molecule. The infrared in gas phase studies for the *cis*-Cbz-Attc(O)-NHMe were challenging, even with high purity sample but resulted in a minor free-C7 conformer was detected. We proposed that this may be due to the high temperature in gas phase caused the conversion of unstable *cis* isomer into more stable *trans* isomer of the Cbz-Attc(O)-NHMe, or it may be a limitation of the gas phase infrared for the sample of *cis*-Cbz-Attc(O)-NHMe. In solution, infrared experimental results showed three conformations: free-C7, free-π_{am} and C5-C6γ forms, supported by theoretical calculations, and were consistent with 1D/2D NMR results. The 1D/2D NMR results suggested the C5-C6γ conformer may be a minor player. The theoretical calculations of the Cbz-Attc(O,O)-NHMe also showed three conformations: free-C7, free-π_{am} and C5-C7δ forms, were consistent with solution phase experimental results (IR, 1D/2D NMR). The 1D/2D NMR results suggested the C5-C7δ conformer may be a minor contribution. Nevertheless, in gas phase, the Cbz-Attc(O,O)-NHMe only showed an extended C5-C7δ conformer, in which an inter-residue N–H···O–S C7δ H-bonding was formed from side chain, and an N–H···O=C C5 interaction formed in the peptide backbone. In solid state, the crystal structure of Cbz-Attc(O,O)-NHMe only exhibited intermolecular H-bond implicating one oxygen atom of the thietane residue and an amide NH from the second molecule. In general, the generated oxygen atom in the heterocyclic residue of these derivatives (excluding *cis*-Cbz-Attc(O)-NHMe) has a significant effect on their conformational behavior. This is due to the formation of a strong C7δ H-bonding, which effectively stabilized the weak C5 interaction in the peptide backbone. Notably, the C7δ interactions formed in *trans*-Cbz-Aatc(Me,O)-NHMe and *trans*-Cbz-Attc(O)-NHMe are stronger than the C6γ interactions of their precursors, (Cbz-Aatc(Me)-NHMe and Cbz-Attc-NHMe). As a result, they are more effective in stabilizing the intra-residue C5 interaction in the peptide backbone.

In the fourth chapter, the conformational behaviors of two ***trans*-ACBC derivatives** were studied. Generally, *trans*-ACBC derivatives adopt a local feature conformation with a C8 H-bonding feature. However, the two *trans*-ACBC derivatives, *N*-capped with benzoxazolinone moiety appeared to decrease this C8 conformation preference and can adopt other conformations, as suggested by infrared and NMR spectroscopic studies in solution. The *trans*-ACBC derivative, *C*-capped with a glycine residue exhibited three conformations: C8, C5 and free. The *trans*-ACBC derivative, *C*-capped with *p*-methoxybenzyl moiety showed two conformations: C8 and free. These findings indicate that the presence of the benzoxazolinone moiety at the *N*-terminal of *trans*-ACBC derivatives has a significant impact, setting it apart from commonly used protective groups such as Boc and Cbz.

This thesis contributes to the understanding of the conformational stabilization of different short peptides by exploring different types of hydrogen bonding involved. As we learned from the third chapter, the N–H···O–N C7δ H-bonding formed in the *trans*-Cbz-Aatc(Me,O)-NHMe is stronger than the N–H···N C6γ H-bonding formed in its precursor Cbz-Aatc(Me)-NHMe, and the N–H···O–S C7δ H-bonding in the *trans*-Cbz-Attc(O)-NHMe is stronger than the N–H···S C6γ H-bonding in its precursor Cbz-Attc-NHMe. A detailed conformational studies of Aatc(Me,O) and Attc(O) oligomers will be possible in the future. Thus, a better understanding of the strength of the C7δ H-bonding in short peptides can be achieved.

PART III

EXPERIMENTAL PART

1 General experimental information

All reagents and solvents were of commercial grade and were used without further purification, with the following exceptions: dichloromethane was passed through a column of alumina; DMF, Et_3N, DIPEA and NMM were dried and distilled from CaH_2 under argon, THF was freshly distilled under an argon atmosphere over Na/benzophenone.

Flash chromatography was performed on silica gel columns (40-63 μm). Analytical thin-layer chromatography was carried out with 0.25 mm commercial silica gel plates (EMD, Silica Gel $60F_{254}$). TLC plates were visualized by fluorescence at 254 nm then revealed using a *p*-anisaldehyde solution (5% in EtOH), phosphomolybdic acid solution (6% in EtOH), a ninhydrin solution (14 mM in EtOH) or a $KMnO_4$ solution (7.5% in water). Retention factors (R_f) are given for such TLC analysis.

^{1}H and **^{13}C NMR** spectra were recorded on Bruker spectrometers operating at 400/360/300 MHz for ^{1}H experiments and at 100/90/75 MHz for ^{13}C experiments. For ^{1}H NMR spectra, chemical shifts (δ) are reported in parts per million (ppm) with reference to residual protonated solvent (δ = 7.26 ppm for $CDCl_3$, δ = 7.58 ppm for Pyr-d_5, δ = 3.31 ppm for CD_3OD, δ = 2.50 ppm for DMSO-d_6) as an internal standard. Splitting patterns for ^{1}H signals are designated as s (singlet), d (doublet), t (triplet), q (quartet), p (pentet), m (multiplet), br (broad), or bs (broad singlet), and coupling constants (*J)* are reported in Hz. For ^{13}C NMR spectra, chemical shifts (δ) are reported in parts per million (ppm) with reference to the deuterated solvent (δ = 77.16 ppm for $CDCl_3$, δ = 135.91 ppm for Pyr-d_5, δ = 49.00 ppm for CD_3OD, δ = 39.52 ppm for DMSO-d_6) as an internal standard.

High-resolution mass spectra (HRMS [ESI(+)]) were recorded on a Bruker MicroTOF-Q spectrometer equipped with an electrospray ionization source in positive mode.

Melting points (Mp) were measured in open capillary tubes on a Büchi B-540 apparatus and are uncorrected.

Fourier transform infrared (IR) spectra were recorded for neat liquid or solid sample on an FT-IR Perkin Elmer Spectrum Two using an ATR diamond accessory, maximum absorbances (ν) are given in cm^{-1}; solution state spectra were recorded for $CHCl_3$ solution in an Omni-cell Specac 1- or 0.2-mm path-length NaCl solution cell, with a $CHCl_3$ background.

Optical rotations were measured in a 10 cm quartz cell using solutions of concentration (*c*) in units of g per 100 mL; $[\alpha]_D^T$ values were deduced for the D-line of sodium at the indicated temperature T.

Preparative High-performance liquid chromatography (HPLC) purification was carried out on an Agilent 1260 Infinity HPLC apparatus equipped with a VL G1311C quaternary pump with online degasser, an ALS G1329B semi-preparative autosampler, a G1315D column oven, a DAD VL G1315D diode array detector and an AS G1364C collector, piloted using ChemStation OpenLab CPL version C.01.04 software. The required solvents were HPLC grade. The mobile phase was filtered through a 0.45 μm PTFE membrane, while injected solutions were filtered through a 0.22 μm PTFE membrane. Separations were performed using a lux cellulose-1 column by Phenomenex® (250 mm × 10 mm; particle size 5 μm) and a mobile phase flow rate of 5 mL/min. The mobile phase and the column were thermostated at 30 °C ± 2 °C. Detection was performed at 210 nm.

The X-ray diffraction data was collected using a VENTURE Photon II 14 CPAD Bruker diffractometer equipped with a mirror monochromator and a MoKα INCOATEC IμS micro-focus source. Crystals were mounted on a CryoLoop (Hampton Research) with mounted on a CryoLoop (Hampton Research) with Paratone-N (Hampton Research) as cryoprotectant and flash-frozen in a nitrogen gas stream, the temperature of the crystals was maintained by means of a 700 series Cryostream cooling device to within an accuracy of ± 1 K. Data were corrected for Lorentz polarization and absorption effects. The structures were solved by direct methods using SHELXS-97[209] and refined against F2 by full-matrix least-squares techniques using SHELXL-2018[210] with anisotropic displacement parameters for all non-hydrogen atoms. Hydrogen atoms were located on a different Fourier map and introduced into the calculations as a riding model with isotropic thermal parameters. All calculations were performed by using the Crystal Structure crystallographic software package WINGX[211].

2 Synthesis of γ/α-hybrid peptides

2.1 General procedures

Procedure A for the deprotection of the *N*-Boc group.

In an argon-flushed flask, **Boc-X^1-OBn/NHBn** (1 eq.) was dissolved in dry CH_2Cl_2 (5 mL/mmol) and then TFA (30 eq.) was added. The reaction was stirred at room temperature for 1 hour. CH_2Cl_2 was removed under reduced pressure, the excess TFA was removed by co-evaporating with $CHCl_3$ for several times and then the resulting residue was left under a high vacuum for 2 hours. The crude TFA salt **TFA·H$_2$N-X^1-OBn/NHBn** was dissolved in dry CH_2Cl_2 (5 mL/mmol), and DIPEA (6 eq.) was added to reach pH 9. The mixture was left to stir at room temperature with a steam of argon and ready for the coupling reaction.

Procedure B for the deprotection of the *O*-benzyl group.

To a solution of **Boc-X^2-OBn** (1 eq.) in CH_2Cl_2/EtOAc (4/1, 33 mL/mmol), Pd/C (10 wt. %, 125 mg/mmol) was added. After degassing the resulting suspension, the mixture was reacted under H_2 at atmospheric pressure for 4 hours. The mixture was then filtered through a celite pad and washed with small portions of EtOAc. The combined filtrate and washings were concentrated under reduced pressure to afford **Boc-X^2-OH**, which was pure enough to be used in the further coupling reaction.

Procedure C for the coupling reactions with TFA salt.

For the synthesis of dipeptides: To a solution of **Boc-(*R*,*R*)-*cis*-^{3,4}CB-GABA-OH (12)** (1 eq.) in a mixture of CH_2Cl_2/DMF (4/1, 10 mL/mmol) in an argon-flushed flask was added DIPEA (2 eq.), followed with the addition of HATU (1.05 eq.). The solution was stirred for 10 minutes at room temperature as the color changed from light to dark brown, then a mixture of the **H$_2$N-X^1-OBn** (1 eq.) (**procedure A**) was incorporated. The resulting mixture was stirred at room temperature for 24 hours. Solvents were removed under reduced pressure and the remaining DMF was removed by co-evaporation with heptane for several times. The resulting residue was dissolved in CH_2Cl_2 (20 mL/mmol) and successively washed by a saturated solution of $NaHCO_3$ (10 mL/mmol), brine (10 mL/mmol), a 1M HCl solution (10 mL/mmol) and brine (10 mL/mmol). The organic phase was dried over Na_2SO_4, filtered and concentrated under reduced pressure. The crude product was purified by flash chromatography on silica to afford the corresponding ***cis*-^{3,4}CB-GABA-X^1-OBn**.

For the synthesis of tetrapeptides and hexapeptides: To a solution of the **Boc-X^2-OH** (1 eq.) (**procedure B**)in a mixture of CH_2Cl_2/DMF (3/1, 10 mL/mmol) in an argon-flushed flask, were added successively DIPEA (2 eq.) and a mixture of the **H$_2$N-X^1-OBn/NHBn** (1 eq.) (**procedure A**), followed by the addition of HATU (1.05 eq.). The resulting mixture was stirred at room temperature for 24 hours. The solvent was removed under reduced pressure and the remaining DMF was removed by co-evaporation with heptane for several times. The resulting residue was dissolved in CH_2Cl_2 (20 mL/mmol) and successively washed by a saturated solution of $NaHCO_3$ (10 mL/mmol), brine (10 mL/mmol), a 1M HCl solution (10 mL/mmol) and brine (10 mL/mmol). The organic phase was then dried over Na_2SO_4, filtered and concentrated under reduced pressure. The crude product was purified by column chromatography or HPLC to afford corresponding **Boc-X^2-X^1-OBn/NHBn**.

Procedure D for the coupling reactions with benzylamine.

To a solution of the **Boc-X^2-OH** (1 eq.) (**procedure B**) in CH_2Cl_2 or CH_2Cl_2/DMF (10 mL/mmol) in an argon-flushed flask, was added **benzylamine** (1.02 eq.). Followed by the addition of

DIPEA (3 eq.) and HATU (1.05 eq.). The mixture was stirred at room temperature for 24 hours. The solvent was removed under reduced pressure and the remaining DMF was removed by co-evaporation with heptane for several times. The resulting residue was dissolved in CH_2Cl_2 (20 mL/mmol) and successively washed by a saturated solution of $NaHCO_3$ (10 mL/mmol), brine (10 mL/mmol), a 1M HCl solution (10 mL/mmol) and brine (10 mL/mmol). The organic phase was then dried over Na_2SO_4, filtered and concentrated under reduced pressure. The crude product was purified by column chromatography to afford corresponding **Boc-X²-NHBn**.

2.2 Synthesis of enantiomers Boc-*cis*-[3,4]CB-GABA-OH **11** and **12**

3,3-Dibromoazepan-2-one (2).

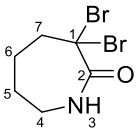

$C_6H_9Br_2NO$
M = 270.95 g/mol

In an ice-cold (0 °C) two-necked argon-flushed flask, caprolactam **1** (5 g, 44.25 mmol, 1 eq.) in $CHCl_3$ (125 mL), PCl_5 (18.4 g, 89.01 mmol, 2 eq.) and ZnI_2 (560 mg, 1.75 mmol, 0.04 eq.) were introduced successively, followed by the slow addition of bromine (4.5 mL, 88.50 mmol, 2 eq.) over 15 minutes. The reaction mixture was allowed to warm to room temperature and stirred overnight. After the reaction was completed (monitored by TLC), the mixture was quenched with ice water (200 mL). The organic phase was separated and successively washed with water (3 × 100 mL) and a 0.5 M solution of $NaHSO_3$ (3 × 100 mL), dried over Na_2SO_4, filtered and concentrated under reduced pressure to give the crude product as a yellow solid. The yellow solid was washed with water (100 mL) to afford **dibrominated caprolactam 2** (9.22 g, 78%) as a white solid and used directly in the next step without further purification.

R_f = 0.60 (PE:EtOAc = 5:5)

^{1}H NMR (360 MHz, $CDCl_3$, 300 K) δ7.06 (bs, 1H, NH^3), 3.57-3.19 (m, 2H, H^7), 2.90-2.54 (m, 2H, H^4), 2.13-1.82 (m, 2H, H^5), 1.82-1.53 (m, 2H, H^6).

The NMR data was in agreement with the literature.[162]

1,3-Dihydro-2H-azepin-2-one (3).

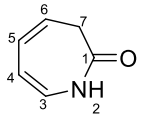

C_6H_7NO
M = 109.13 g/mol

At a solution of compound **2** (9.0 g, 33.47 mmol, 1 eq.) in dry DMF (200 mL), anhydrous LiCl (4.23 g, 99.73 mmol, 3 eq.) was added under an argon atmosphere. The reaction mixture was heated to reflux and reacted for 5 hours, then cooled to room temperature and stirred overnight. The solvent was removed by co-evaporation with heptane under reduced pressure. The residue was diluted in CH_2Cl_2 (100 mL) and H_2O (100 mL), the organic phase was collected, and the aqueous phase was extracted with CH_2Cl_2 (5 × 100 mL). The combined organic phases were dried over Na_2SO_4, filtered and concentrated to give the crude product as a brown oil. The purification was carried out by flash chromatography on silica (PE:EtOAc, gradient from 80:20 to 50:50) to give the product as a yellow solid. Finally, the yellow solid was recrystallized by pentane to obtain **azepinone 3** (2.83 g, 77%) as colorless crystals.

***R**f* = 0.50 (PE:EtOAc = 5:5)

^{1}H NMR (360 MHz, $CDCl_3$, 300 K) δ 8.24 (bs, 1H, NH^2), 6.19 (dd, *J* = 8.8, 4.8 Hz, 2H, $H^{3,5}$), 5.82 (dd, *J* = 8.8, 4.8 Hz, 1H, H^4), 5.61 (dt, *J* = 9.6, 6.8 Hz, 1H, H^6), 2.90 (d, *J* = 6.8 Hz, 2H, H^7).

The NMR data was in agreement with the literature.[158]

cis-2-Azabicyclo[3.2.0]hept-6-en-3-one [(±)-4].

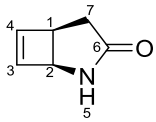

C_6H_7NO
M = 109.13 g/mol

A solution of **azepinone 3** (2.43 g, 22.30 mmol, 1 eq.) in 1 L of dry Et_2O was introduced into a quartz tube equipped with an argon inlet. Argon was bubbling in the solution for 10 minutes. The reaction mixture was cooled to –25 °C with an external cooling system and then irradiated by Rayonet (inside with 16 lamps, λ = 254 nm) for 8 hours. The solvent was removed under reduced pressure to obtain ***cis*-2-azabicyclo[3.2.0]hept-6-en-3-one (±)-4** (2.34 g, 96%) as an orange solid, the crude product was pure enough for the next reaction without purification.

***R**f* = 0.12 (Et_2O)

^{1}H NMR (400 MHz, $CDCl_3$, 300 K) δ 6.55 (bs, 1H, NH^5), 6.40-6.20 (m, 2H, $H^{3,4}$), 4.57-4.28 (m,

1H, H^2), 3.71-3.39 (m, 1H, H^1), 2.47 (dd, *J* = 17.8, 10.2 Hz, 1H, H^7), 2.28 (ddd, *J* = 17.8, 3.2, 1.2 Hz, 1H, H^7).

The NMR data was consistent with the literature.[158]

cis-2-Azabicyclo[3.2.0]heptan-3-one [(±)-5].

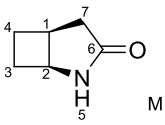

C_6H_9NO
M = 111.14 g/mol

To a solution of compound **(±)-4** (2.3 g, 21.10 mmol, 1 eq.) in EtOAc (165 mL) in an argon-flushed flask, 10% Pd/C (718 mg) was added carefully at room temperature. After degassing the resulting suspension, the solution was stirred overnight under H_2 at atmospheric pressure. The mixture was filtrated through a celite pad, and the celite pad was washed with small portions of EtOAc. The combined filtrate and washings were concentrated under reduced pressure to provide ***cis*-2-azabicyclo[3.2.0]heptan-3-on (±)-5** (2.06 g, 88%) as a colorless oil. The product was used in the following step without further purification.

R_f = 0.12 (Et_2O)

^{1}H NMR (400 MHz, $CDCl_3$, 300 K) δ 6.29 (bs, 1H, H^5), 4.27-3.92 (m, 1H, H^2), 3.27-2.95 (m, 1H, H^1), 2.50 (dd, *J* = 17.6, 8.8 Hz, 1H, H^7), 2.42-2.05 (m, 3H, H^6, $H^{3,4}$), 2.04-1.80 (m, 2H, $H^{3,4}$).

The NMR data was consistent with the literature.[158]

cis-tert-Butyl-3-oxo-2-azabicyclo[3.2.0]heptane-2-carboxylate [(±)-6].

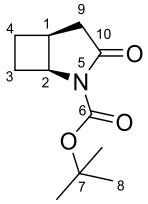

$C_{11}H_{17}NO_3$
M = 211.26 g/mol

To an ice-cold (0 °C) solution of compound **(±)-5** (2.06 g, 18.50 mmol, 1 eq.) in acetonitrile (180 mL) in an argon-flushed flask, Boc_2O (8.25 g, 37.00 mmol, 2 eq.) and DMAP (187 mg, 1.85 mmol, 0.1 eq.) were incorporated successively. The reaction mixture was left to stir at room

temperature overnight. The solvent was removed under reduced pressure, the crude product was purified by flash chromatography on silica (PE:EA = 1:1) to afford ***cis*-*tert*-butyl-3-oxo-2-azabicyclo[3.2.0]heptane-2-carboxylate (±)-6** (3.24 g, 83%) as a pale-yellow solid.

R_f = 0.70 (PE:EtOAc = 5:5)

^{1}H NMR (300 MHz, $CDCl_3$, 300 K) δ 4.42 (tt, *J* = 6.4, 2.2 Hz, 1H, H^2), 3.09-2.84 (m, 1H, H^1), 2.69 (dd, *J* = 18.4, 8.8 Hz, 1H, H^9), 2.57-2.37 (m, 2H, $H^{9,3}$), 2.37-2.19 (m, 1H, H^4), 2.10-1.94 (m, 1H, H^3), 1.94-1.75 (m, 1H, H^4), 1.50 (s, 9H, H^8).

The NMR data was consistent with the literature.[158]

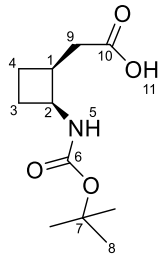

$C_{11}H_{19}NO_4$
M = 229.28 g/mol

***cis*-2-(2-((*tert*-Butoxycarbonyl)amino)cyclobutyl)acetic acid [(±)-7].**

To a solution of compound **(±)6** (3.24 g, 15.36 mmol, 1 eq.) in THF/H_2O (1/1, 50 mL) was added LiOH (6.53 g, 153.60 mmol, 10 eq.), then the reaction mixture was left to stir at room temperature overnight. The solvent was removed under reduced pressure, the resulting aqueous phase was carefully acidified with a 0.5 M HCl solution until pH = 1. The mixture was then extracted with EtOAc (5 × 30 mL) and the combined organic phases were dried over Na_2SO_4, filtered and concentrated under reduced pressure. The crude product was purified by flash chromatography on silica (PE:EtOAc, gradient from 1:1 to 0:1) to give ***cis*-2-(2-((*tert*-butoxycarbonyl)amino) cyclobutyl)acetic acid (±)-7** (3.46 g, 97%) as a white solid.

R_f = 0.35 (PE: EtOAc = 5:5)

^{1}H NMR (360 MHz, $CDCl_3$, 300 K) δ 11.20 (s, 1H, H^{11}), 6.09 (bs, 0.4H, H^5), 4.83 (bs, 0.6H, H^5), 4.46-3.94 (m, 1H, H^2), 3.08-2.75 (m, 1H, H^1), 2.54 (dd, *J* = 15.6, 6.8 Hz, 1H, H^9), 2.42 (dd, *J* = 15.8, 9.0 Hz, 1H, H^9), 2.37-2.19 (m, 1H, H^3), 2.12-1.75 (m, 2H, $H^{3,4}$), 1.65-1.50 (m, 1H, H^4), 1.42 (s, 9H, H^8).

The NMR data was consistent with the literature.[158]

(4*R*,5*S*)-4-Methyl-5-phenyloxazolidin-2-one (9).

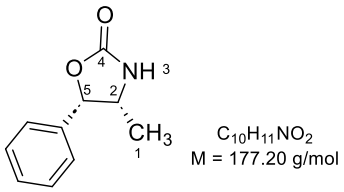

In an argon-flushed flask, (1*S*,2*R*)-2-amino-1-phenylpropan-1-ol **8** (3 g, 19.80 mmol, 1 eq.) in dry CH_2Cl_2 (50 mL) was added at 0 °C, then dry Et_3N (6.09 mL, 43.56 mmol, 2.2 eq.) was injected. A solution of triphosgene (2.06 g, 6.93 mmol, 0.35 eq.) in dry CH_2Cl_2 (10 mL), was added slowly in 30 minutes. The reaction mixture was allowed to warm to room temperature and stirred for 1 hour. A solution of saturated NH_4Cl (21 mL) and CH_2Cl_2 (42 mL) were then introduced, the resulting mixture was stirred for a further 20 minutes. The mixture was extracted with CH_2Cl_2 (3 × 25 mL) and the combined organic phases were dried over Na_2SO_4, filtered and concentrated under reduced pressure to afford **oxazolidinone 9** (3.47 g, 99%) as a pale-yellow solid. This product was pure enough without further purification.

R_f = 0.45 (EtOAc:PE = 5:5)

^{1}H NMR (360 MHz, $CDCl_3$, 300 K) δ 7.69-6.91 (m, 5H, H^{Ar}), 5.92-5.74 (m, 1H, H^5), 5.72 (d, *J* = 7.8 Hz, 1H, H^3), 4.46-3.91 (m, 1H, H^2), 0.81 (d, *J* = 6.6 Hz, 3H, H^1).

$[\alpha]_D^{24}$ = 141.2 (c. 0.55 in $CHCl_3$).

The NMR data was in agreement with the literature.[158]

***tert*-Butyl ((1*S*,2*S*)-2-(2-((4*R*,5*S*)-4-methyl-2-oxo-5-phenyloxazolidin-3-yl)-2-oxoethyl)cyclobutyl)carbamate [(+)-10a] and *tert*-butyl ((1*R*,2*R*)-2-(2-((4*R*,5*S*)-4-methyl-2-oxo-5-phenyloxazolidin-3-yl)-2-oxoethyl)cyclobutyl)carbamate [(–)-10b].**

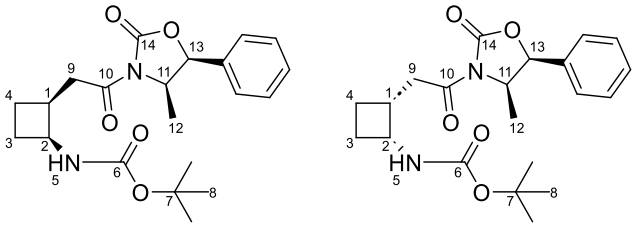

(+)10a

$C_{21}H_{28}N_2O_5$
M = 388.46 g/mol

(–)10b

Flask **A**: To a cold (–78 °C) solution of compound **(±)-7** (3.3 g, 14.45 mmol, 1 eq.) in dry THF (120 mL) in an argon-flushed flask, dry Et_3N (4 mL, 28.90 mmol, 2 eq.) was added. PivCl (1.9 mL, 15.20 mmol, 1.05 eq.) was then introduced into the solution slowly by syringe. The reaction mixture was warmed back to 0 °C and stirred for 1 hour.

Flask **B**: Separately, *n*-BuLi (9 mL, 14.45 mmol, 1 eq.) was carefully added to a solution of **oxazolidinone 9** (2.56 g, 14.45 mmol, 1 eq.) in dry THF (65 mL) at –40 °C. The mixture was stirred for 5 minutes under an argon atmosphere.

The solution from flask **B** was then transferred to flask **A**, and the reaction mixture was stirred for a further 1 hour at –78 °C under argon. After warmed back to 0 °C with an ice-water bath, a saturated aqueous $NaHCO_3$ solution (70 mL) was introduced. THF was removed under reduced pressure and the residue was extracted with CH_2Cl_2 (4 × 60 mL), the combined organic phases were dried over Na_2SO_4, filtered and concentrated under reduced pressure. The crude product was purified by flash chromatography on silica (ultra flash, Et_2O:PE, gradient from 15:55 to 60:40) to give the separable products **(+)-10a** (1.98 g, 41%) as a white solid, and **(–)-10b** (2.3 g, 47%) as a white solid.

For compound *tert*-butyl ((1*S*,2*S*)-2-(2-((4*R*,5*S*)-4-methyl-2-oxo-5-phenyloxazolidin-3-yl)-2-oxoethyl) cyclobutyl)carbamate **[(+)-10a]**:

R_f = 0.35 (Et_2O:PE = 5:5)

Mp = 57-58 °C

^{1}H NMR (300 MHz, $CDCl_3$, 300 K) δ 7.48-7.27 (m, 5H, H^{Ar}), 5.67 (d, *J* = 7.4 Hz, 1H, H^{13}), 4.91 (d, *J* = 8.0 Hz, 1H, H^5), 4.75 (p, *J* = 6.6 Hz, 1H, H^{11}), 4.49-4.16 (m, 1H, H^2), 3.31 (dd, *J* = 16.6, 6.8 Hz, 1H, H^9), 3.16-2.77 (m, 2H, $H^{1,9}$), 2.46-2.18 (m, 1H, H^3), 2.18-1.80 (m, 2H, $H^{3,4}$), 1.57-1.45 (m, 1H, H^4), 1.41 (s, 9H, H^8), 0.88 (d, *J* = 6.6 Hz, 3H, H^{12}).

$[\alpha]_D^{21}$ = –42.6 (c. 0.49 in $CHCl_3$).

For compound *tert*-butyl ((1*R*,2*R*)-2-(2-((4*R*,5*S*)-4-methyl-2-oxo-5-phenyloxazolidin-3-yl)-2-oxoethyl) cyclobutyl)carbamate **[(–)-10b]**.

R_f = 0.44 (Et_2O:PE = 5:5)

Mp = 136-137 °C

^{1}H NMR (300 MHz, $CDCl_3$, 300 K) δ7.50-7.26 (m, 5H, H^{Ar}), 5.67 (d, *J* = 7.2 Hz, 1H, H^{13}), 4.77 (dd, *J* = 15.0, 8.0 Hz, 2H, $H^{5,11}$), 4.54-3.99 (m, 1H, H^{2}), 3.46-2.70 (m, 3H, $H^{9,1}$), 2.50-2.17 (m, 1H, H^{3}), 2.19-1.74 (m, 2H, $H^{3,4}$), 1.64-1.47 (m, 1H, H^{4}), 1.44 (s, 9H, H^{8}), 0.89 (d, *J* = 6.6 Hz, 3H, H^{12}).

$[\alpha]_D^{20}$= 67.2 (c. 0.49 in $CHCl_3$).

The Mp, NMR, OR data were consistent with the literature.[158]

2-((1*S*,2*S*)-2-((*tert*-Butoxycarbonyl)amino)cyclobutyl)acetic acid (11).

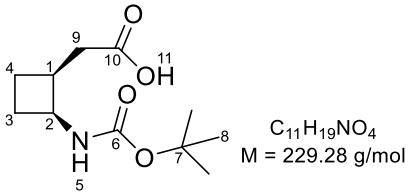

Boc-(*S*,*S*)-*cis*-^{3,4}CB-GABA-OH

To a solution of compound **(+)-10a** (1.98 g, 5.10 mmol, 1 eq.) in THF/H_2O (1:1, 165 mL) were added H_2O_2 (3 mL, 30.60 mmol, 6 eq.) and LiOH (619 mg, 25.50 mmol, 5 eq.) successively. The reaction mixture was stirred at room temperature for 24 hours. A mixture solution of saturated Na_2SO_3 (35 mL) and saturated $NaHCO_3$ (35 mL) was then introduced. THF was removed under reduced pressure, and the aqueous phase was extracted with CH_2Cl_2 (4 × 200 mL). The combined organic phases were dried over Na_2SO_4, filtered and concentrated to obtain **oxazolidinone 9** (864 mg, 96%) as a white solid. The aqueous phase was then cooled to 0 °C and carefully acidified with concentrated HCl solution until pH = 1. The aqueous phase was extracted with CH_2Cl_2 (4 × 200 mL), and the combined organic phases were dried over Na_2SO_4, filtered and concentrated to provide **Boc-(*S*,*S*)-*cis*-^{3,4}CB-GABA-OH 11** (1.12 g, 96%) as a white solid. The product was pure enough to be used without further purification.

R_f = 0.18 (Et_2O:PE = 6:4)

^{1}H NMR (360 MHz, $CDCl_3$, 300 K) δ 11.28 (bs, 1H, H^{11}), 5.97 (bs, 0.3H, H^5), 4.80 (bs, 0.7H, H^5), 4.49-3.92 (m, 1H, H^2), 3.08-2.73 (m, 1H, H^1), 2.55 (dd, *J* = 15.6, 6.0 Hz, 1H, H^9), 2.42 (dd, *J* = 15.6, 9.0 Hz, 1H, H^9), 2.37-2.18 (m, 1H, H^3), 2.15-1.73 (m, 2H, $H^{3,4}$), 1.68-1.50 (m, 1H, H^4), 1.43 (s, 9H, H^8).

^{13}C NMR (100 MHz, $CDCl_3$, 300 K) δ 178.3 (C^{10}), 155.4 (C^6), 79.7 (C^7), 47.0 (C^2), 36.9 (C^1), 34.4 (C^9), 28.4 (C^8), 27.4 (C^3), 21.4 (C^4).

$[\alpha]_D^{21}$ = –75.6 (c. 0.50 in $CHCl_3$).

The NMR and OR data were in agreement with the literature.[158]

2-((1*R*,2*R*)-2-((*tert*-Butoxycarbonyl)amino)cyclobutyl)acetic acid (12).

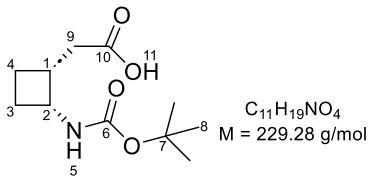

$C_{11}H_{19}NO_4$
M = 229.28 g/mol

Boc-(*R*,*R*)-*cis*-^{3,4}CB-GABA-OH

To a solution of compound **(–)-10b** (2.3 g, 5.93 mmol, 1 eq.) in THF/H_2O (1/1, 195 mL) were successively added H_2O_2 (3.53 mL, 35.58 mmol, 6 eq.) and LiOH (730 mg, 29.65 mmol, 5 eq.). The reaction mixture was stirred at room temperature for 16 hours. A mixture solution of saturated Na_2SO_3 (40 mL) and saturated $NaHCO_3$ (40 mL) was then introduced. THF was removed under reduced pressure, and the aqueous phase was extracted with CH_2Cl_2 (4 × 200 mL). The combined organic phases were dried over Na_2SO_4, filtered and concentrated to obtain **oxazolidinone 9** (1.03 g, 98%) as a white solid. The aqueous phase was then cooled to 0 °C and carefully acidified with concentrated HCl solution until pH = 1. The mixture was extracted with CH_2Cl_2 (4 × 200 mL), and the combined organic phase was dried over Na_2SO_4, filtered and concentrated to afford **Boc-(*R*,*R*)-*cis*-^{3,4}CB-GABA-OH 12** (1.33 g, 98%) as a white solid. The product was pure enough to be used without further purification.

R_f = 0.18 (Et_2O:PE = 6:4)

^{1}H NMR (360 MHz, $CDCl_3$, 300 K) δ 11.15 (bs, 1H, H^{11}), 5.93 (bs, 0.3H, H^5), 4.80 (bs, 0.7H, H^5), 4.57-3.85 (m, 1H, H^2), 3.12-2.72 (m, 1H, H^1), 2.56 (dd, *J* = 15.4, 6.6 Hz, 1H, H^9), 2.43 (dd, *J* = 15.4, 8.4 Hz, 1H, H^9), 2.38-2.19 (m, 1H, H^3), 2.12-1.76 (m, 2H, $H^{3,4}$), 1.68-1.49 (m, 1H, H^8), 1.44 (s, 9H, H^8).

^{13}C NMR (100 MHz, $CDCl_3$, 300 K) δ 178.0 (C^{10}), 157.0 (C^6), 79.7 (C^7), 46.9 (C^2), 36.9 (C^1), 34.4 (C^9), 28.4 (C^8), 27.3 (C^3), 21.4 (C^4).

$[\alpha]_D^{20}$= 76.5 (c. 0.50 in $CHCl_3$).

The NMR and OR data were in agreement with the literature.[158]

2.3 Synthesis of Boc-Ala-OBn **13** and **14**

Benzyl (*tert*-butoxycarbonyl)-D-alaninate (13).

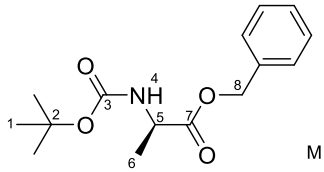

$C_{15}H_{21}NO_4$
M = 279.34 g/mol

Boc-(*R*)-Ala-OBn

To an ice-cold (0 °C) solution of D-alanine (1 g, 11.20 mmol, 1 eq.) in ultra-pure H_2O (25 mL), 1 M NaOH solution (22.5 mL, 24.50 mmol, 2 eq.) was added dropwise and followed by the addition of a solution of Boc_2O (3.6 g, 16.50 mmol, 1.5 eq.) in dioxane (25 mL). The reaction was stirred at room temperature overnight. Dioxane was removed under reduced pressure. The solution was cooled to 0 °C with an ice-water bath and carefully acidified with 1 M HCl to pH = 1. The aqueous phase was extracted with EtOAc (4 × 50 mL) and then the combined organic phases were washed with brine, dried over Na_2SO_4, filtered and concentrated to afford the product Boc-(*R*)-alanine as a white solid and used in the next reaction directly without further purification.

In an argon-flushed flask, a solution of the above-described sample of Boc-(*R*)-alanine (11.20 mmol, 1 eq.) in dry CH_2Cl_2 (55 mL) was added at 0 °C, then successively incorporated benzyl alcohol (1.17 mL, 11.40 mmol, 1.02 eq.), DMAP (136 mg, 1.12 mmol, 0.1 eq.) and DCC (2.55 g, 12.32 mmol, 1.1 eq.). The reaction mixture was then warmed to room temperature and stirred overnight. The solvent was removed under reduced pressure. The crude product was purified by flash chromatography on silica (PE:EtOAc = 4:1) to give **Boc-(*R*)-Ala-OBn 13** (1.87 g, 60%) as a colorless oil.

***R**$_f$* = 0.44 (PE:EtOAc = 4:1)

^{1}H NMR (360 MHz, $CDCl_3$, 300 K) δ 7.42-7.28 (m, 5H, H^{Ar}), 5.16 (dd, *J* = 18.8, 12.2 Hz, 2H, H^8),

5.10-4.96 (m, 1H, H^4), 4.52-4.20 (m, 1H, H^5), 1.43 (s, 9H, H^1), 1.39 (d, *J* = 7.2 Hz, 3H, H^6).

^{13}C NMR (100 MHz, $CDCl_3$, 300 K) δ173.4 (C^7), 155.2 (C^3), 135.6 (C^{Ar}), 128.7, 128.5, 128.3 (CH^{Ar}), 80.0 (C^2), 67.1 (C^8), 49.4 (C^5), 28.4 (C^1), 18.7 (C^6).

$[\alpha]_D^{24}$= 36.4 (c. 1.35 in EtOH).

The NMR data were consistent with the literature.[212]

Benzyl (*tert*-butoxycarbonyl)-L-alaninate (14).

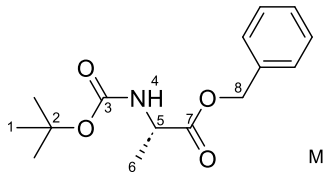

$C_{15}H_{21}NO_4$
M = 279.34 g/mol

Boc-(*S*)-Ala-OBn

In an argon-flushed flask, a solution of Boc-L-alanine (2.07 g, 11.00 mmol, 1 eq.) in dry CH_2Cl_2 (55 mL) was added, then successively incorporated benzyl alcohol (1.15 mL, 11.20 mmol, 1.02 eq.), DMAP (134 mg, 1.10 mmol, 0.1 eq.) and DCC (2.5 g, 12.10 mmol, 1.1 eq.). The reaction mixture was then warmed to room temperature and stirred overnight. The solvent was removed under reduced pressure. The crude product was purified by flash chromatography on silica (PE:EtOAc = 4:1) to give **Boc-(*S*)-Ala-OBn 14** (2.98 g, 97%) as a colorless oil.

***R**$_f$* = 0.44 (PE:EtOAc = 4:1)

^{1}H NMR (300 MHz, $CDCl_3$, 300 K) δ7.46-7.28 (m, 5H, H^{Ar}), 5.17 (dd, *J* = 20.2, 12.4 Hz, 2H, H^8), 5.10-4.93 (m, 1H, H^4), 4.50-4.23 (m, 1H, H^5), 1.43 (s, 9H, H^1), 1.39 (d, *J* = 7.4 Hz, 3H, H^6).

^{13}C NMR (100 MHz, $CDCl_3$, 300 K) δ173.2 (C^7), 155.2 (C^3), 135.5 (C^{Ar}), 128.6, 128.4, 128.1 (CH^{Ar}), 79.8 (C^2), 66.9 (C^8), 49.3 (C^5), 28.3 (C^1), 18.5 (C^6).

$[\alpha]_D^{24}$= –35.7 (c. 1.35 in EtOH).

The NMR data were consistent with the literature.[213]

2.4 Synthesis of peptides alternating *cis*-^{3,4}CB-GABA and alanine

Benzyl (2-((1*R*,2*R*)-2-((*tert*-butoxycarbonyl)amino)cyclobutyl)acetyl)-(*R*)-alaninate (15).

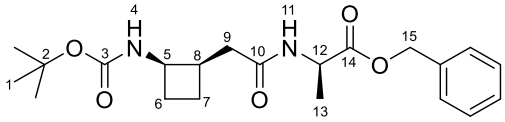

$C_{21}H_{30}N_2O_5$
M = 390.48 g/mol

Boc-(*R*,*R*)-*cis*-^{3,4}CB-GABA-(*R*)-Ala-OBn

According to the general **procedure A**, **Boc-(*R*)-Ala-OBn 13** (243 mg, 0.87 mmol, 1 eq.) was reacted with TFA (2 mL, 26.10 mmol, 30 eq.) in dry CH_2Cl_2 (4 mL) for 1 hour to obtain **TFA·H$_2$N-(*R*)-Ala-OBn**. The TFA salt was then dissolved in dry CH_2Cl_2 (4 mL), and DIPEA (0.91 mL, 5.22 mmol, 6 eq.) was added.

According to the general **procedure C**, **Boc-(*R*,*R*)-*cis*-^{3,4}CB-GABA-OH 12** (200 mg, 0.87 mmol, 1 eq.) was reacted with DIPEA (303 µL, 1.74 mmol, 2 eq.), HATU (347 mg, 0.91 mmol, 1.05 eq.) and the above described **H$_2$N-(*R*)-Ala-OBn** in CH_2Cl_2/DMF (4/1, 8 mL) for 24 hours. After workup and purification on flash chromatography (PE:EtOAc = 3:2) **Boc-(*R*,*R*)-*cis*-^{3,4}CB-GABA-(*R*)-Ala-OBn 15** (316 mg, 93%) was obtained as a white solid.

R_f = 0.31 (PE:EtOAc = 3:2)

Mp = 145-146 °C

^{1}H NMR (360 MHz, $CDCl_3$, 300 K) δ 7.43-7.27 (m, 5H, H^{Ar}), 6.41 (bs, 1H, NH^{11}), 5.25 (bs, 1H, NH^4), 5.18 (dd, *J* = 18.8, 12.2 Hz, 2H, H^{15}), 4.61 (p, *J* = 7.2 Hz, 1H, H^{12}), 4.41-4.02 (m, 1H, H^5), 2.99-2.64 (m, 1H, H^8), 2.46 (dd, *J* = 14.6, 7.6 Hz, 1H, H^9), 2.37-2.28 (m, 1H, H^6), 2.26 (dd, *J* = 14.6, 7.6 Hz, 1H, H^9), 2.04-1.90 (m, 1H, H^7), 1.90-1.77 (m, 1H, H^6), 1.65-1.53 (m, 1H, H^7), 1.42 (s, 9H, H^1), 1.40 (d, *J* = 6.2 Hz, 3H, H^{13}).

^{13}C NMR (90 MHz, $CDCl_3$, 300 K) δ 173.0 (C^{14}), 172.1 (C^{10}), 155.7 (C^3), 135.5 (C^{Ar}), 128.7, 128.6, 128.3 (CH^{Ar}), 79.5 (C^2), 67.2 (C^{15}), 48.3 (C^{12}), 47.7 (C^5), 37.5 (C^8), 36.6 (C^9), 28.5 (C^1), 27.6 (C^6), 21.9 (C^7), 18.3 (C^{13}).

IR ν 3338, 3312, 2990, 2956, 1734, 1675, 1638, 1545, 1514 cm^{-1}.

HRMS [ESI(+)] *m/z* $[M+Na]^+$ calculated for $[C_{21}H_{30}N_2NaO_5]^+$: 413.2047, found: 413.2032.

$[\alpha]_D^{20}$ = 49.7 (c. 0.58 in $CHCl_3$).

***tert*-Butyl ((1*R*,2*R*)-2-(2-(((*R*)-1-(benzylamino)-1-oxopropan-2-yl)amino)-2-oxoethyl) cyclobutyl)carbamate (17).**

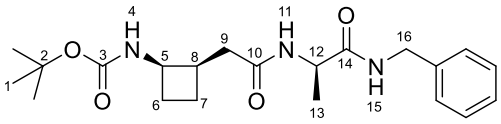

Boc-(*R*,*R*)-*cis*-^{3,4}CB-GABA-(*R*)-Ala-NHBn

According to the general **Procedure B, Boc-(*R*,*R*)-*cis*-^{3,4}CB-GABA-(*R*)-Ala-OBn 15** (422 mg, 1.08 mmol, 1 eq.) was reacted with Pd/C (10 wt. %, 135 mg) in CH_2Cl_2/EtOAc (4/1, 36 mL) under H_2 for 4 hours to afford **Boc-(*R*,*R*)-*cis*-^{3,4}CB-GABA-(*R*)-Ala-OH 16** as a white solid.

According to the general **Procedure D, Boc-(*R*,*R*)-*cis*-^{3,4}CB-GABA-(*R*)-Ala-OH 16** (1.08 mmol, 1 eq.) was reacted with benzylamine (120 μL, 1.10 mmol, 1.02 eq.), DIPEA (564 μL, 3.24 mmol, 3 eq.) and HATU (431 mg, 1.10 mmol, 1.05 eq.) in dry CH_2Cl_2 (10 mL) for 24 hours. After workup and purification on flash chromatography (EtOAc:PE = 3:1) **Boc-(*R*,*R*)-*cis*-^{3,4}CB-GABA-(*R*)-Ala-NHBn 17** (194 mg, 46%) was obtained as a white solid.

R_f = 0.36 (EtOAc:PE = 3:1)

Mp = 166-167 °C

^{1}H NMR (600 MHz, $CDCl_3$, 300 K) δ 7.34-7.19 (m, 5H, H^{Ar}), 6.86 (bs, 1H, NH^{15}), 6.50 (d, *J* = 7.2 Hz, 1H, NH^{11}), 5.14 (d, *J* = 7.2 Hz, 1H, NH^4), 4.48 (p, *J* = 7.2 Hz, 1H, H^{12}), 4.45-4.36 (m, 2H, H^{16}), 4.12 (p, *J* = 7.2 Hz, 1H, H^5), 2.93-2.62 (m, 1H, H^8), 2.39 (dd, *J* = 14.6, 7.6 Hz, 1H, H^9), 2.31-2.24 (m, 1H, H^6), 2.24-2.16 (m, 1H, H^9), 2.02-1.85 (m, 1H, H^7), 1.82-1.73 (m, 1H, H^6), 1.63-1.51 (m, 1H, H^7), 1.42 (s, 9H, H^1), 1.38 (d, *J* = 7.2 Hz, 3H, H^{13}).

^{13}C NMR (90 MHz, $CDCl_3$, 300 K) δ 173.2 (C^{14}), 172.8 (C^{10}), 156.0 (C^3), 137.9 (C^{Ar}), 128.5, 127.4, 127.3 (CH^{Ar}), 79.4 (C^2), 48.8 (C^{12}), 47.1 (C^5), 43.3 (C^{16}), 37.4 (C^8), 36.0 (C^9), 28.2 (C^1), 26.9 (C^6), 21.2 (C^7), 17.9 (C^{13}).

IR ν 3329, 2958, 2934, 1680, 1658, 1636, 1529 cm^{-1}.

HRMS [ESI(+)] *m/z* $[M+Na]^+$ calculated for $[C_{21}H_{31}N_3NaO_4]^+$: 412.2207, found: 412.2191.

$[\alpha]_D^{20}$ = 56.8 (c. 0.52 in $CHCl_3$).

Benzyl (2-((1*R*,2*R*)-2-((*tert*-butoxycarbonyl)amino)cyclobutyl)acetyl)-(*S*)-alaninate (18).

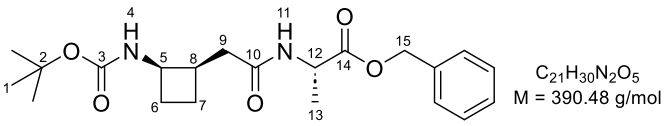

Boc-(*R*,*R*)-*cis*-^{3,4}CB-GABA-(*S*)-Ala-OBn

According to the general **procedure A**, **Boc-(*S*)-Ala-OBn 14** (243 mg, 0.87 mmol, 1 eq.) was reacted with TFA (2 mL, 26.10 mmol, 30 eq.) in dry CH_2Cl_2 (4 mL) for 1 hour to obtain **TFA·H$_2$N-(*S*)-Ala-OBn**. The TFA salt was then dissolved in dry CH_2Cl_2 (4 mL), and added DIPEA (0.91 mL, 5.22 mmol, 6 eq.).

According to the general **procedure C**, **Boc-(*R*,*R*)-*cis*-^{3,4}CB-GABA-OH 12** (200 mg, 0.87 mmol, 1 eq.) was reacted with DIPEA (303 μL, 1.74 mmol, 2 eq.), HATU (347 mg, 0.91 mmol, 1.05 eq.) and the above-described **H$_2$N-(*R*)-Ala-OBn** in CH_2Cl_2/DMF (4/1, 8 mL) for 24 hours. After workup and purification on flash chromatography (PE:EtOAc = 3:2) **Boc-(*R*,*R*)-*cis*-^{3,4}CB-GABA-(*S*)-Ala-OBn 18** (309 mg, 91%) was obtained as a white solid.

R_f = 0.31 (PE:EtOAc = 3:2)

Mp = 157-158 °C

^{1}H NMR (360 MHz, $CDCl_3$, 300 K) δ 7.40-7.27 (m, 5H, H^{Ar}), 6.40 (bs, 1H, NH^{11}), 5.37 (bs, 1H, NH^4), 5.17 (dd, *J* = 20.0, 12.2 Hz, 2H, H^{15}), 4.61 (p, *J* = 7.2 Hz, 1H, H^{12}), 4.31-4.12 (m, 1H, H^5), 2.90-2.77 (m, 1H, H^8), 2.46 (dd, *J* = 14.6, 7.6 Hz, 1H, H^9), 2.36-2.28 (m, 1H, H^6), 2.27 (dd, *J* = 14.6, 7.6 Hz, 1H, H^9), 2.03-1.90 (m, 1H, H^6), 1.90-1.78 (m, 1H, H^7), 1.65-1.51 (m, 1H, H^7), 1.41 (s, 9H, H^1), 1.40 (d, *J* = 6.2 Hz, 3H, H^{13}).

^{13}C NMR (90 MHz, $CDCl_3$, 300 K) δ 173.1 (C^{14}), 172.1 (C^{10}), 155.6 (C^3), 135.4 (C^{Ar}), 128.7, 128.5, 128.2 (CH^{Ar}), 79.4 (C^2), 67.2 (C^{15}), 48.2 (C^{12}), 47.4 (C^5), 37.6 (C^8), 36.5 (C^9), 28.5 (C^1), 27.7 (C^6), 21.6 (C^7), 18.4 (C^{13}).

IR ν 3357, 3272, 2967, 2943, 1719, 1709, 1652, 1534, 1497 cm^{-1}.

HRMS [ESI(+)] *m/z* $[M+Na]^+$ calculated for $[C_{21}H_{30}N_2NaO_5]^+$: 413.2047, found: 413.2035.

$[\alpha]_D^{21}$ = 36.3 (c. 0.60 in $CHCl_3$).

***tert*-Butyl ((1*R*,2*R*)-2-(2-(((*S*)-1-(benzylamino)-1-oxopropan-2-yl)amino)-2-oxoethyl) cyclobutyl)carbamate (20).**

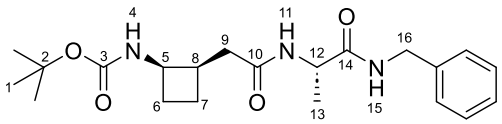

Boc-(*R*,*R*)-*cis*-^{3,4}CB-GABA-(*S*)-Ala-NHBn

According to the general **Procedure B, Boc-(*R*,*R*)-*cis*-^{3,4}CB-GABA-(*S*)-Ala-OBn 18** (422 mg, 1.08 mmol, 1 eq.) was reacted with Pd/C (10 wt. %, 135 mg) in CH_2Cl_2/EtOAc (4/1, 36 mL) under H_2 for 4 hours to afford **Boc-(*R*,*R*)-*cis*-^{3,4}CB-GABA-(*S*)-Ala-OH 19** as a white solid.

According to the general **Procedure D, Boc-(*R*,*R*)-*cis*-^{3,4}CB-GABA-(*S*)-Ala-OH 19** (1.08 mmol, 1 eq.) was reacted with benzylamine (120 μL, 1.10 mmol, 1.02 eq.), DIPEA (564 μL, 3.24 mmol, 3 eq.) and HATU (431 mg, 1.10 mmol, 1.05 eq.) in dry CH_2Cl_2 (10 mL) for 24 hours. After workup and purification on flash chromatography (EtOAc:PE = 3:1) **Boc-(*R*,*R*)-*cis*-^{3,4}CB-GABA-(*S*)-Ala-NHBn 20** (194 mg, 46%) was obtained as a white solid.

R_f = 0.48 (EtOAc:PE = 3:1)

Mp = 194-195 °C

^{1}H NMR (600 MHz, $CDCl_3$, 300 K) δ 7.42-7.12 (m, 5H, H^{Ar}), 6.81 (bs, 1H, NH^{15}), 6.52 (d, *J* = 7.2 Hz, 1H, NH^{11}), 5.23 (d, *J* = 7.2 Hz, 1H, NH^4), 4.51 (p, *J* = 7.2 Hz, 1H, H^{12}), 4.41 (d, *J* = 5.8 Hz, 2H, H^{16}), 4.30-4.11 (m, 1H, H^5), 2.92-2.69 (m, 1H, H^8), 2.44 (dd, *J* = 14.6, 7.6 Hz, 1H, H^9), 2.37-2.27 (m, 1H, H^6), 2.23 (dd, *J* = 14.6, 7.6 Hz, 1H, H^9), 2.03-1.88 (m, 1H, H^7), 1.88-1.78 (m, 1H, H^6), 1.62-1.48 (m, 1H, H^7), 1.42 (s, 9H, H^1), 1.39 (d, *J* = 7.2 Hz, 3H, H^{13}).

^{13}C NMR (90 MHz, $CDCl_3$, 300 K) δ 173.1 (C^{14}), 172.9 (C^{10}), 155.9 (C^3), 137.9 (C^{Ar}), 128.5, 127.4, 127.3 (CH^{Ar}), 79.3 (C^2), 48.7 (C^{12}), 46.9 (C^5), 43.2 (C^{16}), 37.5 (C^8), 36.0(C^9), 28.2 (C^1), 27.1 (C^6), 20.9 (C^7), 17.9 (C^{13}).

IR ν 3327, 2937, 1736, 1682, 1637, 1528 cm^{-1}.

HRMS [ESI(+)] *m/z* $[M+Na]^+$ calculated for $[C_{21}H_{31}N_3NaO_4]^+$: 412.2207, found: 412.2189.

$[\alpha]_D^{22}$ = 13.4 (c. 0.50 in $CHCl_3$).

Benzyl (2-((1*R*,2*R*)-2-((*R*)-2-(2-((1*R*,2*R*)-2-((*tert*-butoxycarbonyl)amino)cyclobutyl) acetamido)propanamido)cyclobutyl)acetyl)-(*R*)-alaninate (21).

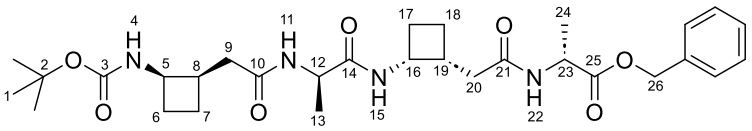

Boc-[(*R*,*R*)-*cis*-^{3,4}CB-GABA-(*R*)-Ala]$_2$-OBn

$C_{30}H_{44}N_4O_7$
M = 572.70 g/mol

According to the general **procedure A**, **Boc-(*R*,*R*)-*cis*-^{3,4}CB-GABA-(*R*)-Ala-OBn 15** (117 mg, 0.30 mmol, 1 eq.) was reacted with TFA (689 μL, 9.00 mmol, 30 eq.) in dry CH_2Cl_2 (2 mL) for 1 hour to obtain **TFA·H$_2$N-(*R*,*R*)-*cis*-^{3,4}CB-GABA-(*R*)-Ala-OBn.** The TFA salt was then dissolved in dry CH_2Cl_2 (2 mL), and DIPEA (314 μL, 1.80 mmol, 6 eq.) was added.

According to the general **procedure C**, **Boc-(*R*,*R*)-*cis*-^{3,4}CB-GABA-(*R*)-Ala-OH 16** (90 mg, 0.30 mmol, 1 eq.) was reacted with DIPEA (105 μL, 0.60 mmol, 2 eq.) and the above-described **H$_2$N-(*R*,*R*)-*cis*-^{3,4}CB-GABA-(*R*)-Ala-OBn**, and HATU (122 mg, 0.32 mmol, 1.05 eq.) in CH_2Cl_2/DMF (3/1, 3 mL) for 24 hours. After workup and purification on flash chromatography (CH_2Cl_2:MeOH, gradient from 100:1 to 100:4) **Boc-[(*R*,*R*)-*cis*-^{3,4}CB-GABA-(*R*)-Ala]$_2$-OBn 21** (125 mg, 73%) was obtained as a white solid.

R_f = 0.31 (CH_2Cl_2:MeOH = 100:4)

Mp = 209-210 °C

^{1}H NMR (360 MHz, $CDCl_3$, 300 K) δ 7.67 (d, *J* = 6.8 Hz, 1H, NH^{15}), 7.48-7.27 (m, 5H, H^{Ar}), 6.85 (d, *J* = 7.6 Hz, 1H, H^{22}), 6.41 (d, *J* = 6.8 Hz, 1H, H^{11}), 5.31 (d, *J* = 7.0 Hz, 1H, H^4), 5.18 (dd, *J* = 21.6, 12.4 Hz, 2H, H^{26}), 4.59 (p, *J* = 7.2 Hz, 1H, H^{23}), 4.50-4.32 (m, 2H, H$^{16, 12}$), 4.32-4.10 (m, 1H, H^5), 3.11-2.70 (m, 2H, H$^{19, 8}$), 2.61-2.40 (m, 2H, H$^{20, 9}$), 2.40-2.16 (m, 4H, H$^{9, 6, 17, 20}$), 2.14-1.90 (m, 3H, H$^{7, 17, 18}$), 1.84-1.75 (m, 1H, H^6), 1.73-1.51 (m, 2H, H$^{7, 18}$), 1.49-1.37 (m, 12H, H$^{1, 24}$), 1.35 (d, *J* = 7.0 Hz, 3H, H^{13}).

^{13}C NMR (90 MHz, $CDCl_3$, 300 K) δ 173.3 (C^{25}), 172.6 (C^{21}), 172.5 (C^{10}), 172.3 (C^{14}), 155.8 (C^3), 135.5 (C^{Ar}), 128.8, 128.6, 128.3 (CH^{Ar}), 79.6 (C^2), 67.3 (C^{26}), 49.5 (C^{12}), 48.4 (C^{23}), 47.9 (C^5), 46.9 (C^{16}), 37.5 (C^8), 37.4 (C^{19}), 37.0 (C^{20}), 36.8 (C^9), 28.5 (C^1), 27.4 (C^6), 27.2 (C^{17}), 22.3 (C$^{7, 18}$), 18.7 (C^{13}), 18.0 (C^{24}).

IR ν 3310, 2981, 1728, 1682, 1637, 1537 cm^{-1}.

HRMS [ESI(+)] *m/z* $[M+Na]^+$ calculated for $[C_{30}H_{44}N_4NaO_7]^+$: 595.3102, found: 595.3093.

$[\alpha]_D^{20}$= 47.8 (c. 0.55 in $CHCl_3$), $[\alpha]_D^{22}$= 156.46 (c. 0.23 in MeOH).

***tert*-Butyl ((1*R*,2*R*)-2-(2-(((*R*)-1-(((1*R*,2*R*)-2-(2-(((*R*)-1-(benzylamino)-1-oxopropan-2-yl)amino)-2-oxoethyl)cyclobutyl)amino)-1-oxopropan-2-yl)amino)-2-oxoethyl) cyclobutyl)carbamate (23).**

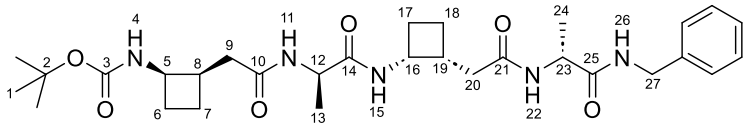

Boc-[(*R*,*R*)-*cis*-^{3,4}CB-GABA-(*R*)-Ala]$_2$-NHBn $C_{30}H_{45}N_5O_6$ M = 571.72 g/mol

According to the general **Procedure B, Boc-[(*R*,*R*)-*cis*-^{3,4}CB-GABA-(*R*)-Ala]$_2$-OBn 21** (80 mg, 0.14 mmol, 1 eq.) was reacted with Pd/C (10 wt. %, 18 mg) in CH_2Cl_2/EtOAc (4/1, 5 mL) under H_2 for 4 hours to afford **Boc-[(*R*,*R*)-*cis*-^{3,4}CB-GABA-(*R*)-Ala]$_2$-OH I-22** as a white solid.

According to the general **Procedure D, Boc-[(*R*,*R*)-*cis*-^{3,4}CB-GABA-(*R*)-Ala]$_2$-OH 22** (0.14 mmol, 1 eq.) was reacted with benzylamine (16 µL, 0.14 mmol, 1.02 eq.), DIPEA (73 µL, 0.42 mmol, 3 eq.) and HATU (56 mg, 0.15 mmol, 1.05 eq.) in dry CH_2Cl_2 (2 mL) for 24 hours. After workup and purification on flash chromatography (CH_2Cl_2:MeOH, gradient from 100:1 to 100:4) **Boc-[(*R*,*R*)-*cis*-^{3,4}CB-GABA-(*R*)-Ala]$_2$-NHBn 23** (47 mg, 59%) was obtained as a white solid.

R_f = 0.35 (CH_2Cl_2:MeOH = 100:5)

Mp = 214-215 °C

^{1}H NMR (400 MHz, Pyr-d_5, 300 K) δ9.15 (s, 1H, NH^{26}), 8.96 (d, *J* = 5.8 Hz, 1H, NH^{22}), 8.85 (d, *J* = 5.4 Hz, 1H, NH^{11}), 8.81 (d, *J* = 7.6 Hz, 1H, NH^{15}), 8.10 (d, *J* = 7.0 Hz, 1H, NH^4), 7.56-7.46 (m, 2H, H^{Ar}), 7.33 (t, *J* = 7.4 Hz, 2H, H^{Ar}), 7.28-7.24 (m, 1H, H^{Ar}), 5.06-5.02 (m, 1H, H^{23}), 4.82 (dd, *J* = 14.8, 6.2 Hz, 1H, H^{27}), 4.78-4.61 (m, 3H, $H^{27, 16, 12}$), 4.59-4.43 (m, 1H, H^5), 3.45-3.11 (m, 2H, $H^{8, 19}$), 2.99-2.73 (m, 2H, $H^{9, 20}$), 2.68-2.42 (m, 2H, $H^{9, 20}$), 2.37-2.24 (m, 1H, H^6), 2.24-2.14 (m, 1H, H^{17}), 2.14-2.01 (m, 2H, $H^{17, 6}$), 2.00-1.81 (m, 4H, $H^{7, 18, 18, 7}$), 1.66 (d, *J* = 7.2 Hz, 3H, H^{24}), 1.47 (d, *J* = 7.2 Hz, 3H, H^{13}), 1.46 (s, 9H, H^1).

^{13}C NMR (100 MHz, Pyr-d_5, 300 K) δ174.1 (C^{25}), 173.9 (C^{14}), 173.9 (C^{10}), 173.2 (C^{21}), 156.9 (C^3), 140.9 (C^{Ar}), 129.2, 128.4, 127.6 (CH^{Ar}), 78.9 (C^2), 51.3 (C^{12}), 50.9 (C^{23}), 49.3 (C^5), 47.9 (C^{16}), 43.7

(C^{27}), 38.8 (C^{8}), 38.7 (C^{19}), 37.5 (C^{9}), 36.9 (C^{20}), 28.9 (C^{1}), 27.2 (C^{6}), 26.7 (C^{17}), 23.8 (C^{7}), 23.6 (C^{18}), 19.1 (C^{24}), 19.0 (C^{13}).

IR ν 3325, 3291, 2976, 2934, 1680, 1638, 1530 cm^{-1}.

HRMS [ESI(+)] *m/z* $[M+Na]^+$ calculated for $[C_{30}H_{45}N_5NaO_6]^+$: 594.3262, found: 594.3239.

$[\alpha]_D^{24}$= 2.2 (c. 0.10 in pyridine).

Benzyl (2-((1*R*,2*R*)-2-((*S*)-2-(2-((1*R*,2*R*)-2-((*tert*-butoxycarbonyl)amino)cyclobutyl) acetamido)propanamido)cyclobutyl)acetyl)-(*S*)-alaninate (24).

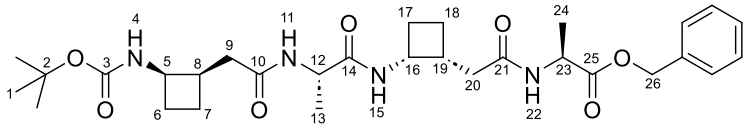

Boc-[(*R*,*R*)-*cis*-^{3,4}CB-GABA-(*S*)-Ala]$_2$-OBn $C_{30}H_{44}N_4O_7$ M = 572.70 g/mol

According to the general **procedure A**, **Boc-(*R*,*R*)-*cis*-^{3,4}CB-GABA-(*S*)-Ala-OBn 20** (117 mg, 0.30 mmol, 1 eq.) was reacted with TFA (689 µL, 9.00 mmol, 30 eq.) in dry CH_2Cl_2 (2 mL) for 1 hour to obtain **TFA·H_2N-(*R*,*R*)-*cis*-^{3,4}CB-GABA-(*S*)-Ala-OBn.** The TFA salt was then dissolved in dry CH_2Cl_2 (2 mL), and DIPEA (314 µL, 1.80 mmol, 6 eq.) was added.

According to the general **procedure C**, **Boc-(*R*,*R*)-*cis*-^{3,4}CB-GABA-(*S*)-Ala-OH 19** (90 mg, 0.30 mmol, 1 eq.) was reacted with DIPEA (105 µL, 0.60 mmol, 2 eq.), the above-described **H_2N-(*R*,*R*)-*cis*-^{3,4}CB-GABA-(*S*)-Ala-OBn** and HATU (122 mg, 0.32 mmol, 1.05 eq.) in a mixture of CH_2Cl_2/DMF (3/1, 3 mL) for 24 hours. After workup and purification on flash chromatography (CH_2Cl_2:MeOH, gradient from 100:1 to 100:4) **Boc-[(*R*,*R*)-*cis*-^{3,4}CB-GABA-(*S*)-Ala]$_2$-OBn 24** (116 mg, 68%) was obtained as a white solid.

R_f = 0.31 (CH_2Cl_2:MeOH = 100:4)

Mp = 198-199 °C

^{1}H NMR (360 MHz, $CDCl_3$, 300 K) δ 8.00 (d, *J* = 5.8 Hz, 1H, NH^{22}), 7.85 (d, *J* = 8.4 Hz, 1H, H^{15}), 7.57-7.26 (m, 5H, H^{Ar}), 6.86 (d, *J* = 6.0 Hz, 1H, H^{11}), 5.67 (d, *J* = 6.8 Hz, 1H, H^{4}), 5.19 (dd, *J* = 23.0, 12.4 Hz, 2H, H^{26}), 4.64 (p, *J* = 7.4 Hz, 1H, H^{23}), 4.58-4.42 (m, 1H, H^{16}), 4.36-4.04 (m, 2H, $H^{5, 12}$), 2.95-2.74 (m, 2H, $H^{19, 8}$), 2.48 (dd, *J* = 14.0, 7.8 Hz, 1H, H^{9}), 2.40-2.09 (m, 6H, $H^{20, 6, 9, 20,}$

$^{17, 18}$), 2.08-1.90 (m, 3H, H$^{17, 18, 7}$), 1.90-1.78 (m, 1H, H^{6}), 1.65-1.51 (m, 1H, H^{7}), 1.50-1.39 (m, 12H, H$^{24, 1}$), 1.35 (d, *J* = 7.2 Hz, 3H, H^{13}).

^{13}C NMR (90 MHz, $CDCl_3$, 300 K) δ 175.5 (C^{25}), 173.4 (C^{10}), 173.2 (C^{21}), 172.7 (C^{14}), 155.6 (C^{3}), 135.4 (C^{Ar}), 128.7, 128.6, 128.2 (CH^{Ar}), 79.4 (C^{2}), 67.5 (C^{26}), 49.7 (C^{12}), 48.3 (C^{23}), 47.4 (C^{5}), 46.9 (C^{16}), 37.9 (C^{8}), 37.9 (C^{19}), 36.5 (C^{9}), 35.3 (C^{20}), 28.6 (C^{1}), 27.7 (C^{6}), 26.8 (C^{17}), 21.4 (C^{7}), 19.9 (C^{18}), 17.7 (C^{13}), 17.1 (C^{24}).

IR ν 3313, 2981, 2942, 1730, 1682, 1638, 1536 cm^{-1}.

HRMS [ESI(+)] *m/z* $[M+Na]^+$ calculated for $[C_{30}H_{44}N_4NaO_7]^+$: 595.3102, found: 595.3078.

$[\alpha]_D^{23}$ = 83.9 (c. 0.53 in $CHCl_3$).

***tert*-Butyl ((1*R*,2*R*)-2-(2-(((*S*)-1-(((1*R*,2*R*)-2-(2-(((*S*)-1-(benzylamino)-1-oxopropan-2-yl)amino)-2-oxoethyl)cyclobutyl)amino)-1-oxopropan-2-yl)amino)-2-oxoethyl) cyclobutyl)carbamate (26).**

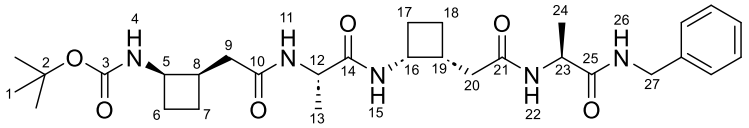

Boc-[(*R*,*R*)-*cis*-^{3,4}CB-GABA-(*S*)-Ala]$_2$-NHBn $C_{30}H_{45}N_5O_6$ M = 571.72 g/mol

According to the general **Procedure B, Boc-[(*R*,*R*)-*cis*-^{3,4}CB-GABA-(*S*)-Ala]$_2$-OBn 24** (80 mg, 0.14 mmol, 1 eq.) was reacted with Pd/C (10 wt. %, 18 mg) in CH_2Cl_2/EtOAc (4/1, 5 mL) under H_2 for 4 hours to afford **Boc-[(*R*,*R*)-*cis*-^{3,4}CB-GABA-(*S*)-Ala]$_2$-OH 25** as a white solid.

According to the general **Procedure D, Boc-[(*R*,*R*)-*cis*-^{3,4}CB-GABA-(*S*)-Ala]$_2$-OH 25** (0.14 mmol, 1 eq.) was reacted with benzylamine (16 µL, 0.14 mmol, 1.02 eq.), DIPEA (73 µL, 0.42 mmol, 3 eq.) and HATU (56 mg, 0.15 mmol, 1.05 eq.) in dry CH_2Cl_2 (2 mL) for 24 hours. After workup and purification on flash chromatography (CH_2Cl_2:MeOH, gradient from 100:1 to 100:4) **Boc-[(*R*,*R*)-*cis*-^{3,4}CB-GABA-(*S*)-Ala]$_2$-NHBn 26** (70 mg, 88%) was obtained as a white solid.

R_f = 0.35 (CH_2Cl_2:MeOH = 100:5)

Mp = 222-223 °C

^{1}H NMR (400 MHz, Pyr-d_5, 300 K) δ 9.51 (t, *J* = 5.8 Hz, 1H, NH^{26}), 9.17 (d, *J* = 7.4 Hz, 1H, NH^{22}),

9.10 (d, *J* = 6.8 Hz, 1H, NH^{11}), 9.07 (d, *J* = 7.8 Hz, 1H, NH^{15}), 7.80 (d, *J* = 7.2 Hz, 1H, NH^{4}), 7.54-7.46 (m, 2H, H^{Ar}), 7.32 (t, *J* = 7.6 Hz, 2H, H^{Ar}), 7.28-7.23 (m, 1H, H^{Ar}), 5.02 (p, *J* = 7.2 Hz, 1H, H^{23}), 4.94-4.89 (m, 1H, H^{12}), 4.86-4.81 (m, 1H, H^{16}), 4.71 (d, *J* = 5.8 Hz, 2H, H^{27}), 4.67-4.53 (m, 1H, H^{5}), 3.29-3.14 (m, 1H, H^{8}), 3.14-3.03 (m, 1H, H^{19}), 2.86 (dd, *J* = 14.2, 6.2 Hz, 1H, H^{9}), 2.76-2.57 (m, 3H, $H^{9,\ 20,\ 20}$), 2.37-2.15 (m, 4H, $H^{18,\ 17,\ 17,\ 6),}$ 2.17-2.04 (m, 1H, H^{6}), 2.04-1.79 (m, 3H, $H^{7,\ 18,\ 7}$), 1.64 (d, *J* = 7.2 Hz, 3H, H^{24}), 1.49 (d, *J* = 6.2 Hz, 3H, H^{13}), 1.48 (s, 9H, H^{1}).

^{13}C NMR (100 MHz, Pyr-d_5, 300 K) δ175.4 (C^{25}), 173.8 (C^{10}), 173.5 (C^{21}), 173.5 (C^{14}), 156.5 (C^{3}), 140.3 (C^{Ar}), 129.2 , 128.2, 127.7 (CH^{Ar}), 78.5 (C^{2}), 50.4 (C^{12}), 50.2 (C^{23}), 48.2 (C^{5}), 47.7 (C^{16}), 43.9 (C^{27}), 39.2 (C^{8}), 39.2 (C^{19}), 36.8 (C^{9}), 36.2 (C^{20}), 28.9 (C^{1}), 27.6 (C^{6}), 27.1 (C^{17}), 22.1 (C^{7}), 21.2 (C^{18}), 18.7 (C^{24}), 18.5 (C^{13}).

IR ν3326, 3300, 2975, 2934, 1681, 1638, 1531 cm^{-1}.

HRMS [ESI(+)] *m/z* $[M+Na]^+$ calculated for $[C_{30}H_{45}N_5NaO_6]^+$: 594.3262, found: 594.3241.

$[\alpha]_{\mathbf{D}}^{\mathbf{25}}$= 28.8 (c. 0.2 in pyridine).

Benzyl (2-((1*R*,2*R*)-2-((*R*)-2-(2-((1*R*,2*R*)-2-((*R*)-2-(2-((1*R*,2*R*)-2-((*tert*-butoxycarbonyl) amino)cyclobutyl)acetamido)propanamido)cyclobutyl)acetamido)propanamido)cyclobutyl)acetyl)-(*R*)-alaninate (27).

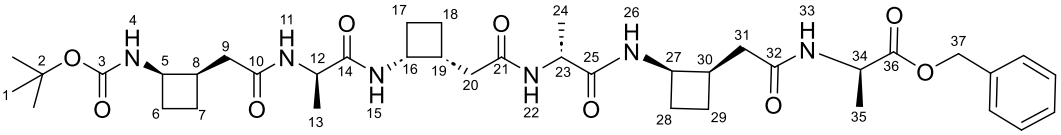

Boc-[(*R*,*R*)-*cis*-^{3,4}CB-GABA-(*R*)-Ala]$_3$-OBn

$C_{39}H_{58}N_6O_9$
M = 754.93 g/mol

According to the general **procedure A**. **Boc-[(*R*,*R*)-*cis*-^{3,4}CB-GABA-(*R*)-Ala]$_2$-OBn 21** (132 mg, 0.23 mmol, 1 eq.) was reacted with TFA (528 μL, 6.90 mmol, 30 eq.) in dry CH_2Cl_2 (5 mL) for 1 hour to obtain **TFA·H$_2$N-[(*R*,*R*)-*cis*-^{3,4}CB-GABA-(*R*)-Ala]$_2$-OBn.** The TFA salt was then dissolved in dry CH_2Cl_2 (5 mL), and DIPEA (240 μL, 1.38 mmol, 6 eq.) was added.

According to the general **procedure C**, **Boc-(*R*,*R*)-*cis*-^{3,4}CB-GABA-(*R*)-Ala-OH 16** (69 mg, 0.23 mmol, 1 eq.) was reacted with DIPEA (80 μL, 0.46 mmol, 2 eq.), **H$_2$N-[(*R*,*R*)-*cis*-^{3,4}CB-GABA-(*R*)-Ala]$_2$-OBn** and HATU (92 mg, 0.24 mmol, 1.05 eq.) in a mixture of CH_2Cl_2/DMF (3/1, 3 mL) for 24 hours. After workup, the crude product was purified by preparative HPLC (mobile phase *n*-hexane:EtOH = 65:35). The product elution (with baseline separation) was collected at 14.6 minutes, followed by solvent evaporation **Boc-[(*R*,*R*)-*cis*-^{3,4}CB-GABA-(*R*)-Ala]$_3$-OBn 27** (104

mg, 60%) was obtained as a white solid.

R_f = 0.43 (CH_2Cl_2: MeOH = 100: 6)

Mp = 233-234 °C

^{1}H NMR (360 MHz, DMSO-d_6, 300 K) δ 8.38 (d, J = 6.8 Hz, 1H, NH^{33}), [8.14 (d, J = 7.8 Hz, 1H), 8.11 (d, J = 7.8 Hz, 1H), 8.03 (d, J = 7.6 Hz, 1H), 7.99 (d, J = 9.4 Hz, 1H), 4H, $NH^{11, 15, 22, 26}$], 7.56-7.18 (m, 5H, H^{Ar}), 7.07 (d, J = 7.8 Hz, 1H, NH^4), 5.09 (s, 2H, H^{37}), 4.39-4.12 (m, 5H, $H^{12, 16, 23, 27, 34}$), 4.12-3.97 (m, 1H, H^5), 2.73-2.60 (m, 3H, $H^{8, 19, 30}$), 2.35-1.44 (m, 18H, $H^{9, 31, 20, 6, 7, 17, 18, 28, 29}$), 1.36 (s, 9H, H^1), [1.27 (d, J = 7.4 Hz, 3H), 1.17 (dd, J = 7.1, 1.2 Hz, 6H), 9H, $H^{13, 24, 35}$].

^{13}C NMR (90 MHz, DMSO-d_6, 300 K) δ [171.9, 171.9, 171.7, 171.6, 171.5, 171.2 ($C^{10, 14, 21, 25, 32, 36}$)], 154.8 ($C^3$), 136.0 ($C^{Ar}$), 128.4, 128.0, 127.7 ($CH^{Ar}$), 77.5 ($C^2$), 65.7 ($C^{37}$), [48.1, 48.1, 47.6, 46.5, 45.1, 44.9 ($C^{5, 12, 16, 23, 27, 34}$)] , [37.5, 37.4, 37.3 ($C^{8, 19, 30}$)], [35.0, 35.0, 34.8 ($C^{9, 20, 31}$)], 28.2 ($C^1$), [25.9, 25.7, 25.6 ($C^{6, 17, 28}$)], [21.0, 20.7, 20.6 ($C^{7, 18, 29}$)], [18.8, 18.7, 16.8 ($C^{13, 24, 35}$)].

IR ν 3318, 3299, 2982, 2958, 2922, 2855, 1739, 1678, 1660, 1639, 1531 cm^{-1}.

HRMS [ESI(+)] *m/z* $[M+Na]^+$ calculated for $[C_{39}H_{58}N_6NaO_9]^+$: 777.4157, found: 777.4141.

***tert*-Butyl ((1*R*,2*R*)-2-(2-(((*R*)-1-(((1*R*,2*R*)-2-(2-(((*R*)-1-(((1*R*,2*R*)-2-(2-(((*R*)-1-(benzyl amino)-1-oxopropan-2-yl)amino)-2-oxoethyl)cyclobutyl)amino)-1-oxopropan-2-yl)amino)-2-oxoethyl)cyclobutyl)amino)-1-oxopropan-2-yl)amino)-2-oxoethyl)cyclobutyl)carbamate (28).**

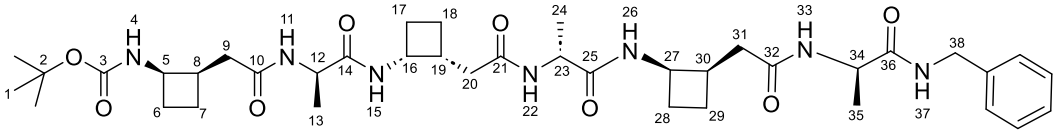

Boc-[(*R*,*R*)-*cis*-^{3,4}CB-GABA-(*R*)-Ala]$_3$-NHBn

$C_{39}H_{59}N_7O_8$
M = 753.94 g/mol

According to the general **procedure A**. **Boc-[(*R*,*R*)-*cis*-^{3,4}CB-GABA-(*R*)-Ala]$_2$-NHBn 23** (51 mg, 0.09 mmol, 1 eq.) was reacted with TFA (207μL, 2.70 mmol, 30 eq.) in dry CH_2Cl_2 (5 mL) for 1 hour to obtain **TFA·H_2N-[(*R*,*R*)-*cis*-^{3,4}CB-GABA-(*R*)-Ala]$_3$-NHBn.** The TFA salt was then dissolved in dry CH_2Cl_2 (5 mL), and DIPEA (94 μL, 0.54 mmol, 6 eq.) was added.

According to the general **procedure C**, **Boc-(*R*,*R*)-*cis*-^{3,4}CB-GABA-(*R*)-Ala-OH 16** (27 mg, 0.09

mmol, 1 eq.) was reacted with DIPEA (31 μL, 0.18 mmol, 2 eq.), the above-described **H_2N-[(*R*,*R*)-*cis*-^{3,4}CB-GABA-(*R*)-Ala]$_2$-NHBn** and HATU (38 mg, 0.10 mmol, 1.05 eq.) in a mixture of CH_2Cl_2/DMF (3/1, 2 mL) for 24 hours. After workup, the crude product was purified by preparative HPLC (mobile phase *n*-hexane:EtOH = 40:60). The product elution (with baseline separation) was collected at 10.5 minutes, followed by solvent evaporation **Boc-[(*R*,*R*)-*cis*-^{3,4}CB-GABA-(*R*)-Ala]$_3$-NHBn 28** (41 mg, 61%) was obtained as a white solid.

The sample was not sufficient soluble in DMSO-d_6 and gave unsatisfactory NMR spectra.

R_f = 0.51 (CH_2Cl_2:MeOH = 100:6)

Mp = 245-246 °C

IR ν 3319, 3290, 3210, 2982, 2959, 2931, 2854, 1679, 1660, 1637, 1554, 1527 cm^{-1}.

HRMS [ESI(+)] *m/z* $[M+Na]^+$ calculated for $[C_{39}H_{59}N_7NaO_8]^+$: 776.4317, found: 777.4283.

Benzyl (2-((1*R*,2*R*)-2-((*S*)-2-(2-((1*R*,2*R*)-2-((*S*)-2-(2-((1*R*,2*R*)-2-((*tert*-butoxycarbonyl) amino)cyclobutyl)acetamido)propanamido)cyclobutyl)acetamido)propanamido)cyclobutyl)acetyl)-(*S*)-alaninate (29).

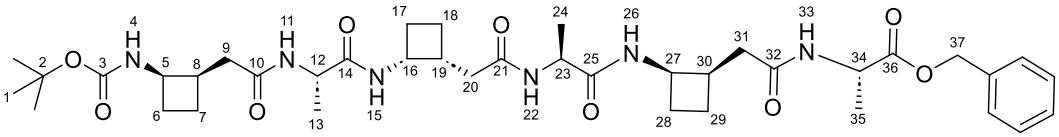

Boc-[(*R*,*R*)-*cis*-^{3,4}CB-GABA-(*S*)-Ala]$_3$-OBn

$C_{39}H_{58}N_6O_9$
M = 754.93 g/mol

According to the general **procedure A**. **Boc-[(*R*,*R*)-*cis*-^{3,4}CB-GABA-(*S*)-Ala]$_2$-OBn 24** (132 mg, 0.23 mmol, 1 eq.) was reacted with TFA (528 μL, 6.90 mmol, 30 eq.) in dry CH_2Cl_2 (5 mL) for 1 hour to obtain **TFA·H_2N-[(*R*,*R*)-*cis*-^{3,4}CB-GABA-(*S*)-Ala]$_2$-OBn.** The TFA salt was then dissolved in dry CH_2Cl_2 (5 mL), and DIPEA (240 μL, 1.38 mmol, 6 eq.) was added.

According to the general **procedure C**, **Boc-(*R*,*R*)-*cis*-^{3,4}CB-GABA-(*S*)-Ala-OH 19** (69 mg, 0.23 mmol, 1 eq.) was reacted with DIPEA (80 μL, 0.46 mmol, 2 eq.), **H_2N-[(*R*,*R*)-*cis*-^{3,4}CB-GABA-(S)-Ala]$_2$-OBn** and HATU (92 mg, 0.24 mmol, 1.05 eq.) in a mixture of CH_2Cl_2/DMF (3/1, 3 mL) for 24 hours. After workup and purification by flash chromatography (CH_2Cl_2:MeOH, gradient from 100:1 to 100:4) **Boc-[(*R*,*R*)-*cis*-^{3,4}CB-GABA-(*S*)-Ala]$_3$-OBn 29** (95 mg, 55%) was obtained as a white solid.

R_f = 0.43 (CH_2Cl_2:MeOH = 100:6)

Mp = 245-246 °C

^{1}H NMR (400 MHz, Pyr-d_5, 310 K) δ 9.13 (d, *J* = 7.2 Hz, 1H, H^{22}), 9.06 (d, *J* = 7.0 Hz, 1H, H^{33}), 9.02 (d, *J* = 6.8 Hz, 1H, H^{11}), 8.96 (d, *J* = 7.6 Hz, 1H, H^{15}), 8.80 (d, *J* = 7.6 Hz, 1H, H^{26}), 7.69 (s, 1H, H^4), 7.49-7.26 (m, 5H, H^{Ar}), 5.29 (dd, *J* = 25.6, 12.6 Hz, 2H, H^{37}), 4.95-4.86 (m, 1H, H^{34}), 4.89-4.80 (m, 3H, $H^{16, 12, 27}$), 4.72-4.67 (m, 1H, H^{23}), 4.65-4.52 (m, 1H, H^5), 3.31-2.98 (m, 3H, $H^{8, 30, 19}$), 2.87-2.55 (m, 6H, $H^{9, 31, 20}$), 2.35-2.04 (m, 8H, $H^{17, 18, 28, 6}$), 2.04-1.81 (m, 6H, $H^{29, 18, 7}$), 1.56 (d, *J* = 7.2 Hz, 3H, H^{24}), 1.52 (d, *J* = 7.2 Hz, 3H, H^{13}), 1.49 (s, 9H, H^1), 1.47 (d, *J* = 7.2 Hz, 3H, H^{35}).

^{13}C NMR (100 MHz, Pyr-d_5, 300 K) δ [174.98, 174.77, 173.98, 173.98, 173.49, 173.46 ($C^{10, 14, 21, 25, 32, 36}$)], 156.46 ($C^3$), 136.91 ($C^{Ar}$), [129.30, 128.91, 128.79 (CH^{Ar})], 78.56 (C^2), 67.38 (C^{37}), [50.55, 50.43, 49.26, 48.27, 47.75, 47.75 ($C^{5, 12, 16, 23, 27, 34}$)] , [40.07, 39.15, 38.96 ($C^{8, 19, 30}$)], [36.74, 36.18, 36.08 ($C^{9, 20, 31}$)], 28.92 (C^1), [27.61, 26.99, 26.96 ($C^{6, 17, 28}$)], [22.16, 21.77, 21.07 ($C^{7, 18, 29}$)], [18.44, 18.30, 17.62 ($C^{13, 24, 35}$)].

IR ν 3281, 2934, 1737, 1680, 1635, 1525 cm^{-1}.

HRMS [ESI(+)] *m/z* $[M+Na]^+$ calculated for $[C_{39}H_{58}N_6NaO_9]^+$: 777.4157, found: 777.4127.

***tert*-Butyl ((1*R*,2*R*)-2-(2-(((*S*)-1-(((1*R*,2*R*)-2-(2-(((*S*)-1-(((1*R*,2*R*)-2-(2-(((*S*)-1-(benzyl amino)-1-oxopropan-2-yl)amino)-2-oxoethyl)cyclobutyl)amino)-1-oxopropan-2-yl)amino)-2-oxoethyl)cyclobutyl)amino)-1-oxopropan-2-yl)amino)-2-oxoethyl) cyclobutyl)carbamate (30).**

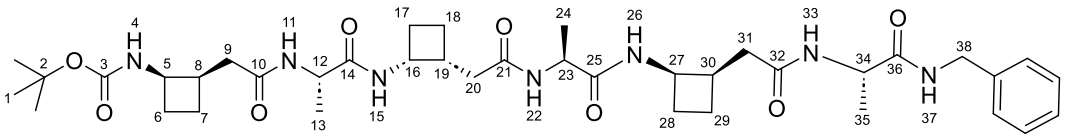

Boc-[(*R*,*R*)-*cis*-^{3,4}CB-GABA-(*S*)-Ala]$_3$-NHBn

$C_{39}H_{59}N_7O_8$
M = 753.94 g/mol

According to the general **procedure A**, **Boc-[(*R*,*R*)-*cis*-^{3,4}CB-GABA-(*S*)-Ala]$_2$-NHBn 26** (51 mg, 0.09 mmol, 1 eq.) was reacted with TFA (207 μL, 2.70 mmol, 30 eq.) in dry CH_2Cl_2 (5 mL) for 1 hour to obtain **TFA·H$_2$N-[(*R*,*R*)-*cis*-^{3,4}CB-GABA-(*S*)-Ala]$_3$-NHBn**. The TFA salt was then dissolved in dry CH_2Cl_2 (5 mL), and DIPEA (94 μL, 0.54 mmol, 6 eq.) was added.

According to the general **procedure C**, **Boc-(*R*,*R*)-*cis*-^{3,4}CB-GABA-(*S*)-Ala-OH 19** (27 mg, 0.09 mmol, 1 eq.) was reacted with DIPEA (31 μL, 0.18 mmol, 2 eq.), **[(*R*,*R*)-*cis*-^{3,4}CB-GABA-(*S*)-Ala]$_2$-NHBn** and HATU (38 mg, 0.10 mmol, 1.05 eq.) in a mixture of CH_2Cl_2/DMF (3/1, 2 mL) for 24 hours. After workup, the crude product was purified by preparative HPLC (mobile phase *n*-hexane:EtOH = 40:60). The product elution (with baseline separation) was collected at 6.7 minutes, followed by solvent evaporation **Boc-[(*R*,*R*)-*cis*-^{3,4}CB-GABA-(*S*)-Ala]$_3$-NHBn 30** (32 mg, 48%) was obtained as a white solid.

***R**$_f$* = 0.51 (CH_2Cl_2:MeOH = 100:6)

Mp = 255-257 °C

^{1}H NMR (400 MHz, Pyr-d_5, 330 K) δ 9.30 (s, 1H, H^{37}), 9.13 (d, *J* = 7.8 Hz, 1H, H^{26}), 9.08 (d, *J* = 6.2 Hz, 1H, H^{22}), 8.96 (d, *J* = 7.4 Hz, 1H, H^{33}), 8.89 (d, *J* = 7.8 Hz, 1H, H^{15}), 8.83 (d, *J* = 6.6 Hz, 1H, H^{11}), 7.49 (d, *J* = 7.6 Hz, 2H, H^{Ar}), 7.41 (s, 1H, H^4), 7.33 (t, *J* = 7.6 Hz, 2H, H^{Ar}), 7.28-7.24 (m, 1H, H^{Ar}), 5.01-4.91 (m, 1H, H^{34}), 4.91-4.75 (m, 4H, H$^{23, 16, 12, 27}$), 4.73-4.66 (m, 2H, H^{38}), 4.52-4.51 (m, 1H, H^5), 3.23-3.12 (m, 1H, H^8), 3.12–2.99 (m, 2H, H$^{30, 19}$), 2.83 (dd, *J* = 14.2, 6.4 Hz, 1H, H^9), 2.77-2.60 (m, 4H, H$^{31, 20, 9, 31}$), 2.55 (dd, *J* = 14.2, 6.2 Hz, 1H, H^{20}), 2.46-2.17 (m, 8H, H$^{28, 17, 17, 6, 18, 29, 18, 28}$), 2.17-2.05 (m, 1H, H^6), 2.05-1.91 (m, 3H, H$^{29, 7}$), 1.91-1.80 (m, 1H, H^7), 1.61 (d, *J* = 7.4 Hz, 3H, H^{35}), 1.59 (d, *J* = 7.0 Hz, 3H, H^{24}), 1.52 (d, *J* = 7.6 Hz, 3H, H^{13}), 1.50 (s, 9H, H^1).

^{13}C NMR (100 MHz, Pyr-d_5, 300 K) δ 175.7 (C^{36}), [174.6, 174.2, 173.8, 173.3 (C$^{10, 21, 25, 32}$)], 173.1 (C^{14}), 156.0 (C^3), 139.7 (C^{Ar}), 128.8, 127.8, 127.3 (CH^{Ar}), 78.1 (C^2), 50.4 (C^{12}), 50.4 (C^{34}), 50.0 (C^{23}), 47.9 (C^5), 47.6 (C^{16}), 47.4 (C^{27}), 43.5 (C^{38}), 38.8 (C$^{8, 19, 30}$), 36.3 (C^9), 35.5 (C^{20}), 35.3 (C^{31}), 28.5 (C^1), 27.2 (C^6), 26.5 (C^{17}), 26.5 (C^{28}), 21.7 (C^7), 20.3 (C^{18}), 20.1 (C^{29}), 18.1 (C^{24}), 17.9 (C^{35}), 17.7 (C^{13}).

IR ν 3284, 3063, 2936, 1681, 1638, 1532 cm^{-1}.

HRMS [ESI(+)] *m/z* [M+Na]$^+$ calculated for [$C_{39}H_{59}N_7NaO_8$]$^+$: 776.4317, found: 776.4279.

3 Synthesis of Cbz-Aatc(Me)-NHMe and derivatives

3.1 General procedures

Procedure E for the deprotection of the Cbz group

To a solution of Cbz capped compound (1 eq.) in MeOH (70 mL/mmol) under argon, was added 10% Pd/C (72 mg/mmol) carefully at room temperature. The suspension was degassed then stirred for 30 minutes under H_2 at atmospheric pressure. The mixture was filtered through a celite pad, and the celite pad was washed with small portions of MeOH. The combined filtrate and washings were passed through a 0.45 μm PTFE membrane then evaporated to dryness under reduced pressure to leave the deprotected amine used directly in the following step.

Procedure F for the coupling reactions with compound **33**

To a cold (–30 °C) solution of compound **33** (1 eq.) in dry DMF (5 mL/mmol) in an argon-flushed flask, were added successively NMM (1 eq.) and IBCF (1 eq.). The solution was stirred for 1.5 hours just below –20 °C, then a solution of the above-described amine in dry DMF (3 mL/mmol) was added; the source flask was rinsed with dry DMF (2 mL/mmol) which was then introduced to the reaction mixture. The mixture was stirred at –20 °C for 18 hours then allowed to warm to room temperature. The solvent was removed by co-evaporation with heptane under reduced pressure and the residue was partitioned between CH_2Cl_2 (20 mL/mmol) and 5% aqueous $NaHCO_3$ (20 mL/mmol). The organic layer was collected, and the aqueous layer was extracted with CH_2Cl_2 (6 × 10 mL/mmol). The combined organic layers were washed with 5% aqueous $NaHCO_3$ (2 × 10 mL/mmol), dried over Na_2SO_4, filtered and concentrated under reduced pressure. The residue was purified by flash chromatography to give the resulting peptide.

Procedure G for the deprotection of the *N*-Boc group

To an ice-cooled solution of Aatc(Boc) compound (1 eq.) in dry CH_2Cl_2 (1 mL/mmol) under argon, 4 M HCl solution in dioxane (200 eq.) was added dropwise. The resulting solution was stirred at 0 °C for 30 minutes then allowed to warm to room temperature and reacted for 3-15 hours. After the reaction was completed, the solution was concentrated under reduced pressure and the remaining volatiles were co-evaporation with $CHCl_3$ (4 × 1 ml/mmol) under reduced pressure to leave the deprotected azetidine as its hydrochloride salt, used directly in the next step.

3.2 Synthesis of Cbz-Aatc(Me)-NHMe **42**

3-Benzyloxycarbonylamino-1-(*tert*-butoxycarbonyl)azetidine-3-carboxylic acid (33).

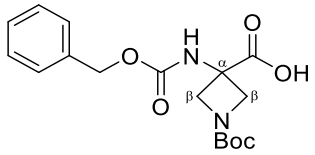

$C_{17}H_{22}N_2O_6$
M = 350.37 g/mol

In a 250 mL flask were added 3-amino-1-(*tert*-butoxycarbonyl)azetidine-3-carboxylic acid (3.0 g, 13.86 mmol, 1 eq.) and Na_2CO_3 (4.4 g, 41.58 mmol, 4.5 eq.) successively, then a mixture of H_2O/dioxane (2/1, 90 mL) was added. When all the solids had dissolved, the solution was cooled to 0 °C in an ice-water bath and CbzCl (1.0 mL, 6.93 mmol, 0.5 eq.) was added dropwise. The solution was allowed warm to room temperature and stirred for 24 hours. The solution was then cooled to 0 °C and more CbzCl (1.0 mL, 6.93 mmol, 0.5 eq.) was added dropwise. This procedure was repeated one more time, so that a total of 1.5 eq. of CbzCl had been added to the solution. After a further 24 hours at room temperature, dioxane was removed slowly under reduced pressure. The remaining aqueous solution was washed with hexane (3 × 150 mL) then cooled to 0 °C and slowly acidified with 2 M HCl aqueous solution until pH = 1. The solution was then extracted with CH_2Cl_2 (6 × 150 mL) and the combined organic layers were dried over Na_2SO_4, filtered and concentrated to dryness under reduced pressure. The residue was purified by flash chromatography (CH_2Cl_2:MeOH:AcOH, 100:1:1) compound **33** (4.55 g, 93%) was obtained as a white solid.

***R**f* = 0.25 (CH_2Cl_2:MeOH:AcOH = 95:5:1)

Mp = 173-175 °C

^{1}H NMR (400 MHz, CD_3OD, 300 K) δ 7.64-7.08 (m, 5H, CH^{Ar}), 5.11 (s, 1H, CH_2^{Cbz}), 4.52-4.14 (m, 2H, $C^{\beta}H$), 4.14-3.86 (m, 2H, $C^{\beta}H$), 1.47 (s, 9H, *t*Bu).

^{13}C NMR (100 MHz, CD_3OD, 300 K) δ 174.2 (CO^{acid}), 157.9 (CO^{Boc}, CO^{Cbz}), 137.9 (C^{Ar}), 129.5, 129.0, 128.8 (CH^{Ar}), 81.5 (C^{tBu}), 67.7 (CH_2^{Cbz}), 59.5, 58.2 (br, $C^{\beta}H_2$), 54.1 (C^{α}), 28.6 (CH_3^{Boc}).

IR ν 3242, 2970, 1715, 1667, 1529 cm^{-1}.

HRMS [ESI(+)] *m/z* $[M+Na]^+$ calculated for $[C_{17}H_{22}N_2NaO_6]^+$: 373.1376; found: 373.1358.

***tert*-Butyl 3-benzyloxycarbonylamino-3-(methylcarbamoyl)azetidine-1-carboxylate (34).**

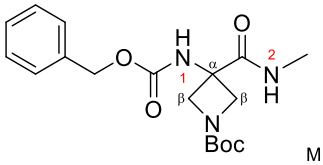

$C_{18}H_{25}N_3O_5$
M = 363.41 g/mol

Cbz-Aatc(Boc)-NHMe

To a cold (–20 °C) solution of compound **33** (200 mg, 0.57 mmol, 1 eq.) in dry THF (2 mL) under argon were added successively NMM (63 µL, 0.57 mmol, 1 eq.) and IBCF (74 µL, 0.57 mmol, 1 eq.). The activation period was 10 minutes at –20 °C. Then a solution of 40% aqueous $MeNH_2$ (0.5 mL, 5.7 mmol, 10 eq.) in THF (0.5 mL) was added and the resulting solution was stirred at –20 °C for 1.5 hours. 5% aqueous $NaHCO_3$ (5 mL) was added to the solution and the mixture was stirred at room temperature for 1 hour. CH_2Cl_2 (20 mL) was added, and the organic layer was collected. The aqueous layer was extracted with CH_2Cl_2 (5 × 20 mL). The combined organic layers were washed with 5% aqueous $NaHCO_3$ (2 × 5 mL), then dried over Na_2SO_4, filtered and concentrated under reduced pressure. The residue was purified by flash chromatography (CH_2Cl_2:MeOH, gradient from 100:3 to 100:5) to give **Cbz-Aatc(Boc)-NHMe 34** (176 mg, 85%) as a white solid.

***R**$_f$* = 0.25 (CH_2Cl_2:MeOH = 100:3)

Mp = 63-65 °C

^{1}H NMR (400 MHz, $CDCl_3$, 310 K) δ 7.44-7.21 (m, 5H, CH^{Ar}), 6.57 (bs, 1H, NH^2), 6.11 (bs, 1H, NH^1), 5.10 (s, 2H, $CH_2{}^{Cbz}$), 4.22 (d, *J* = 9.0 Hz, 2H, $C^{\beta}H^b$), 4.08 (d, *J* = 9.0 Hz, 2H, $C^{\beta}H^a$), 2.80 (d, *J* = 4.8 Hz, 3H, N^2CH_3), 1.43 (s, 9H, *t*Bu).

^{13}C NMR (100 MHz, $CDCl_3$, 310 K) δ 171.5 (CO^{amide}), 156.6 (CO^{Boc}), 155.5 (CO^{Cbz}), 135.9 (C^{Ar}), 128.7, 128.5, 128.2 (CH^{Ar}), 80.4 (C^{tBu}), 67.3 ($CH_2{}^{Cbz}$), 57.8 (br, $C^{\beta}H_2$), 53.6 (C^{α}), 28.4 ($CH_3{}^{tBu}$), 26.8 (N^2CH_3).

IR ν 3307, 2975, 1657, 1523 cm^{-1}.

HRMS [ESI(+)] *m/z* $[M+Na]^+$ calculated for $[C_{18}H_{25}N_3NaO_5]^+$: 386.1686; found: 386.1675.

Benzyl (1-methyl-3-(methylcarbamoyl)azetidin-3-yl)carbamate (42).

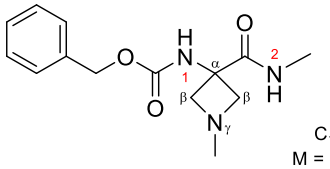

$C_{14}H_{19}N_3O_3$
M = 277.32 g/mol

Cbz-Aatc(Me)-NHMe

According to the general **procedure G**, **Cbz-Aatc(Boc)-NHMe 34** (138 mg, 0.38 mmol, 1 eq.) was reacted with 4 M HCl solution in dioxane (4.8 mL, 19.00 mmol, 50 eq.) in dry CH_2Cl_2 (10 mL) at 0 °C for 30 minutes, then at room temperature for 3 hours. After solvent evaporation to leave the deprotected azetidine **41** as its hydrochloride salt.

To an ice-cooled solution of the above-described azetidine hydrochloride in MeOH (3 mL) were added successively acetic acid (109 µL, 1.90 mmol, 5 eq.), 37% aqueous formaldehyde (285 µL, 3.80 mmol, 10 eq.) and $NaBH_3CN$ (72 mg, 1.14 mmol, 3 eq.). The mixture was then allowed warm to room temperature and stirred overnight. The solvent was removed under reduced pressure and the residue was partitioned between CH_2Cl_2 (30 mL) and saturated aqueous $NaHCO_3$ solution (30 mL). The organic layer was collected, and the aqueous layer was extracted with CH_2Cl_2 (9 × 30 mL). The combined organic layers were dried over Na_2SO_4, filtered and concentrated under reduced pressure. The residue was purified by flash chromatography (CH_2Cl_2:MeOH, gradient from 10:1 to 1:1). Appropriate fractions were pooled and evaporated. The residue was taken up in $CHCl_3$ (5 mL) and the turbid solution was filtered through a 0.45 µm PTFE membrane and the filtrate was evaporated, **Cbz-Aatc(Me)-NHMe 42** (87 mg, 83%) was obtained as a white solid.

***R**$_f$* = 0.20 (CH_2Cl_2:MeOH = 10:1)

Mp = 161-163 °C

^{1}H NMR (400 MHz, $CDCl_3$, 300 K) δ 8.23 (bs, 1H, NH^2), 7.45-7.28 (m, 5H, CH^{Ar}), 6.35 (bs, 1H, NH^1), 5.11 (s, 2H, $CH_2{}^{Cbz}$), 4.18-3.87 (m, 2H, $C^{\beta}H^a$), 3.75-3.36 (m, 2H, $C^{\beta}H^b$), 2.90 (d, *J* = 4.8 Hz, 3H, N^2CH_3), 2.51 (s, 3H, $N^{\gamma}CH_3$).

^{13}C NMR (100 MHz, $CDCl_3$, 300 K) δ 172.9 (CO^{amide}), 155.3(CO^{Cbz}), 136.4 (C^{Ar}), 128.7, 128.3, 128.1 (CH^{Ar}), 66.6 ($CH_2{}^{Cbz}$), 63.1 (br, $C^{\beta}H_2$), 53.7 (C^{α}), 44.7 ($N^{\gamma}CH_3$), 26.7 (N^2CH_3).

IR ν 3305, 2780, 1712, 1649, 1573, 1546 cm^{-1}.

HRMS [ESI(+)] *m/z* $[M+Na]^+$ calculated for $[C_{14}H_{19}N_3NaO_3]^+$: 300.1319; found: 300.1313.

3.3 Synthesis of Cbz-[Aatc(Me)]$_2$-NHMe **44**

***tert*-Butyl 3-benzyloxycarbonylamino-3-((1-*tert*-butoxycarbonyl)-3-(methyl carbamoyl)azetidin-3-yl)carbamoyl)azetidine-1-carboxylate (36).**

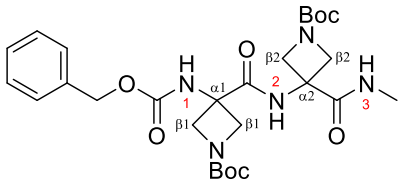

$C_{27}H_{39}N_5O_8$
M = 561.64 g/mol

Cbz-[Aatc(Boc)]$_2$-NHMe

According to the general **procedure E**, **Cbz-Aatc(Boc)-NHMe 34** (363 mg, 1.00 mmol, 1 eq.) was reacted with 10% Pd/C (72 mg) in MeOH (70 mL) for 30 minutes under H_2 at atmospheric pressure. After solvent evaporation to leave the deprotected amine **35** as a white solid.

According to the general **procedure F**, compound **33** (350 mg, 1.00 mmol, 1 eq.) was reacted with NMM (111 µL, 1.00 mmol, 1 eq.) and IBCF (130 µL, 1.00 mmol, 1 eq.) in dry DMF (5 mL) at –20 °C for 1.5 hours. Then a solution of the above-described deprotected amine in dry DMF (5 mL) was added and the mixture was stirred at –20 °C for 18 hours. After workup and purification on flash chromatography (CH_2Cl_2:MeOH, gradient from 100:3 to 100:5) **Cbz-[Aatc(Boc)]$_2$-NHMe 36** (399 mg, 71%) was obtained as a white solid.

***R**$_f$* = 0.30 (CH_2Cl_2:MeOH = 100:5)

Mp = 201-203 °C

^{1}H NMR (400 MHz, $CDCl_3$, 300 K) δ 7.41-7.29 (m, 5H, CH^{Ar}), 7.24 (bs, 1H, NH^2), 6.78 (bs, 1H, NH^3), 6.20 (bs, 1H, NH^1), 5.14 (s, 2H, CH_2^{Cbz}), 4.53-4.16 (m, 4H, $C^{\beta}H^b$), 3.95 (d, *J* = 9.2 Hz, 2H, $C^{\beta2}H^a$), 3.89 (d, *J* = 9.2 Hz, 2H, $C^{\beta1}H^a$), 2.77 (d, *J* = 4.4 Hz, 3H, N^3CH_3), 1.43 (s, 9H, *t*Bu), 1.43 (s, 9H, *t*Bu).

^{13}C NMR (100 MHz, $CDCl_3$, 300 K) δ 170.7, 170.4 (CO^{amide}), 156.5 (CO^{Cbz}), 156.4, 156.2 (CO^{Boc}), 135.6 (C^{Ar}), 128.9, 128.4 (CH^{Ar}), 80.7, 80.6 (C^{tBu}), 68.1 (CH_2^{Cbz}), 57.9 (br, $C^{\beta}H_2$), 54.1, 53.9 (C^{α}), 28.4 (CH_3^{tBu}), 26.9 (N^3CH_3).

IR ν 3344, 3285, 3230, 2918, 2948, 1694, 1679, 1643 cm^{-1}.

HRMS [ESI(+)] *m/z* $[M+Na]^+$ calculated for $[C_{27}H_{39}N_5NaO_8]^+$: 584.2696; found: 584.2667.

Benzyl (1-methyl-3-((1-methyl-3-(methylcarbamoyl)azetidin-3 yl)carbamoyl) azetidin-3-yl)carbamate (44).

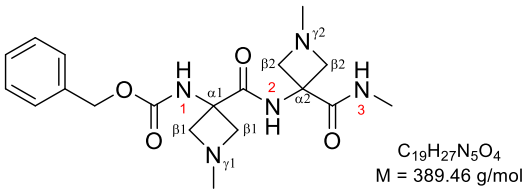

Cbz-[Aatc(Me)]$_2$-NHMe

According to the general **procedure G**, **Cbz-[Aatc(Boc)]$_2$-NHMe 36** (105 mg, 0.19 mmol, 1 eq.) was reacted with 4 M HCl solution in dioxane (4.6 mL, 19.00 mmol, 100 eq.) in dry CH_2Cl_2 (5 mL) at 0 °C for 30 minutes, then at room temperature for 4 hours. After solvent evaporation to leave the deprotected diazetidine **43** as its dihydrochloride salt.

To an ice-cooled solution of the above-described diazetidine dihydrochloride in MeOH (4 mL) were added successively acetic acid (57 µL, 1.00 mmol, 5 eq.), 37% aqueous formaldehyde solution (143 µL, 1.90 mmol, 10 eq.) and $NaBH_3CN$ (36 mg, 0.57 mmol, 3 eq.). The mixture was allowed to warm to room temperature and stirred for 10 hours. The mixture was cooled to 0 °C, then acetic acid (57 µL, 1.00 mmol, 5 eq.), 37% aqueous formaldehyde solution (143 µL, 1.90 mmol, 10 eq.) and $NaBH_3CN$ (36 mg, 0.57 mmol, 3 eq.) were added. The mixture was allowed to warm to room temperature and stirred for a further 10 hours. The solvent was removed under reduced pressure and the residue was partitioned between CH_2Cl_2 (10 mL) and saturated aqueous $NaHCO_3$ solution (20 mL). The organic layer was collected, and the aqueous layer was extracted with CH_2Cl_2 (10 × 10 mL). The combined organic layers were dried over Na_2SO_4, filtered and concentrated under reduced pressure. The residue was purified by preparative HPLC (mobile phase CH_3CN:MeOH = 43:57, + 1% aq. NH_4OH). The product elution (with baseline separation) was collected at 8.7 minutes, followed by solvent evaporation **Cbz-[Aatc(Me)]$_2$-NHMe 44** (56 mg, 75%) was obtained as a white solid.

R_f = 0.35 (CH_3CN:MeOH:NH_4OH = 1:1:0.1)

Mp = 183-185 °C

^{1}H NMR (400 MHz, $CDCl_3$, 300 K) δ9.05 (bs, 1H, NH), 7.94 (bs, 1H, NH), 7.39-7.26 (m, 5H, CH^{Ar}), 6.13 (bs, 1H, NH^{1}), 5.10 (s, 2H, CH_2^{Cbz}), 3.98-3.68 (m, 4H, $C^{\beta}H^{a}$), 3.64-3.53 (m, 4H, $C^{\beta}H^{b}$), 2.89 (d, J = 4.8 Hz, 3H, $N^{3}CH_3$), 2.44 (s, 6H, $N^{\gamma}CH_3$).

^{13}C NMR (100 MHz, $CDCl_3$, 300 K) δ 173.1, 173.0 (CO^{amide}), 155.4 (CO^{Cbz}), 136.5 (C^{Ar}), 128.6, 128.2, 128.0 (CH^{Ar}), 66.6 (CH_2^{Cbz}), 63.3, 63.2 ($C^{\beta}H_2$), 54.5, 54.4 (C^{α}), 45.3, 45.2 ($N^{\gamma}CH_3$), 26.6 ($N^{3}CH_3$).

IR ν 3374, 3268, 2918, 2772, 1696, 1661, 1587, 1518 cm^{-1}.

HRMS [ESI(+)] *m/z* $[M+Na]^+$ calculated for $[C_{19}H_{28}N_5NaO_8]^+$: 412.1955; found: 412.1933.

3.4 Synthesis of Cbz-[Aatc(Me)]$_3$-NHMe **46**

tert-Butyl 3-benzyloxycarbonylamino-3-((1-(_tert_-butoxycarbonyl)-3-((1-(_tert_-butoxycarbonyl)-3-(methylcarbamoyl)azetidin-3-yl)carbamoyl)azetidin-3-yl)carbamoyl)azetidine-1-carboxylate (38)

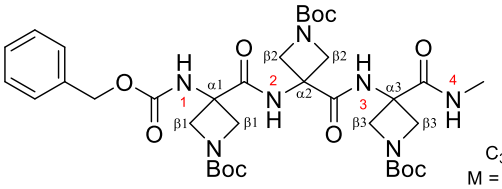

Cbz-[Aatc(Boc)]$_3$-NHMe

According to the general **procedure E**, **Cbz-[Aatc(Boc)]$_2$-NHMe 36** (421 mg, 0.75 mmol, 1 eq.) was reacted with 10% Pd/C (54 mg) in MeOH (50 mL) for 30 minutes under H_2 at atmospheric pressure. After solvent evaporation to leave the deprotected amine **37** as a white solid.

According to the general **procedure F**, compound **33** (291 mg, 0.83 mmol, 1.1 eq.) was reacted with NMM (124 µL, 1.13 mmol, 1.5 eq.) and IBCF (147 µL, 1.13 mmol, 1.5 eq.) in dry DMF (5 mL) at –20 °C for 1.5 hours. Then a solution of the above-described deprotected amine in dry DMF (5 mL) was added and stirred at –20 °C for 18 hours. After workup and purification on flash chromatography (CH_2Cl_2:EtOAc:MeOH, gradient from 40:40:1 to 10:10:1) **Cbz-[Aatc(Boc)]$_3$-NHMe 38** (325 mg, 57%) was obtained as a white solid.

***R**$_f$* = 0.31 (CH_2Cl_2:MeOH = 100:5)

Mp = 172-174 °C

^{1}H NMR (400 MHz, $CDCl_3$, 310 K) δ 7.69 (bs, 1H, NH^3), 7.66 (bs, 1H, NH^2), 7.39-7.32 (m, 5H, CH^{Ar}), 6.85 (bs, 1H, NH^1), 6.79 (d, J = 4.8 Hz, 1H, NH^4), 5.16 (s, 2H, CH_2^{Cbz}), 4.63-4.22 (m, 6H, $C^{\beta}H^b$), 3.93-3.77 (m, 6H, $C^{\beta}H^a$), 2.79 (d, J = 4.8 Hz, 3H, N^4CH_3), 1.44 (s, 9H, *t*Bu), 1.43 (s, 9H, *t*Bu), 1.42 (s, 9H, *t*Bu).

^{13}C NMR (100 MHz, $CDCl_3$, 300 K) δ 173.1, 172.0, 170.9 (CO^{amide}), 157.7 (CO^{Cbz}), 156.0, 155.91 (CO^{Boc}), 135.8 (C^{Ar}), 128.9, 128.5, 127.5 (CH^{Ar}), 80.5, 80.3, 80.2 (C^{tBu}), 68.0 (CH_2^{Cbz}), 57.4 (br, $C^{\beta}H_2$), 54.0, 53.9, 53.8 (C^{α}), 28.4 (CH_3^{tBu}), 26.9 (N^4CH_3).

IR ν 3521, 3305, 2978, 1670, 1523 cm^{-1}.

HRMS [ESI(+)] *m/z* $[M+Na]^+$ calculated for $[C_{36}H_{53}N_7NaO_{11}]^+$: 782.3695; found: 782.3665.

Benzyl (1-methyl-3-((1-methyl-3-((1-methyl-3-(methylcarbamoyl)azetidin-3-yl)carbamol)azetidin-3-yl)carbamoyl)azetidin-3-yl)carbamate (46).

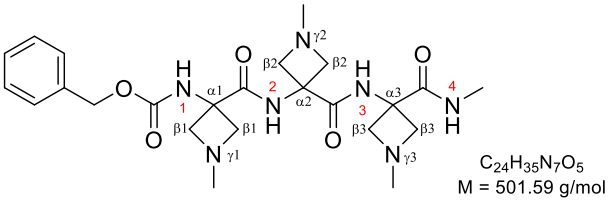

Cbz-[Aatc(Me)]$_3$-NHMe

According to the general **procedure G**, **Cbz-[Aatc(Boc)]$_3$-NHMe 38** (95 mg, 0.13 mmol, 1 eq.) was reacted with 4 M HCl solution in dioxane (6.7 mL, 25.00 mmol, 200 eq.) in dry CH_2Cl_2 (8 mL) at 0 °C for 30 minutes, then at room temperature for 5 hours. After solvent evaporation to leave the deprotected triazetidine **45** as its trihydrochloride salt.

To an ice-cooled solution of the above-described triazetidine trihydrochloride in MeOH (4 mL) were added successively acetic acid (43 µL, 0.75 mmol, 6 eq.), 37% aqueous formaldehyde solution (141 µL, 1.88 mmol, 15 eq.) and $NaBH_3CN$ (71 mg, 1.13 mmol, 9 eq.). The mixture was allowed to warm to room temperature and stirred for 10 hours. The mixture was cooled to 0 °C, then acetic acid (43 µL, 0.75 mmol, 6 eq.), 37% aqueous formaldehyde (141 µL, 1.88 mmol, 15 eq.) and $NaBH_3CN$ (71 mg, 0.38 mmol, 9 eq.) were added. The mixture was allowed to warm to room temperature and stirred for a further 10 hours. This procedure was repeated one more time, so that three aliquots of reagents had been added to the solution. After a final 10 hours stirring period at room temperature, the solvent was removed under reduced

pressure and the residue was partitioned between CH_2Cl_2 (10 mL) and saturated aqueous $NaHCO_3$ solution (20 mL). The organic layer was collected, and the aqueous layer was extracted with CH_2Cl_2 (10 × 10 mL). The combined organic layers were dried over Na_2SO_4, filtered, and concentrated under reduced pressure. The residue was purified by preparative HPLC (mobile phase CH_3CN:MeOH = 55:45, + 0.4% aq. NH_4OH). The product elution (with baseline separation) was collected at 5.9 minutes, followed by solvent evaporation **Cbz-[Aatc(Me)]$_3$-NHMe 46** (41 mg, 65%) was obtained as a white solid.

***R**$_f$* = 0.25 (CH_3CN:MeOH:NH_4OH = 1:1:0.1)

Mp = 58-60 °C

^{1}H NMR (400 MHz, $CDCl_3$, 300 K) δ8.79 (bs, 1H, NH), 8.48 (bs, 1H, NH), 7.78 (bs, 1H, NH), 7.42-7.28 (m, 5H, CH^{Ar}), 6.27 (bs, 1H, NH^1), 5.09 (s, 2H, CH_2^{Cbz}), 3.87-3.68 (m, 6H, $C^{\beta}H^a$), 3.65-3.57 (m, 6H, $C^{\beta}H^b$), 2.87 (d, *J* = 4.8 Hz, 3H, N^4CH_3), 2.43 (s, 6H, $N^{\gamma}CH_3$), 2.42 (s, 3H, $N^{\gamma}CH_3$).

^{13}C NMR (100 MHz, $CDCl_3$, 300 K) δ 173.0, 172.6, 171.6 (CO^{amide}), 155.9 (CO^{Cbz}), 136.2 (C^{Ar}), 128.7, 128.4, 128.2 (CH^{Ar}), 67.0 (CH_2^{Cbz}), 63.3, 63.2 ($C^{\beta}H_2$), 55.3, 54.8, 54.6 (C^{α}), 45.3, 45.1, 45.0 ($N^{\gamma}CH_3$), 26.7 (N^4CH_3).

IR ν 3309, 2923, 2854, 1652, 1523 cm^{-1}.

HRMS [ESI(+)] *m/z* $[M+Na]^+$ calculated for $[C_{24}H_{35}N_7NaO_5]^+$: 524.2592; found: 524.2576.

3.5 Synthesis of Cbz-[Aatc(Me)]$_4$-NHMe **48**

***tert*-Butyl 3-benzyloxycarbonylamino-3-((1-(*tert*-butoxycarbonyl)-3-((1-(*tert*-butoxycarbonyl)-3-((1-(*tert*-butoxycarbonyl)-3-(methylcarbamoyl)azetidin-3-yl)carbamoyl)azetidin-3-yl)carbamoyl)azetidin-3-yl)carbamoyl)azetidine-1-carboxylate (40).**

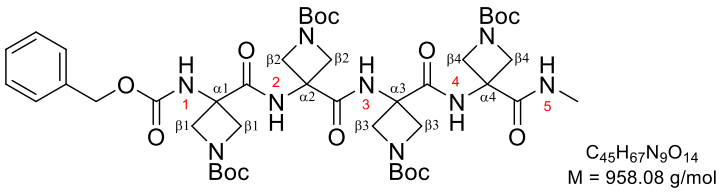

Cbz-[Aatc(Boc)]$_4$-NHMe

According to the general **procedure E**, **Cbz-[Aatc(Boc)]$_3$-NHMe 38** (152 mg, 0.20 mmol, 1 eq.) was reacted with 10% Pd/C (14 mg) in MeOH (15 mL) for 30 minutes under H_2 at atmospheric pressure. After solvent evaporation to leave the deprotected amine **39** as a white solid.

According to the general **procedure F**, compound **33** (85 mg, 0.22 mmol, 1.1 eq.) was reacted with NMM (33 µL, 0.30 mmol, 1.5 eq.) and IBCF (26 µL, 0.21 mmol, 1.05 eq.) in dry DMF (2 mL) at –20 °C for 1.5 hours. Then a solution of the above-described deprotected amine in dry DMF (3 mL) was added and stirred at –20 °C for 18 hours. After workup and purification on flash chromatography (Et_2O:CH_2Cl_2:MeOH, gradient from 30:0:1 to 30:10:1) **Cbz-[Aatc(Boc)]$_4$-NHMe 40** (115 mg, 60%) was obtained as a white solid.

***R**$_f$* = 0.45 (Et_2O:MeOH = 20:1)

Mp = 182-184°C

^{1}H NMR (400 MHz, $CDCl_3$, 315 K) δ 8.48 (bs, 1H), 8.11 (bs, 1H), 7.80 (bs, 1H), 7.71 (bs, 1H), 7.44-7.29 (m, 5H, CH^{Ar}), 7.01 (d, *J* = 4.4 Hz, 1H, NH^5), 5.20 (s, 2H, CH_2^{Cbz}), 4.63-4.18 (m, 8H, $C^{\beta}H^b$), 4.07-3.71 (m, 8H, $C^{\beta}H^a$), 2.78 (d, *J* = 4.4 Hz, 3H, N^5CH_3), 1.44 (s, 9H, *t*Bu), 1.43 (s, 9H, *t*Bu), 1.42 (s, 9H, *t*Bu), 1.42 (s, 9H, *t*Bu).

^{13}C NMR (100 MHz, $CDCl_3$, 315 K) δ 173.3, 172.1, 171.9, 170.8 (CO^{amide}), 157.8 (CO^{Cbz}), 156.6, 156.0, 155.9, (CO^{Boc}), 135.7 (C^{Ar}), 129.1, 128.8, 128.0 (CH^{Ar}), 80.9, 80.7, 80.4, 80.3 (C^{tBu}), 68.6 (CH_2^{Cbz}), 57.9 (br, $C^{\beta}H_2$), 54.4, 54.3, 54.1, 54.0 (C^{α}), 28.6, 28.5 (CH_3^{tBu}), 26.9 (N^5CH_3).

IR ν 3298, 2976, 2936, 2885, 1658, 1526 cm^{-1}.

HRMS [ESI(+)] *m/z* $[M+Na]^+$ calculated for $[C_{45}H_{67}N_9NaO_{14}]^+$: 980.4700; found: 980.4654.

Benzyl (1-methyl-3-((1-methyl-3-((1-methyl-3-((1-methyl-3 (methylcarbamoyl)azetidin-3-yl)carbamoyl)azetidin-3-yl)carbamoyl)azetidin-3-yl)carbamoyl)azetidin-3-yl)carbamate (48).

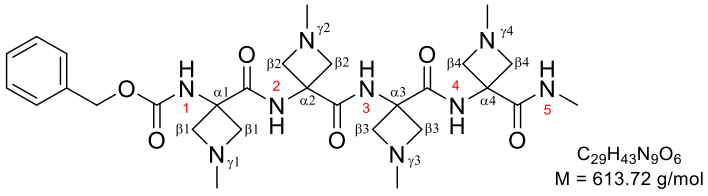

$C_{29}H_{43}N_9O_6$
M = 613.72 g/mol

Cbz-[Aatc(Me)]$_4$-NHMe

According to the general **procedure G**, **Cbz-[Aatc(Boc)]$_4$-NHMe 40** (96 mg, 0.10 mmol, 1 eq.) was reacted with 4 M HCl solution in dioxane (5.4 mL, 20.00 mmol, 200 eq.) in dry CH_2Cl_2 (10 mL) at 0 °C for 30 minutes, then at room temperature for 15 hours. After solvent evaporation to leave the deprotected tetraazetidine **47** as its tetrahydrochloride salt.

To an ice-cooled solution of the above-described tetraazetidine tetrahydrochloride in MeOH (3 mL) were added successively acetic acid (32 µL, 0.60 mmol, 6 eq.), paraformaldehyde (15 mg, 0.50 mmol, 5 eq.) and $NaBH_3CN$ (17 mg, 0.30 mmol, 3 eq.). The mixture was allowed to warm to room temperature and stirred for 10 hours. The mixture was cooled to 0 °C, then acetic acid (32 µL, 0.60 mmol, 6 eq.), paraformaldehyde (15 mg, 0.50 mmol, 5 eq.) and $NaBH_3CN$ (17 mg, 0.30 mmol, 3 eq.) were added. The mixture was allowed to warm to room temperature and stirred for a further 10 hours. This procedure was repeated two more times, so that four aliquots of reagents had been added to the solution. After the final 10 hours stirring period at room temperature, the solvent was removed under reduced pressure and the residue was partitioned between CH_2Cl_2 (10 mL) and saturated aqueous $NaHCO_3$ solution (20 mL). The organic layer was collected, and the aqueous layer was extracted with CH_2Cl_2 (10 × 10 mL). The combined organic layers were dried over Na_2SO_4, filtered and concentrated under reduced pressure. The residue was purified by preparative HPLC (mobile phase CH_3CN:MeOH = 65:35, + 0.25% aq. NH_4OH). The product elution (with baseline separation) was collected at 10.4 minutes, followed by solvent evaporation **Cbz-[Aatc(Me)]$_4$-NHMe 48** (28 mg, 46%) was obtained as a white solid.

***R**$_f$* = 0.12 (CH_3CN:MeOH:NH_4OH = 1:1:0.1)

Mp = 131-134 °C

^{1}H NMR (400 MHz, $CDCl_3$, 300 K) δ 8.79 (bs, 1H), 8.26 (bs, 1H), 7.98 (bs, 1H), 7.42-7.30 (m, 5H, CH^{Ar}), 7.29 (signal masked by aromatic protons, NH), 6.77 (bs, 1H, NH^1), 5.08 (s, 2H, CH_2^{Cbz}), 3.79-3.46 (m, 16H, $C^{\beta}H_2$), 2.82 (d, *J* = 4.8 Hz, 3H, N^5CH_3), 2.44-2.33 (m, 12H, $N^{\gamma}CH_3$).

^{13}C NMR (100 MHz, $CDCl_3$, 300 K) δ 174.4, 172.3, 170.8, 170.7 (CO^{amide}), 156.6 (CO^{Cbz}), 136.0 (C^{Ar}), 128.8, 128.6, 128.5 (CH^{Ar}), 67.4 (CH_2^{Cbz}), 63.9, 63.3, 62.9, 62.5 ($C^{\beta}H_2$), 55.7, 55.4, 55.3, 54.9 (C^{α}), 45.3, 45.2, 44.5, 43.4 ($N^{\gamma}CH_3$), 26.9 (N^5CH_3).

IR ν 3314, 2954, 2919, 2850, 1655, 1528 cm^{-1}.

HRMS [ESI(+)] *m/z* $[M+Na]^+$ calculated for $[C_{29}H_{43}N_9NaO_6]^+$: 636.3229; found: 636.3200

4 Synthesis of Aatc and Attc oxide derivatives

4.1 Purification of *m*-CPBA

Commercial *m*-CPBA (10 g, 70%-75% purity) was washed thrice with buffer solution (500 mL, pH = 7.5, a mixture of 0.1 M NaOH:0.2 M KH_2PO_4:H_2O = 41:25:34), filtered and then left under vacuum to afford *m*-CPBA as a dry, white solid (6.1 g, detected by ^{1}H NMR was pure).

4.2 Synthesis of Cbz-Aatc(Me,O)-NHMe *trans* **49**

3-(((Benzyloxy)carbonyl)amino)-1-methyl-3-(methylcarbamoyl)azetidine-1-oxide (49).

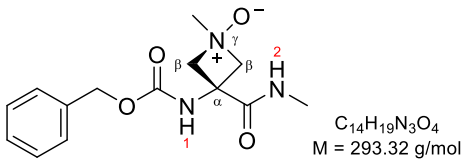

Cbz-Aatc(Me,O)-NHMe *trans*

A solution of **Cbz-Aatc(Me)-NHMe 42** (28 mg, 0.10 mmol, 1 eq.) in dry CH_2Cl_2 (4 mL) under an argon atmosphere, was cooled at –78 °C. Potassium carbonate (28 mg, 0.20 mmol, 2 eq.) and *m*-CPBA (21 mg, 0.10 mmol, 1 eq.) were added successively. The mixture was stirred for 3 hours at –78 °C and then allowed to warm to room temperature. The suspension was filtered through a 0.45 μm PTFE membrane, the filtrate was collected and evaporated under reduced pressure. The crude product was purified by flash chromatography (CH_3CN:MeOH:NH_4OH, gradient from 20:20:1 to 20:20:2), **Cbz-Aatc(Me,O)-NHMe *trans* 49** (24 mg, 83%) was obtained as a white solid.

***R**$_f$* = 0.21 (CH_3CN:MeOH:NH_4OH = 20:20:1)

Mp = 149-151 °C

^{1}H NMR (400 MHz, $CDCl_3$, 300 K) δ 11.61 (bs, 1H, NH^2), 7.42-7.31 (m, 5H, CH^{Ar}), 6.76 (bs, 1H, NH^1), 5.38 (d, *J* = 11.6 Hz, 2H, $C^{\beta}H^a$), 5.13 (s, 2H, CH_2^{Cbz}), 4.22 (d, *J* = 11.6 Hz, 2H, $C^{\beta}H^b$), 3.43 (s, 3H, $N^{\gamma}CH_3$), 2.92 (d, *J* = 4.5 Hz, 3H, N^2CH_3).

^{13}C NMR (100 MHz, $CDCl_3$, 300 K) δ 170.3 (CO^{amide}), 155.1 (CO^{Cbz}), 136.0 (C^{Ar}), 128.8, 128.5, 128.0 (CH^{Ar}), 77.7 ($C^{\beta}H_2$), 67.0 (CH_2^{Cbz}), 58.5 ($N^{\gamma}CH_3$), 51.8 (C^{α}), 27.0 (N^2CH_3).

IR ν 3512, 3369, 2923, 2854, 1698, 1670, 1574, 1537 cm^{-1}.

HRMS [ESI(+)] *m/z* $[M+Na]^+$ calculated for $[C_{14}H_{19}N_3NaO_4]^+$: 316.1268, found: 316.1260.

4.3 Synthesis of Cbz-Attc-NHMe **54**

2-Thia-5,7-diazaspiro[3.4]octane-6,8-dione (51).

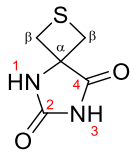

$C_5H_6N_2O_2S$
M = 158.18 g/mol

To a suspension of $(NH_4)_2CO_3$ (960 mg, 10.00 mmol, 2.2 eq.) in MeOH (25 mL) was added KCN (320 mg, 5.00 mmol, 1.1 eq.). The suspension was stirred for 30 minutes at 40 °C until all the solids were dissolved, then a solution of thietane-3-one **50** (400 mg, 4.50 mmol, 1 eq.) in MeOH (6 mL) was added. The mixture was stirred for 30 minutes at 40 °C, then 3 days at 25 °C. The solvent was removed under reduced pressure. The resulting dark brown sticky solid was treated with 6 M aqueous HCl solution until pH = 1. Then the mixture was filtered and washed with a small amount of ice water, the crude **hydantoin 51** (584 mg, 82%) was obtained as a brown solid. This compound was used directly in the next reaction without further purification.

R_f = 0.60 (EtOAc:MeOH = 98:2).

^{1}H NMR (400 MHz, DMSO-d_6, 300 K) δ 10.62 (bs, 1H, NH^3), 8.80 (bs, 1H, NH^1), 3.52-2.42 (m, 4H, $C^\beta H$).

^{13}C NMR (100 MHz, DMSO-d_6, 300 K) δ 175.6 (CO^4), 155.4 (CO^2), 63.3 (C^α), 34.7 ($C^\beta H_2$).

The NMR data were in agreement with the literature.[196]

Benzyl (3-(methylcarbamoyl)thietan-3-yl)carbamate (53).

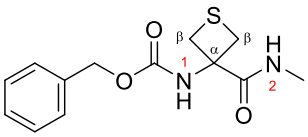

$C_{13}H_{16}N_2O_3S$
M = 280.34 g/mol

Cbz-Attc-NHMe

A solution of **hydantoin 51** (256 mg, 1.62 mmol, 1 eq.) in 3 M NaOH (6 mL, 11 eq.) was reflux for 18 hours. The solvent was removed under reduced pressure. The light-yellow residue was treated with 3 M aqueous HCl solution until pH = 1. The solution was concentrated under reduced pressure to give the hydrochloride as a pale-yellow solid, which was used in the next step without further purification.

To a solution of the above-described sample of hydrochloride in a mixture of H_2O/THF (1 : 1, 12 mL) in an argon-flushed flask was added CbzOSu (653 mg, 2.62 mmol, 1.6 eq.), followed with the addition of Na_2CO_3 (139 mg, 2.12 mmol, 1.3 eq.). The solution was stirred for 6 days at room temperature. THF was then removed under reduced pressure. The aqueous layer was washed with hexane (3 × 10 mL), then slowly acidified with a 2M aqueous HCl at 0 °C to reach pH 1. The aqueous phase was extracted with CH_2Cl_2 (6 × 10 mL). The combined organic phases were dried over Na_2SO_4, filtered and concentrated under reduced pressure. The purification was carried out by flash chromatography (from CH_2Cl_2: EtOAc = 5:1 to CH_2Cl_2:MeOH:AcOH = 98:2:1) to give crude **53** as a pale-yellow oil and used directly in the next step.

To a cold (–20 °C) solution of the above-described sample of **53** in THF (4 mL) under argon were added successively NMM (196 μL, 1.78 mmol, 1.1 eq.) and IBCF (231 μL, 1.78 mmol, 1.1 eq.). The activation period was of 10 minutes at –20 °C. Then a solution of 40% aqueous $MeNH_2$ (1.4 mL, 16.20 mmol, 10 eq.) in THF (3 mL) was added and the resulting solution was stirred at –20 °C for 1.5 hours. 5% aqueous $NaHCO_3$ (5 mL) was added to the solution and the mixture was stirred at room temperature for 1 hour. CH_2Cl_2 (20 mL) was added, and the organic layer was collected. The aqueous layer was extracted with CH_2Cl_2 (5 × 20 mL). The combined organic layers were washed with 5% aqueous $NaHCO_3$ (2 × 5 mL), then dried over Na_2SO_4, filtered and concentrated under reduced pressure. The purification was carried out by flash chromatography (PE:EtOAc, gradient from 7:3 to 0:1) to give **Cbz-Attc-NHMe 54** (164 mg, 36%) as a white solid.

R_f = 0.60 (PE:EtOAc = 2:8)

^{1}H NMR (400 MHz, $CDCl_3$, 300 K) δ 7.96 (bs, 1H, NH^2), 7.53-7.26 (m, 5H, CH^{Ar}), 6.47 (bs, 1H, NH^1), 5.14 (s, 2H, CH_2^{Cbz}), 4.25 (d, *J* = 8.0 Hz, 2H, $C^{\beta}H^a$), 3.24 (d, *J* = 10.0 Hz, 2H, $C^{\beta}H^b$), 2.95 (d, *J* = 5.2 Hz, 3H, N^2CH_3).

^{13}C NMR (90 MHz, $CDCl_3$, 300 K) δ 172.3 (CO^{amide}), 155.1 (CO^{Cbz}), 136.3 (C^{Ar}), 129.2, 128.2, 127.8 (CH^{Ar}), 66.9 (CH_2^{Cbz}), 61.0 (C^{α}), 35.6 ($C^{\beta}H_2$), 26.7 (N^2CH_3).

The NMR data were in agreement with the literature.[196]

4.4 Synthesis of Cbz-Attc(O)-NHMe *trans* **55** and *cis* **56**

***trans*-Benzyl (3-(methylcarbamoyl)-1-oxidothietan-3-yl)carbamate (55) and *cis*-benzyl (3-(methylcarbamoyl)-1-oxidothietan-3-yl)carbamate (56).**

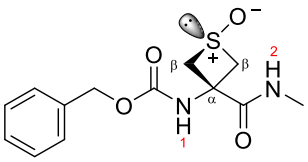

Cbz-Attc(O)-NHMe *trans*

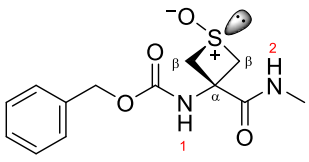

Cbz-Attc(O)-NHMe *cis*

$C_{13}H_{16}N_2O_4S$
M = 296.34 g/mol

Procedure H for the oxidation using H_2O_2-AcOH

To a cold (10 °C) solution of **Cbz-Attc-NHMe 54** (28 mg, 0.10 mmol, 1 eq.) in dry CH_2Cl_2 (1 mL) in an argon-flushed flask, was added dropwise a mixture of H_2O_2 (35%, 40 µL) in glacial acetic acid (40 µL). Then the solution was stirred for 30 minutes at 10 °C. The reaction mixture was alkalized with a 1M NaOH aqueous solution, then extracted with CH_2Cl_2 (5 × 5 mL). The combined organic layers were dried over Na_2SO_4, filtered and concentrated under reduced pressure to give the crude product as a white solid. The crude product was purified by flash chromatography on silica (EtOAc:CH_2Cl_2:MeOH, from 30:10:0 to 10:10:1) to give respectively the **Cbz-Attc(O)-NHMe *trans* 55** (9 mg, 30%) as a white solid and **Cbz-Attc(O)-NHMe *cis* 56** (17 mg, 60%) as a white solid.

Procedure I for the oxidation using *m*-CPBA

To a cold (–78 °C) solution of **Cbz-Attc-NHMe 54** (28 mg, 0.10 mmol, 1 eq.) in dry CH_2Cl_2 (4 mL) in an argon-flushed flask, potassium carbonate (27.8 mg, 0.20 mmol, 2 eq.) and *m*-CPBA (21 mg, 0.10 mmol, 1 eq.) were added successively. The mixture was stirred for 3 hours at –78 °C and then allowed to warm to room temperature. The suspension was filtered through a 0.45 µm PTFE membrane, the filtrate was collected and then concentrated under reduced pressure. The crude product was purified by flash chromatography on silica (EtOAc:CH_2Cl_2:MeOH, from 30:10:0 to 10:10:1) to give respectively the **Cbz-Attc(O)-NHMe *trans* 55** (16 mg, 53%) and the **Cbz-Attc(O)-NHMe *cis* 56** (8 mg, 27%).

For **Cbz-Attc(O)-NHMe *trans* 55**.

***R*$_f$** = 0.29 (EtOAc:CH_2Cl_2:MeOH = 30:10:1)

Mp = 190-192 °C

^{1}H NMR (400 MHz, $CDCl_3$, 300 K) δ 8.78 (bs, 1H, NH^{2}), 7.43-7.27 (m, 5H, CH^{Ar}), 6.69 (bs, 1H, NH^{1}), 5.12 (s, 2H, CH_2^{Cbz}), 4.53 (d, *J* = 14.4 Hz, 2H, $C^{\beta}H^{a}$), 3.31 (d, *J* = 14.4 Hz, 2H, $C^{\beta}H^{b}$), 2.93 (d, *J* = 4.4 Hz, 3H, $N^{2}CH_3$).

^{13}C NMR (100 MHz, $CDCl_3$, 300 K) δ 170.1 (CO^{amide}), 154.9 (CO^{Cbz}), 136.0 (C^{Ar}), 128.8, 128.5, 128.2 (CH^{Ar}), 67.1 (CH_2^{Cbz}), 59.5 (C^{α}), 56.2 ($C^{\beta}H_2$), 27.5 ($N^{2}CH_3$).

IR ν 3323, 3217, 3033, 1719, 1651, 1541 cm^{-1}.

HRMS [ESI(+)] *m/z* $[M+Na]^+$ calculated for $[C_{13}H_{16}N_2NaO_4S]^+$: 319.0723, found: 319.0716.

For **Cbz-Attc(O)-NHMe *cis* 56**.

***R**$_f$* = 0.24 (EtOAc:CH_2Cl_2:MeOH = 30:10:1)

Mp = 193-195 °C

^{1}H NMR (400 MHz, $CDCl_3$, 300 K) δ 7.46-7.29 (m, 5H, CH^{Ar}), 6.42 (bs, 1H, NH^{2}), 5.84 (bs, 1H, NH^{1}), 5.13 (s, 2H, CH_2^{Cbz}), 4.20 (d, *J* = 12.0 Hz, 2H, $C^{\beta}H^{b}$), 3.22 (d, *J* = 12.0 Hz, 2H, $C^{\beta}H^{a}$), 2.80 (d, *J* = 4.8 Hz, 3H, $N^{2}CH_3$).

^{13}C NMR (100 MHz, $CDCl_3$, 300 K) δ 172.0 (CO^{amide}), 154.5 (CO^{Cbz}), 135.4 (C^{Ar}), 128.9, 128.9, 128.5 (CH^{Ar}), 68.1 (CH_2^{Cbz}), 61.5 ($C^{\beta}H_2$), 53.1 (C^{α}), 26.9 ($N^{2}CH_3$).

IR ν 3319, 3227, 3029, 1716, 1637, 1531 cm^{-1}.

HRMS [ESI(+)] *m/z* $[M+Na]^+$ calculated for $[C_{13}H_{16}N_2NaO_4S]^+$: 319.0723, found: 319.0716.

4.5 Synthesis of Cbz-Attc(O,O)-NHMe **57**

Benzyl (3-(methylcarbamoyl)-1,1-dioxidothietan-3-yl)carbamate (57).

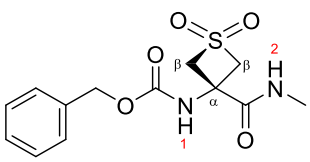

$C_{13}H_{16}N_2O_5S$
M = 312.34 g/mol

Cbz-Attc(O,O)-NHMe

To a solution of **Cbz-Attc-NHMe 54** (28 mg, 0.10 mmol, 1 eq.) in dry CH_2Cl_2 (4 mL) in an argon-flushed flask at 0 °C, potassium carbonate (27.8 mg, 0.20 mmol, 2 eq.) and *m*-CPBA (21 mg, 0.20 mmol, 2 eq.) were added successively. The mixture was stirred for 2 hours at 0 °C and then allowed to warm to room temperature. The suspension was filtered, and the solution was evaporated under reduced pressure. The purification was carried out by flash chromatography on silica (EtOAc:CH_2Cl_2 = 3:1), **Cbz-Attc(O,O)-NHMe 57** (29 mg, 92%) was obtain as a white solid.

***R**$_f$* = 0.78 (EtOAc:CH_2Cl_2:MeOH = 30:10:1)

Mp = 177-179 °C

^{1}H NMR (400 MHz, $CDCl_3$, 300 K) δ 7.58-7.27 (m, 5H, CH^{Ar}), 6.80 (bs, 1H, NH^2), 6.07 (bs, 1H, NH^1), 5.16 (s, 2H, $CH_2{}^{Cbz}$), 4.71 (d, *J* = 12.4 Hz, 2H, $C^{\beta}H^b$), 4.33 (d, *J* = 12.4 Hz, 2H, $C^{\beta}H^a$), 2.85 (d, *J* = 4.8 Hz, 3H, N^2CH_3).

^{13}C NMR (100 MHz, $CDCl_3$, 300 K) δ 169.1 (CO^{amide}), 155.5 (CO^{Cbz}), 135.4 (C^{Ar}), 128.9, 128.8, 128.5 (CH^{Ar}), 72.9 ($C^{\beta}H_2$), 68.2 ($CH_2{}^{Cbz}$), 47.5 (C^{α}), 27.3 (N^2CH_3).

IR ν 3383, 3231, 3038, 1725, 1662, 1538 cm^{-1}.

HRMS [ESI(+)] *m/z* $[M+Na]^+$ calculated for $[C_{13}H_{16}N_2NaO_5S]^+$: 335.0672, found: 335.0671.

5 NMR data of *trans*-ACBC derivatives **58** and **59**

For a detailed description of two ACBC derivatives **58** and **59**, see the literature.[205]

(1*R*,2*R*)-*N*-(4-Methoxyphenyl)-2-(2-oxobenzo[d]oxazol-3(2*H*)-yl)cyclobutane-1-carboxamide (58).

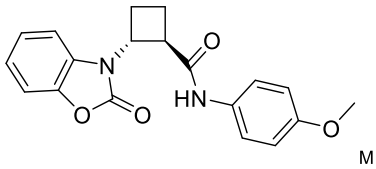

$C_{19}H_{18}N_2O_4$
M = 338.36 g/mol

^{1}H NMR (400 MHz, $CDCl_3$, 300 K) δ 8.25 (bs, 1H, NH), 7.45 (d, *J* = 9.0 Hz, 2H), 7.25-7.07 (m, 3H), 7.09-7.01 (m, 1H), 6.84 (d, *J* = 9.0 Hz, 2H), 4.71 (q, *J* = 8.6 Hz, 1H), 4.15 (q, *J* = 9.0 Hz, 1H), 3.78 (s, 3H), 2.68-2.52 (m, 1H), 2.52-2.29 (m, 2H), 2.26-2.14 (m, 1H).

Methyl ((1*R*,2*R*)-2-(2-oxobenzo[d]oxazol-3(2*H*)-yl)cyclobutane-1-carbonyl)glycinate (59).

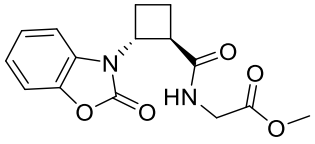

$C_{15}H_{16}N_2O_5$
M = 304.30 g/mol

^{1}H NMR (400 MHz, $CDCl_3$, 300 K) δ7.23-7.01 (m, 4H), 6.54 (bs, 1H, NH), 4.73 (q, *J* = 8.8 Hz, 1H), 4.13-3.93 (m, 3H), 3.73 (s, 3H), 2.71 (p, *J* = 10.2 Hz, 1H), 2.47-2.29 (m, 1H), 2.27-2.11 (m, 2H).

BIBLIOGRAPHY

Bibliography

(1) Lewis, G. N. Monograph series (American Chemical Society); The Chemical Catalog Company, Inc.: New York, **1923**.

(2) Pauling, L. *J. Am. Chem. Soc.* **1935**, *57*, 2680–2684.

(3) Ketema, A.; Worku, A. *J. Chem.* **2020**, *2020*, 1–7.

(4) Amdursky, N.; Głowacki, E. D.; Meredith, P. *Adv. Mater.* **2019**, *31*, 1802221.

(5) Garcia, D.; Starkweather Jr., H. W. *J. Polym. Sci. Polym. Phys. Ed.* **1985**, *23*, 537–555.

(6) Schroeder, L. R.; Cooper, S. L. *J. Appl. Phys.* **1976**, *47*, 4310–4317.

(7) Watson, J. D.; Crick, F. H. C. *Nature* **1953**, *171*, 737–738.

(8) Kagra, D.; Jangra, R.; Sharma, P. *ChemPhysChem* **2022**, *23*, e202100731.

(9) Mirsky, A. E.; Pauling, L. *Proc. Natl. Acad. Sci.* **1936**, *22*, 439–447.

(10) Pauling, L.; Corey, R. B.; Branson, H. R. *Proc. Natl. Acad. Sci.* **1951**, *37*, 205–211.

(11) Pauling, L.; Corey, R. B. *Proc. Natl. Acad. Sci.* **1951**, *37*, 251–256.

(12) Chothia, C. *J. Mol. Biol.* **1976**, *105*, 1–12.

(13) Richards, F. M. *Annu. Rev. Biophys. Bioeng.* **1977**, *6*, 151–176.

(14) Barlow, D. J.; Thornton, J. M. *J. Mol. Biol.* **1988**, *201*, 601–619.

(15) Armen, R.; Alonso, D. O. V.; Daggett, V. *Protein Sci.* **2003**, *12*, 1145–1157.

(16) Eisenberg, D. *Proc. Natl. Acad. Sci.* **2003**, *100*, 11207–11210.

(17) Kendrew, J. C.; Bodo, G.; Dintzis, H. M.; Parrish, R. G.; Wyckoff, H.; Phillips, D. C. *Nature* **1958**, *181*, 662–666.

(18) Perutz, M. F.; Rossmann, M. G.; Cullis, A. F.; Muirhead, H.; Will, G.; North, A. C. T. *Nature* **1960**, *185*, 416–422.

(19) Kumar, P.; Bansal, M. *FEBS J.* **2015**, *282*, 4415–4432.

(20) Cooley, R. B.; Arp, D. J.; Karplus, P. A. *J. Mol. Biol.* **2010**, *404*, 232–246.

(21) Chapman, R.; Kulp, III, J. L.; Patgiri, A.; Kallenbach, N. R.; Bracken, C.; Arora, P. S. *Biochemistry* **2008**, *47*, 4189–4195.

(22) Chothia, C. *J. Mol. Biol.* **1973**, *75*, 295–302.

(23) Nyquist, R. A. *Spectrochim. Acta* **1963**, *19*, 1595–1605.

(24) Burgess, A. W.; Scheraga, H. A. *Biopolymers* **1973**, *12*, 2177–2183.

(25) Pohl, G.; Perczel, A.; Vass, E.; Magyarfalvi, G.; Tarczay, G. *Phys. Chem. Chem. Phys.* **2007**, *9*, 4698.

(26) Newberry, R. W.; Raines, R. T. *Nat. Chem. Biol.* **2016**, *12*, 1084–1088.

(27) Murray, K. A.; Evans, D.; Hughes, M. P.; Sawaya, M. R.; Hu, C. J.; Houk, K. N.; Eisenberg, D. *ACS Nano* **2022**, *16*, 2154–2163.

(28) Zhbankov, R. G. *J. Mol. Struct.* **1992**, *270*, 523–539.

(29) Klemm, D.; Heublein, B.; Fink, H.-P.; Bohn, A. *Angew. Chem. Int. Ed.* **2005**, *44*, 3358–3393.
(30) Slater, S. J.; Ho, C.; Taddeo, F. J.; Kelly, M. B.; Stubbs, C. D. *Biochemistry* **1993**, *32*, 3714–3721.
(31) Boggs, J. M. *Biochim. Biophys. Acta BBA - Rev. Biomembr.* **1987**, *906*, 353–404.
(32) Díez-González, S.; Marion, N.; Nolan, S. P. *Chem. Rev.* **2009**, *109*, 3612–3676.
(33) D'Souza, D. M.; Müller, T. J. J. *Chem. Soc. Rev* **2007**, *36*, 1095–1108.
(34) Trouvé, J.; Gramage-Doria, R. *Chem. Soc. Rev.* **2021**, *50*, 3565–3584.
(35) Natale, D.; Mareque-Rivas, J. C. *Chem Commun* **2008**, No. 4, 425–437.
(36) Grotjahn, D. B.; Incarvito, C. D.; Rheingold, A. L. *Angew. Chem. Int. Ed.* **2001**, *40*, 3884–3887.
(37) Rajabimoghadam, K.; Darwish, Y.; Bashir, U.; Pitman, D.; Eichelberger, S.; Siegler, M. A.; Swart, M.; Garcia-Bosch, I. *J. Am. Chem. Soc.* **2018**, *140*, 16625–16634.
(38) Li, J.-Y.; Xie, P.-P.; Zhou, T.; Qian, P.-F.; Zhou, Y.-B.; Li, H.-C.; Hong, X.; Shi, B.-F. *ACS Catal.* **2022**, *12*, 9083–9091.
(39) Gimeno, M. C.; Herrera, R. P. *Eur. J. Org. Chem.* **2020**, *2020*, 1057–1068.
(40) Curran, D. P.; Kuo, L. H. *J. Org. Chem.* **1994**, *59*, 3259–3261.
(41) Curran, D. P.; Kuo, L. H. *Tetrahedron Lett.* **1995**, *36*, 6647–6650.
(42) Taylor, M. S.; Jacobsen, E. N. *Angew. Chem. Int. Ed.* **2006**, *45*, 1520–1543.
(43) Yu, X.; Wang, W. *Chem. – Asian J.* **2008**, *3*, 516–532.
(44) Dalko, P. I.; Moisan, L. *Angew. Chem. Int. Ed.* **2001**, *40*, 3726–3748.
(45) Houk, K. N.; List, B. *Acc. Chem. Res.* **2004**, *37*, 487–487.
(46) Tanaka, K.; Mori, A.; Inoue, S. *J. Org. Chem.* **1990**, *55*, 181–185.
(47) Takemoto, Y. *Org. Biomol. Chem.* **2005**, *3*, 4299.
(48) Sigman, M. S.; Jacobsen, E. N. *J. Am. Chem. Soc.* **1998**, *120*, 4901–4902.
(49) Sohtome, Y.; Tanatani, A.; Hashimoto, Y.; Nagasawa, K. *Tetrahedron Lett.* **2004**, *45*, 5589–5592.
(50) Menger, F. M. *Acc. Chem. Res.* **1985**, *18*, 128–134.
(51) Bruice, T. C.; Lightstone, F. C. *Acc. Chem. Res.* **1999**, *32*, 127–136.
(52) Pàmies, O.; Bäckvall, J.-E. *Chem. Rev.* **2003**, *103*, 3247–3262.
(53) Knowles, R. R.; Jacobsen, E. N. *Proc. Natl. Acad. Sci.* **2010**, *107*, 20678–20685.
(54) Scavetta, R. D.; Thomas, C. B.; Walsh, M. A.; Szegedi, S.; Joachimiak, A.; Gumport, R. I.; Churchill, M. E. A. *Nucleic Acids Res.* **2000**, *28*, 3950–3961.
(55) Mako, T. L.; Racicot, J. M.; Levine, M. *Chem. Rev.* **2019**, *119*, 322–477.
(56) Drain, C. M.; Russell, K. C.; Lehn, J.-M. *Chem. Commun.* **1996**, No. 3, 337.
(57) Zhang, D.-W.; Wang, W.-K.; Li, Z.-T. *Chem. Rec.* **2015**, *15*, 233–251.
(58) Archer, E. A.; Gong, H.; Krische, M. J. *Tetrahedron* **2001**, *57*, 1139–1159.

(59) Garcia-Tellado, F.; Geib, S. J.; Goswami, S.; Hamilton, A. D. *J. Am. Chem. Soc.* **1991**, *113*, 9265–9269.

(60) Geib, S. J.; Vicent, C.; Fan, E.; Hamilton, A. D. *Angew. Chem. Int. Ed.* **1993**, *32*, 119–121.

(61) Kawamura, S.; Chu, H.; Felding, J.; Baran, P. S. *Nature* **2016**, *532*, 90–93.

(62) Winkler, J. D.; Axten, J. M. *J. Am. Chem. Soc.* **1998**, *120*, 6425–6426.

(63) Couladouros, E. A.; Mihou, A. P.; Bouzas, E. A. *Org. Lett.* **2004**, *6*, 977–980.

(64) Lynch, J. E.; Zanatta, S. D.; White, J. M.; Rizzacasa, M. A. *Chem. – Eur. J.* **2011**, *17*, 297–304.

(65) Appella, D. H.; Christianson, L. A.; Karle, I. L.; Powell, D. R.; Gellman, S. H. *J. Am. Chem. Soc.* **1996**, *118*, 13071–13072.

(66) Gellman, S. H. *Acc. Chem. Res.* **1998**, *31*, 173–180.

(67) Möhle, K.; Günther, R.; Thormann, M.; Sewald, N.; Hofmann, H.-J. *Biopolymers* **1999**, *50*, 167–184.

(68) Doerksen, R. J.; Chen, B.; Yuan, J.; Winkler, J. D.; Klein, M. L. *Chem Commun* **2003**, No. 20, 2534–2535.

(69) Gademann, K.; Häne, A.; Rueping, M.; Jaun, B.; Seebach, D. *Angew. Chem. Int. Ed.* **2003**, *42*, 1534–1537.

(70) Claridge, T. D. W.; Goodman, J. M.; Moreno, A.; Angus, D.; Barker, S. F.; Taillefumier, C.; Watterson, M. P.; Fleet, G. W. J. *Tetrahedron Lett.* **2001**, *42*, 4251–4255.

(71) Hetényi, A.; Mándity, I. M.; Martinek, T. A.; Tóth, G. K.; Fülöp, F. *J. Am. Chem. Soc.* **2005**, *127*, 547–553.

(72) Jagadeesh, B.; Kiran, M. U.; Sudhakar, A.; Chandrasekhar, S. *Chem. – Eur. J.* **2009**, *15*, 12592–12595.

(73) Appella, D. H.; Christianson, L. A.; Klein, D. A.; Richards, M. R.; Powell, D. R.; Gellman, S. H. *J. Am. Chem. Soc.* **1999**, *121*, 7574–7581.

(74) LePlae, P. R.; Fisk, J. D.; Porter, E. A.; Weisblum, B.; Gellman, S. H. *J. Am. Chem. Soc.* **2002**, *124*, 6820–6821.

(75) Peelen, T. J.; Chi, Y.; English, E. P.; Gellman, S. H. *Org. Lett.* **2004**, *6*, 4411–4414.

(76) Hetényi, A.; Szakonyi, Z.; Mándity, I. M.; Szolnoki, É.; Tóth, G. K.; Martinek, T. A.; Fülöp, F. *Chem Commun* **2009**, No. 2, 177–179.

(77) Mándity, I. M.; Fülöp, L.; Vass, E.; Tóth, G. K.; Martinek, T. A.; Fülöp, F. *Org. Lett.* **2010**, *12*, 5584–5587.

(78) Sharma, G. V. M.; Reddy, N. Y.; Ravi, R.; Sreenivas, B.; Sridhar, G.; Chatterjee, D.; Kunwar, A. C.; Hofmann, H.-J. *Org. Biomol. Chem.* **2012**, *10*, 9191.

(79) Shin, S.; Lee, M.; Guzei, I. A.; Kang, Y. K.; Choi, S. H. *J. Am. Chem. Soc.* **2016**, *138*, 13390–13395.

(80) Thodupunuri, P.; Katukuri, S.; Ramakrishna, K. V. S.; Sharma, G. V. M.; Kunwar, A. C.; Sarma, A. V. S.; Hofmann, H.-J. *J. Org. Chem.* **2017**, *82*, 2018–2031.

(81) Raguse, T. L.; Porter, E. A.; Weisblum, B.; Gellman, S. H. *J. Am. Chem. Soc.* **2002**, *124*, 12774–12785.

(82) Chandrasekhar, S.; Reddy, M. S.; Jagadeesh, B.; Prabhakar, A.; Ramana Rao, M. H. V.; Jagannadh, B. *J. Am. Chem. Soc.* **2004**, *126*, 13586–13587.

(83) Korendovych, I. V.; Shandler, S. J.; Montalvo, G. L.; DeGrado, W. F. *Org. Lett.* **2011**, *13*, 3474–3477.

(84) Mándity, I. M.; Wéber, E.; Martinek, T. A.; Olajos, G.; Tóth, G. K.; Vass, E.; Fülöp, F. *Angew. Chem. Int. Ed.* **2009**, *48*, 2171–2175.

(85) Szolnoki, É.; Hetényi, A.; Martinek, T. A.; Szakonyi, Z.; Fülöp, F. *Org Biomol Chem* **2012**, *10*, 255–259.

(86) Szolnoki, É.; Hetényi, A.; Mándity, I. M.; Fülöp, F.; Martinek, T. A. *Eur. J. Org. Chem.* **2013**, *2013*, 3555–3559.

(87) Seebach, D.; Overhand, M.; Kühnle, F. N. M.; Martinoni, B.; Oberer, L.; Hommel, U.; Widmer, H. *Helv. Chim. Acta* **1996**, *79*, 913–941.

(88) Seebach, D.; Ciceri, P. E.; Overhand, M.; Jaun, B.; Rigo, D.; Oberer, L.; Hommel, U.; Amstutz, R.; Widmer, H. *Helv. Chim. Acta* **1996**, *79*, 2043–2066.

(89) Gorrea, E.; Pohl, G.; Nolis, P.; Celis, S.; Burusco, K. K.; Branchadell, V.; Perczel, A.; Ortuño, R. M. *J. Org. Chem.* **2012**, *77*, 9795–9806.

(90) Fernandes, C.; Faure, S.; Pereira, E.; Théry, V.; Declerck, V.; Guillot, R.; Aitken, D. J. *Org. Lett.* **2010**, *12*, 3606–3609.

(91) Imani, Z.; Guillot, R.; Declerck, V.; Aitken, D. J. *J. Org. Chem.* **2020**, *85*, 6165–6171.

(92) Ragab, S. S.; Kassir, A. F.; Guillot, R.; Scherrmann, M.-C.; Boddaert, T.; Aitken, D. J. *Chem. Commun.* **2018**, *54*, 1968–1971.

(93) Tanda, K.; Eto, R.; Kato, K.; Oba, M.; Ueda, A.; Suemune, H.; Doi, M.; Demizu, Y.; Kurihara, M.; Tanaka, M. *Tetrahedron* **2015**, *71*, 3909–3914.

(94) Baldauf, C.; Günther, R.; Hofmann, H.-J. *Helv. Chim. Acta* **2003**, *86*, 2573–2588.

(95) Awada, H.; Grison, C. M.; Charnay-Pouget, F.; Baltaze, J.-P.; Brisset, F.; Guillot, R.; Robin, S.; Hachem, A.; Jaber, N.; Naoufal, D.; Yazbeck, O.; Aitken, D. J. *J. Org. Chem.* **2017**, *82*, 4819–4828.

(96) Vasudev, P. G.; Shamala, N.; Ananda, K.; Balaram, P. *Angew. Chem. Int. Ed.* **2005**, *117*, 5052–5055.

(97) Sharma, G. V. M.; Jayaprakash, P.; Narsimulu, K.; Ravi Sankar, A.; Ravinder Reddy, K.; Radha Krishna, P.; Kunwar, A. C. *Angew. Chem. Int. Ed.* **2006**, *45*, 2944–2947.

(98) Mathieu, L.; Legrand, B.; Deng, C.; Vezenkov, L.; Wenger, E.; Didierjean, C.; Amblard, M.; Averlant-Petit, M.-C.; Masurier, N.; Lisowski, V.; Martinez, J.; Maillard, L. T. *Angew. Chem. Int. Ed.* **2013**, *52*, 6006–6010.

(99) Hintermann, T.; Gademann, K.; Jaun, B.; Seebach, D. *Helv. Chim. Acta* **1998**, *81*, 983–1002.

(100) Hanessian, S.; Luo, X.; Schaum, R.; Michnick, S. *J. Am. Chem. Soc.* **1998**, *120*, 8569–8570.
(101) Seebach, D.; Brenner, M.; Rueping, M.; Schweizer, B.; Jaun, B. *Chem. Commun.* **2001**, 2, 207–208.
(102) Seebach, D.; Brenner, M.; Rueping, M.; Jaun, B. *Chem. – Eur. J.* **2002**, *8*, 573–584.
(103) Baldauf, C.; Günther, R.; Hofmann, H.-J. *Pept. Sci.* **2006**, *84*, 408–413.
(104) Baldauf, C.; Günther, R.; Hofmann, H.-J. *J. Org. Chem.* **2006**, *71*, 1200–1208.
(105) De Pol, S.; Zorn, C.; Klein, C. D.; Zerbe, O.; Reiser, O. *Angew. Chem. Int. Ed.* **2004**, *43*, 511–514.
(106) Sharma, G. V. M.; Nagendar, P.; Jayaprakash, P.; Radha Krishna, P.; Ramakrishna, K. V. S.; Kunwar, A. C. *Angew. Chem. Int. Ed.* **2005**, *117*, 6028–6032.
(107) Srinivasulu, G.; Kumar, S. K.; Sharma, G. V. M.; Kunwar, A. C. *J. Org. Chem.* **2006**, *71*, 8395–8400.
(108) Schmitt, M. A.; Choi, S. H.; Guzei, I. A.; Gellman, S. H. *J. Am. Chem. Soc.* **2006**, *128*, 4538–4539.
(109) Hayen, A.; Schmitt, M. A.; Ngassa, F. N.; Thomasson, K. A.; Gellman, S. H. *Angew. Chem. Int. Ed.* **2004**, *43*, 505–510.
(110) Choi, S. H.; Guzei, I. A.; Spencer, L. C.; Gellman, S. H. *J. Am. Chem. Soc.* **2008**, *130*, 6544–6550.
(111) Horne, W. S.; Price, J. L.; Keck, J. L.; Gellman, S. H. *J. Am. Chem. Soc.* **2007**, *129*, 4178–4180.
(112) Chatterjee, S.; Vasudev, P. G.; Raghothama, S.; Shamala, N.; Balaram, P. *Pept. Sci.* **2008**, *90*, 759–771.
(113) Guo, L.; Chi, Y.; Almeida, A. M.; Guzei, I. A.; Parker, B. K.; Gellman, S. H. *J. Am. Chem. Soc.* **2009**, *131*, 16018–16020.
(114) Misra, R.; Saseendran, A.; George, G.; Veeresh, K.; Raja, K. M. P.; Raghothama, S.; Hofmann, H.-J.; Gopi, H. N. *Chem. – Eur. J.* **2017**, *23*, 3764–3772.
(115) Sharma, G. V. M.; Jadhav, V. B.; Ramakrishna, K. V. S.; Jayaprakash, P.; Narsimulu, K.; Subash, V.; Kunwar, A. C. *J. Am. Chem. Soc.* **2006**, *128*, 14657–14668.
(116) Giuliano, M. W.; Maynard, S. J.; Almeida, A. M.; Guo, L.; Guzei, I. A.; Spencer, L. C.; Gellman, S. H. *J. Am. Chem. Soc.* **2014**, *136*, 15046–15053.
(117) Vasudev, P. G.; Chatterjee, S.; Ananda, K.; Shamala, N.; Balaram, P. *Angew. Chem. Int. Ed.* **2008**, *120*, 6530–6532.
(118) Guo, L.; Almeida, A. M.; Zhang, W.; Reidenbach, A. G.; Choi, S. H.; Guzei, I. A.; Gellman, S. H. *J. Am. Chem. Soc.* **2010**, *132*, 7868–7869.
(119) Horne, W. S.; Gellman, S. H. *Acc. Chem. Res.* **2008**, *41*, 1399–1408.
(120) Grison, C. M.; Robin, S.; Aitken, D. J. *Chem. Commun.* **2016**, *52*, 7802–7805.
(121) Tavassoli, A. Royal Society of Chemistry, **2020**.
(122) Saraogi, I.; Hamilton, A. D. *Biochem. Soc. Trans.* **2008**, *36*, 1414–1417.

(123) Azzarito, V.; Long, K.; Murphy, N. S.; Wilson, A. J. *Nat. Chem.* **2013**, *5*, 161–173.

(124) Choi, S. H.; Guzei, I. A.; Spencer, L. C.; Gellman, S. H. *J. Am. Chem. Soc.* **2008**, *130*, 6544–6550.

(125) Checco, J. W.; Lee, E. F.; Evangelista, M.; Sleebs, N. J.; Rogers, K.; Pettikiriarachchi, A.; Kershaw, N. J.; Eddinger, G. A.; Belair, D. G.; Wilson, J. L.; Eller, C. H.; Raines, R. T.; Murphy, W. L.; Smith, B. J.; Gellman, S. H.; Fairlie, W. D. *J. Am. Chem. Soc.* **2015**, *137*, 11365–11375.

(126) Grison, C. M.; Miles, J. A.; Robin, S.; Wilson, A. J.; Aitken, D. J. *Angew. Chem. Int. Ed.* **2016**, *55*, 11096–11100.

(127) S. Nowick, J.; M. Smith, E.; Pairish, M. *Chem. Soc. Rev.* **1996**, *25*, 401–415.

(128) Brandmeier, V.; Sauer, W. H. B.; Feigel, M. *Helv. Chim. Acta* **1994**, *77*, 70–85.

(129) Kemp, D. S.; Bowen, B. R. *Tetrahedron Lett.* **1988**, *29*, 5077–5080.

(130) Cashman, T. J.; Linton, B. R. *Org. Lett.* **2007**, *9*, 5457–5460.

(131) Ramírez-Alvarado, M.; Kortemme, T.; Blanco, F. J.; Serrano, L. *Bioorg. Med. Chem.* **1999**, *7*, 93–103.

(132) DeGrado, W. f.; Schneider, J. p.; Hamuro, Y. *J. Pept. Res.* **1999**, *54*, 206–217.

(133) Toniolo, C.; Crisma, M.; Formaggio, F.; Alemán, C.; Ramakrishnan, C.; Kalmankar, N.; Balaram, P. *Pept. Sci.* **2017**, *108*, e22911.

(134) Baruah, P. K.; Sreedevi, N. K.; Gonnade, R.; Ravindranathan, S.; Damodaran, K.; Hofmann, H.-J.; Sanjayan, G. J. *J. Org. Chem.* **2007**, *72*, 636–639.

(135) Srinivas, D.; Gonnade, R.; Ravindranathan, S.; Sanjayan, G. J. *J. Org. Chem.* **2007**, *72*, 7022–7025.

(136) Gademann, K.; Kimmerlin, T.; Hoyer, D.; Seebach, D. *J. Med. Chem.* **2001**, *44*, 2460–2468.

(137) Peggion, C.; Moretto, A.; Formaggio, F.; Crisma, M.; Toniolo, C. *Pept. Sci.* **2013**, *100*, 621–636.

(138) Crisma, M.; Formaggio, F.; Alemán, C.; Torras, J.; Ramakrishnan, C.; Kalmankar, N.; Balaram, P.; Toniolo, C. *Pept. Sci.* **2018**, *110*, e23100.

(139) Benedetti, E.; Barone, V.; Bavoso, A.; Di Blasio, B.; Lelj, F.; Pavone, V.; Pedone, C.; Bonora, G. M.; Toniolo, C.; Leplawy, M. T.; Kaczmarek, K.; Redlinski, A. *Biopolymers* **1988**, *27*, 357–371.

(140) Toniolo, C.; Bonora, G. M.; Bavoso, A.; Benedetti, E.; Di Blasio, B.; Pavone, V.; Pedone, C.; Barone, V.; Lelj, F.; Leplawy, M. T.; Kaczmarek, K.; Redlinski, A. *Biopolymers* **1988**, *27*, 373–379.

(141) Aubry, A.; Del Duca, V.; Pantano, M.; Formaggio, F.; Crisma, M.; Toniolo, C.; Kamphuis, J. *Lett. Pept. Sci.* **1995**, *1*, 157–162.

(142) James, W. H.; Baquero, E. E.; Choi, S. H.; Gellman, S. H.; Zwier, T. S. *J. Phys. Chem. A* **2010**, *114*, 1581–1591.

(143) Alauddin, M.; Biswal, H. S.; Gloaguen, E.; Mons, M. *Phys. Chem. Chem. Phys.* **2015**, *17*, 2169–2178.

(144) Gloaguen, E.; Tardivel, B.; Mons, M. *Struct. Chem.* **2016**, *27*, 225–230.

(145) Yatsyna, V.; Mallat, R.; Gorn, T.; Schmitt, M.; Feifel, R.; Rijs, A. M.; Zhaunerchyk, V. *J. Phys. Chem. A* **2019**, *123*, 862–872.

(146) Kumar, S.; Mishra, K. K.; Singh, S. K.; Borish, K.; Dey, S.; Sarkar, B.; Das, A. *J. Chem. Phys.* **2019**, *151*, 104309.

(147) Habka, S.; Sohn, W. Y.; Vaquero-Vara, V.; Géléoc, M.; Tardivel, B.; Brenner, V.; Gloaguen, E.; Mons, M. *Phys. Chem. Chem. Phys.* **2018**, *20*, 3411–3423.

(148) Cabezas, C.; Varela, M.; Alonso, J. L. *Angew. Chem.* **2017**, *129*, 6520–6525.

(149) Imani, Z.; Mundlapati, V. R.; Brenner, V.; Gloaguen, E.; Le Barbu-Debus, K.; Zehnacker-Rentien, A.; Robin, S.; Aitken, D. J.; Mons, M. *Chem. Commun.* **2023**, *59*, 1161–1164.

(150) Loquais, Y.; Gloaguen, E.; Habka, S.; Vaquero-Vara, V.; Brenner, V.; Tardivel, B.; Mons, M. *J. Phys. Chem. A* **2015**, *119*, 5932–5941.

(151) Buchanan, E. G.; James, W. H.; Choi, S. H.; Guo, L.; Gellman, S. H.; Müller, C. W.; Zwier, T. S. *J. Chem. Phys.* **2012**, *137*, 094301.

(152) James, W. H.; Baquero, E. E.; Choi, S. H.; Gellman, S. H.; Zwier, T. S. *J. Phys. Chem. A* **2010**, *114*, 1581–1591.

(153) Imani, Z.; Mundlapati, V. R.; Goldsztejn, G.; Brenner, V.; Gloaguen, E.; Guillot, R.; Baltaze, J.-P.; Barbu-Debus, K. L.; Robin, S.; Zehnacker, A.; Mons, M.; Aitken, D. J. *Chem. Sci.* **2020**, *11*, 9191–9197.

(154) Mundlapati, V. R.; Imani, Z.; D'mello, V. C.; Brenner, V.; Gloaguen, E.; Baltaze, J.-P.; Robin, S.; Mons, M.; Aitken, D. J. *Chem. Sci.* **2021**, *12*, 14826–14832.

(155) McCarson, K. E.; Enna, S. J. *Neurochem. Res.* **2014**, *39*, 1948–1963.

(156) Levandovskiy, I. A.; Sharapa, D. I.; Shamota, T. V.; Rodionov, V. N.; Shubina, T. E. *Future Med. Chem.* **2011**, *3*, 223–241.

(157) Crittenden, D. L.; Park, A.; Qiu, J.; Silverman, R. B.; Duke, R. K.; Johnston, G. A. R.; Jordan, M. J. T.; Chebib, M. *Bioorg. Med. Chem.* **2006**, *14*, 447–455.

(158) Awada, H.; Robin, S.; Guillot, R.; Yazbeck, O.; Naoufal, D.; Jaber, N.; Hachem, A.; Aitken, D. J. *Eur. J. Org. Chem.* **2014**, *2014*, 7148–7155.

(159) André, V.; Gras, M.; Awada, H.; Guillot, R.; Robin, S.; Aitken, D. J. *Tetrahedron* **2013**, *69*, 3571–3576.

(160) Baldauf, C.; Günther, R.; Hofmann, H.-J. *J. Org. Chem.* **2006**, *71*, 1200–1208.

(161) Mansour, A. T. These de doctorat, Université Paris-Saclay, **2018**.

(162) Grimm, J. B.; Stables, J. P.; Brown, M. L. *Bioorg. Med. Chem.* **2003**, *11*, 4133–4141.

(163) Tedeschi, T.; Corradini, R.; Marchelli, R.; Pushl, A.; Nielsen, P. E. *Tetrahedron Asymmetry* **2002**, *13*, 1629–1636.

(164) Al-Warhi, T. I.; Al-Hazimi, H. M. A.; El-Faham, A. *J. Saudi Chem. Soc.* **2012**, *16*, 97–116.

(165) Mándity, I. M.; Wéber, E.; Martinek, T. A.; Olajos, G.; Tóth, G. K.; Vass, E.; Fülöp, F. *Angew. Chem. Int. Ed.* **2009**, *48*, 2171–2175.

(166) M. Grison, C.; Robin, S.; J. Aitken, D. *Chem. Commun.* **2015**, *51*, 16233–16236.

(167) Grison, C. M.; Miles, J. A.; Robin, S.; Wilson, A. J.; Aitken, D. J. *Angew. Chem. Int. Ed.* **2016**, *55*, 11096–11100.

(168) Altmayer-Henzien, A.; Declerck, V.; Farjon, J.; Merlet, D.; Guillot, R.; Aitken, D. J. *Angew. Chem. Int. Ed.* **2015**, *127*, 10957–10960.

(169) Crisma, M.; Peggion, C.; Moretto, A.; Banerjee, R.; Supakar, S.; Formaggio, F.; Toniolo, C. *Pept. Sci.* **2014**, *102*, 145–158.

(170) Toniolo, C.; Crisma, M.; Formaggio, F.; Peggion, C. *Pept. Sci.* **2001**, *60*, 396–419.

(171) Toniolo, C.; Benedetti, E. *Macromolecules* **1991**, *24*, 4004–4009.

(172) Prasad, S.; Rao, R. B.; Balaram, P. *Biopolymers* **1995**, *35*, 11–20.

(173) Toniolo, C.; Crisma, M.; Formaggio, F.; Benedetti, E.; Santini, A.; Iacovino, R.; Saviano, M.; Di Blasio, B.; Pedone, C.; Kamphuis, J. *Pept. Sci.* **1996**, *40*, 519–522.

(174) Gatos, M.; Formaggio, F.; Crisma, M.; Toniolo, C.; Bonora, G. M.; Benedetti, Z.; Di Blasio, B.; Iacovino, R.; Santini, A.; Saviano, M.; Kamphuis, J. *J. Pept. Sci.* **1997**, *3*, 110–122.

(175) Peggion, C.; Moretto, A.; Formaggio, F.; Crisma, M.; Toniolo, C. *Pept. Sci.* **2013**, *100*, 621–636.

(176) Wolf, W. M.; Stasiak, M.; Leplawy, M. T.; Bianco, A.; Formaggio, F.; Crisma, M.; Toniolo, C. *J. Am. Chem. Soc.* **1998**, *120*, 11558–11566.

(177) Scaffidi, A.; Skelton, B. W.; Stick, R. V.; White, A. H.; Scaffidi, A.; Skelton, B. W.; Stick, R. V.; White, A. H. *Aust. J. Chem.* **2007**, *60*, 93–94.

(178) Cho, J.; Tanaka, M.; Sato, S.; Kinbara, K.; Aida, T. *J. Am. Chem. Soc.* **2010**, *132*, 13176–13178.

(179) Žukauskaitė, A.; Moretto, A.; Peggion, C.; Zotti, M. D.; Šačkus, A.; Formaggio, F.; Kimpe, N. D.; Mangelinckx, S. *Eur. J. Org. Chem.* **2014**, *2014*, 2312–2321.

(180) Liu, D.; Imani, Z.; Gourson, C.; Guillot, R.; Robin, S.; Aitken, D. J. *Synlett* **2023**.

(181) Gilheany, D.; Bieszczad, B. US pat. WO2015181182A1, **2015**.

(182) Sharma, K.; Strizhak, A. V.; Fowler, E.; Wang, X.; Xu, W.; Hatt Jensen, C.; Wu, Y.; Sore, H. F.; Lau, Y. H.; Hyvönen, M.; Itzhaki, L. S.; Spring, D. R. *Org. Biomol. Chem.* **2019**, *17*, 8014–8018.

(183) Gerard, B.; O'Shea, M. W.; Donckele, E.; Kesavan, S.; Akella, L. B.; Xu, H.; Jacobsen, E. N.; Marcaurelle, L. A. *ACS Comb. Sci.* **2012**, *14*, 621–630.

(184) Mnich, S. J.; Hiebsch, R. R.; Huff, R. M.; Muthian, S. *J. Pharmacol. Exp. Ther.* **2010**, *333*, 445–453.

(185) Žukauskaitė, A.; Mangelinckx, S.; Buinauskaitė, V.; Šačkus, A.; De Kimpe, N. *Amino Acids* **2011**, *41*, 541–558.

(186) Ciganek, E. *J. Org. Chem.* **1990**, *55*, 3007–3009.

(187) Rayburn, C. H.; Harlan, W. R.; Hanmer, H. R. *J. Am. Chem. Soc.* **1950**, *72*, 1721–1723.
(188) O'Neil, I. A.; Miller, N. D.; Peake, J.; Barkley, J. V.; Low, C. M. R.; Kalindjian, S. B. *Synlett* **1993**, *1993*, 515–518.
(189) O'Neil, I. A.; Miller, N. D.; Barkley, J. V.; Low, C. M. R.; Kalindjian, S. B. *Synlett* **1995**, *1995*, 619–621.
(190) Watson, A. A.; Fairlie, D. P.; Craik, D. J. *Biochemistry* **1998**, *37*, 12700–12706.
(191) Jiang, L.; Burgess, K. *J. Am. Chem. Soc.* **2002**, *124*, 9028–9029.
(192) Menguy, L.; Drouillat, B.; Marrot, J.; Couty, F. *Tetrahedron Lett.* **2012**, *53*, 4697–4699.
(193) Kozikowski, A. P.; Fauq, A. H. *Synlett* **1991**, *1991*, 783–784.
(194) Volynskii, N. P.; Shevchenko, S. E. *Pet. Chem.* **2007**, *47*, 109–117.
(195) Imani, Z.; Mundlapati, V. R.; Brenner, V.; Gloaguen, E.; Barbu-Debus, K. L.; Zehnacker-Rentien, A.; Robin, S.; Aitken, D. J.; Mons, M. *Chem. Commun.* **2023**, *59*, 1161–1164.
(196) Imani, Z.; Mundlapati, V. R.; Goldsztejn, G.; Brenner, V.; Gloaguen, E.; Guillot, R.; Baltaze, J.-P.; Barbu-Debus, K. L.; Robin, S.; Zehnacker, A.; Mons, M.; Aitken, D. J. *Chem. Sci.* **2020**, *11*, 9191–9197.
(197) Malloum, A.; Conradie, J. *Data Brief* **2022**, *42*, 108024.
(198) Namyslo, J. C.; Kaufmann, D. E. *Chem. Rev.* **2003**, *103*, 1485–1537.
(199) Lee-Ruff, E.; Mladenova, G. *Chem. Rev.* **2003**, *103*, 1449–1483.
(200) Fülöp, F. *Chem. Rev.* **2001**, *101*, 2181–2204.
(201) Fülöp, F.; Martinek, T. A.; Tóth, G. K. *Chem. Soc. Rev.* **2006**, *35*, 323–334.
(202) Brannock, K. C.; Bell, A.; Burpitt, R. D.; Kelly, C. A. *J. Org. Chem.* **1964**, *29*, 801–812.
(203) Declerck, V.; Aitken, D. J. *Amino Acids* **2011**, *41*, 587–595.
(204) Zhong, X.; Tang, Q.; Zhou, P.; Zhong, Z.; Dong, S.; Liu, X.; Feng, X. *Chem. Commun.* **2018**, *54*, 10511–10514.
(205) Barranco, S.; Cuccu, F.; Liu, D.; Robin, S.; Guillot, R.; Secci, F.; Brenner, V.; Mons, M.; Caboni, P.; Aitken, D. J.; Frongia, A. *Eur. J. Org. Chem.* **2023**, *26*, e202300183.
(206) Alauddin, M.; Gloaguen, E.; Brenner, V.; Tardivel, B.; Mons, M.; Zehnacker-Rentien, A.; Declerck, V.; Aitken, D. J. *Chem. – Eur. J.* **2015**, *21*, 16479–16493.
(207) Torres, E.; Gorrea, E.; Silva, E. D.; Nolis, P.; Branchadell, V.; Ortuño, R. M. *Org. Lett.* **2009**, *11*, 2301–2304.
(208) M. Grison, C.; Robin, S.; J. Aitken, D. *Chem. Commun.* **2016**, *52*, 7802–7805.
(209) Sheldrick, G. M. **1997**.
(210) Sheldrick, G. M. *Acta Crystallogr. A* **2008**, *64*, 112–122.
(211) Farrugia, L. J. *J. Appl. Crystallogr.* **1999**, *32*, 837–838.
(212) García-Calvo, J.; Torroba, T.; Brañas-Fresnillo, V.; Perdomo, G.; Cózar-Castellano, I.; Li, Y.-H.; Legrand, Y.-M.; Barboiu, M. *Chem. – Eur. J.* **2019**, *25*, 9287–9294.
(213) Feng, J.; Liang, S.; Chen, S.-Y.; Zhang, J.; Fu, S.-S.; Yu, X.-Q. *Adv. Synth. Catal.* **2012**, *354*, 1287–1292.

Résumé en Langue Française

L'objectif de cette thèse était d'acquérir une compréhension globale des différents types de liaisons H et de leurs contributions à la conformation. Pour étudier la liaison H à longue portée entre le squelette et le dos, une série de peptides hybrides γ/α composés de *cis*-^{3,4}CB-GABA et d'alanine ont été synthétisés. La liaison H à courte portée entre le squelette et le squelette C5 et la liaison H entre la chaîne latérale et le squelette N-H···N C6γ ont été étudiées à l'aide de dérivés de l'Aatc(Me). En outre, pour estimer le rôle de l'atome d'oxygène des dérivés oxydés dans la stabilisation de l'interaction C5, des dérivés Aatc(Me,O), Attc(O) et Attc(O,O) ont été préparés. Enfin, le comportement conformationnel de deux dérivés trans-ACBC a également été étudié afin d'évaluer les caractéristiques de la conformation locale.

Dans le premier chapitre, nous nous sommes concentrés sur les études conformationnelles des peptides hybrides γ/α incorporant du (*R*,*R*)-*cis*-^{3,4}CB-GABA et de la (*R*)- ou de la (*S*)-alanine. Les peptides hybrides γ/α pertinents ont été synthétisés avec succès en solution à l'aide d'une stratégie synthétique convergente, ce qui a permis d'obtenir efficacement des di-, tétra- et hexapeptides. Afin de tenir compte des coopérations diédriques pour la formation d'hélices, les deux énantiomères de l'alanine ont été utilisés, ce qui a donné des peptides de la série *R*,*R*,*R* et de la série *R*,*R*,*S*. En outre, des peptides avec un ester de benzyle et un amide de benzyle au niveau de la partie C-terminale ont été préparés pour évaluer la contribution du NH supplémentaire aux comportements conformationnels. Au total, douze peptides ont donc été synthétisés.

Le comportement conformationnel de ces peptides a été étudié dans des solutions de chloroforme et de pyridine à l'aide d'un ensemble de techniques spectroscopiques (titrage DMSO-d_6, ^{1}H-^{1}H ROESY 2D NMR, IR) et de calculs théoriques (recherche conformationnelle Hybrid Monte Carlo Multiple Minima). Ces recherches ont révélé que les peptides de la série *R*,*R*,*R* γ/α ne présentaient aucune indication claire d'une préférence conformationnelle particulière, ni aucune preuve qu'ils se replient dans une conformation en hélice 12/10. Les peptides de la série *R*,*R*,*S* γ/α semblent adopter une conformation en hélice 12/10, comme le suggèrent les expériences de RMN 1D/2D, l'infrarouge en solution et la modélisation moléculaire. Ce travail a fourni un nouveau cas de peptides hybrides γ/α qui peuvent se replier dans une conformation en hélice 12/10.

Le deuxième chapitre est consacré aux études de conformation des dérivés de l'Aatc(Me). La stratégie de modification post-synthétique a été employée pour préparer des dérivés Aatc(Me) allant du monomère au di-, tri- et tétramère. Chaque substrat Aatc(Boc) a d'abord été déprotégé puis méthylé sur tous les résidus aminés libres présents dans l'oligomère, ce qui a permis d'obtenir des rendements modérés à bons de produits méthylés. Le

comportement conformationnel de ces dérivés Aatc(Me) (mono-, di- et trimères) a été étudié dans une solution de chloroforme à l'aide de techniques spectroscopiques (UV/IR en phase gazeuse, IR en solution, titrage DMSO-d_6, variation de température, RMN ^{1}H-^{1}H NOESY 2D) et de calculs de chimie quantique. Ces recherches ont montré l'existence concomitante d'une liaison H inter-résidus N-H···N, chaîne latérale-backbone C6γ et d'une interaction intra-résidus N-H···O=C, C5 pour ces dérivés Aatc(Me). Les systèmes de liaison H C5-C6γ successifs présentent une conformation étendue.

Dans le monomère Cbz-Aatc(Me)-NHMe, cette conformation C5-C6γ étendue a été identifiée par des calculs théoriques et a été suggérée par des études en phase gazeuse et en solution. Les motifs de liaison H C5-C6γ consécutifs semblent également présenter une conformation C5-C6γ/C5-C6γ entièrement étendue du dimère Cbz-[Aatc(Me)]$_2$-NHMe identifiée par des calculs théoriques, ce qui est en accord avec les résultats obtenus par infrarouge en phase gazeuse. Ces deux C5-C6γ motifs sont liés par une interaction C=O···H(N)···N à 3 centres. Cependant, les résultats obtenus par infrarouge en solution ont montré que la conformation C5-C6γ/C5-C6γ entièrement étendue était accompagnée d'une conformation C5-C6γ/π_{am} semi-étendue et d'une conformation a β-turn. La conformation C5-C6γ/π_{am} conformation semi-étendue, dans laquelle une liaison H C5-C6γ a été remplacée par une interaction π_{am}. D'autres résultats de la spectroscopie RMN étaient compatibles avec le paysage conformationnel du dimère en solution. Les conformations les moins énergétiques du trimère Cbz-[Aatc(Me)]$_3$-NHMe, calculées théoriquement en phase gazeuse, présentaient principalement une forme C5-C6γ/C5-C6γ/C5-C6γ entièrement étendue et une forme C5-C6γ/π_{am}/C5-C6γ form semi-étendue, ce qui est cohérent avec les résultats obtenus en phase gazeuse par infrarouge. En solution, les études infrarouges suggèrent que la forme C5-C6γ/C5-C6γ/C5-C6γ conformer entièrement étendue n'est pas compétitive et a été remplacée par des conformations C5-C6γ/π_{am}/C5-C6γ and à 3_{10} hélices semi-étendues. Le C5-C6γ/π_{am}/C5-C6γ form semi-étendu était présent, comme le suggèrent les études de RMN 1D/2D (déplacements chimiques ^{1}H des signaux NH, titrage DMSO-d_6, expériences de variation de température et RMN 2D NOESY). La présence de la nouvelle conformation en hélice 3_{10} a été mise en évidence par la RMN ^{1}H-^{1}H NOESY 2D, où une corrélation à longue portée entre CH_2 du groupe Cbz et C$^\beta$Ha du troisième résidu azétidine a été observée. Globalement, du monomère au trimère, les caractéristiques de liaison H C5-C6γ étaient présentes dans le paysage conformationnel des trois composés, mais les motifs C5-C6γ consécutifs sont moins compétitifs que les structures alternatives partiellement repliées. Les études de conformation du tétramère Cbz-[Aatc(Me)]$_4$-NHMe ont également été tentées, mais le processus de fragmentation indésirable en phase gazeuse de l'échantillon a empêché la poursuite des études en phase gazeuse. En solution, une expérience de spectroscopie infrarouge a été réalisée et peut suggérer que la conformation en hélice 3_{10} est présente en solution. Ces

résultats de conformation du monomère au tétramère peuvent indiquer que plus la chaîne de l'oligomère Aatc(Me) est longue, plus il est probable qu'elle ait une conformation repliée.

Dans le troisième chapitre, les comportements conformationnels de quatre dérivés oxydés, dont *trans*-Cbz-Aatc(Me,O)-NHMe, *trans*-Cbz-Attc(O)-NHMe, *cis*-Cbz-Attc(O)-NHMe et Cbz-Attc(O,O)-NHMe, ont été étudiés. La température élevée utilisée pour l'infrarouge en phase gazeuse a entraîné la dégradation de Cbz-Aatc(Me,O)-NHMe en une structure d'alanine déshydrogénée, et les calculs théoriques n'ont pas été effectués sur cette structure. Cependant, en solution, les résultats de la spectroscopie infrarouge ont montré une conformation étendue C5-C7δ prédominante, dans laquelle une liaison H inter-résidus N-H···O-N C7δ a été formée à partir de la chaîne latérale, ainsi qu'une interaction N-H···O=C C5 formée dans l'épine dorsale du peptide. Les résultats de la RMN 1D/2D (déplacements chimiques 1H des signaux NH, titrage DMSO-d_6, variation de température et expériences RMN ^{1}H-^{1}H NOESY 2D) étaient en parfait accord avec la conformation étendue C5-C7δ présentée dans Cbz-Aatc(Me,O)-NHMe. À l'état solide, la structure cristalline de Cbz-Aatc(Me,O)-NHMe ne présente qu'une liaison H intermoléculaire impliquant l'atome d'oxygène de la fraction azétidine et un NH amide d'une deuxième molécule. Les calculs théoriques pour *trans*-Cbz-Attc(O)-NHMe ont montré une conformation étendue C5-C7δ prédominante, dans laquelle une liaison H inter-résidus N-H···O-S C7δ a été formée à partir de la chaîne latérale, ainsi qu'une interaction N-H···O=C C5 formée dans le squelette du peptide, comme le suggèrent les études infrarouges en phase gazeuse et en solution, ainsi que les études RMN. En solution, outre une forme étendue C5-C7δ dominante, des contributions mineures d'une forme N-H···N π_{am} interaction et/ou d'un conformère C7 libre sont également présentes. À l'état solide, la structure cristalline de *trans*-Cbz-Attc(O)-NHMe a montré une liaison H intermoléculaire impliquant l'atome d'oxygène du résidu thiétane et un NH amide d'une deuxième molécule. Les études infrarouges en phase gazeuse pour le *cis*-Cbz-Attc(O)-NHMe ont été difficiles, même avec un échantillon de grande pureté, mais elles ont permis de détecter un conformère C7 libre mineur. Nous avons proposé que cela puisse être dû à la température élevée en phase gazeuse qui a provoqué la conversion de l'isomère *cis* instable en isomère *trans* plus stable du Cbz-Attc(O)-NHMe, ou qu'il puisse s'agir d'une limitation de l'infrarouge en phase gazeuse pour l'échantillon de *cis*-Cbz-Attc(O)-NHMe. En solution, les résultats expérimentaux dans l'infrarouge ont révélé trois conformations : les formes C7 libre, C5-π_{am} libre et C5-C6γ libre, confirmées par les calculs théoriques, et étaient cohérentes avec les résultats de la RMN 1D/2D. Les résultats de la RMN 1D/2D suggèrent que le conformère C5-C6γ pourrait jouer un rôle mineur. Les calculs théoriques du Cbz-Attc(O,O)-NHMe ont également révélé trois conformations : les formes C7 libre, C5-π_{am} libre et C5-C7δ, qui concordent avec les résultats expérimentaux en phase de solution (IR, RMN 1D/2D). Les résultats de la RMN 1D/2D suggèrent que le conformère C5-C7δ pourrait représenter une

contribution mineure. Néanmoins, en phase gazeuse, le Cbz-Attc(O,O)-NHMe ne présentait qu'un conformère C5-C7δ étendu, dans lequel une liaison H inter-résidus N-H···O-S C7δ a été formée à partir de la chaîne latérale, et une interaction N-H···O=C C5 s'est formée dans le squelette du peptide. À l'état solide, la structure cristalline de Cbz-Attc(O,O)-NHMe ne présente qu'une liaison H intermoléculaire impliquant un atome d'oxygène du résidu thiétane et un NH amide de la deuxième molécule. En général, l'atome d'oxygène généré dans le résidu hétérocyclique de ces dérivés (à l'exception du *cis*-Cbz-Attc(O)-NHMe) a un effet significatif sur leur comportement conformationnel. Ceci est dû à la formation d'une forte liaison H C7δ, qui stabilise efficacement la faible interaction C5 dans le squelette du peptide. Notamment, les interactions C7δ formées dans *trans*-Cbz-Aatc(Me,O)-NHMe et *trans*-Cbz-Attc(O)-NHMe sont plus fortes que les interactions C6γ de leurs précurseurs (Cbz-Aatc(Me)-NHMe et Cbz-Attc-NHMe). Par conséquent, ils sont plus efficaces pour stabiliser l'interaction intra-résidus C5 dans le squelette du peptide.

Dans le quatrième chapitre, les comportements conformationnels de deux dérivés *trans*-ACBC ont été étudiés. En général, les dérivés *trans*-ACBC adoptent une conformation locale avec une liaison H en C8. Cependant, les deux dérivés *trans*-ACBC, *N*-capped with benzoxazolinone moiety semblent diminuer cette préférence de conformation C8 et peuvent adopter d'autres conformations, comme le suggèrent les études spectroscopiques infrarouges et RMN en solution. Le dérivé *trans*-ACBC, coiffé en C par un résidu glycine, présentait trois conformations : C8, C5 et libre. Le dérivé *trans*-ACBC, coiffé en C par une partie *p*-méthoxybenzyle, présente deux conformations : C8 et libre. Ces résultats indiquent que la présence du groupement benzoxazolinone à l'extrémité *N*-terminale des dérivés *trans*-ACBC a un impact significatif, le distinguant des groupements protecteurs couramment utilisés tels que Boc et Cbz.

Cette thèse contribue à la compréhension de la stabilisation conformationnelle de différents peptides courts en explorant les différents types de liaison hydrogène impliqués.